GAS HYDRATE CONTROL BY LOW DOSAGE HYDRATE INHIBITORS

by

MOSAYYEB ARJMANDI

BSc., MSc.

Submitted for the Degree of Doctor of Philosophy in

Petroleum Engineering

Heriot-Watt University

Institute of Petroleum Engineering

October 2007

ABSTRACT

Gas hydrates are ice-like crystalline compounds, which form through a combination of water and suitably sized 'guest' molecules under low temperature and elevated pressure conditions. The formation of gas hydrates in subsea pipelines can cause pipeline blockage, resulting in serious economic and safety issues. Gas hydrate formation is generally prevented by employment of so-called 'thermodynamic inhibitors', which include salts and organic compounds such as methanol and ethylene glycol. However, the use of thermodynamic inhibitors can become uneconomical when high concentrations are required and/or water cut is high. There are also important associated issues with respect to inhibitor recovery and environmental damage. In the light of this, other methods for hydrate prevention such as making use of natural hydrate inhibitors in oil systems and application of a new family of hydrate inhibitors, termed 'Low Dosage Hydrate Inhibitors' (LDHI), are becoming attractive options. In this work both methods have been addressed by investigating the primary mechanism and the parameters involved in hydrate inhibition by the mentioned methods, using novel experimental techniques, and an in-house hydrate model.

It is known that water/oil (W/O) emulsions can reduce gas hydrate blockage risks. Natural surfactants such as asphaltenes and resins in the oil are commonly identified as the agents responsible for stabilising W/O emulsions. In this work, it was shown that oil properties, mixing rate and mixing history, water content, and operational conditions (e.g. pressure) play significant role in reducing hydrate blockage risks in oil/water systems. The effect of mixing rate on the induction time before hydrate formation was shown to be a function of system mixing history (degree of emulsification of water in oil). Before formation of stable emulsion, the induction time increased with mixing rate. However after formation of stable water/oil emulsion induction time was not a strong function of the mixing rate. Water content found to be the most important factor in controlling the risk. It was shown that for the oils tested, water cuts up to 20% do not pose any risk of blockage in the system tested while at 30% water cut a low dosage hydrate inhibitor will be needed for preventing hydrate blockage. A novel experimental set up (Glass Micromodel set-up) was used to obtain visual information regarding the state of water oil emulsion, size of water droplets in the emulsion, hydrates particle size and morphology and distribution of different phases in the system. The results showed

that heavier components in the oil phase are attracted on gas hydrate crystals formed in a water /oil emulsion (the oil surrounding the hydrate particles became brighter and more transparent). Furthermore, it was demonstrated that at static condition the agglomeration of hydrate particles appears to be easier than in flowing conditions in the Micromodel set-up. That was in line with the results obtained from the kinetic rig tests (where long shut-in times resulted in stirrer blockage).

The principal limitation to current Kinetic Hydrate Inhibitor (KHI) design techniques is a lack of verified molecular mechanisms for LDHI activity. In the framework of a joint project between Heriot-Watt and Warwick Universities, a new approach has been used in the design and testing of new LDHIs. Chemicals designed using molecular dynamic simulation were subsequently synthesised (Warwick University) and tested using novel experimental techniques under simulated offshore pipeline conditions to evaluate their potential for use in offshore operations and factors affecting their performance and to study primary mechanism of hydrate inhibition (Heriot-Watt University). The new KHIs showed mild hydrate inhibition effect. In natural gas-water system, their performance was not as good as conventional KHIs (poly-vinylcaprolactam (PVCap) and poly vinyl pyrrolidone (PVP)), however in methane water system, one of them performed better than PVP. Furthermore, the new KHIs demonstrated good anti-agglomeration characteristics (after failure and hydrate formation). Visual observation of hydrate formation and growth in the presence of new KHI showed that it prevents agglomeration of the hydrate particles and cause deformation of the hydrate crystals. In general the performance of the KHIs tested in this study including conventional KHIs were better in structure II hydrate systems compared to structure I hydrates.

Identification of the parameters affecting the performance of Kinetic Hydrate Inhibitors (KHI) is crucial for effective design, screening and deployment of them in deepwater applications. In this work, some of the influential parameters on the performance of PVCap were experimentally studied by application of a kinetic rig and a visual rig. The effect of mixing, pressure, polymer molecular weight, the solvent, subzero conditions, and different gas hydrate structures on the performance of a KHI, PVCap were investigated. The negative effect of static conditions on the performance of PVCap was shown in a visual kinetic rig. By the experiments in a kinetic rig, the negative effect of pressure at constant subcooling on the performance of PVCap was demonstrated. It was shown that the low molecular weight PVCap inhibit hydrate formation better than high molecular weight PVCap. At constant subcooling, PVCap was shown to inhibit structure II hydrate more effectively than structure I hydrate. The negative impact of

corrosion inhibitor on the performance of PVCap was shown. The results showed that ethylene glycol (as a carrier fluid) does not have any significant effect on the performance of PVCap. Furthermore, it was shown that PVCap can inhibit hydrate formation at subzero conditions in the presence of ethylene glycol.

Anti-Agglomerants (AA) are another class of LDHIs developed over the last decade, which prevent hydrates from agglomerating and depositing in pipelines. In this work, after a brief description and literature survey on the development and testing of AA chemicals, a new methodology for testing AAs using the Kinetic Rig and the Glass Micromodel set up was presented. The performance of AAs was evaluated in kinetic rig by torque measurements in different conditions. Two different types of impellers were used for torque measurement and it was shown that the torque measurement was improved by using a helical tube instead of paddle-shape impeller. It was shown that the information obtained from torque measurement technique can be used for screening AAs, however it is not sufficient for selection of an AA for field application. The complementary information such as hydrate particles size, morphology and their distribution in different phases can be obtained from Glass Micromodel set-up. Preliminary experiments, using a proven AA chemical in comparison with another similar compound and an un-inhibited system, showed that the techniques developed in this study are suitable and effective for the testing of AAs.

In studying the kinetics of hydrate formation and inhibition at different conditions, a thermodynamic hydrate model is essential for predicting hydrate phase boundary from which the driving force for hydrate formation can be calculated. In this work an in-house hydrate model (Heriot-Watt Hydrate Model (HWHYD model) has been used for thermodynamic description of the phases and prediction of hydrate phase boundary. As part of the above model, a new approach in modelling phase equilibria and gas solubility in saline solutions has been proposed. Salts were introduced as components in the EoS by calculating their EoS parameters from corresponding cation and anion parameters. A non-density dependent mixing rule was used for calculating a, b, and c parameters of the EoS. The inclusion of salts in the EoS resulted in the omission of Debye-Huckel electrostatic contribution term in the fugacity coefficient calculations. Water-salt binary interaction parameters were optimised using freezing point depression and boiling point elevation data of aqueous electrolyte solutions. Gas solubility data in aqueous electrolyte solution were used for optimising salt-gas BIPs. The predictions of the model have been compared with independent experimental data, demonstrating the reliability of the approach.

The degree of subcooling is usually used as the driving force for hydrate formation; however, it does not encompass the effect of pressure. In this work, by application of the two latest driving force expressions for hydrate formation, and an in-house hydrate model the relationships between subcooling and the calculated driving force at different conditions for pure gas–water and natural gas–water systems have been analysed. The relationship between the driving force and the degree of subcooling for methane, ethane and propane demonstrated that subcooling is a good representative of driving force for pure compounds over a wide pressure range. For natural gas systems at isothermal conditions, between 5 and 20 MPa, subcooling underestimates the calculated driving force for hydrate formation; however, above 20 MPa, subcooling is a good representative of real driving force. Constant degree of subcooling is an appropriate criterion for up-scaling the tests with pure gas and natural gas. For natural gas–water systems at constant driving force/subcooling conditions, the induction time does not seem to be a function of pressure, while in the presence of PVCap, increasing the system pressure had a negative effect on the induction time. This was attributed to the effect of KHI and pressure on the kinetic barriers for hydrate formation in a system. Therefore, testing KHIs at similar field conditions is recommended.

Dedicated to:

My parents, **Ahmad** and **Azam,**

for their heartfelt encouragement and endless support

ACKNOWLEDGMENTS

I would like to express my sincere gratitude and appreciation to Professors Bahman Tohidi and Ali Danesh for their excellent supervision, invaluable guidelines, and continues supports and encouragements. I also owe my thanks to Dr. Shao Ran Ren for his very helpful guidance and his assistance in the experimental side of this work.

I am privileged to be a member of Gas Hydrate Research Group at Heriot-Watt University. Hence, the contribution of all the members in this group is highly appreciated.

The co-operation of all colleagues including the academics, senior and associate researchers and members of support staff of the Institute of Petroleum Engineering at Heriot-Watt University is also appreciated.

The financial support from Engineering and Physical Sciences Research Council (EPSRC) and Heriot-Watt University through their full scholarship to conduct this study is gratefully acknowledged.

The research project, of which this work is a part, is supported by BASF, BP, Clariant Oil Services, Gaz de France, OMV Aktiengesellschaft, TOTAL and the UK Department of Trade and Industry, which is gratefully acknowledged.

Last but not least, I will always remember the encouragement and support of all members of my family, without which all the challenges associated with pursuing this degree would have been very difficult to surmount if not impossible.

ACADEMIC REGISTRY
Research Thesis Submission

Name:	Mosayyeb Arjmandi		
School/PGI:	Petroleum Engineering		
Version: *(i.e. First, Resubmission, Final)*	Final	Degree Sought:	PhD

Declaration

In accordance with the appropriate regulations I hereby submit my thesis and I declare that:

1) the thesis embodies the results of my own work and has been composed by myself
2) where appropriate, I have made acknowledgement of the work of others and have made reference to work carried out in collaboration with other persons
3) the thesis is the correct version of the thesis for submission*.
4) my thesis for the award referred to, deposited in the Heriot-Watt University Library, should be made available for loan or photocopying, subject to such conditions as the Librarian may require
5) I understand that as a student of the University I am required to abide by the Regulations of the University and to conform to its discipline.

* *Please note that it is the responsibility of the candidate to ensure that the correct version of the thesis is submitted.*

Signature of Candidate:	M. Arjmandi	Date:	12/10/2007

Submission

Submitted By *(name in capitals)*:	MOSAYYEB ARJMANDI
Signature of Individual Submitting:	M. Arjmandi
Date Submitted:	14/10/2007

For Completion in Academic Registry

Received in the Academic Registry by *(name in capitals)*:	VAL MURDOCH		
Method of Submission *(Handed in to Academic Registry; posted through internal/external mail)*:	BY EXTERNAL MAIL (DHL)		
Signature:	Valerie A Murdoch	Date:	15/10/07

TABLE OF CONTENTS

LIST OF PUBLICATIONS BY THE CANDIDATE

Arjmandi, M, Tohidi, B., Danesh, A., and Todd, A.C., 2005, " "Is Subcooling the Right Driving Force For Testing Low Dosage Hydrate Inhibitors?", Chemical Engineering Science, Volume 60, Issue 5, pp. 1313-1321, March.

Arjmandi, M., Ren, S. and Tohidi, B., 2005, " Anti-agglomeration and synergism effect of quaternary ammonium zwitterions", Proceeding of 5th International Conference on Gas Hydrates, Trondheim, Norway, 13-16 June.

Tohidi, B., Danesh, A., and Todd, A.C., Anderson, R., Burgass, R.W., **Arjmandi, M.**, Masoudi, R., Ji, H.Y., Mohammadi, A.H., Yang, J.H., Ren, S.R., Zain, Z., Mali, G., and Jadhawar, P., 2004, "Gas hydrates and flow assurance studies", *Proceeding of DTI Maximising Hydrocarbon Recovery from the UKCS Seminar 2004*, 22nd-23rd June 2004, Aberdeen, UK.

Masoudi, R., **Arjmandi, M.** and Tohidi, B., 2003, "Extension of Valderrama-Patel-Teja equation of state to modelling single and mixed electrolyte solutions", *Chemical Engineering Science*, 58(9), 1743-1749.

Arjmandi, M., Ren, S.R., Tohidi, B., 2003, "Progress in Design and Assessment of Low Dosage Hydrate Inhibitors", Proceedings of Offshore Mediterranean Conference, Ravenna, Italy, 26-28 March.

Yang, J., Ren, S.R., **Arjmandi, M.**, and Tohidi, B., 2003, "Application of Glass Micromodel in Design and Evaluation of Kinetic Hydrate Inhibitors", Proceedings of Offshore Mediterranean Conference, Ravenna, Italy, 26 March.

Ren, S.R., Biderkab, A.-B., **Arjmandi, M.**, Yang, J., and Tohidi, 2003, "Avoiding Gas Hydrate Problems in Deepwater Operations", proceedings of BHR Group Multiphase Technology conference, San Remo, Italy, 11-13 June.

Tohidi, B., Anderson, R., Masoudi, R., **Arjmandi, M.**, Burgass, R.W., Yang, J.H., 2003, "A Review of Clathrate Hydrate Research at Heriot-Watt University", *Russian Chemical Journal*, 47(3), 49-58.

Tohidi, B., Danesh, A., Todd, A.C., Yang, J., Ren, S.R., **Arjmandi, M.**, Burgass, R.W.,

Carnegie, E., Anderson, R., Biderkab, A.-B., and Zain, 2003,"Flow assurance: micro- and macro-scale evaluation of low dosage hydrate inhibitors", UK DTI IOR Seminar, Aberdeen, Scotland, UK, 24 June.

Arjmandi, M.,. and Tohidi, B., 2002, "Design and Testing of Low Dosage Hydrate Inhibitors", **3rd Prize winner,** presented at the *SPE Europec Student Paper Contest*, Aberdeen, Scotland, October (2002).

Tohidi, B., Danesh, A., and Todd, A.C., Burgass, R.W., Ren, S.R., Anderson, R., Yang, J.H., **Arjmandi, M.**, Reid, A., Ji, H.Y., Masoudi, R., Biderkab, A.B., and Mohammadi, A.H., 2002, "Gas hydrates in offshore production and drilling", *Proceeding of DTI Improved Oil Recovery (IOR) Research Dissemination Seminar*, 25th June 2002, Aberdeen, UK.

Tohidi, B., Danesh, A., Todd, A. C., Østergaard, K. K., Burgass, R. W., Anderson, R., Yang, J.-H., Ren, S.-R., **Arjmandi, M.**, Reid, A., Ji, H.Y., Massoudi, R., 2001, Gas Hydrates in Offshore Production and Drilling", DTI IOR Seminar, 26th June, London, UK.

Arjmandi, M, Ren, S.R., Biderkab, A.-B, Tohidi, B,"Oil Natural Hydrate Inhibition in Subsea Operation and Multi-Phase Transportation". In preparation.

Arjmandi, M, Ren, S.R., Tohidi, B, "Parameters Affecting the Kinetic Hydrate Inhibitors Performance". In preparation.

Arjmandi, M, Ren, S.R.,Yang, J., Ren, S.R., Tohidi, B, "Evaluation of Anti-Agglomerants Using Kinetic Rig and Micromodel Set-Up". In preparation.

CHAPTER 1

INTRODUCTION

1.1 CLATHRATE GAS HYDRATES

Humphry Davy's observation of chlorine hydrate in 1810 is generally regarded as the discovery of gas hydrate (Davy, 1811). Sir Davy formed a solid from an aqueous solution of chlorine cooled to below 9 °C. In the following decades, hydrates of other, mainly inorganic compounds were found. However, gas hydrates were not linked to matters outside the laboratory, and indeed the petroleum industry, until the 1930's when Hammerschmidt concluded that natural gas hydrates were responsible for blockage of gas transmission lines (Hammerschmidt, 1934).

The term of gas hydrates refers to nonstoichiometric species, belonging to the group of clathrates. They should be distinguished from the stoichiometric hydrates common to inorganic chemistry, e.g., $CaCl_2.6H_2O$ (antarcticite). Clathrates are inclusion compounds, consisting of a host and a guest species. Clathrates can be aqueous, e.g., gas hydrates with water as the host, as well as non-aqueous, e.g., clathrasils with SiO_2 acting as the host.

Gas hydrates are, as other clathrates, crystalline compounds. By hydrogen bonding water molecules arrange into cavities, which become stable by entrapping guest molecules. When different sized cavities arrange themselves into crystals, different hydrate structures appear. Not all cavities in the crystal structure need to be occupied by a guest molecule in order for the structure to be stable.

Three gas hydrate structures are commonly known to the petroleum industry. They are, hydrate structure-I (sI), structure-II (sII), and structure-H (sH). Some properties of the three hydrate structures are given in Table 1.1. Figure 1.1 presents the shape of the different gas hydrate cavities in the three structures.

Hydrate sI consists of a 12 Å cube consisting of 46 water molecules, which form two types of small and large cavities. The two small cavities are pentagonal dodecahedra (5^{12}), whereas the six large cavities are tetradecanhedra having two opposite hexagonal faces and twelve pentagonal faces ($5^{12}6^2$). The smaller cavities are almost spherical, whereas the larger cavities of sI are slightly oblate. Hydrate sI can accommodate guests with diameters up to 6 Å in size.

The unit cell of structure-II (sII), which is a 17.3 Å cube with 136 water molecules, also contains two types of cavities. The 16 smaller cavities are distorted pentagonal dodecahedra and the 8 larger cavities are hexadecahedra having 4 hexagonal faces and twelve pentagonal faces ($5^{12}6^4$). The latter cavities are almost spherical in shape. Hydrate sII accommodates molecules up to around 7 Å in diameter. Properties of hydrate structures I and II were detailed in depth by Jeffrey (1984).

Hydrate sH was recently discovered and reported by Ripmeester et al. (1987). It is a new hexagonal hydrate structure, which requires both large and small molecules to stabilise the structure. The unit cell of sH consists of 34 water molecules forming a hexagonal lattice with parameters a = 12.26 Å and c = 10.17 Å. The sH has three different types of cavities, three 5^{12} cavities which is common to all known hydrate structures, two new 12 faces $4^3 5^6 6^3$ cavities and one new large $5^{12}6^8$ cavity. The $4^3 5^6 6^3$ cavity has three-square faces, six pentagonal faces, and three hexagonal faces, whereas the $5^{12}6^8$ has 12 pentagonal faces and eight hexagonal faces. Due to the large $5^{12}6^8$ cavity sH can accommodate molecules as large almost 10 Å in diameter (Sloan, 1998).

Knowing the three types of hydrate structures, the structure formed depends primarily on the size of the molecules involved. Very small molecules, such as helium and neon do not form gas hydrates, because they are too small to be trapped in any of the above-mentioned cavities. Slightly larger molecules, such as methane, ethane, etc., are known to form sI hydrates. The stable hydrate structure changes back to sII for larger molecules such as propane and isobutane. For binary and multicomponent systems, generally the size of the largest molecule determines the hydrate structure (except structure H, and some binaries like C_1/C_2). Hydrates made of pure compounds are known as simple gas hydrates. However, some large molecules such as normal butane cannot form simple hydrates and they need some smaller molecules, known as help gases, to

fill small cavities and stabilise the structure. These types of hydrates are known as double hydrates. Before the discovery of sH, normal butane was known to be the heaviest hydrate former and anything heavier than that was a non-hydrate former, inhibiting hydrate formation. However, it has been proved that much heavier molecules, such as methylcyclohexane, can form gas hydrates, providing that a help gas fills the small cavities in the sH (Mehta and Sloan, 1993; Ripmeester et al., 1991, Danesh et al., 1994).

Gas Hydrates depending on pressure can form at temperatures considerably higher than the freezing point of water when light hydrocarbons (or light gases) and water are present together. Figure 1.2 illustrates methane hydrate phase boundary (the pressure and temperature conditions at which methane gas, water and hydrate are in equilibrium), hydrate free zone and stable hydrate zone. Gas hydrates have been reviewed in depth by Sloan (1998).

1.2 GAS HYDRATES IN OIL AND GAS INDUSTRY

While naturally occurring hydrates may yield an abundant source of primary energy, and hydrates may also prove useful in the transportation of natural gas, in conventional oil and gas drilling and production operations occurrence of hydrates presents serious operational and safety problems together with substantial potential losses of revenue. Low seabed temperatures combined with high fluid pressures available in subsea pipelines promote formation of clathrates in reservoir hydrocarbon-water fluid mixtures. Hydrates can block pipelines, subsea transfer lines, and, in the event of a gas kick during drilling, form in the well, in risers, BOPs (Blow-Out Preventers) and choke lines (Barker and Gomez, 1989). As the offshore industry advances in to the new deepwater provinces, the difficulties associated with hydrate formation are becoming more significant.

1.3 PREVENTION OF GAS HYDRATES

As mentioned earlier, the formation of hydrates requires four essential elements to be present: hydrate-forming gases (or liquids), water or ice, low temperatures and moderate to high pressures. Strategies for hydrate mitigation and remediation often modify one or more of these elements to destabilise the hydrate and thus remove the problem. However, hydrates can also be prevented by injection of chemical inhibitors, which modify the chemistry of hydrate formation. Various methods for hydrate control can be summarised as follows:

Pressure Control: Design and operate the system with pressure low enough to maintain the fluids in the hydrate free zone (Figure 1.2). This method is often impractical for normal operation since the pressure required for transportation of production fluids would usually exceed the hydrate formation pressure at the ambient temperature. However, for the removal of hydrates following unplanned shutdowns, various depressurisation techniques to shift the system to outside the hydrate phase boundary is normal practice.

Temperature Control: Maintain the temperature of production fluids by either insulation or heating in order to prevent the system entering the hydrate zone. Temperature control by insulation only offers hydrate control during operation when system is being continually heated by hot production fluids. Following a shut down the production fluids will cool down and can enter the hydrate zone. Under these circumstances the traditional approach has been to depressurise the system as discussed above, although heating can be used to prevent cooldown into the hydrate region by maintaining temperatures (Mehta et al. 2001).

Dehydration: Prevent the formation of hydrates by removing the supply of water using separation and dehydration. This approach has proved popular for the export of sales gas.

Hydrate Former Removal: Reduce the risk of hydrate blockage and/or reduce the inhibitor requirement by removing the supply of gas (hydrate former) by gas liquid separation. This approach has been proposed for subsea operation where gas and liquids are separated subsea and are transported to the processing facilities in separate pipelines.

Injection of Chemical Inhibitors: Chemical hydrate inhibitors (e.g. methanol and ethylene glycol), also known as thermodynamic inhibitors, reduce water activity and hence affect the equilibrium conditions where hydrate can form. Hydrate phase boundary in the presence of thermodynamic inhibitors is shifted to lower temperatures and higher pressures. This provides a wider hydrate free zone for operations (Figure 1.3). Conventional chemical inhibitors are a major tool in current hydrate prevention strategies (Urdahl et al, 1995, Notz et al, 1995, Argo et al, 2000, Frostman, 2000) but must be used in large volumes, *e.g.*, up to 50 mass% methanol in the water-rich phase. This imposes severe capital and operational costs. Recent international estimates of the cost of the conventional

inhibitor, methanol, alone are in excess of $150million per year (Long et al., 1994). Furthermore, the transportation, storage, injection, and recovery of conventional chemical inhibitors such as methanol have associated health, safety and environmentally (HS&E) concerns (Phillips and Grainger, 1998).

In the past decade, in response to the economic and HS&E concerns, a new group of non-thermodynamic chemical inhibitors has been developed which has received considerable attention from the industry. A number of laboratory studies and field trials have been reported in literature (Phillips and Grainger, 1998, Mitchell and Talley 1999, Argo et al., 2000, Frostman and Przybylinski, 2001, Lovell and Pakulski 2002). These chemicals do not shift the thermodynamic phase boundary of hydrate formation, but interfere with the process of hydrate formation by means of a number of mechanisms proposed by many researchers (Sloan, 1998, King et al. 2000, Koh et al 2002, Makogon and Sloan, 2002). Because the effective dosage for these new chemicals is much lower than those required for thermodynamic inhibitors, often around 0.3–0.5 mass% compared with 10–50 mass% needed for conventional inhibitors (Phillips and Grainger, 1998), the new inhibitors are known as Low Dosage Hydrate Inhibitors (LDHI). LDHIs are typically divided by different active mechanisms such as, Kinetic Hydrate Inhibitor (KHI) and Anti-Agglomerants (AA).

Kinetic hydrate inhibitors (KHI) were among the first LDHIs utilised to control hydrates in oil and gas systems. The KHIs work by delaying hydrate nucleation and/or growth. An inhibitor molecule retards crystal growth by either adsorbing onto the crystal surface (the growth sites) or fitting into the crystal lattice. By doing so, the KHI distorts the crystal lattice or growth steps thus preventing the crystal from growing rapidly in a regular crystal structure. The anti-agglomerate technique is based on preventing the agglomeration and deposition of hydrate crystals so that a transportable hydrate slurry could be formed (Behar et al, 1994, Frostman, 2000). Current anti-agglomerate inhibitors must be used in the presence of an oil phase. The anti-agglomerant inhibitors are incorporated into the hydrate crystal lattice and serve to disrupt further growth of the crystals.

1.4 OVERVIEW OF THE THESIS

The knowledge of gas hydrate phase behaviour is, on a whole, well documented. Especially the issue of hydrate phase boundary determination has received much

attention over the years. Today, comprehensive thermodynamic models, mostly based on equations of state and statistical thermodynamics, are available for hydrate equilibrium predictions. Hydrate kinetics pose the largest challenge to future understanding, which now rests on a comparatively sound thermodynamic foundation (Sloan, 2003).

Competitive oil and gas prices together with increasing concern for the environment necessitates novel hydrate control procedures. Areas of concern are the development of low dosage hydrate inhibitors, use of natural inhibitors in some oils, and introduction of environmental friendly chemical inhibitors. Lately, a significant shift in research efforts from thermodynamics to kinetics of gas hydrate formation and inhibition has also been observed (Sloan, 1998).

The focus of this thesis is prevention of gas hydrate problems in the oil and gas industry by low dosage hydrate inhibitors and making use of some components already available in the oil production fluids (i.e. salt in produced water and natural surfactants in some oils).

For investigating the kinetics of hydrate formation and inhibition in any system, knowing the hydrate phase boundary of the system is essential in order to calculate available driving force of hydrate formation at specific system conditions. In the absence of experimental data, a reliable predictive thermodynamic model for generating hydrate phase boundaries in different systems is crucial. Furthermore, as the water-cut in oil wellstreams is formation water which inhibits hydrate formation to some extent, for more economical use of expensive inhibitors an efficient thermodynamic hydrate model should be able to predict the effect of salts on the hydrate phase boundary of the system. In Chapter 2, first the thermodynamic formulations for fugacity calculations in the different phases in Heriot-Watt Hydrate Model, which has been used in this study, are detailed. Then the improvement of the model in this work for modelling single and mixed electrolyte solutions and gas solubility in saline water, by a rigorous thermodynamic approach, is described.

It is known that the formation of water/oil (W/O) emulsions reduces gas hydrate blockage risks in subsea pipelines. Natural surfactants such as asphaltenes and resins in the oil are commonly identified as the agents responsible for stabilising W/O emulsions. With economical and environmental concerns associated with

the application of different conventional methods for preventing gas hydrate, making use of natural inhibition of hydrates in some oils is becoming an attractive option. Different parameters such as type of oil, water content, mixing rate, mixing history and pressure may play role on the induction time (the period before hydrate formation when the system get into the stable temperature and pressure inside the hydrate forming region) and transportability of the system. In Chapter 3 the results of the experimental investigations made on the kinetics of hydrate formation in water-oil-natural gas systems at subsea operation conditions, addressing the above-mentioned factors, are presented.

While the LDHIs developed over the past decade have been applied in many oil and gas fields for controlling hydrate, there is much scope for further development. The mechanism of KHIs is still far from comprehensive apart from the adsorption theory (Sloan 1998, Koh et al., 2002). Three problems in particular arise: the extent of subcooling (the temperature difference between operating (in hydrate zone) and equilibrium conditions at a specific pressure) induced, the operating pressure, and the environmental acceptability. Subcooling and operating pressure affect the induction time of the system. The current generation of KHIs allows only 10–12 °C subcooling at medium pressure conditions for achieving an acceptable induction time in the system whereas about 20 °C at high-pressure conditions is needed in many applications. There is still a need for the development of KHIs suitable for high degree of subcooling and for high pressures. The performance of current KHIs at various conditions has not been fully investigated. There is little information available regarding hydrate formation and the mechanism and effect of KHIs at micro-scales. As a result the design and deployment of current KHIs have been on a trial and error basis. In this thesis the above-mentioned problems have been addressed.

In Chapter 4 a new methodology for designing and testing of KHIs is presented. The preliminary mechanism of hydrate formation and inhibition, which was studied by visual observations, is also presented in Chapter 4.

Knowing the parameters that affect the performance of kinetic hydrate inhibitors at different conditions is important for designing new inhibitors and efficient deployment of existing inhibitors. In this study some of the influential factors on the kinetic inhibitor performance, such as pressure, hydrate structure, mixing,

polymer molecular weight and solvent, compatibility with other inhibitors (e.g. corrosion inhibitor), and subzero conditions, have been investigated and detailed in Chapter 5.

In the systems where oil and water exist and due to high degree of subcooling and high pressure conditions application of kinetic hydrate inhibitors is not possible, anti-agglomerants are used to form a transportable hydrate slurry. Screening and testing the performance of the hydrate anti-agglomerants which are suitable for specific pipeline conditions is of high importance in flow assurance studies. In this work, a brief description and literature survey on the development and testing of AA chemicals is presented. A methodology for testing anti-agglomerants by new experimental set-ups is also presented in Chapter 6.

For testing LDHIs, subcooling is usually considered as the driving force for hydrate formation and a criterion for simulating field conditions. In many cases, it is a routine industrial practice to scale up the experiments conducted at low-pressure conditions to high pressures based on some similarity principles. As subcooling does not encompass the effect of pressure, its application as a driving force and scale-up criterion may be unreliable in some cases. A comprehensive driving force for hydrate formation is a function of pressure, temperature, and gas composition; however, its calculation is not as simple as that of subcooling. A comprehensive driving force for hydrate formation in a gas-water system, derived on the basis of thermodynamics principles, should be applicable to any system in the presence of low dosage hydrate inhibitors due to their very low concentrations in the aqueous phase and their negligible effect on the hydrate phase boundary. In this thesis, Chapter 7, by application of the two latest driving force expressions for hydrate formation, the relationships between subcooling and the true driving force at different conditions for different systems has been analysed. The suitability of subcooling as driving force in testing LDHIs at different systems has been identified. Following that the results of tests are presented, which show the impact of pressure on the induction time in the absence and presence of a kinetic hydrate inhibitor when the driving force for hydrate formation is constant.

The conclusions of this thesis and recommendations for future work are presented in Chapter 8.

1.5 TABLES

Table 1.1. Hydrate unit cell characteristics of structures-I, II, and H (Tohidi, 1995).

Structure	I		II		H		
Crystal system	Cubic		Cubic		Hexagonal		
Lattice parameter/ Å	12		17.3		a=12.26, c=10.17		
H_2O/unit cell	46		136		34		
Total No. of cavities/ unit cell	8		24		6		
Cavity type	5^{12}	$5^{12}6^2$	5^{12}	$5^{12}6^4$	5^{12}	$4^3 5^6 6^3$	$5^{12}6^8$
Radius of cavity/ Å	3.95	4.3	3.91	4.73	3.91	4.06	5.71
Coordination No.	20	24	20	28	20	20	36
Cavities/unit cell	2	6	16	8	3	2	1

1.6 FIGURES

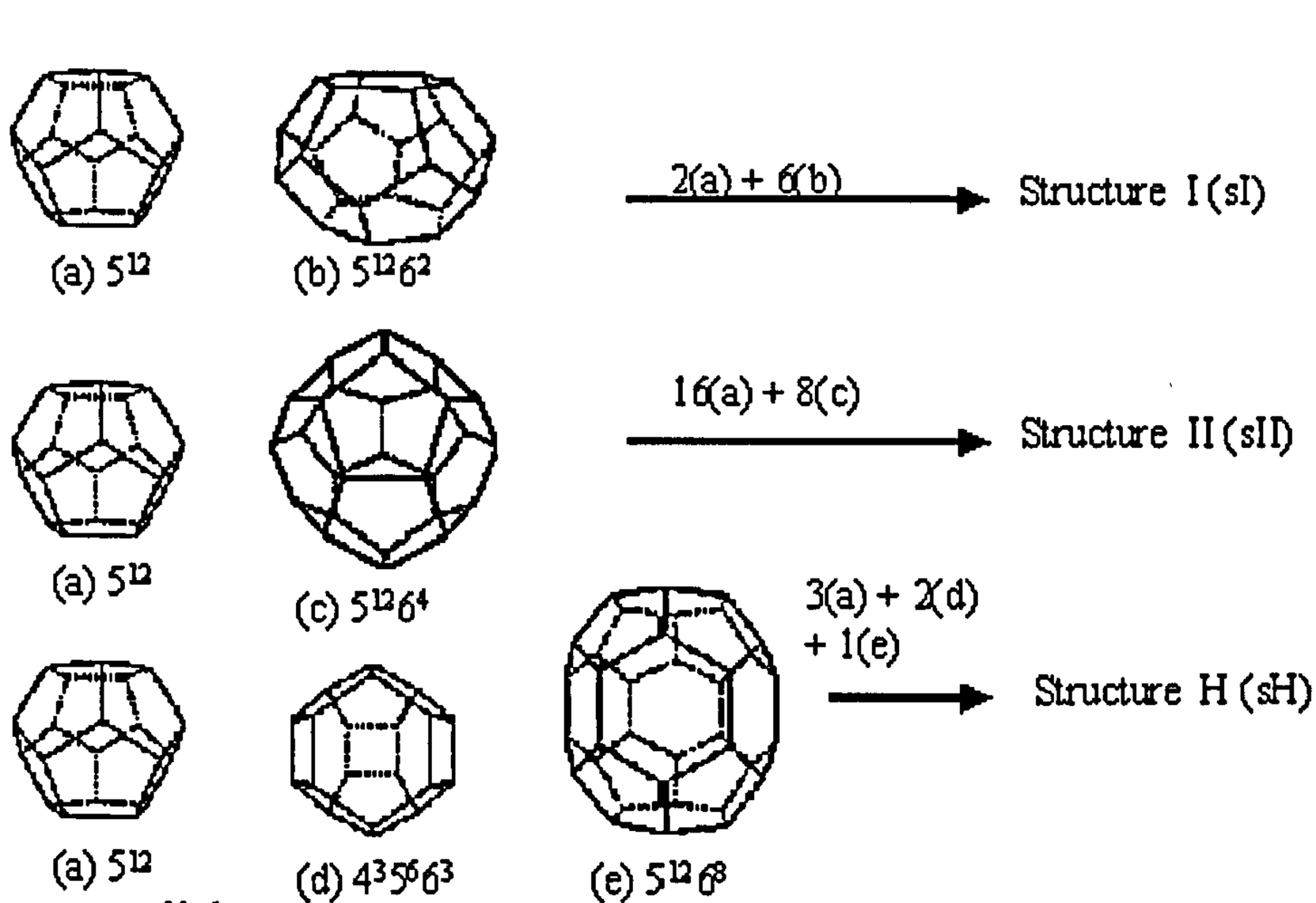

Figure 1.1. Cavities in gas hydrate structures.

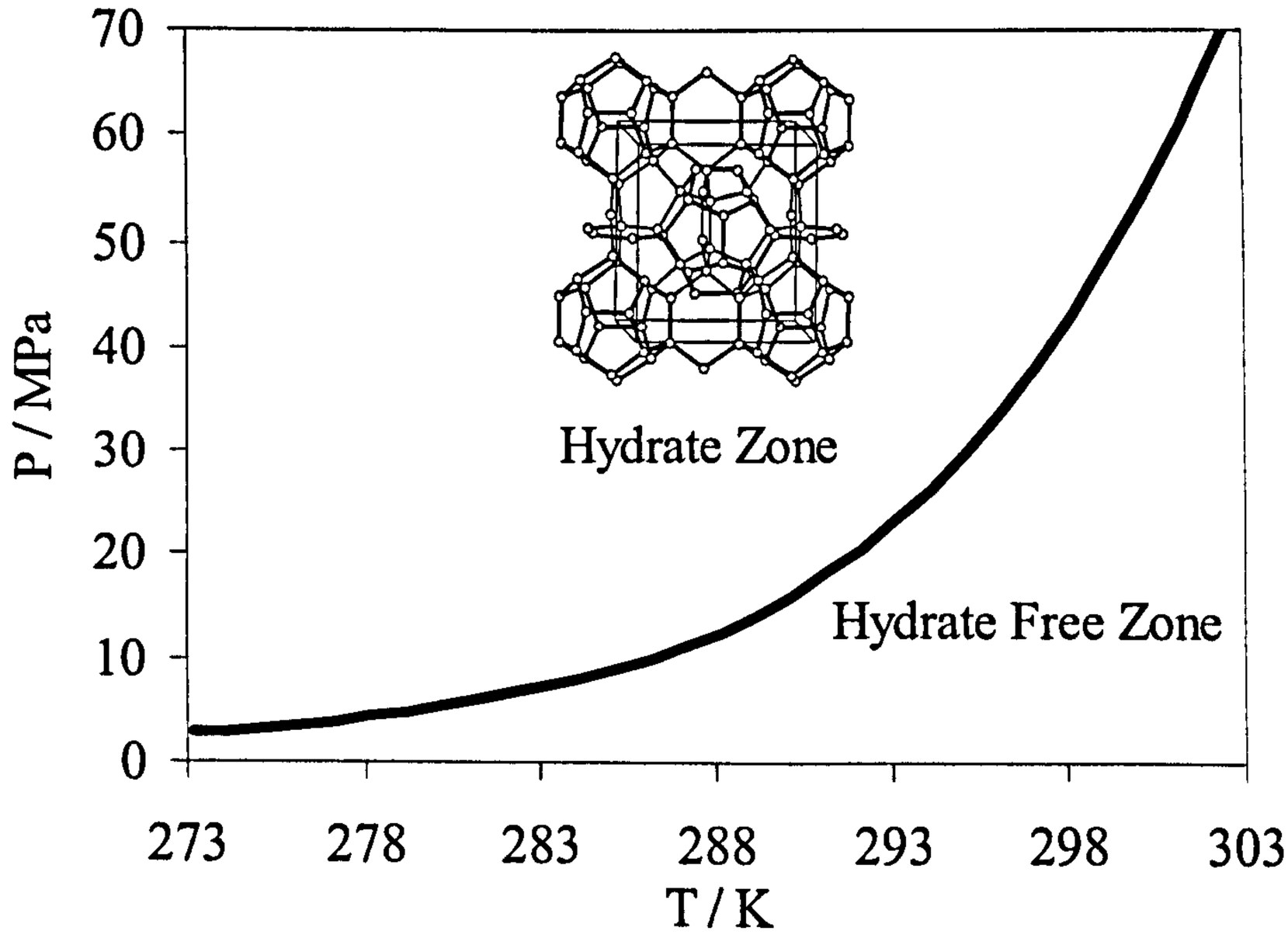

Figure 1.2. Methane hydrate phase boundary.

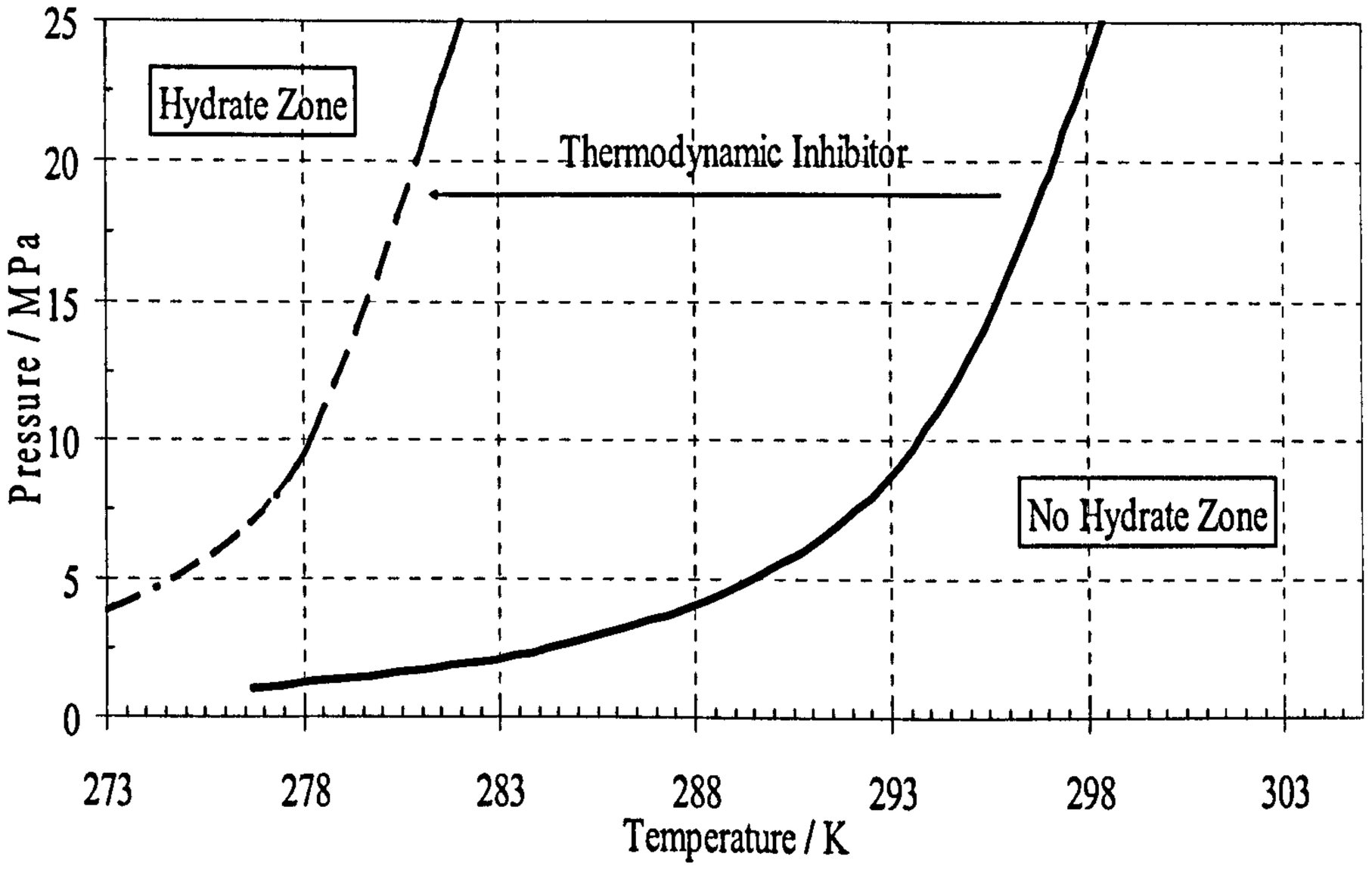

Figure 1.3. Shift of hydrate phase boundary by thermodynamic inhibitors.

CHAPTER 2

A SIMPLIFIED MODEL FOR PHASE EQUILIBRIA IN ELECTROLYTE SOLUTIONS

2.1 INTRODUCTION

For efficient and economical petroleum exploration and production, phase equilibria, vapour-liquid as well as the hydrate phase boundary must be precisely known in order to find the hydrate free zone conditions. It is well known that when electrolytes are present in liquid water, hydrate formation is inhibited as they can prevent the ordering of the water molecules around hydrate formers. In the gas and oil industries, formation water (Table 1 presents a typical composition) may be present in the reservoirs and hydrocarbon transfer lines, as well as in the surface separation facilities. In such systems accurate experimental and theoretical knowledge of phase equilibria, hydrate phase boundaries in the presence of electrolytes are crucial to the success of any flow assurance strategy. The salts in formation water prevent hydrate formation to some extend by reducing water activity.

In relation to testing the performance of low dosage hydrate inhibitors (LDHI) in subsea pipeline conditions, it is necessary to know the system driving force for hydrate formation in order to know the range of inhibitor applicability. The driving force of hydrate formation in a system is usually considered as degree of subcooling which is defined as the difference of system temperature and equilibrium temperature at system pressure. For calculation of the degree of subcooling in a system, prediction of the hydrate phase boundary is essential by a reliable thermodynamic model.

In this chapter, first the description of phases in Heriot-Watt Hydrate Model (HWHYD), which has been used in later chapters for predicting the hydrate phase boundaries, is presented. A simplified vapour liquid equilibrium (VLE) model in the presence of salts, which was developed in this work, will then be presented.

2.2 DESCRIPTION OF PHASES IN HWHYD MODEL

A typical hydrate system consists of several phases, i.e., vapour (V), water rich (L_w), liquid hydrocarbon (L_{HC}), hydrate (H), and ice (I). Furthermore, thermodynamic inhibitors, e.g., methanol and salts may also be present, leading to more complicated systems. As far as the hydrate phase boundary is concerned, a calculation algorithm was developed by Parrish and Prausnitz (1972), for determining the dissociation curve of gas hydrate. The algorithm operates by finding the point at which the chemical potential difference between the water in the hydrate phase and in the coexisting phases is zero. Despite shortcomings, the above algorithm, which is known as conventional formulation, is still widely used in the industry. Briefly, in this type of calculation it is necessary to specify the number and type of phases present, the hydrocarbon composition on a water free basis, the inhibitor concentration, and temperature (or pressure). After performing the calculations, the algorithm will provide values of pressure (or temperature), the composition of all phases and the amount of each hydrocarbon phase.

However, there are several calculations that could provide important information regarding gas hydrate phases, in addition to potential hydrate formation conditions. These include the ability to perform flash calculations in the presence of gas hydrates, which is to calculate the amount of hydrate that will form under given circumstances, and the composition of all equilibrium phases. Another important calculation is the distribution of inhibitor throughout the equilibrium phases, which has many applications in determining the amount of methanol lost in the vapour phase. All of the above calculations are possible when using the multi-phase flash calculation procedure developed by Michelsen (1982) and adopted by Cole and Goodwin (1990) for a combination of vapour and liquid phases, in conjunction with an equation of state or an activity model.

2.2.1 MULTI PHASE EQUILIBRIUM

Bishnoi *et al.* (1989) adopted the methodology for multiphase equilibrium flash calculations of Gupta (1988) for systems containing gas hydrates. Cole and Goodwin (1990) rearranged the hydrate phase model to a form compatible with the Michelsen flash algorithm, to give explicit expressions for the fugacities of all the components of the hydrate lattice as functions of the overall composition of the hydrate phase. Avlonitis (1992) proposed an alternative algorithm for multiphase flash calculations.

A combined employment of two stability criteria was used in his method. Either the fugacity ratios between any phase under test and a reference phase converge to unity or the mass of the test phase is zero. His approach is particularly efficient when water and hydrate former are present in the feed and generally up to six phases may be present at equilibrium.

For the description of a typical hydrate problem more than one model is usually needed. For a system to be at thermodynamic equilibrium, the chemical potential of each component throughout the system must be uniform:

$$\mu_{i1} = \ldots = \mu_{ij} = \ldots = \mu_{i\pi} \quad , \qquad i=1, 2, \ldots, N \tag{2.1}$$

where μ_{ij} is the chemical potential of component i in phase j, N is the number of components and π is the number of phases. For an isothermal system this will reduce to equality of fugacity for each component in all phases.

$$f_{i1} = \ldots = f_{ij} = \ldots = f_{i\pi} \quad , \qquad i=1, 2, \ldots, N \tag{2.2}$$

In the most general case, i.e., when all components are present in all phases, there will be $N(\pi\text{-}1)$ such equations. In addition, material balance imposes another set of $N+\pi$ equations:

$$z_i = \sum_j^{\pi} F_j x_{ij} \tag{2.3}$$

and

$$\sum_i^{N} x_{ij} = 1 \tag{2.4}$$

where z_i is the specified composition of the feed, F_j the fraction in moles of phase j and x_{ij} the mole fraction of component i in phase j. Totally there are $\pi(N+1)$ equations with an equal number of unknowns, which may be chosen to be either (x_{ij}, F_j) at specified temperature T and pressure P or (x_{ij}, F_j=r, P) at specified T with $F_r = 0$. The first is the typical isothermal flash problem and the second the general phase boundary problem. In summary, after determination of the correct number of equilibrium phases and their corresponding compositions at fixed temperature and pressure by a multiphase algorithm, the hydrate phase boundary and flash calculation is reduced to finding

suitable equations of state for calculating the fugacity in different equilibrium phases.

In the following sections, the models and equations used for evaluating the fugacities in various phases common to hydrate calculations are described in more details.

2.2.2 VAPOUR, LIQUID HYDROCARBON, AND WATER PHASES

An Equation of State (EoS) which is cubic in volume and gives pressure in terms of volume and temperature of a substance is called a cubic equation of state. They are more successful than any other type of equation of state with a simpler form (Walas,1985). Cubic equations of state are commonly used in the petroleum industry for volumetric and phase behaviour modelling of reservoir fluids. Since the introduction of van der Waals equation in 1873, numerous equations (e.g. Redlich-Kwong equation, the Soave-Redlich-Kwong equation and the Peng-Robinson equation) have been published in the literature and promising new equations keep appearing. All these cubic equations of state have two constants, an attraction parameter a and a repulsion parameter b, hence they are called two-constant equations of state. The latter parameter is also referred as the co-volume parameter and is sometimes called the effective molecular volume. The Peng-Robinson equation of state is given as

$$P = \frac{RT}{(v-b)} - \frac{a(T)}{v(v+b)+b(v-b)} \tag{2.5}$$

Application of the equation of state to mixtures requires the evaluation of parameters a and b (in equation 2.5) using the corresponding pure component parameters and the composition of the mixture. The rules governing the combination of pure component parameters and composition to derive the mixture properties are known as mixing rules. van der Waals proposed a quadratic mixing rule, known as classical or random mixing rules, which can provide good results for simple mixtures where the molecules do not differ appreciably in size, shape or polarity.

In classical mixing rules, which are applied to describe the nonpolar-nonpolar binary interactions in fluid mixtures, the parameters a, and b for a mixture, are calculated from the following equations:

$$a = \sum_i \sum_j x_i x_j \left(a_i a_j\right)^{0.5} \left(1 - k_{ij}\right) \tag{2.6}$$

$$b = \sum_i x_i b_i \tag{2.7}$$

where x_i is the mole fraction of component i and k_{ij} is the so-called standard binary interaction parameter (BIP) between component i and component j. Binary interaction parameter takes into account the difference in the interaction of unlike molecules. The purpose of the binary interaction parameter is to enhance the capability of an equation of state to predict the desired phase behaviour; hence most of the methods to fit the binary interaction parameter match laboratory-data with that calculated by the equation of state.

Introduction of a third parameter in the EoS relaxes the assumption of a fixed value for the critical compressibility factor and improves the prediction of volumetric properties. Patel and Teja (1982) introduced a third parameter in the EoS in such a way that the EoS critical compressibility factor may be chosen freely to match the vapour pressure and saturated liquid density. The 3-parameter PT (Patel-Teja) EoS has been shown to give satisfactory results for both vapour pressure and liquid density even for heavy and polar compounds. In the PT EoS, the acentric factor has been extensively used to correlate the parameters of the equation of state. However, the acentric factor is a parameter representing the behaviour of a substance at a relatively low temperature range. Therefore, Valderrama and Cisternas (1986) and later Valderrama (1990) modified the Patel and Teja equation of state (modification know as the VPT EoS) by using the critical compressibility factor to correlate parameters of PT EoS.

Danesh *et al.* (1991) evaluated the reliability of 10 equations of state with classical mixing rules for predicting the phase behaviour and volumetric properties of hydrocarbon fluids, with particular relevance to the North Sea gas injection systems. They concluded that the Valderrama modification of the Patel and Teja equation of state (VPT EoS) was superior to other equations of state, particularly without using any binary interaction parameter which is to enhance the capability of an equation of state to predict the desired phase behaviour.

However, the random mixing rule is not satisfactory for polar-nonpolar liquid mixtures. Avlonitis *et al.* (1994) proposed a non density dependent (NDD) mixing rule and showed its superiority to density dependent (DD) mixing rules in representing the phase behaviour of multicomponent mixtures containing hydrocarbons up to n-octane, nitrogen, carbon dioxide, hydrogen sulphide, water and methanol.

In Heriot-Watt hydrate model, the well-proven Valderrama modification of the Patel and Teja equation of state (VPT EoS) with the non-density dependent (NDD) mixing rule (Avlonitis *et al.*, 1994) has been used to model all the fluid phases, i.e., V, L_{HC}, and L_W. Binary Interaction Parameters for hydrocarbon gases and water have been determined by matching published binary vapour liquid equilibria data.

The VPT EoS has the following form:

$$P = \frac{RT}{v-b} - \frac{a(T)}{v^2 + (b+c)v - bc} \tag{2.8}$$

where $a = a_c \alpha(T_r)$. For a pure component the four parameters of Eq. (2.5) are obtained as follows:

$$a_c = \Omega_{a_c} \frac{R^2 T_C^2}{P_C} \tag{2.9}$$

$$b = \Omega_b \frac{R\ T_C}{P_C} \tag{2.10}$$

$$c = \Omega_c \frac{R\ T_C}{P_C} \tag{2.11}$$

$$\alpha(T_r) = \left(1 + m(1 - T_r^{0.5})\right)^2 \tag{2.12}$$

where P is the pressure, T is the temperature, v is the molar volume, and R is the universal gas constant. The subscripts c and r denote critical and reduced properties, respectively. Ω_a and Ω_b in a two parameter EoS or Ω_c in a three parameter EoS may be found by satisfying Equation (2.5) and the following two critical point conditions:

$$\left(\frac{\partial P}{\partial v}\right)_{T_c} = 0 \tag{2.13}$$

$$\left(\frac{\partial^2 P}{\partial v^2}\right)_{T_c} = 0 \tag{2.14}$$

In the VPT EoS, the parameters in the Eqs. (2.6) - (2.9) are calculated by the following equations:

$$\Omega_{a_c} = 0.66121 - 0.76105 Z_C \tag{2.15}$$

$$\Omega_b = 0.02207 + 0.20868 Z_C \tag{2.16}$$

$$\Omega_c = 0.57765 - 1.87080 Z_C \tag{2.17}$$

$$m = 0.46283 + 3.5823\,\omega Z_C + 8.19417(\omega Z_C)^2 \tag{2.18}$$

where ω and Z_C are the acentric factor and critical compressibility factor respectively. Avlonitis et al. (1994) relaxed the correlation of $\alpha(T_r)$ of VPT EoS for water and methanol and regressed a more specific correlation for temperatures up to critical point:

$$\alpha(T_r) = \left(1 + m(1 - T_r^{\Psi})\right)^2 \tag{2.19}$$

Methanol: m=0.76757, Ψ=0.67933

Water: m=0.72318, Ψ=0.52084

In classical mixing rules, for mixture, the parameters *a and b* are calculated from equations 2.6 and 2.7, and parameter *c* is calculated from the following equation:

$$c = \sum_i x_i c_i \tag{2.20}$$

where x_i is the mole fraction of component i .

For polar-nonpolar interaction the NDD mixing rules are applied. In these mixing rules, the attraction parameter (a) has been separated into two parts, the classical mixing rule part (a^C) and the asymmetric contribution part (a^A), as follows:

$$a = a^C + a^A \tag{2.21}$$

$$a^C = \sum_i \sum_j x_i x_j (a_i a_j)^{0.5} (1 - k_{ij}) \tag{2.22}$$

$$a^A = \sum_p x_p^2 \sum_i x_i a_{pi} l_{pi} \tag{2.23}$$

$$a_{pi} = \sqrt{a_p a_i} \tag{2.24}$$

where p stands for polar component and l_{pi} is the binary interaction parameter between the polar component and the other components, which is a function of temperature, calculated by the following expression:

$$l_{pi} = l_{pi}^{0} - l_{pi}^{1}(T-T_0) \tag{2.25}$$

where l_{pi}^{0} and l_{pi}^{1} are binary interaction parameters and T_0 is the ice point in K. It should be noted that in the classical mixing rules the binary interaction parameters, k_{ij} and k_{ji}, have the same values for nonpolar-nonpolar pairs. However, these values are not necessarily equal for the nonpolar-polar or polar-polar pairs.

Using the above EoS and associated mixing rules the fugacity of each component in all fluid phases can be calculated from:

$$f_i = x_i \varphi_i P \tag{2.26}$$

where P is the pressure, f_i, x_i and φ_i are the fugacity, mole fraction and fugacity coefficient of component i, respectively in vapour or liquid phases.

2.2.3 HYDRATE PHASES EQUILIBRIA

Van der Waals and Platteeuw (1959) derived the basic statistical thermodynamic equations by using the ideal solution theory to model the gas hydrate phases. In their approach, hydrate-forming molecules are viewed as adsorbed in the cavity sites, which is described by the Langmuir adsorption theory. The fundamental assumptions in developing this theory are:

1. The host molecules contribution to the free energy is independent of the occupation of the cavity. This assumption also implies that the encased molecule does not distort the cavity.
2. Each cavity can contain at most one guest molecule, which cannot diffuse from the cavity.
3. There are no interactions between the guest molecules, i.e., the energy of an encased guest molecule is independent of the number and types of other guest molecules.
4. No quantum effects are needed; classical statistics are valid.

Using the Parrish and Prausnitz (1972) approach, Mehta and Sloan (1994) extended the van der Waals and Platteeuw thermodynamic model to the new structure-H hydrates.

The fugacity of water in the hydrate phase is given by Anderson and Prausnitz (1986):

$$f_w^H = f_w^\beta \exp\left(-\frac{\Delta\mu_w^{\beta-H}}{RT}\right) \tag{2.27}$$

where f_w^β is the fugacity of water in the empty hydrate lattice, R and T are the gas constant and absolute temperature, respectively. $\Delta\mu_w^{\beta-H}$ is the chemical potential difference of water between the empty hydrate lattice, μ_w^β, and the hydrate phase, μ_w^H, and is obtained from the van der Waals and Platteeuw expression (Parrish and Prausnitz, 1972):

$$\Delta\mu_w^{\beta-H} = \mu_w^\beta - \mu_w^H = RT\sum_m v_m \ln\left(1+\sum_j C_{jm} f_j\right) \tag{2.28}$$

where v_m is the number of cavities of type m per water molecule in the unit cell, f_j is the fugacity of the gas component j. C_{jm} is the Langmuir constant, which accounts for the gas-water interaction in the cavity. Numerical values for the Langmuir constant can be calculated if a model for the guest-host interaction is chosen. van der Waals and Platteeuw (1959) used the Lennard-Jones potential function and showed that the Langmuir constant is a function of temperature according to the relation:

$$C_{jm}(T) = \frac{4\pi}{kT}\int_0^\infty \exp\left(-\frac{w(r)}{kT}\right) r^2 dr \tag{2.29}$$

where k is Boltzmann's constant and $w(r)$ is the spherically symmetric cell potential in the cavity, with r measured from centre, and depends on the intermolecular potential function chosen for describing the encaged gas-water interaction. Here the Kihara potential parameters (Kihara, 1953) with a spherical core, as illustrated in Figure 2.1 are used:

$$\Gamma(r) = \infty \qquad \text{, for} \qquad r = 2\alpha \tag{2.30}$$

$$\Gamma(r) = 4\varepsilon\left[\left(\frac{\sigma^*}{r-2\alpha}\right)^{12} - \left(\frac{\sigma^*}{r-2\alpha}\right)^{6}\right] \quad \text{, for} \qquad r > 2\alpha \tag{2.31}$$

where $\Gamma(r)$ is the potential energy of interaction between two molecules, α is the hard core radius, $\sigma = \sigma^* + 2\alpha$ is the collision diameter and ε is the depth of the energy well.

McKoy and Sinanoglu (1963) summed up all these guest-water binary interactions inside the cell to yield an overall cell potential:

$$w(r) = 2z\varepsilon\left[\frac{(\sigma^*)^{12}}{R^{11}r}\left(\delta^{10} + \frac{\alpha}{R}\delta^{11}\right) - \frac{(\sigma^*)^{6}}{R^{5}r}\left(\delta^{4} + \frac{\alpha}{R}\delta^{5}\right)\right] \tag{2.32}$$

where z is the coordination number of the cavity, that is, the number of oxygen molecules at the periphery of each cavity, R is the radius of the cavity and δ^N is a polynomial given by the equation:

$$\delta^N = \left[\left(1 - \frac{r}{R} - \frac{a}{R}\right)^{-N} - \left(1 + \frac{r}{R} - \frac{a}{R}\right)^{-N}\right] \tag{2.33}$$

here N is an integer equal to 4, 5, 10, or 11.

Tohidi (1995) describes the optimisation procedure employed for determining the Kihara parameters, as well as lists Kihara parameters for conventional gas hydrate forming components. For simplicity, σ^* and ε/k have been chosen as optimisation parameters, instead of σ and ε, respectively.

The fugacity of water in the empty hydrate lattice, f_w^β in Equation (2.26), is given by:

$$f_w^\beta = f_w^{I/L} \exp\left(\frac{\Delta\mu_w^{\beta-I/L}}{RT}\right) \tag{2.34}$$

where $f_w^{I/L}$ is the fugacity of pure ice or liquid water and the quantity inside the parentheses is given by the following equation:

$$\begin{aligned}\frac{\Delta\mu_w^{\beta-I/L}}{RT} &= \frac{\mu_w^\beta(T,P)}{RT} - \frac{\mu_w^{I/L}(T,P)}{RT} \\ &= \frac{\Delta\mu_w^0}{RT_0} - \int_{T_0}^{T}\frac{\Delta h_w^{\beta-I/L}}{RT^2}dT + \int_{P_0}^{P}\frac{\Delta v_w^{\beta-I/L}}{RT}dP\end{aligned} \tag{2.35}$$

where μ^β_w and $\mu_w^{I/L}$ are the chemical potential of the empty hydrate lattice and of pure water in the ice (I) or the liquid (L) state, respectively. P is the equilibrium pressure and T_0 is the absolute temperature at the ice point. $\Delta\mu_w^0$ is the reference chemical

potential difference between water in the empty hydrate lattice and pure water in the ice phase at 273.15 K. $\Delta h_w^{\beta-I/L}$ and $\Delta v_w^{\beta-I/L}$ are molar enthalpy and volume differences between an empty hydrate lattice and ice or liquid water. $\Delta h_w^{\beta-I/L}$ is given with the following equation:

$$\Delta h_w^{\beta-I/L} = \Delta h_w^0 + \int_{T_0}^{T} \Delta C_{pw} dT \tag{2.36}$$

where Δh_w^0 is the enthalpy difference between the empty hydrate lattice and ice at ice point and zero pressure. The heat capacity difference between the empty hydrate lattice and the pure liquid water phase is also temperature dependent and the equation recommended by Holder *et al.* (1980) is used:

$$\Delta C_{pw} = -37.32 + 0.179(T - T_0) \qquad \text{, for} \quad T > T_0 \tag{2.37}$$

Furthermore, the heat capacity difference between hydrate structures and ice is set equal to zero. In HWHYD model, for the heat capacity difference between the empty hydrate lattice and the pure liquid water the equation recommended by Holder et al. (1980) is used.

Table 2.2 presents the reference properties of the hydrate structures used in the model, as reported by Parrish and Prausnitz (1972), Dharmawardhana *et al.* (1980), and Mehta and Sloan (1994). The table includes $\Delta\mu_w^0$, which is the reference chemical potential difference between water in the empty hydrate lattice and pure water in the ice phase at 273.15 K, Δh_w^0, which is the enthalpy difference between the empty hydrate lattice and ice at ice point and zero pressure, and Δv_w^0, which is molar volume differences between an empty hydrate lattice and ice or liquid water.

Predictions from the described hydrate fugacity model are relatively good at moderate pressures and temperatures. However, at high pressures (P>20 MPa) and for natural gas hydrates the model predictions deviate from experimental data (Ballard and Sloan, 2002). The deviation at high pressures has been attributed to the assumption of hydrate lattice constant volume in Van der Waals and Platteeuw model. Ballard and Sloan (2002) developed a new hydrate model in which the distortion of the cages by the guest molecules was taken into account.

2.2.4 ICE PHASE

The fugacity of a pure solid can, as for a supersaturated pure liquid, be calculated using the Poynting correction, i.e., assuming that the volume of the supersaturated phase is constant at the volume for the saturated phase (Anderson and Prausnitz, 1986). For ice the expression becomes:

$$f_w^I = \phi_w^{sat} P_I^{sat} \exp\left(\frac{v_I (P - P_I^{sat})}{RT}\right) \tag{2.38}$$

where f_w^I is the fugacity of water in the ice phase, ϕ_w^{sat} is the water fugacity coefficient in the vapour phase at pressure equal to the ice vapour pressure, P_I^{sat} is the ice vapour pressure, v_I is the ice molar volume, R is the universal gas constant, and P and T are the system pressure and temperature, respectively.

The ice molar volume (cc/mol) is calculated using the following expression (Tohidi, 1995):

$$v_I = 19.629 + 2.2364 \times 10^{-3} (T - 273.15) \tag{2.39}$$

and the ice vapour pressure (mmHG) is also calculated using (Tohidi, 1995):

$$P_I^{Sat} = \log\left[(-1.032 \times 10^{-3}) / T + 5.106 \log T - 9.771 \times 10^{-2} T + 7.036 \times 10^{-5} T^2 - 9.851 \right] \tag{2.40}$$

where T is the temperature in Kelvin.

2.2.5 SALINE WATER PHASE

Several thermodynamic models have been developed to represent the vapour-liquid equilibria (VLE) in aqueous electrolyte solutions (Li and Nghiem, 1986; Sander et al., 1986; Macedo et al., 1990). Early models for predicting vapour-liquid equilibria in systems containing aqueous electrolyte solutions were either based on an activity coefficient approach or did not include non-condensable gases. Aasberg-Peterson et al. (1991) adopted a new approach. They divided the fugacity coefficient of each component in the liquid water phase into two terms: an equation of state term (short-range interactions), which is employed to calculate the effect of non-ionic (molecular) species in the aqueous phase and a Debye-Hückel electrostatic term (long-range

interactions), which is used for calculating the effect of salts on the fugacity coefficients of molecular species in the solution.

$$\ln\varphi_I = \ln\varphi_I^{EoS} + \mathrm{Ln}\gamma_I^{EL} \qquad I=1,\ldots\ldots, N \qquad (2.41)$$

Where N is the number of non-electrolyte components, φ_I is the fugacity coefficient of component I, φ_i^{EoS} is the fugacity coefficient of component I neglecting the electrostatic effect calculated by an EoS, and γ_i^{EL} is the contribution of the electrostatic term. It is worth mentioning that they did not consider salt as a component in the EoS, but took into account its effect on the fugacity coefficient of other molecular species.

In the Heriot-Watt model, the fugacities in water rich phase are calculated by combining the VPT Eos with the Debye-Huckel electrostatic contribution for taking into account the effect of salt.

$$\mathrm{Ln}\gamma_i^{DH} = 2A\, h_{is}\, M_m\, f(BI^{1/2})/B^3 \qquad (2.42)$$

where M_m is the salt-free mixture molecular weight determined as a molar average, I is the ionic strength, and h_{is} is the interaction coefficient between the dissolved salt and a non-electrolyte component (gas and water). The water-salt and gas salt interaction coefficients need to be optimised using experimental data. The function $f(BI^{1/2})$ is obtained from:

$$f(BI^{1/2}) = 1 + BI^{1/2} - 1/(1+BI^{1/2}) - 2\ln(1+BI^{1/2}) \qquad (2.43)$$

The parameters A and B are given by:

$$A = 1.327757*10^5 d_m^{0.5}/(\eta_m T)^{1.5} \qquad (2.44)$$

$$B = 6.359696*d_m^{0.5}/(\eta_m T)^{0.5} \qquad (2.45)$$

Where η_m is the salt free mixture dielectric constant and d_m is salt free mixture density (kg/m^3). Tohidi et al. (1995) modified the Aasberg-Peterson approach by expressing the interaction coefficients in the Debye-Hückel electrostatic term as a function of the electrolyte concentration and temperature of the system. The modification was to extend the model capabilities to handle lower temperatures, and wider salt concentrations. They also optimised the relevant parameters for a larger number of salts and extended the model to mixed electrolyte solutions by using Kumar and Patwardhan approach (Kumar and Patwardhan, 1986).

2.3 THE NEW MODEL IN SALINE WATER PHASE

The aim of this work is to develop a simplified thermodynamic model for predicting the phase behaviour of aqueous electrolyte solutions as well as solubility in these systems.

2.3.1 SALTS AS COMPONENTS

Zuo and Guo (1991) presented their model for predicting gas solubility in a saline solution under both high and low-pressure conditions. In their model ions/salts in solution are considered as components in the EoS. They suggested the following equation for calculating the fugacity coefficient of each component:

$$\ln\varphi_i = \ln\varphi_i^{EoS} + \ln\varphi_i^{DH} \qquad (2.46)$$

For the first term in the above equation they employed Patel-Teja EoS, and extended its application to ions (cations and anions) in solution by definition of "a", "b", and "c" parameters for them as follows:

$$a = 2.57012\,\pi\,\varepsilon\,N_a^2\,\sigma^3\,f \qquad (2.47)$$

$$c = b = (2/3)\,\pi N_a\,\sigma^3 \qquad (2.48)$$

where N_a is the Avogadro number, σ is the ionic diameter, f is an empirical constant equal to 6, ε is the ionic energy parameter estimated from the dispersion theory (Mavroyannis and Stephen, 1962):

$$\varepsilon = 2.2789 * 10^{-8}\,\eta^{0.5}\chi^{1.5}\sigma^{-6}k \qquad (2.49)$$

where η is the number of electrons in an ion, χ is the polarizability of an ion, and k is the Boltzmann's constant.

The Kurihara (1987) mixing rule for the energy parameter "a" was used along with the van der Waals mixing rule. The second term of Eq. (2.46) is a Debye-Hückel expression using the fully dissociated salt as the standard state (Li and Pitzer, 1986):

$$\ln\phi_i^{DH} = -A\left[\frac{2Z_i^2}{B}\ln\left(\frac{1+BI^{0.5}}{1+B/\sqrt{2}}\right) + \left(\frac{I^{0.5}Z_i^2 - 2I^{1.5}}{1+BI^{0.5}}\right)\right]. \qquad (2.50)$$

where

$$I = 0.5\,\Sigma\,x_i Z_i^2 \qquad (2.51)$$

$$A = \frac{1}{3}\left(\frac{2\pi N_s d_o}{M_s}\right)^{0.5}\left(\frac{e^2}{DkT}\right)^{1.5} \quad (2.52)$$

$$B = 2150\left(\frac{d_o}{DT}\right)^{0.5} \quad (2.53)$$

where D, e, Z, M_s and d_o denote the dielectric constant, electronic charge, number of charges, molecular weight of solvent, and solvent density, respectively.

2.3.2 THE NEW APPROACH

In this approach, an equation of state based (EoS) model has been adopted for modelling all fluid phases, including the water-rich phase. The Valderrama-Patel-Teja (VPT) EoS, together with a NDD mixing rule, is used in this approach. Salts are treated as components in the EoS, similar to other components in the system. Equations (2.47) and (2.48) are used to calculate the *a*, *b*, and *c* parameters in the EoS for individual ions. The following relations are suggested and used for calculating the *a*, *b*, and *c* for the resulting salts:

$$a_s=(a_a a_c)^{1/2} \quad (2.54)$$

$$b_s=(b_a+b_c)/2 \quad (2.55)$$

$$c_s=(c_a+c_c)/2 \quad (2.56)$$

where subscripts *s*, *a*, and *c* denote salts, anions, and cations, respectively.

By including salts in the VPT EoS and using NDD mixing rules, the Debye-Hückel electrostatic contribution term was eliminated from Equation (2.46). This resulted in a simple and flexible approach for modelling aqueous electrolyte solutions. It should be noted that the effect of Debye-Hückel term, in the original approach (Zuo and Guo, 1991), has been studied and it appeared to be negligible.

Therefore, the following equation is applied in this approach instead of Equation (2.46):

$$\ln\varphi_i = \ln\varphi_i^{EoS} \quad (2.57)$$

where *i* denotes each component in the system, including salt (i.e., fugacity of salt in the aqueous phase can be calculated from the above equation). Binary Interaction Parameters (BIPs) between salt and water are optimised using water freezing point depression and boiling point elevation data. A similar approach is used to optimise

salt-salt BIPs. In addition, gas solubility data in aqueous electrolyte solutions have been used in optimisation of gas-salt BIPs. Table 2.3 shows all Binary Interaction Parameters (BIPs) of water-salt, salt-salt, and gas-salt for the NDD mixing rule obtained through the optimisation process.

2.3.3 PHASE BEHAVIOUR OF SINGLE AND MIXED ELECTROLYTE AQUEOUS SOLUTION

The new simplified approach has been applied to model NaCl and KCl aqueous solutions. The resulting model is capable of predicting the phase behaviour of aqueous electrolyte solutions, as detailed below:

Initially water-salt binary interaction parameters were optimised, using data on freezing point depression and boiling point elevation of their aqueous solutions. This provided a reliable water-salt phase behaviour model over a wide temperature range (i.e., -25 °C to 125 °C). Figure 2.2 presents the experimental (CRC, 1989) and calculated freezing point of NaCl aqueous solutions. Figure 2.3 presents the vapour pressure lowering of NaCl and KCl aqueous solutions at 353.15 K, 373.15 K, and 273.15 K. It should be noted that the vapour pressure lowering experimental data (from International Critical Tables, ICT (Washburn, 19 26-1930) has not been used in optimising the BIPs, so they could be regarded as independent data. Excellent agreement between experimental data and model predictions is observed.

To model mixed electrolyte aqueous solutions, experimental data on boiling point elevation (ICT (Washburn, 1926-1930)) and freezing point depression data (Hall et al., 1988) of NaCl and KCl aqueous solutions have been used to optimise the BIPs between NaCl and KCl. Figure 2.4 shows the experimental and predicted water freezing point temperatures in the presence of NaCl and KCl at 0.6 NaCl mass fraction [NaCl/(NaCl+KCl)]. The predictions are in excellent agreement with the experimental data, considering that only the freezing point depression data at 0.2 and 0.8 NaCl mass fractions have been used in the optimisation process.

2.3.4 GAS SOLUBILITY IN SINGLE AND MIXED ELECTROLYTE AQUEOUS SOLUTIONS

The gas solubility data in aqueous electrolyte solutions has been used for optimising gas-salt binary interaction parameters. Figure 2.5 presents the experimental data (Takenouchi and Kennedy, 1965) and the calculated methane solubility in pure water and NaCl aqueous solutions. Figure 2.6 presents the experimental data (O'Sullivan &

Smith, 1970) and the calculated carbon dioxide solubility in pure water and NaCl aqueous solutions. The agreement between experimental data and model predictions is very good.

Limited data is available on the phase behaviour of mixed electrolyte systems. Independent gas solubility data has been used in validating the developed thermodynamic model. Table 2.4 shows the only available experimental data (Byrne & Stoessell, 1982) on CH_4 solubility in a NaCl/KCl/water ternary system. The thermodynamic model prediction is also presented in the table, demonstrating the reliability of the developed model.

2.4 CONCLUSIONS

In a typical hydrate problem several phases are potentially present. In this Chapter, the formulations used in Heriot-Watt hydrate model for thermodynamic equilibrium and models to determine fugacities in different phases, including hydrate and saline water, have been outlined. As detailed, the Valderrama modification of the Patel and Teja cubic equation of state with non-density dependent mixing rules has been used for fugacity calculations in all fluid phases. The hydrate phases are described by the solid solution theory and ice is regarded as subcooled liquid. The saline water phase was described by a modification of Aasberg-Peterson approach. The previous approaches (Zuo & Guo, 1991 and Tohidi et al., 1995) in modelling phase equilibria in the presence of aqueous electrolyte solutions have been improved by introducing salts as components in the equation of state and eliminating the Debye-Hückel electrostatic contribution term in the fugacity coefficient calculations. Water-salt and gas-salt binary interaction parameters are calculated from the literature data.

The above approach, which could be applied to other EoS, provides a much simpler method for predicting phase equilibria in the presence of aqueous electrolyte solutions, at a wide temperature and pressure ranges. The predicted water freezing point depression, boiling point elevation, and gas solubility in aqueous electrolyte solutions are compared with independent literature data, demonstrating the reliability of the simplified model.

2.5 TABLES

Table 2.1. Typical formation water composition.

Ion	Concentration (mg/litre)
Na^+	15860
K^+	250
Ca^{++}	757
Mg^{++}	102
Ba^{++}	3.01
Sr^{++}	122
Fe^{++}	2.63
B^{+++}	56.4
Mn^{++}	0.25
Cl^-	25550
Br^-	53
I^-	58.2
HCO_3^-	1068
SO_4^{--}	390

Table 2.2. Thermodynamic reference properties for structures-I, II, and H.

Structure	I	II	H
$\Delta\mu_w^0$ (J/mol)	1297[#]	937[#]	914.38[¤]
Δh_w^0 (J/mol)[†]	1389[#]	1025[#]	846.57[¤]
Δv_w^0 (cm^3/mol)[††]	3.0[§]	3.4[§]	3.85[¤]

[†] In the liquid water region subtract 6009.5 J/mol from Δh_w^0.

[††] In the liquid water region add 1.601 cm^3/mol to Δv_w.

[#] Dharmawardhana *et al.* (1980).

[§] Parrish and Prausnitz (1972).

[¤] Mehta and Sloan (1994).

Table 2.3. Binary Interaction Parameters (BIPs) for the NDD mixing rule.

K_{ij}	H2O	CH4	CO2	NaCl	KCl
H_2O	0	0.5058	0.2659	0.3213	-0.2836
CH_4	0.5058	0	0	0.8738	1.482
CO_2	0.2659	0	0	0.206	-
NaCl	0.3791	0.8738	0.206	0	-1.377
KCl	-0.2386	1.482	-	-1.737	0

l^0_{ij}	H2O	CH4	CO2	NaCl	KCl
H_2O	0	1.818	0.81386	1.951	-0.0957
NaCl	2.62	103.438	-24.68	0	-4.278
KCl	0.4476	146.357	-	-9.374	0

l^1_{ij}*1E+4	H2O	CH4	CO2	NaCl	KCl
H_2O	0	49	18.3228	-9.468	3.951
NaCl	135.615	14670.5	-12.598	0	-1117.1
KCl	21.679	68393.4	-	2493.2	0

Table 2.4. Experimental and predicted CH_4 solubility in NaCl/KCl/water system

NaCl (Mass%)	KCl (Mass%)	T (K)	P (MPa)	Experimental solubility (Mole%)	Predicted solubility (Mole%)	Error (%)
5.158	6.58	298.15	3.795	0.051	0.045	11.76

2.6 FIGURES

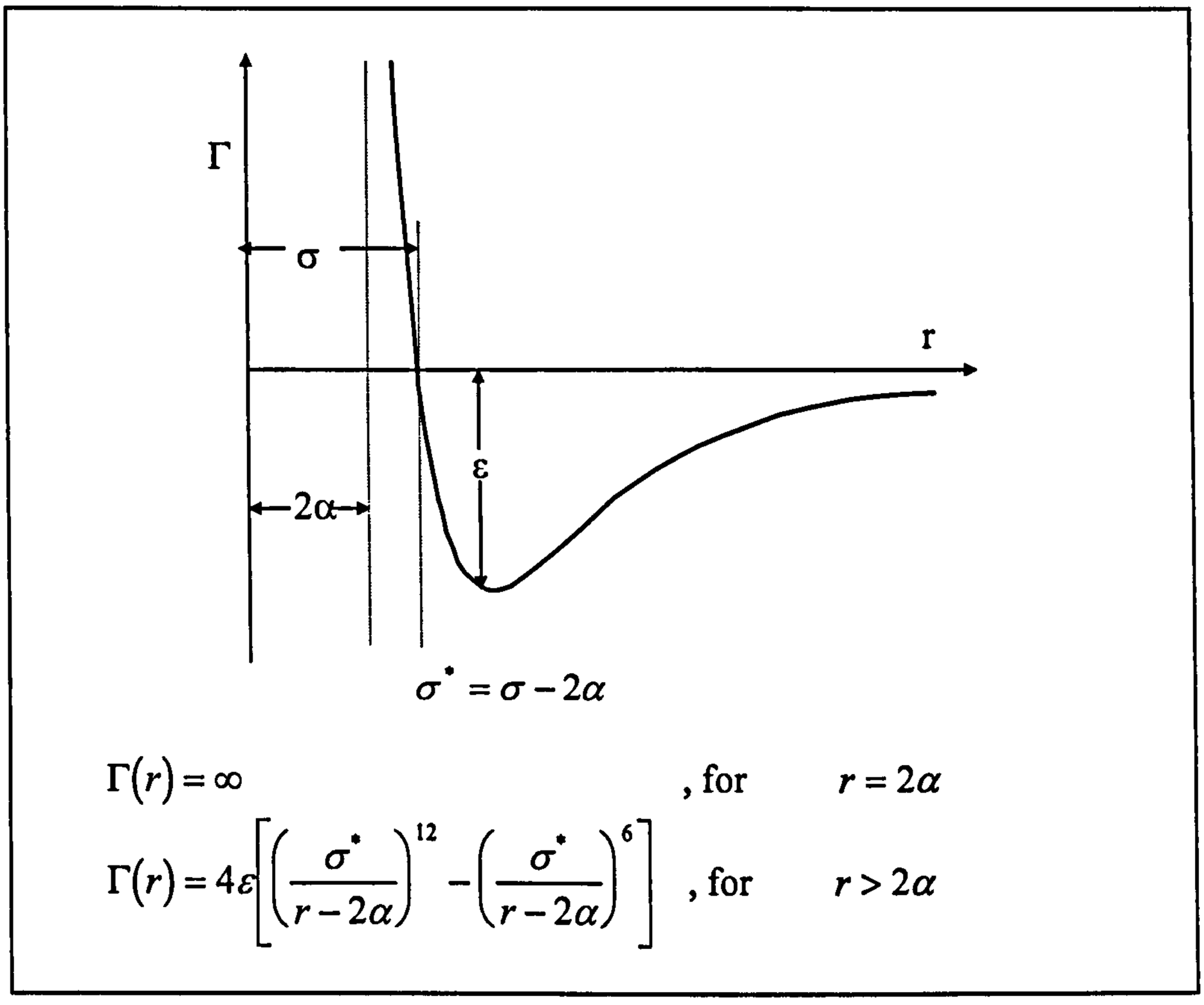

Figure 2.1. Potential function in the Kihara model with three adjustable parameters.

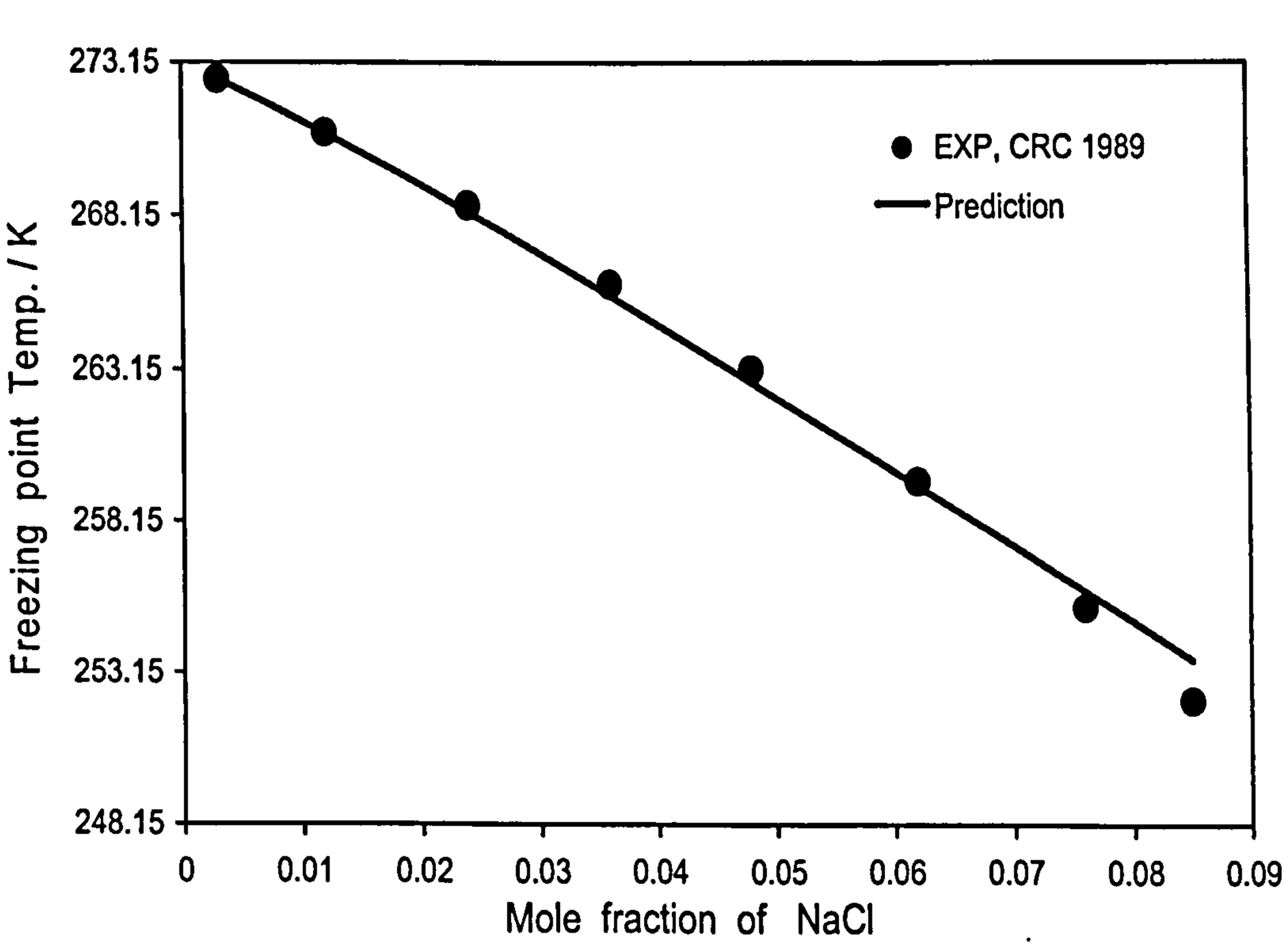

Figure 2.2. Experimental and calculated freezing points of NaCl aqueous solutions (0 to 24.3 mass% NaCl).

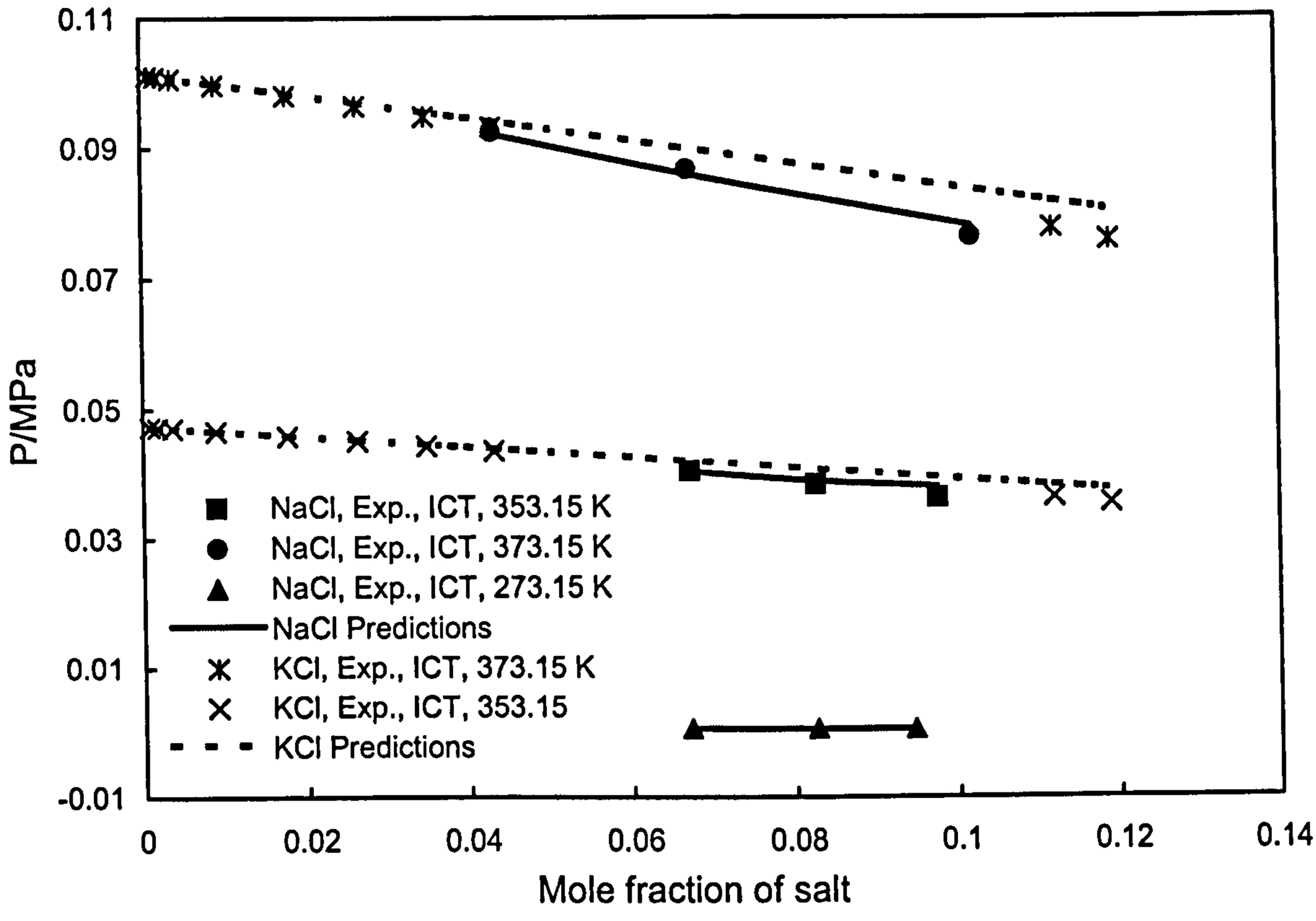

Figure 2.3. Experimental and predicted vapour pressure lowering of NaCl and KCl aqueous solutions at various temperatures (up to 36 mass%).

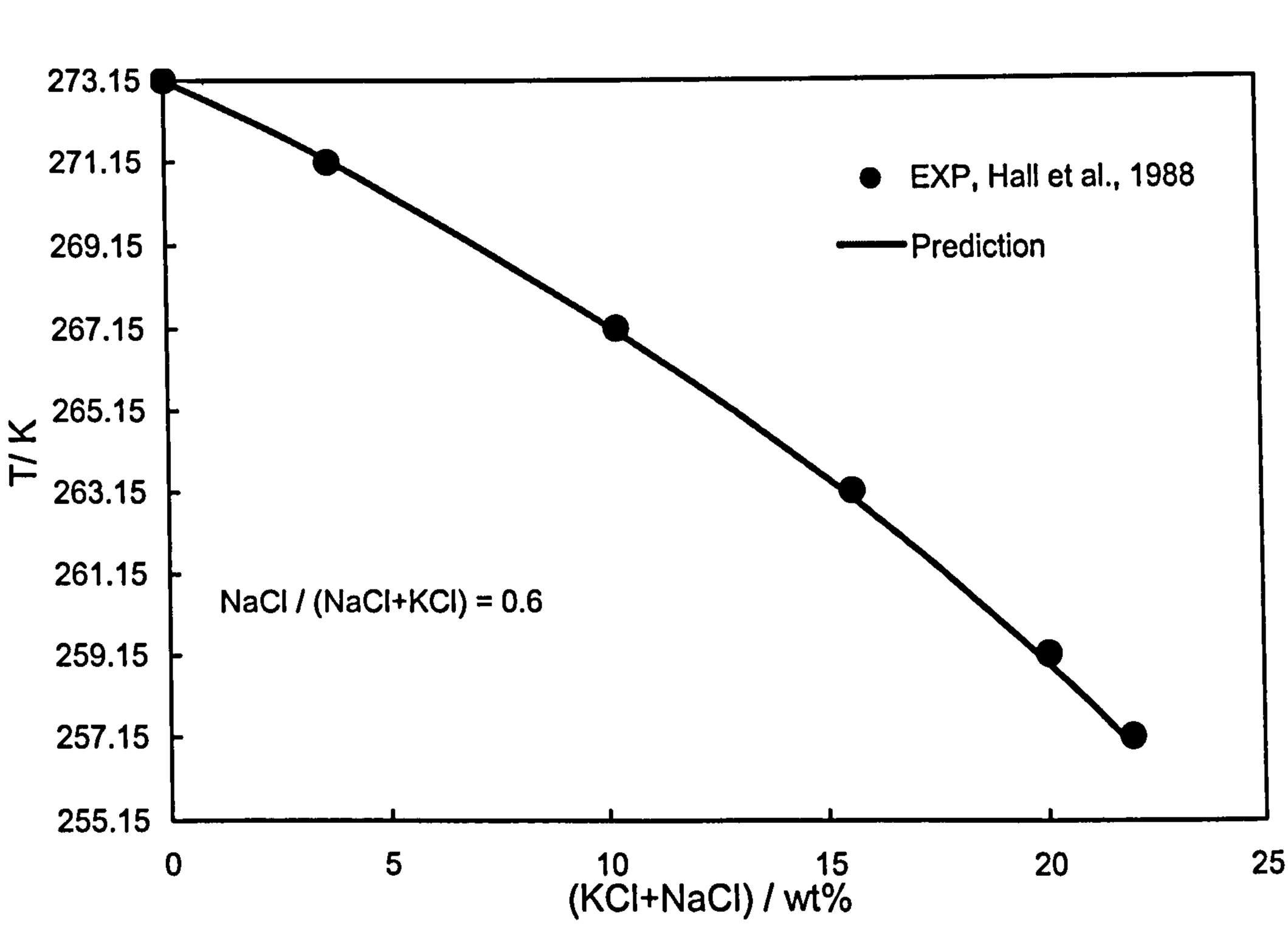

Figure 2.4. Experimental and predicted water freezing point temperature in the presence of NaCl and KCl.

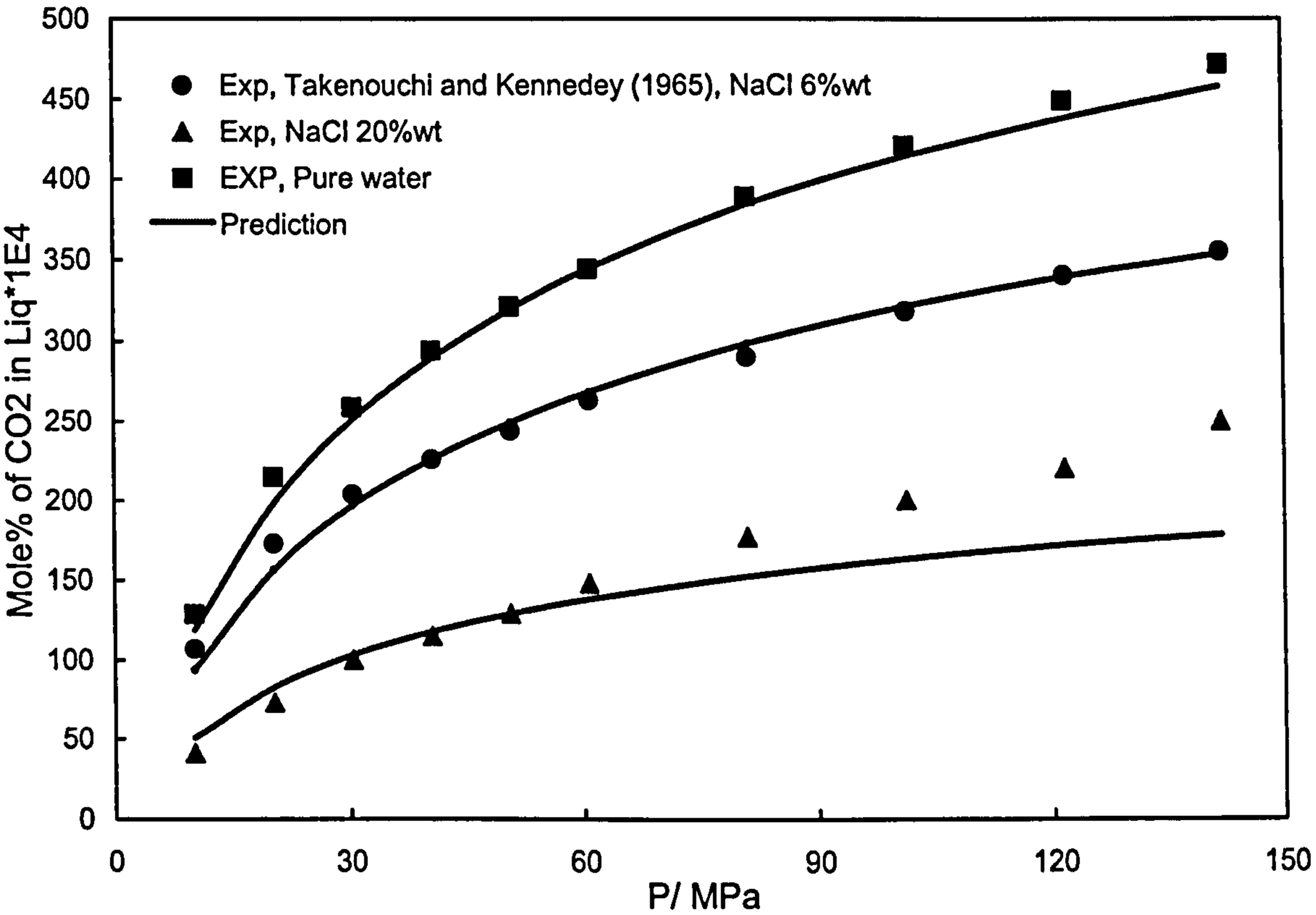

Figure 2.5. Experimental and predicted methane solubility in pure water and NaCl aqueous solutions at 324.65 K.

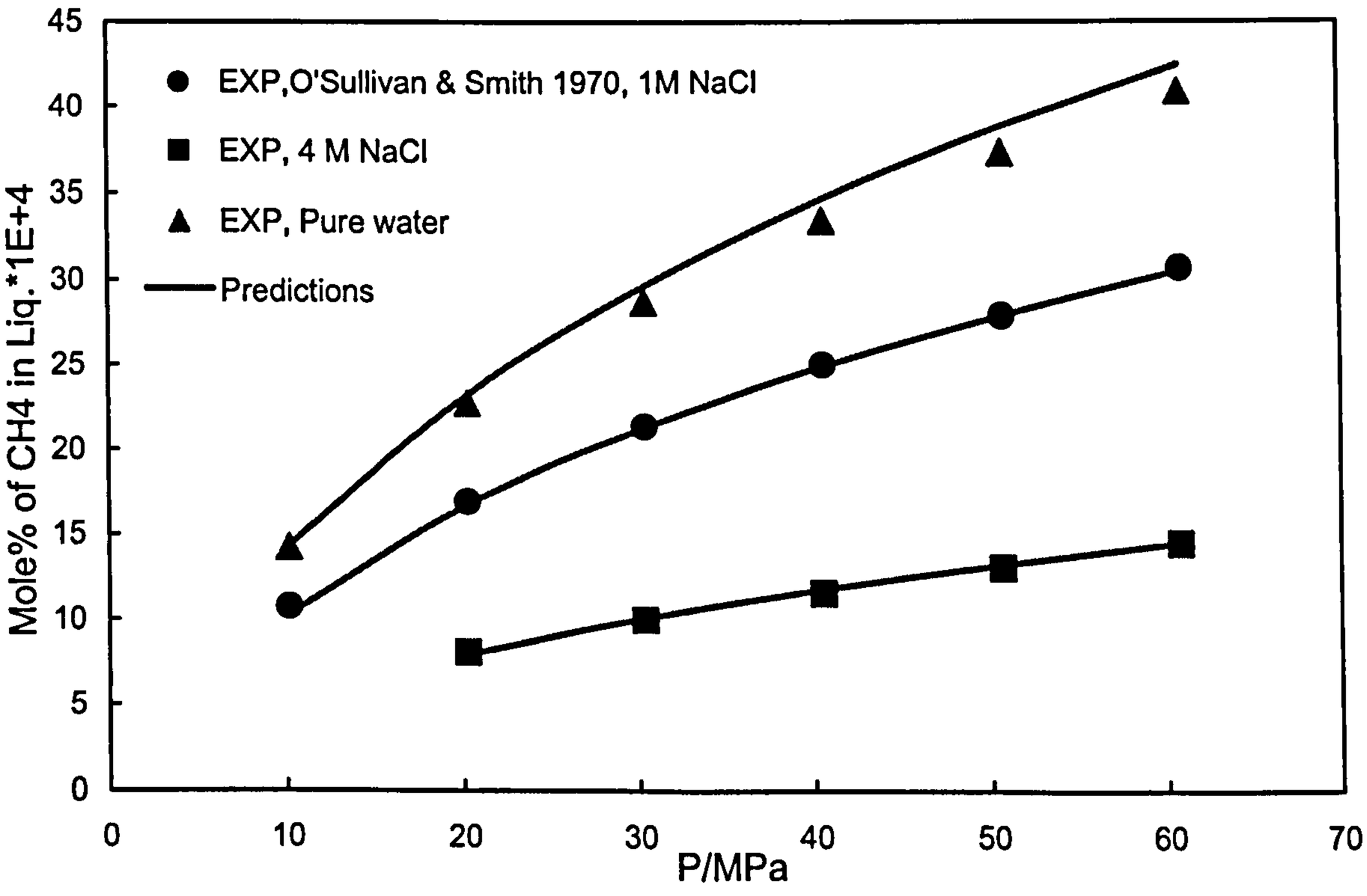

Figure 2.6. Experimental and predicted carbon dioxide solubility in pure water and NaCl aqueous solutions at 423.15 K.

CHAPTER 3

OIL NATURAL HYDRATE INHIBITION IN SUBSEA OPERATION AND MULTIPHASE TRANSPORTATION

3.1 INTRODUCTION

In deepwater exploration and production, long distance tieback multiphase pipelines are becoming a preferred economic option for many fields. Flow assurance is of great importance in these systems, where high pressures, low temperatures, and long residence times of fluids mean the risk of hydrate blockage is very high. The presence of a liquid hydrocarbon phase in water/gas systems may have a great impact on hydrate formation and control remedies deployed. To prevent hydrate blockage, traditional techniques, such as insulation, heating, depressurisation or injection of thermodynamic inhibitors, may be overly expensive or insufficiently effective for long tiebacks. For this reason, new technologies, such as subsea water separation, injection of low dosage hydrate inhibitors (kinetic inhibitors and/or anti-agglomerants), and making use of the natural inhibition effect of oil and formation water, have received considerable attention.

It is known that the formation of water/oil (W/O) emulsions reduces gas hydrate blockage risks. This could be due to the dispersion of water and gas hydrates in the continuous oil phase and/or slower rates of gas hydrate formation. Natural surfactant such as asphaltenes and resins in the oil are commonly identified as the agents responsible for stabilising W/O emulsions. Natural surfactant can be adsorbed on the water/hydrocarbon interface and stabilise emulsions by decreasing the interfacial tension between oil and water. The presence of asphaltenes at this interface can have a great influence on hydrate formation, which takes place at the W/O interface. The presence of an emulsion can influence the quantity and the kinetics of hydrates formed. A few publications dealing with the effect of natural surfactants (present in crudes) on hydrates transportation have been published (Fadnes, 1996, Leporcher et al., 1998,

Camargo et al., 2000, Sinquin et al., 2001) and most of these articles concluded that the presence of W/O emulsion helps the transportation of hydrate "slurry" in the pipeline. Sinquin and co-workers (Sinquin et al., 2001) reported that condensate and paraffinic crude oils show very violent and rapid hydrate formation, while hydrate formation with the asphaltenic oils is delayed and the crystallisation is less rapid. However no direct correlation between the quantity of surfactants in a crude and its ability to transport hydrates has been reported. On the other hand the effect of paraffinic compounds is not clearly demonstrated but is generally presented as an advantage (Leporcher et al., 1998).

Not many articles concerning the kinetic of hydrates formation in the presence of crude oil have been published. Some researchers (Nygaard, 1989, Sinquin et al., 2002) have reported that the hydrocarbon phase delays the hydrates formation, that is to say natural kinetic inhibitor exists in the crudes. On the contrary, Skovborg (Skovborg, 1993) concludes that the presence of crude will accelerate the hydrate formation. In summary, the results published in the literature are few and inconsistent.

This study presents the experimental investigations made on the kinetics of hydrate formation in water-oil-natural gas systems at subsea operating conditions using a kinetic reactor and a new experimental set-up (Glass Micromodel). Two different types of oils were used in the tests. Experiments have been conducted in a kinetic rig to examine the effect of different parameters such as water content, mixing rate, mixing history and pressure on the induction time (the period of time before hydrate formation when the system reaches the stable temperature and pressure conditions inside the hydrate stability region). The effects of water content and pressure on transportability of the system have been investigated under various operating conditions, including flowing, shut-in and restart. The micromodel set up has been used for visualisation of the hydrate formation in water/oil emulsion and the distribution of phases in the system at flowing and static conditions.

3.2 MATERIALS AND EXPERIMENTAL METHODS

In the absence of live oil samples from different fields, two different dead oils and saline water (9.8% NaCl) and a synthetic natural gas were used in the experiments. The compositions of the oils (named as Oil (A), Oil (B)) have been shown in Table 3.1. A BOC standard bottled natural gas was used in the tests. The natural gas composition was given as: C_1 - 86.36%, C_2 - 5.43%, C_3 - 1.49%, C_{4+} - 0.61%, N_2 - 4.99% and CO_2 - 1.12%.

A Hydrate Kinetics Rig was used in this study. Figure 3.1 illustrates the schematic diagram of the rig. It consisted of a jacket vessel (2400 ml, internal diameter of 150 mm), a stirrer with magnetic motor and a glycol circulation system for controlling the temperature in the cell. The pressure capacity of the system is up to 40 MPa. The maximum cooling rate is 15 K/hr. The test fluid is stirred using the magnetic agitator with a paddle type impeller. The rheology of the hydrate slurry is monitored by measuring the power input to the agitator (equivalent to torque on the stirrer shaft). The test cell and stirrer used were made of stainless steel. The rates of hydrate formation/dissociation can be calculated from the pressure reduction rates. The equipment can be used to measure the phase boundary of various hydrocarbon systems, to study the inhibiting effects of different hydrate inhibitors, and to assess the transportability of water-hydrocarbon system under hydrate forming conditions. The relatively large volume of the test cell is an advantage for simulating oil/water/gas multiphase systems under various dynamic/static (shut-in) conditions during various subsea processes.

In the hydrate formation and dissociation experiments, the required amount of oil and water were first loaded into the test cell, and then the natural gas was charged into the cell up to the required pressure. To form hydrates, the system was cooled down to a set temperature (e.g. to 277.15 K) at 15 K/hr and at a specified stirring rate. The system was then left to form hydrates. The pressure, temperature and torque were measured during the process. To measure the hydrate dissociation point, a step-heating (0.5 °C/ 5-10 hrs) was used. The method of step-heating ensures equilibrium at each step, and only equilibrium data is used in determining dissociation conditions. This procedure results in reliable and repeatable measurements (Tohidi et al., 2000).

After dissociation, the system was normally heated up to 298.15-307.15 K for 4-5 hours to remove water history (i.e., the influence of hydrate memory in the water phase) before the next experiment. This was on the basis of previous experiments for successful removal of hydrate memory in the water.

An intermediate pressure (8 MPa) glass micromodel was also used in the tests to visually observe the hydrates formed in oil/water emulsions. The micromodel set-up is shown in Figure 3.2, which consists of an etched glass base-plate topped with a sealed glass cover plate. Geometrically designed networks of pores can be used to construct the glass micromodel by etching with hydrofluoric acid (20-200 mm pore size in width). The cover plate has an inlet and outlet, which allows fluids to be pumped through the enclosed

network of pores. The model is mounted in a vessel that exerts an overburden pressure, and is submersed in a temperature-controlled bath. A magnifying camera is mounted above the model to observe the fluid behaviour inside the micromodel. Video footage can be recorded during the experiments. The pictures presented here are still images digitally captured from video recordings, or directly from the camera.

3.3 KINETIC RIG EXPERIMENTS RESULTS

3.3.1 OIL (A)

The first study targeted the hydrate problems associated with multiphase (oil-water-natural gas) transportation in oil (A). Nine experiments were carried out on the Oil (A)-saline water/water-natural gas system with different water / oil ratios in the kinetic rig to study different parameters affecting natural hydrate inhibition by oil. The results of the tests have been summarised in Table 3.2 (Test No.1-5). The recorded pressure, temperature and torque profiles for Tests No. 1-3a are shown in Figures 3.3 to 3.5. Tests 3b to 3e were series of repeated tests following Test 3a after hydrate dissociation (and holding at 313.15 K under stirring for 4 hours to destroy water hydrate history). In interpreting the pressure profiles in above-mentioned Figures, the first steady pressure reduction was due to the system being cooled down to the temperature set point. After that, the pressure was normally remained constant until a second drop (while temperature was constant) due to hydrate formation. A rise in temperature and torque usually follows hydrate formation. A hydrate induction time (t_i) may be observed as the time lapse after the temperature levelling out at the set point and before hydrate formation (as noticed by pressure drop). The experimental conditions of the tests and the induction times (t_i) are summarised in Table 3.2. The stirrer speed was 400 rpm in all tests, except for test 3e where a stirrer speed of 100 rpm was used.

The hydrate dissociation points for the Oil (A)-saline water-natural gas systems with different water contents were also measured (Tests No. 1, 2 and 3b) to estimate the degrees of subcooling in the systems. By comparing the hydrate formation conditions and dissociation points the degrees of subcooling are around 5.4-7.1 K.

As shown in Figures 3.3-3.6 and Table 3.2, by increasing the water cut the induction time decreases. It is interesting to note that the presence of the oil in water/gas systems has some inhibition effect, which increases the hydrate induction time. In the absence of the oil and at lower pressure range of 3.75 MPa (Table 3.2, Test No.5 and Figure 3.7) no induction time before hydrate formation was observed. The test results show that

the observed induction time is not only dependent on water content, but also being affected by the mixing history (Test No.3a-3d) and the mixing rate (Test 3e) as well. Tests No. 3a to 3d were carried out under a similar mixing rate, while Tests 3b, 3c and 3d went through longer mixing time at high temperatures (313.15 K) for removing the water history. This could change the degree of the water/oil/gas emulsion in the system.

The above kinetic tests indicate that hydrates may form at different water cuts under subsea conditions though the presence of oil may increase the induction time prior to hydrate formation. However, the main concern, in terms of pipeline transportation, is whether it will lead to pipeline blockage. The hydrate-plugging tendency can be evaluated by measuring torque on the stirrer during mixing. The experimental results show that the maximum torque after hydrate formation increases with water content (Figures 3.3 to 3.7). It should be noted that in all the Figures the torque (with an arbitrary unit) has been shown on the pressure axis and in Figures 3.5-3.6 "torque/5" has been drawn with time in order to use the same axis scale for both pressure and torque quantities. In Test No.5, where only water was loaded in the system, a dramatic torque increase was observed, which led to a seize-up of the stirrer (Figure 3.7). In test No.4 (Figure 3.6), where the water cut was 50%, the torque increased from 8 to 35 after massive hydrate formation during cooling, but the stirrer was not blocked. Therefore, as mentioned by other researchers, the presence of oil could reduce the risks of hydrate plugging. It has been reported (Fadnes, 1996, Leporcher et al., 1998) that the presence of a water-oil emulsion helps greatly the transportation of hydrate slurry in the pipeline. For further study on the effect of mixing on the induction time / natural inhibition, four other tests were conducted on the above oil with 30% water cut in the presence of natural gas at testing conditions of 277 K and 7.67 MPa with different rate of mixing (150-500 rpm). In order to eliminate the effect of memory and conditioning in the fluids, each test carried out with a fresh batch of water-oil solution. Before starting each test, the kinetic rig was first washed thoroughly with xylene. Acetone was used for second wash. Then the rig was washed by distilled water and dried.

The pressure profiles of the tests have been presented in Figure 3.8. The observed induction times at various rates of mixing suggest that higher mixing rates leads to better hydrate inhibition in the oil system. The composition of oil is not known, there is also possibility of wax drop out at tests conditions.

It has been reported that shut-in / start up conditions in the pipelines are the worst case in terms of hydrate formation and blockage (Urdahl, et al., 1997, Rasch et al., 2001). To simulate a shut-in situation in subsea operations, the stirrer was switched off. The first test was carried out following Test No.4 (Table 3.2), which was the worst case tested for oil systems, with 50 volume% water. In order to evaluate hydrate blockage after shut-in and during re-start, the stirrer was switched off and the system was kept at hydrate forming conditions for one day. The result showed that the stirrer could be restarted to restore mixing after the shut-in. A second test was carried out to check the hydrate formation during shut-in, which was also using the system described in Test No.4. The pressure, temperature and torque profiles of the test are shown in Figure 3.9. During the experiment, the stirrer was first switched on during cooling starting from 310 K until temperature reached to 279.15 K, then the stirrer was switched off for 20 hours. There were no signs of hydrate formation during the shut-in period. However, the hydrate formed immediately after stirrer was switched on. As shown in Figure 3.9, the system pressure dropped dramatically and the torque registered on the stirrer reached to a value of 35. The tests results show that in oil system tested, although after shut-in period, hydrate forms at restart but it does not block the stirrer and the slurry is transportable.

3.3.2 OIL (B)

For further investigating the above results and the effect of pressure, a series of experiments conducted on another type of oil (B) in the kinetic rig. The first series of tests carried out on the oil (B)-saline water (30 volume %)-natural gas system at different rates of mixing (rpm). The results of the tests in a chronological order have been summarised in Table 3.3 and the pressure, temperature and torque profiles of the tests are shown in Figures 3.10-3.13. The tests carried out at similar conditions (10 MPa and 277.5-279.3 K). The first test (Test No. 1, Figure 3.10) was carried out just after the gas was charged at 294.2 K, then the system was cooled down to a set point of 278.1 K under a stirring rate of 500 rpm without previous shearing and thermal history. A short induction time (0.5 hour) was observed in this test. The following tests (Tests No. 2-4, Figures 311-3.13) were carried out after a hydrate dissociation process at a high temperature (307.15 K) for about 4 hours using the same loading. Therefore, different shearing and thermal histories were imposed on the subsequent tests. Different rates of mixing were applied in Tests No.2-4. It has been noticed that the measured induction time is related to shearing history and thermal history in previous experiments due to an emulsification process between water and oil. The results

suggest that after formation of a stable emulsion (e.g. Test No.2, with 800rpm), the rate of mixing does not have significant effect on the system's induction time before hydrate formation (Tests No.3-4). In this case, approximately 3.5 hours of induction time was observed for a fully mixed (and emulsified) water/oil system.

The effect of pressure on the induction time at different rates of mixing was studied by conducting three tests at high pressure (21 MPa) conditions on the above system (oil (B) -saline water (30 volume %)-natural gas). Table 3.4 lists all the experimental results generated in the high pressure case and the temperature, pressure and torque profiles of the tests are presented in Figures 3.14-3.16. The experiments were carried out at different stirring speeds, but with a similar set point of temperature. At high pressures, hydrates formed straightaway during cooling with no apparent induction time for all the cases. It appeared that the high driving force (ΔP) made the system much more vulnerable to hydrate attack than at medium pressure conditions (Table 3.3, Tests No.1-4) where some induction time was observed before hydrate formation. It should be mentioned that there was a significant torque increase after hydrate formation in both cases; 11-16% torque increase in the medium-pressure case and 22-31% torque increase in the high-pressure case. The lower torques increase after hydrate formation in medium pressure conditions suggests better transportability of the hydrate slurry at those conditions.

To investigate the effect of water content on the induction time before hydrate formation and the transportability of the system after hydrate formation similar tests have been carried out for the oil (B) containing 10% of water as for the case of 30% water content. Three tests conducted at a medium pressure of 7.6 MPa and similar temperature range of 277.3-277.8 K with different rate of mixing 250-500 rpm. The summary of the results is shown in Table 3.5 and the pressure, temperature and torque profiles of the tests are presented in Figures 3.17-3.19. As shown in Table 3.5 by increasing the rate of mixing longer induction times were observed, which were expected from the discussion about the effect of mixing in section 3.3.1. By comparing the induction times (0.5-4 hours) observed in 30% water cut tests (Table 3.3) with those of 10% water cut experiments (9-15 hours, Table 3.5), it can be concluded that the lower the water content the longer the induction times and the better natural inhibition of hydrate by oil. It is worth to note that the torque increase after hydrate formation for the tests with 10% water cut is negligible (3-5%) in comparison with those of tests at

30% water cut (11-16%), denoting the improvement in the system transportability by reducing the water content.

As described before to simulate a shut-in situation, the stirrer was first switched off (before hydrate formation) for a certain period of time (e.g. 1-2 days) while the system was kept at the required pressure and temperature conditions (e.g. 10 MPa, 277.15 K). The pressure and temperature in the system were monitored to check if hydrate could form during the shut-in. The stirrer was then restarted, and the torque was checked for stirrer blockage. Hydrate formation during re-start was also monitored. Three tests were carried out on the 30% and 10% water cut systems at the low and high pressure conditions.

Figure 3.20 shows the shut-in experiment for the 30% water cut case at 9.7 MPa and 275. K. It was observed that there was no hydrate formation during the shut-in (stirrer off) period of 50 hours. Hydrate was formed immediately after restart of stirring (up to 500 rpm), however it did not block the stirrer. Figure 3.21 shows the result at the high pressure (20 MPa) test. The stirrer was switched off before cooling. It was noticed that hydrate formed during cooling, at 277.5 K, before reaching to the 275.2 K set point. Restarts of the stirrer were tried after 45 hours shut-in. But the stirrer was completely blocked. Similar test was performed for the 10% water cut as shown in Figure 3.22, in which the pressure and restart torque profiles are plotted. The set point temperature was 276.15 K for P=20 MPa. It appeared that there was no hydrate formation at high pressure condition during the shut-in period of over 33 hours. Restart of the stirrer could be reassured, with a slightly higher torque required to restart the stirring slowly. The data suggest that for the oils tested, there could be a hydrate problem when water content is 30% during shut-in and restart, while this risk could be reduced significantly with a reduction in the water content (e.g., 10%). The results suggest that for systems similar to above mentioned system, LDHI might be required for field application at water cut higher than 30%.

3.4 MICROMODEL EXPERIMENTS RESULTS

Micromodels have been used extensively in reservoir fluid studies, revealing important visual information on the phase behaviour in porous media (Sohrabi et al., 2000). However, their adoption for use in the study of gas hydrates appears to be an entirely novel approach. Results presented by Tohidi et al. (Tohidi et. al. 2001, Tohidi et. al. 2002) demonstrate the potential micromodels have in this field. In this study a medium-pressure (8.3 MPa) glass micromodel has been used to visually observe hydrate

formation in water in oil systems. (The Micromodel experiments in this section were contributed by Mr. Ali Bashir Biderkab, which is gratefully acknowledged).

In the first test, gas was added to the oil (B) and 30% water at around 7 MPa in the piston vessel connected to the micromodel. The system was left for 24 hours at room temperature to achieve equilibrium. The piston vessel was mixed and connected to the micromodel. The micromodel was flooded with the mixture and cooled down to around 273.15 K. Initially no hydrate formation was observed at static conditions for 24 hours. The outlet valve was opened and closed to initiate flow in the system. Hydrate formation was observed. Figure 3.23 shows formation and re-distribution of gas hydrates in the inlet section of the micromodel. As shown in Figure 3.23(a-d), large hydrate masses developed in this poorly mixed emulsion system. It is interesting to note that the oil phase left after hydrate formation became lighter in colour, while the hydrate masses became darker. This may be due to the adsorption of heavy components of the oil by hydrate crystals during the hydrate formation process. In order to study the effect of low temperature conditions on the heavy components of the oil, an experiment was conducted on the oil (B) alone without water (to eliminate the effect of hydrate formation) at similar conditions to the above test to see if cooling the oil to subzero temperatures can cause any deposition in oil. Figure 3.24 shows the oil in micromodel at 303.15 and 268.35K. As can be seen, by cooling down the system there was no sign of deposition of oil heavy components. This shows that in the system of study hydrate particles caused adsorption / deposition of oil heavy components.

In the next test, the objective was to investigate hydrate formation and crystal growth in stable water-oil emulsions, as well as water droplets and hydrate crystal sizes and their distribution in such systems. A stable water in oil emulsion (30 volume% water and 70 volume % oil) was prepared using a high shear stirrer (10,000 rpm), as shown in Figure 3.25. The sizes of water droplets in oil were around 5-10 micrometer. Natural gas was added to the emulsion at 7 MPa in the piston vessel connected to the micromodel. The system was left for 24 hours at room temperature to achieve equilibrium. The piston vessel was mixed and connected to the micromodel. The micromodel was flooded with the mixture and cooled down to around 273.15 K. The system left for one day and the inlet and outlet valves were opened and closed to induce the hydrate formation, but the hydrates did not form. In order to form hydrate, higher degree of subcooling was needed. Due to the pressure limitation of the existing glass micromodel, the system temperature was reduced to 269.15 K. No hydrate formation was observed at static conditions. A pressure difference was established across the micromodel to initiate

flowing conditions. Gas hydrate formation was observed as shown in Figure 3.26. As can be seen, oil near hydrate crystals looks lighter, potentially due to the adsorption of heavier compounds on gas hydrates. In addition, gas hydrates adopted the shape of water droplet, which became deformed due to fluid flow and hydrate formation. Gas hydrates within the emulsion were transportable, and no hydrate particles agglomeration was observed during the flow conditions.

At this stage the outlet valve was closed in order to investigate hydrates under static conditions. Initially, the gas hydrates were dissociated, most probably due to the introduction of warm fluid to the system. The dissociation of gas hydrates resulted in larger water droplets, as expected. The system was left to achieve equilibrium and hydrate formation was initiated by opening and closing the outlet valve. Figure 3.27 shows hydrate formation after 6 and 24 hours at static conditions. As shown in Figure 3.27, it appears that a layer of hydrates is formed at the oil-water interface, with more water being converted into hydrates with time. Another observation is agglomeration of hydrate particles at static conditions with time, resulting in larger hydrate crystals, which may explain the higher risk of hydrate blockage in the pipelines at shut-in conditions compared to flowing conditions.

3.5. SUMMARY AND CONCLUSIONS

A series of experiments conducted on two different types of oil at subsea pipeline conditions using a kinetic rig and a glass micromodel set-up to investigate the parameters involving in natural inhibition of gas hydrates in oil-water-natural gas systems at flowing (mixing) and shut-in/restart conditions. The kinetic rig was used to evaluate the oil natural hydrate inhibition by measuring the induction time before hydrate formation. The torque measurement on stirring was used to assess the transportability of hydrate slurry and the risk of hydrate blockage in the pipeline.

Several important features of the hydrate forming process relating to multiphase transportation under subsea conditions were identified. From the results of the tests it was found that the presence of a crude oil phase in water/gas system could increase the induction time for hydrate formation. Formation of water in oil emulsion could play an important role in natural hydrate inhibition and the transportability of hydrocarbon systems. This can be attributed to the dispersion effect of oil on hydrate particles formed in flowing conditions, which may prevent the formation of massive hydrate blocks and stop hydrate sticking on the wall. The induction time in oil systems appears

be a function of oil properties, mixing rate and mixing history, water content, and operational conditions (e.g. pressure).

For separate batches of oil/water/gas system tested, the induction time was increased with mixing rate. However it was observed that after formation of a stable emulsion in a batch, mixed at high rpm, the effect of rate of mixing on induction time was not significant.

In the tests at flow conditions, reduction of water content lead to extension of induction time before hydrate formation and improvement of transportability (reduction in measured torques) of the hydrate slurry. In shut-in restart cases, reduction of water cut prevented hydrate blockage even at high pressure conditions. The results showed that water content in a black oil system is the most important factor in terms of hydrate risks. For instance, 30% water in the oil (B) system tested, will pose a serious hydrate problem: hydrates will form when pressure is over 19 MPa either in flowing or in shut-in conditions, leading to high pumping pressure and possible blockage. At low pressure conditions (<8 MPa), hydrates will also form with a limited induction time (a few hours), but in the pipeline it is expected that high pumping pressure will be required to keep the flow and restart the flow after shut-in. Pipeline blockage could not be ruled out. The test with 10% water cut has shown some positive aspects to reduce the hydrate problems both at low and high pressure conditions. It is anticipated that hydrate might form even when the water cut is less than 10%, but it would not cause any serious problem in terms of pumping pressure and pipeline blockage. The results of the experiments in this study are inline with the results of the tests conducted by SINTEF/BP in a wheel flow loop (Vebenstad et al., 2005). In that study the hydrate plugging potential of a Golf of Mexico oil (King oil) was assessed at different water cuts and it was shown that at 5% and 10% water cuts there was a non-plugging hydrate slurries.

The micromodel set up was utilised to study the hydrate formation in water/oil emulsion and the distribution of phases in the system. The micromodel tests have shown that different shapes and sizes of hydrate particles can form in the water/oil emulsions, which can be a good indication to check the hydrate morphology if it poses risks for pipeline blockage. The micromodel tests provided a unique insight to the mechanism of hydrate formation and the morphology of hydrates formed in water/oil emulsions. The initial results showed that gas hydrates remove some heavier components from oil systems as indicated by light colour oil around hydrate particles.

This could be due to adsorption of heavier/darker compounds to the surface of hydrates. The results showed that hydrate particles at static conditions change shape and size (as a result of agglomeration) with time, which to some extent confirms the results obtained from the kinetic rig tests (where long shut-in times resulted in stirrer blockage).

3.6 TABLES

Table 3.1 Composition of the dead oils used in the experiments.

Composition of the Dead Oils / Mol%		
	Oil (A)	Oil (B)
i-C_4	0.27	0.19
n-C_4	0.64	0.84
i-C_5	3.41	0.92
n-C_5	4.71	1.62
C_6	5.94	3.51
C_7	8.59	5.96
C_8	10.01	7.02
C_9	6.97	5.89
C_{10}+	59.47	74.06

Table 3.2 Experimental conditions and results of the experiments on the oil (A)-saline water / water-natural gas systems in the kinetic rig. Test No.6-9 were conducted with separate batches of oil and water.

Test No.	NaCl mass%	Water cut	P&T at hydrate formation MPa/K	Induction time, t_i/hrs	Mixing Rate/rpm	Diss. Points P/T, MPa/K
1	9.8	10	7.83 / 277.01	5.2	400	8.12/283.75
2	9.8	20	7.52 / 277.75	2.0	400	7.71/283.15
3a	9.8	30	7.54 / 273.85	1.5	400	
3b	9.8	30	7.50 / 277.01	7.5	400	7.85/284.15
3c	9.8	30	7.50 / 273.97	3.2	400	
3d	9.8	30	7.48 / 273.93	5.2	400	
3e	9.8	30	7.47 / 273.71	2.2	100	
4	0	50	8.10 / 282.65	0	400	
5	0	100	3.75 / 283.15	0	400	
6	0	30	7.75 / 277	1.5	150	
7	0	30	7.75 / 277	2	200	
8	0	30	7.75 / 277	3	300	
9	0	30	7.75 / 277	6.5	500	

* *Stirrer was set at 100 rpm in this test. The stirrer was set at 400 rpm for all other tests.*

** *Volume of water to total volume of oil and water at room T&P.*

\+ *No oil in the system (only natural gas and water).*

Table 3.3 Experimental conditions and results of the tests on the oil (B)-saline water (30 volume%)-natural gas system in the kinetic rig with different mixing rate at medium pressure conditions.

Test	RPM	NaCl	Testing Conditions	Induction
No.		mass%	T/K & P/MPa	Time / hrs
1	500	9.8	278.1 / 10	0.5
2	800	9.8	279.3 / 10.1	3.5
3	250	9.8	277.5 / 10	4

4	550	9.8	278.1 / 10	4

Table 3.4 Experimental conditions and results of the tests on the oil (B)-saline water (30 volume%)-natural gas system in the kinetic rig with different mixing rates at high pressure conditions.

Test	RPM	NaCl	Testing Conditions	Induction
order		mass%	T/K & P/MPa	Time / hrs
1	600	9.8	280.1 / 21.4	0
2	200	9.8	277.4 / 21.0	0
3	750	9.8	279.2 / 21.3	0

Table 3.5 Experimental conditions and results of the tests on the oil (B)-saline water (10 volume%)-natural gas system in the kinetic rig with different mixing rate at medium pressure conditions.

Test	RPM	NaCl	Testing Conditions	Induction
No.		mass%	T/K & P/MPa	Time / hrs
1	250	9.8	277.3 / 7.6	10
2	400	9.8	277.4 / 7.6	9
3	500	9.8	277.8 / 7.6	15

3.7 FIGURES

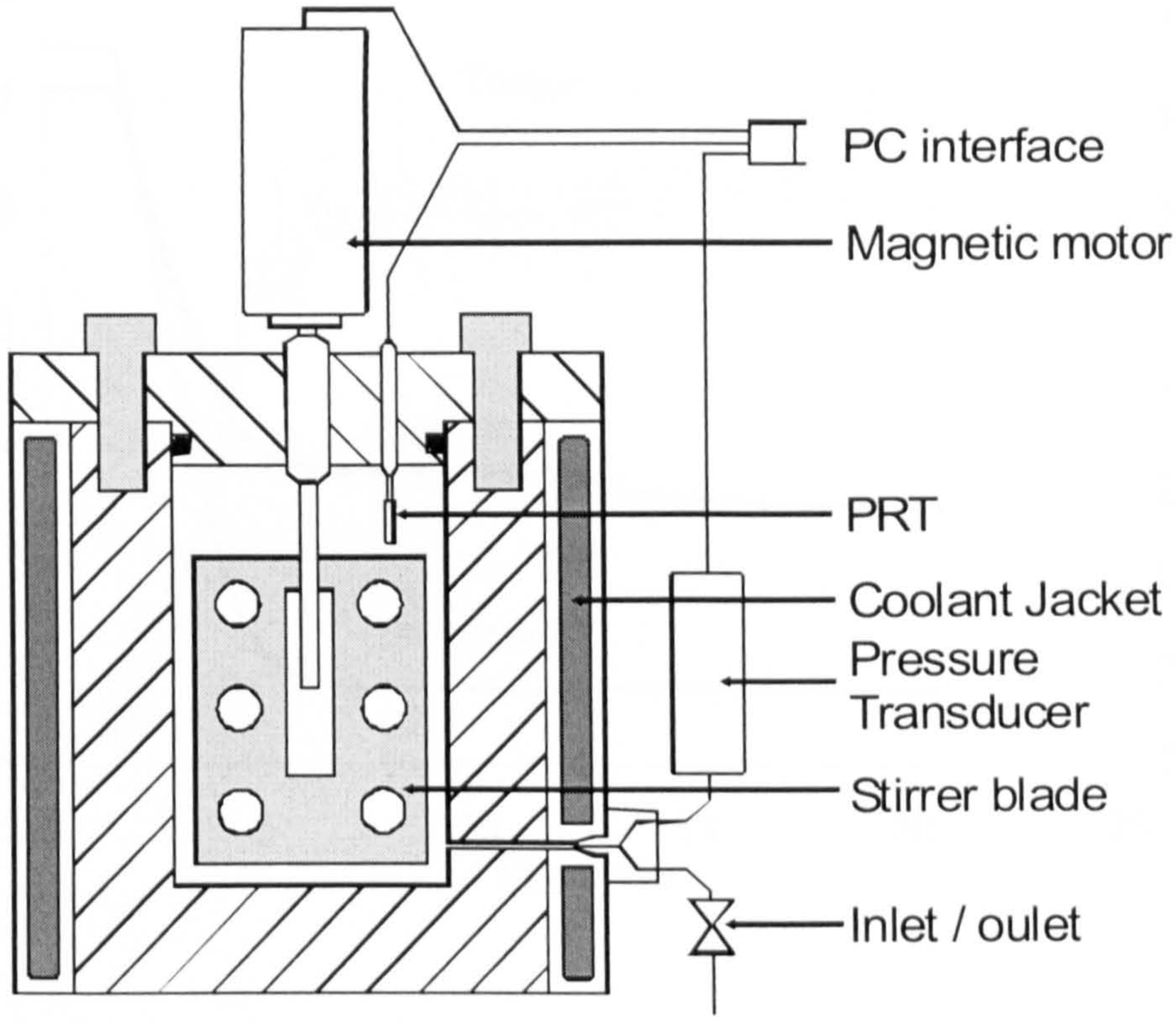

Figure 3.1 Schematic Diagram of the Hydrate Kinetic Rig.

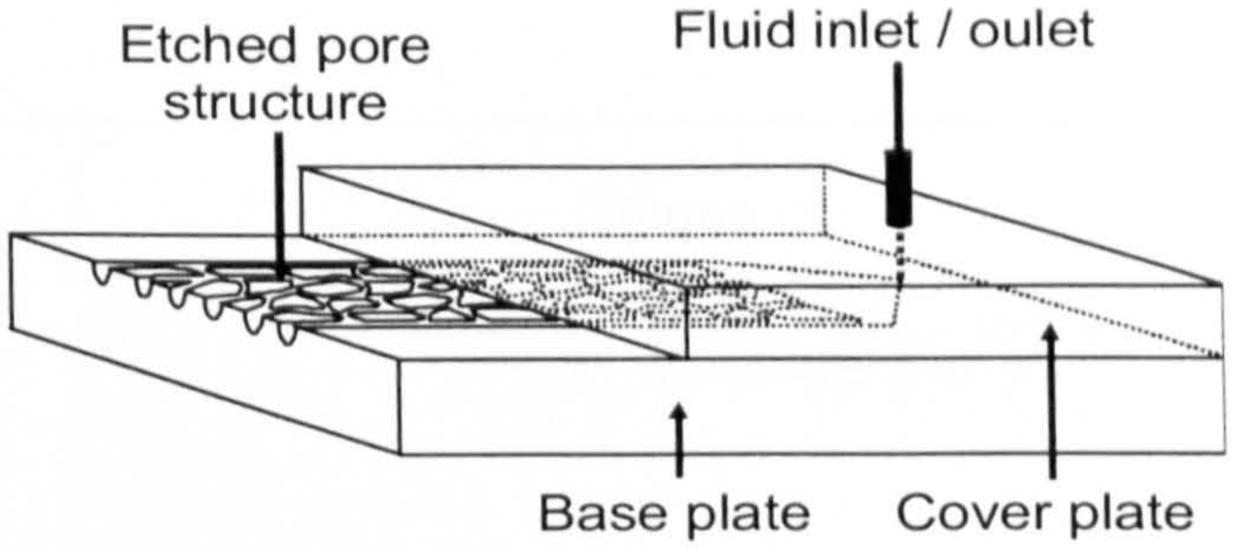

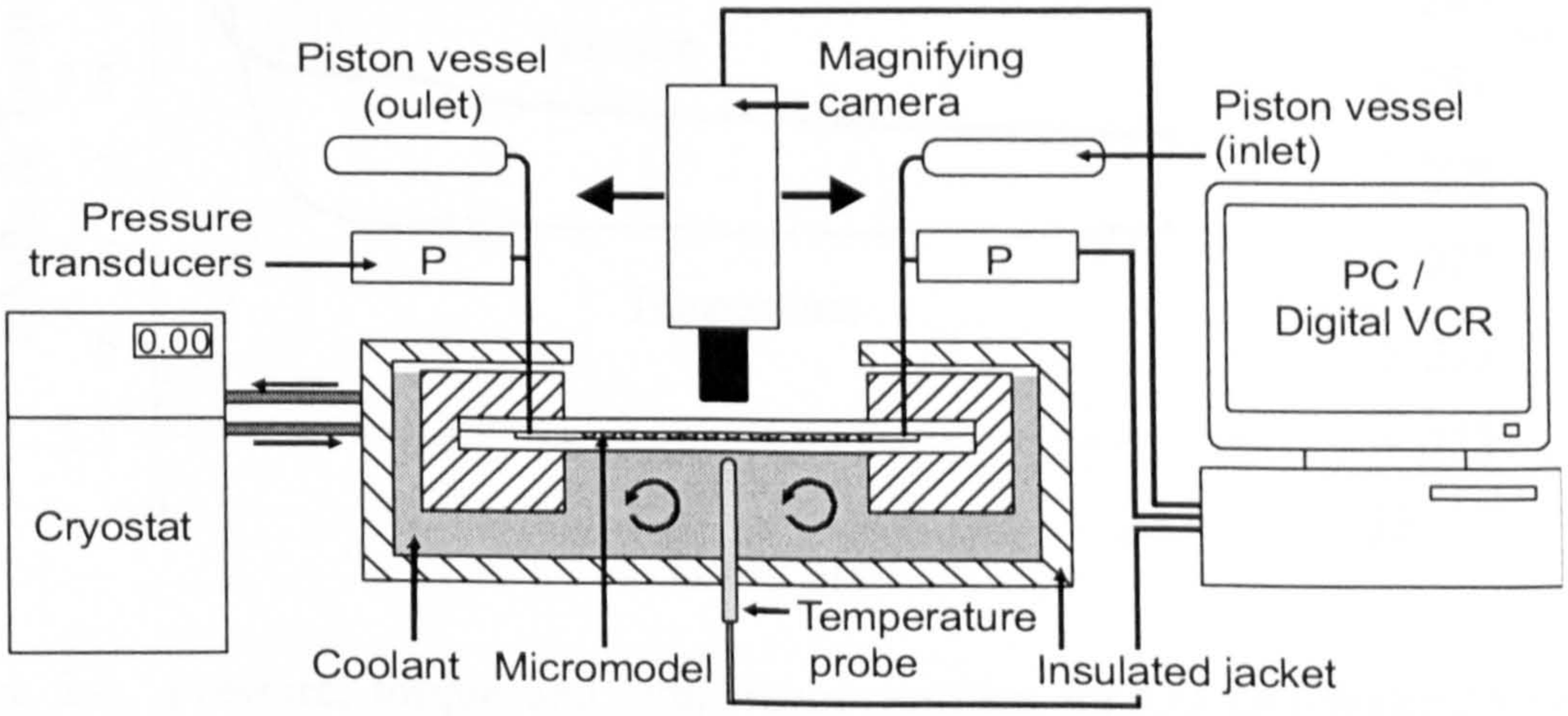

Figure 3.2 Schematic illustration of the micromodel experimental set-up.

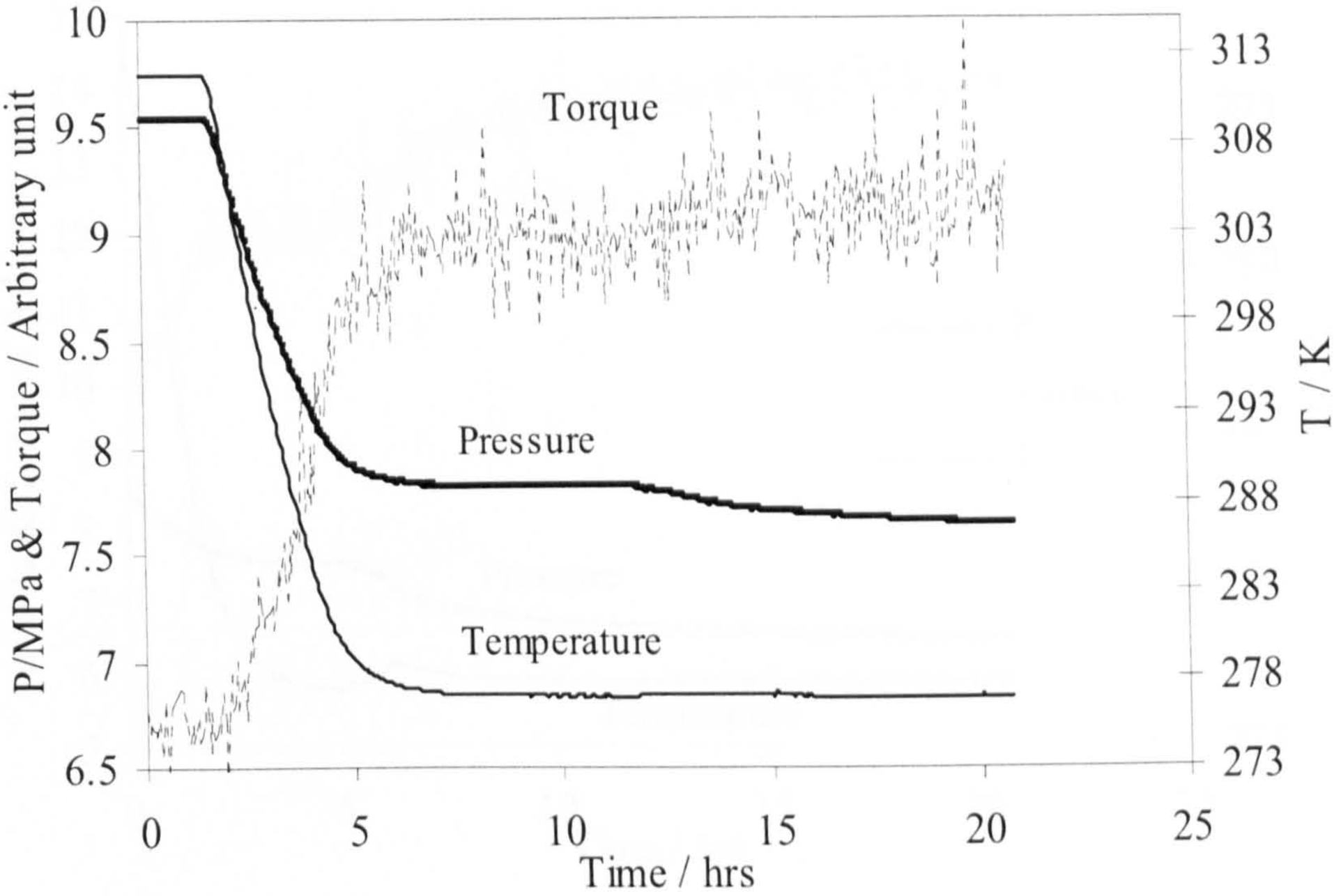

Figure 3.3 Pressure, torque and temperature profiles for Oil (A)-Water (10 vol%)-Natural gas system. After cooling down the system, 5.2 hours induction time was observed before hydrate formation. The formation of hydrates has resulted in a decrease in pressure and an increase in the measured torque.

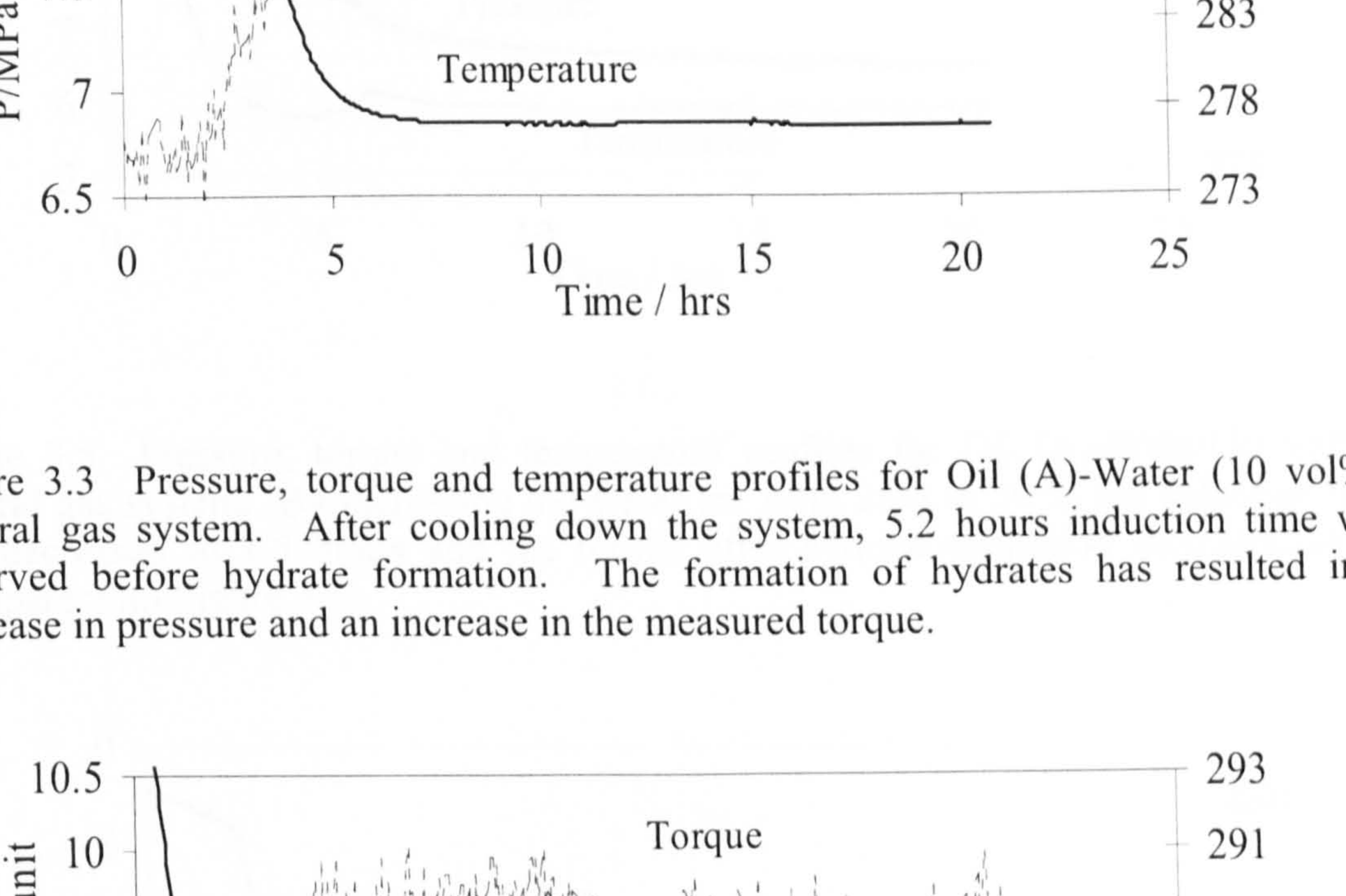

Figure 3.4 Pressure, torque and temperature profiles for Oil (A)-Water(20 vol%)-Natural gas system. By increasing the water cut from 10% to 20 % the induction time decreased to 2 hours and the torque after hydrate formation increased to 9.5 (compare with Figure 3.3).

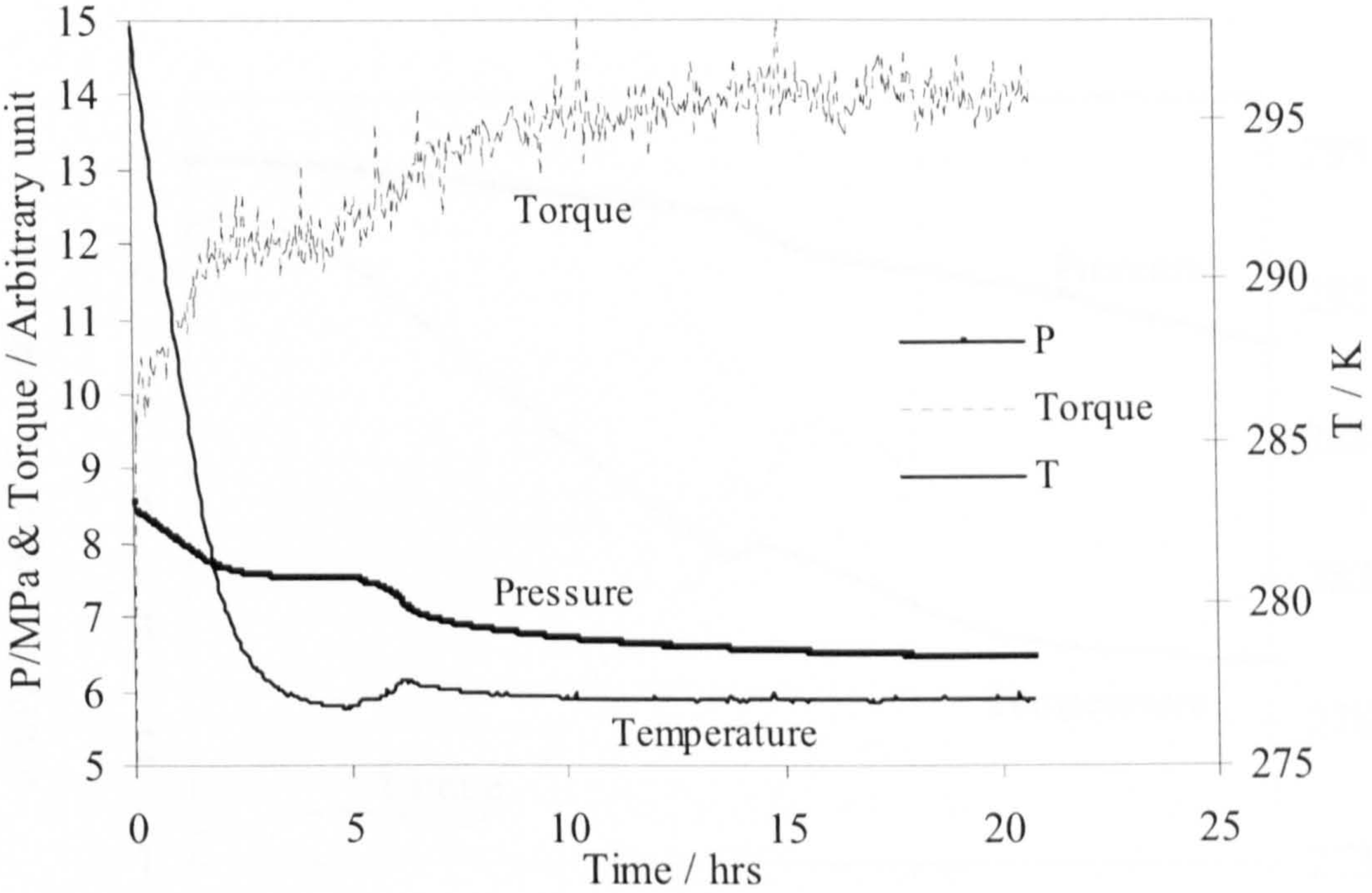

Figure 3.5 Pressure, torque and temperature profiles for Oil (A)-Water(30 vol%)-Natural gas system. By increasing the water cut from 20% to 30 % the induction time was decreased to 1.5 hours and the torque after hydrate formation increased to 14 (compare with Figure 3.4).

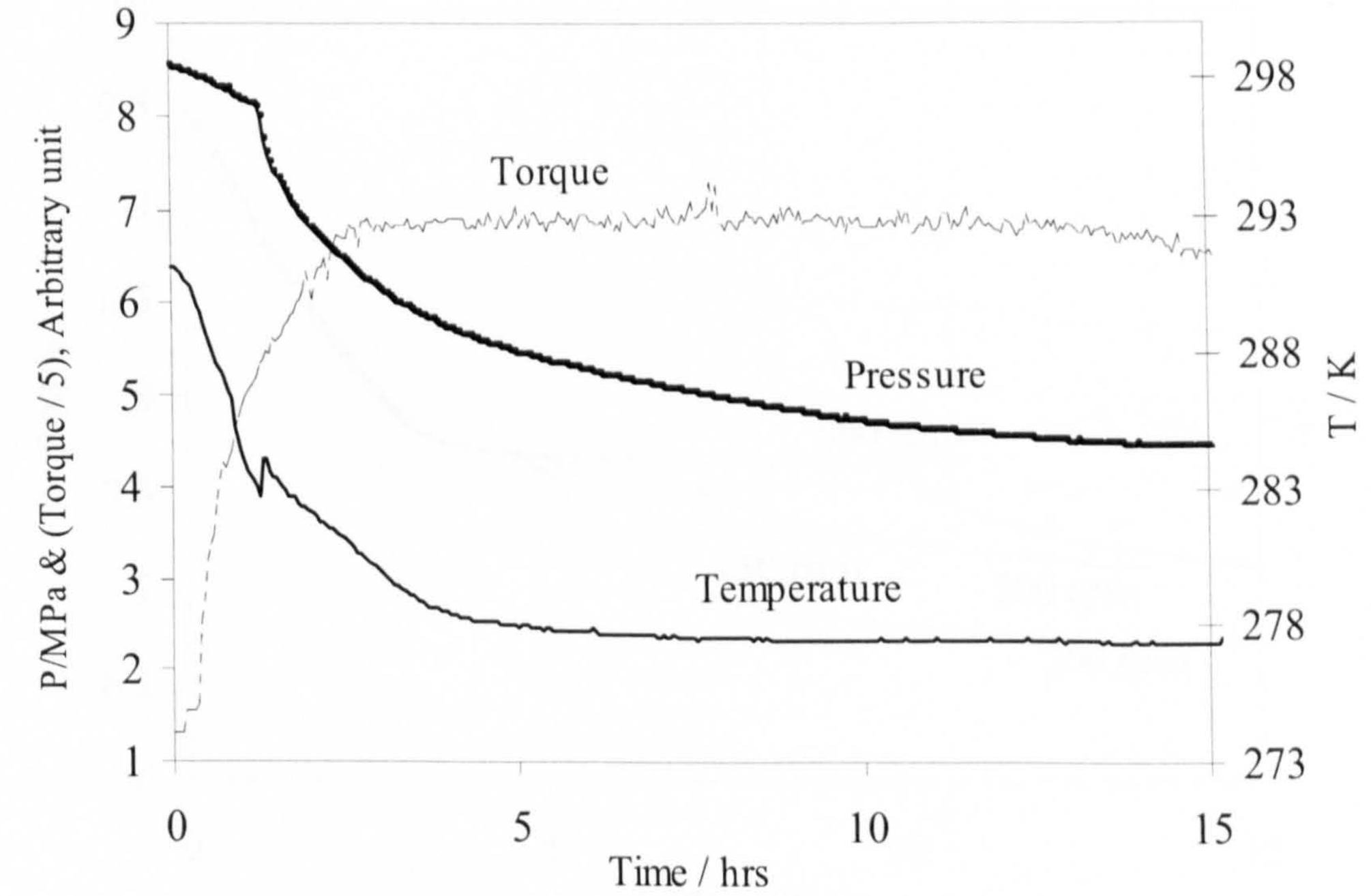

Figure 3.6 Pressure, torque and temperature profiles for Oil (A)-Water (50 vol%)-Natural gas system. By increasing the water cut from 30% to 50 % no induction time was observe before hydrate formation and the torque after hydrate formation increased to 35 (compare with Figure 3.5).

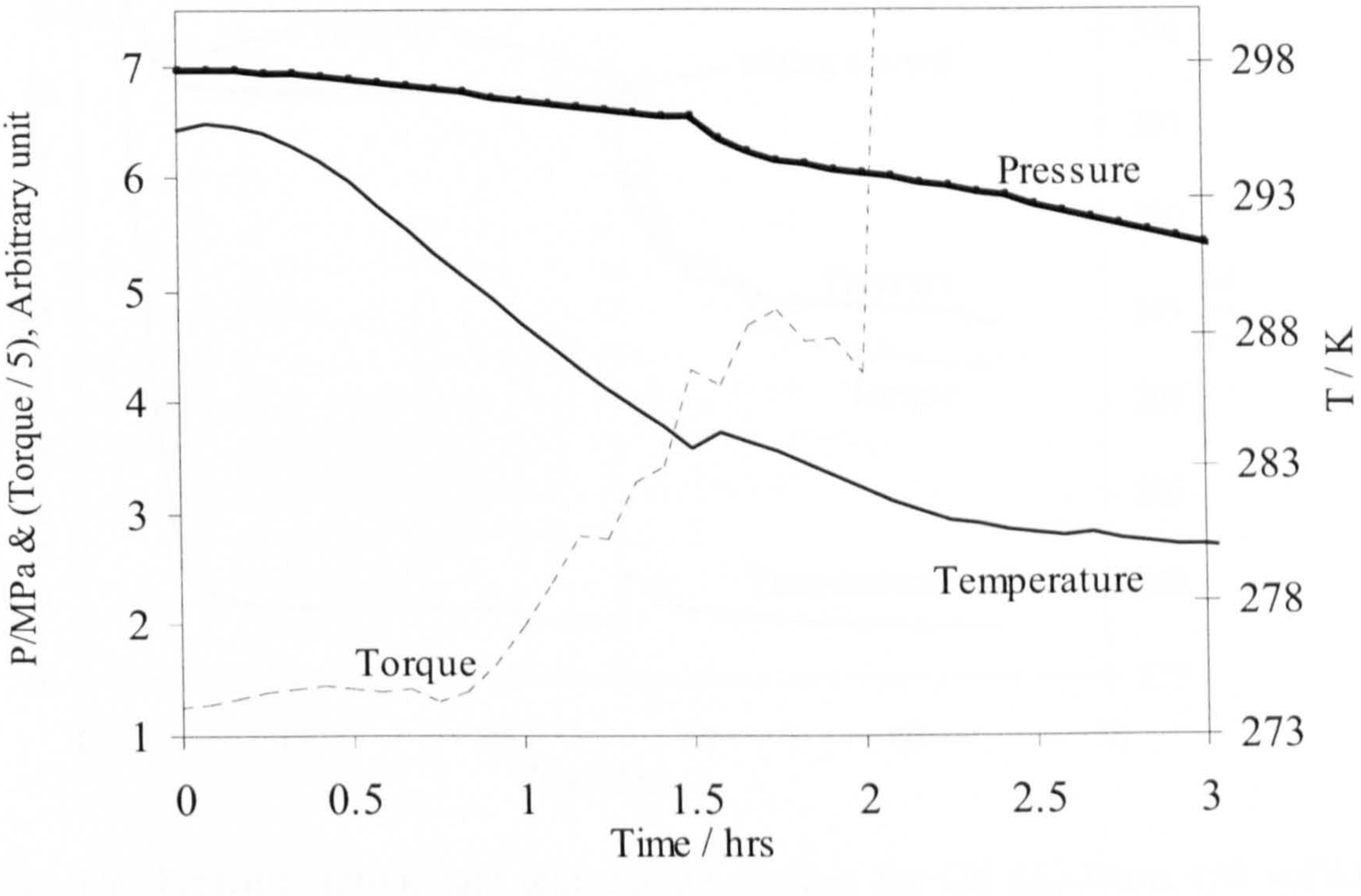

Figure 3.7 Pressure, torque and temperature profiles for Water -Natural gas system. The stirrer was blocked as a result of hydrate formation. In the absence of oil phase no induction time before hydrate formation was observed.

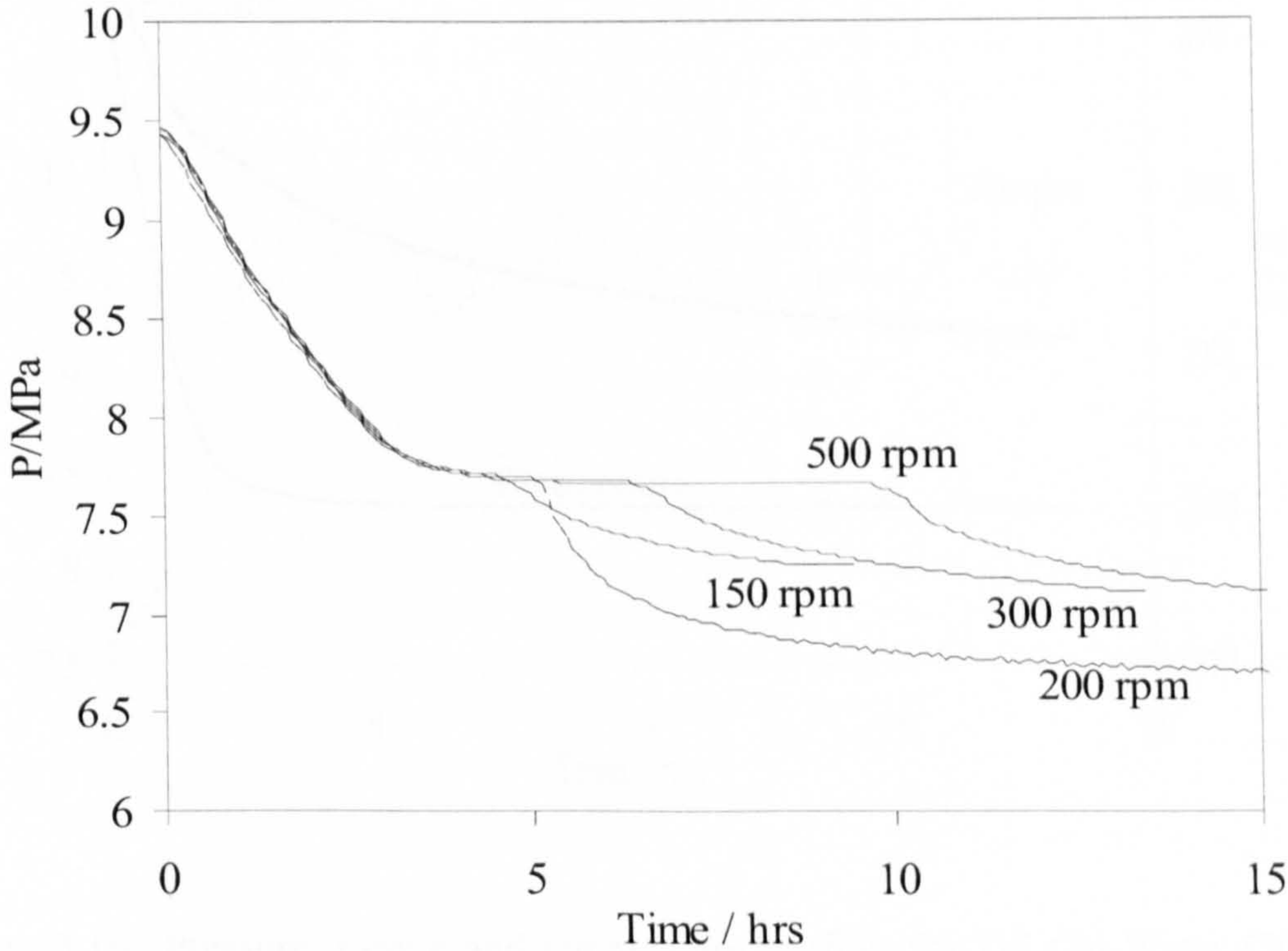

Figure 3.8 Measured pressure profiles for different batches of oil (A) and water (30 volume%) at set point temperature of 277 K and various rpms. The observed induction times at various rates of mixing suggest that higher mixing rates leads to better hydrate inhibition in the oil system.

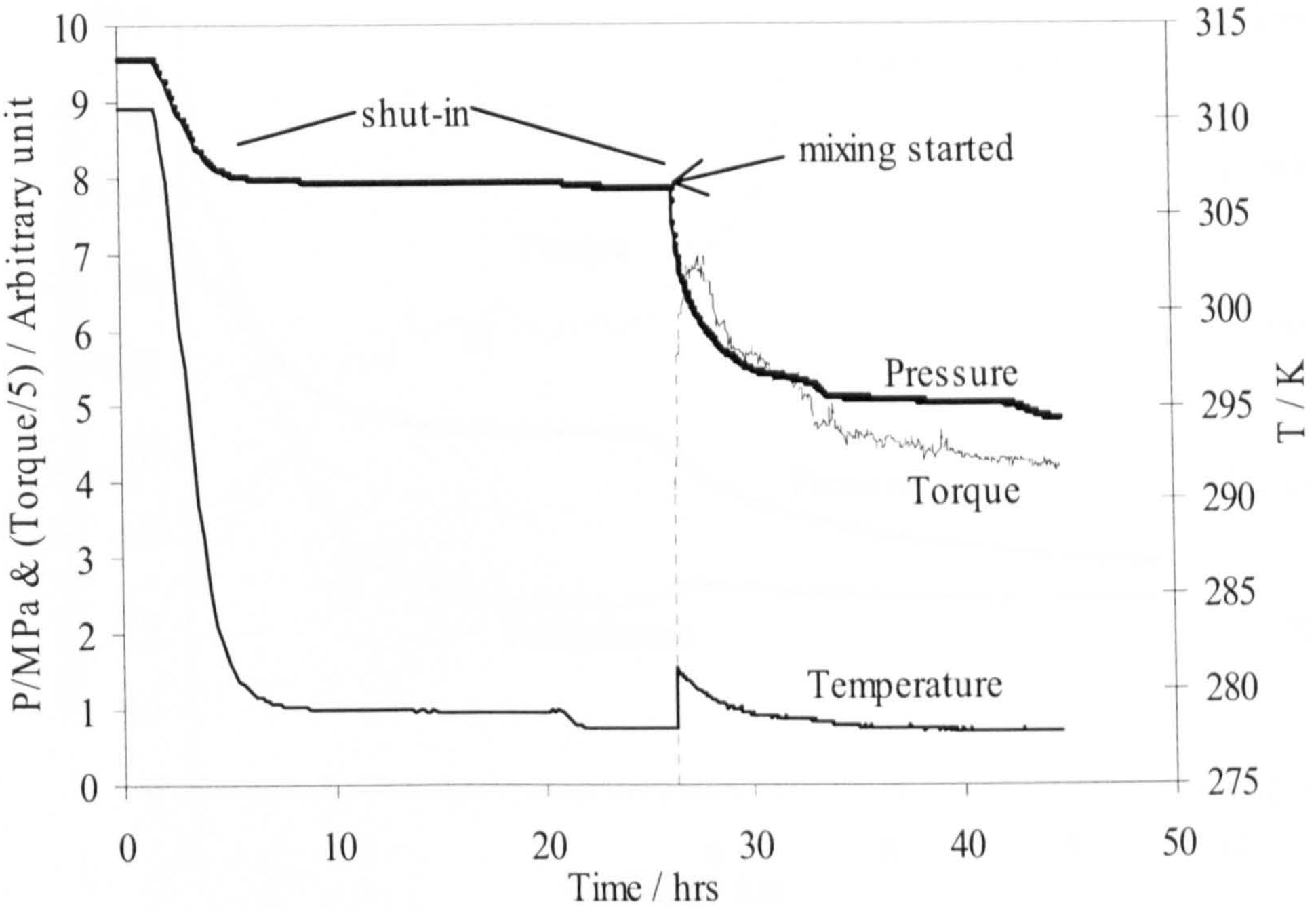

Figure 3.9 Pressure, torque and temperature profiles for Oil (A)-Water (50 vol%)-Natural gas system. Stirrer was switched off from time 0 to 26 hours. Hydrates formed immediately after switching on the stirrer, but the stirrer was not blocked by hydrates.

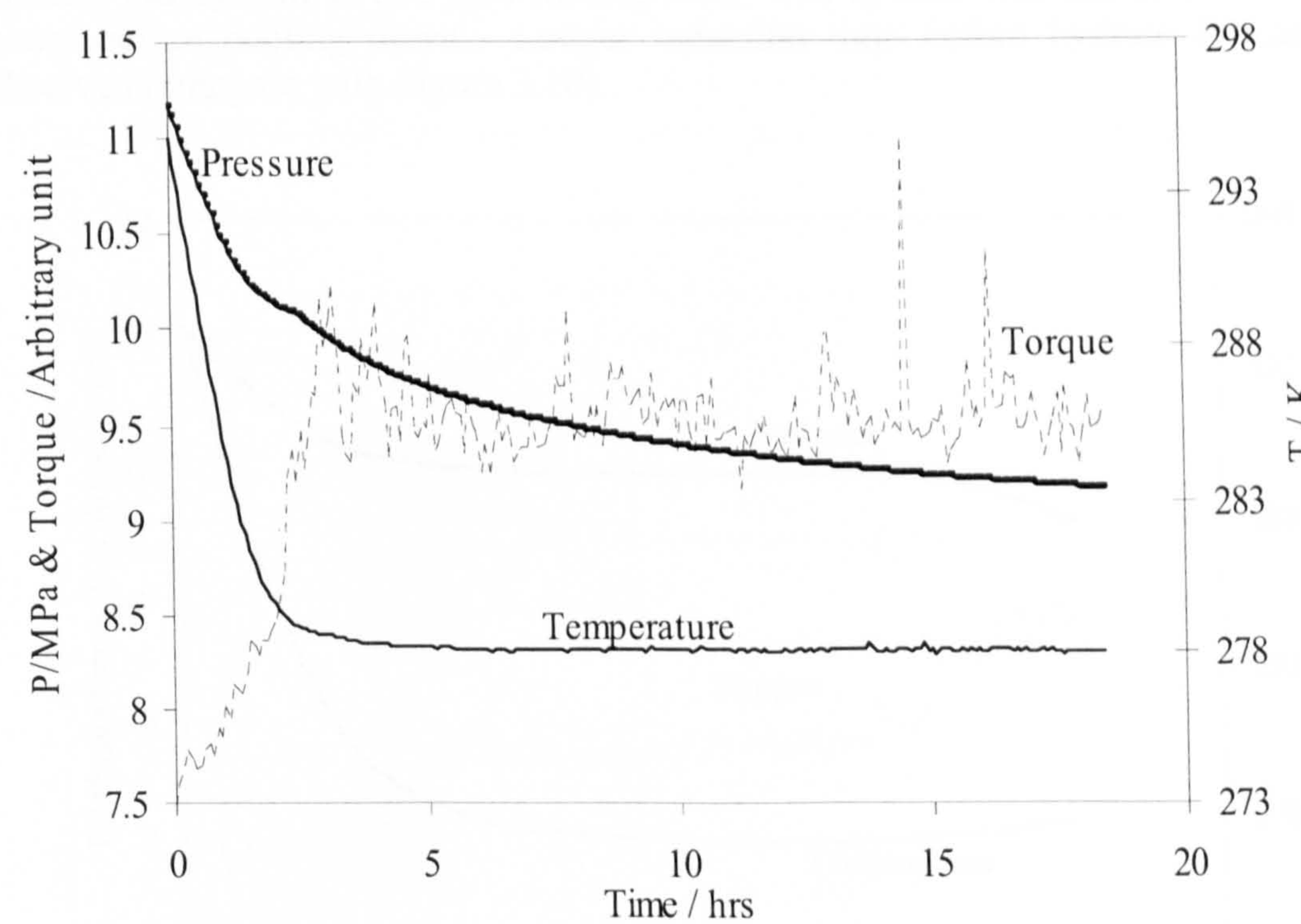

Figure 3.10 Pressure, torque and temperature profiles for Oil (B)-Water (30 vol%)-Natural gas system at 500 rpm mixing rate. Short induction time was observed before hydrate formation in the system without previous shearing and thermal history.

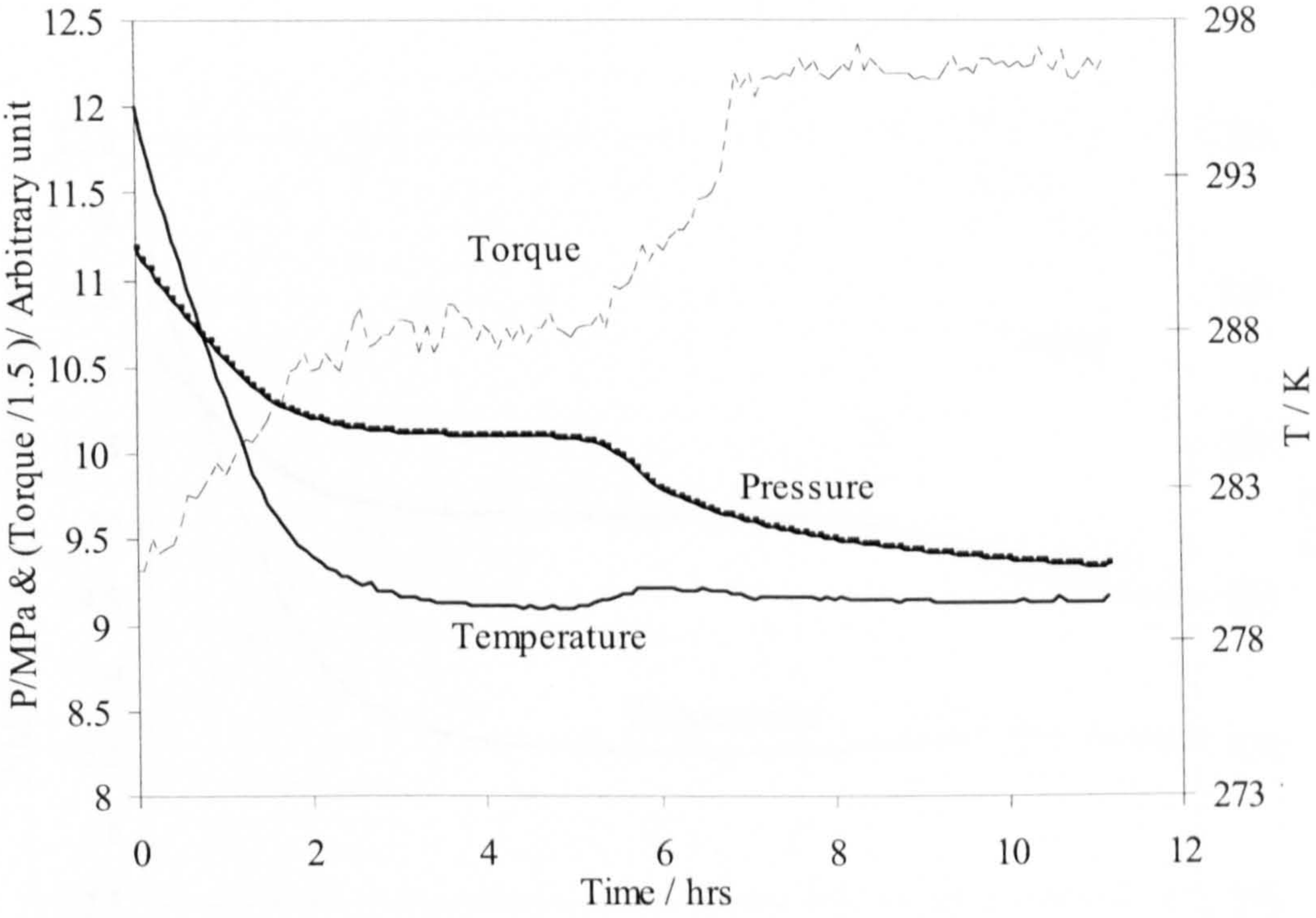

Figure 3.11 Pressure, torque and temperature profiles for Oil (B)-Water (30 vol%)-Natural gas system at 800 rpm mixing rate. The system was left at 307.15 K for 4 hours before cooling down. Longer induction time before hydrate formation was observed (compare with Figure 3.10).

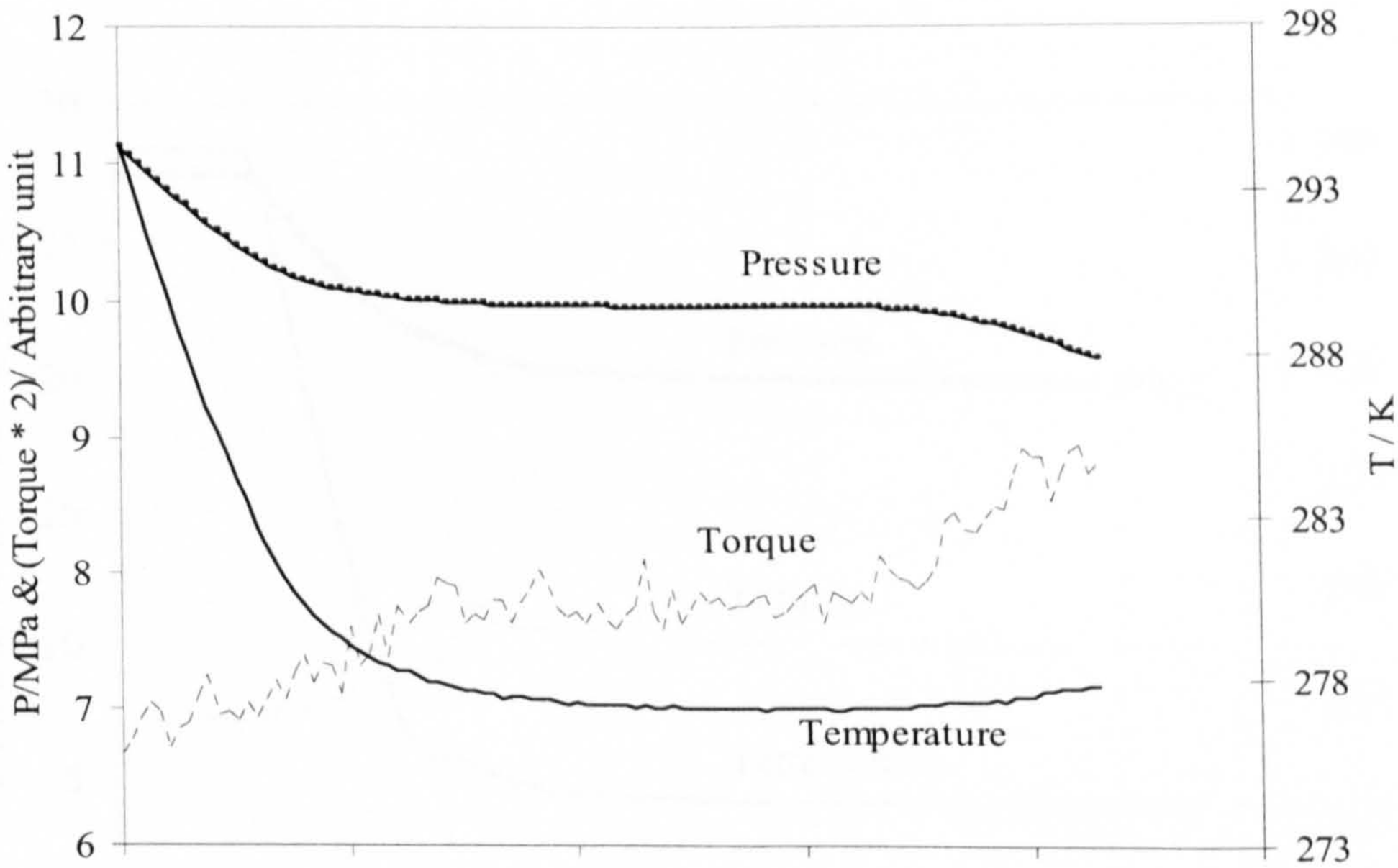

Figure 3.12 Pressure, torque and temperature profiles for Oil (B)-Water (30 vol%)-Natural gas system at 250 rpm mixing rate. The system was left at 307.15 K for 4 hours before cooling down. After formation of a stable emulsion (e.g. Figure 3.11, with 800rpm), the rate of mixing does not have significant effect on the system's induction time.

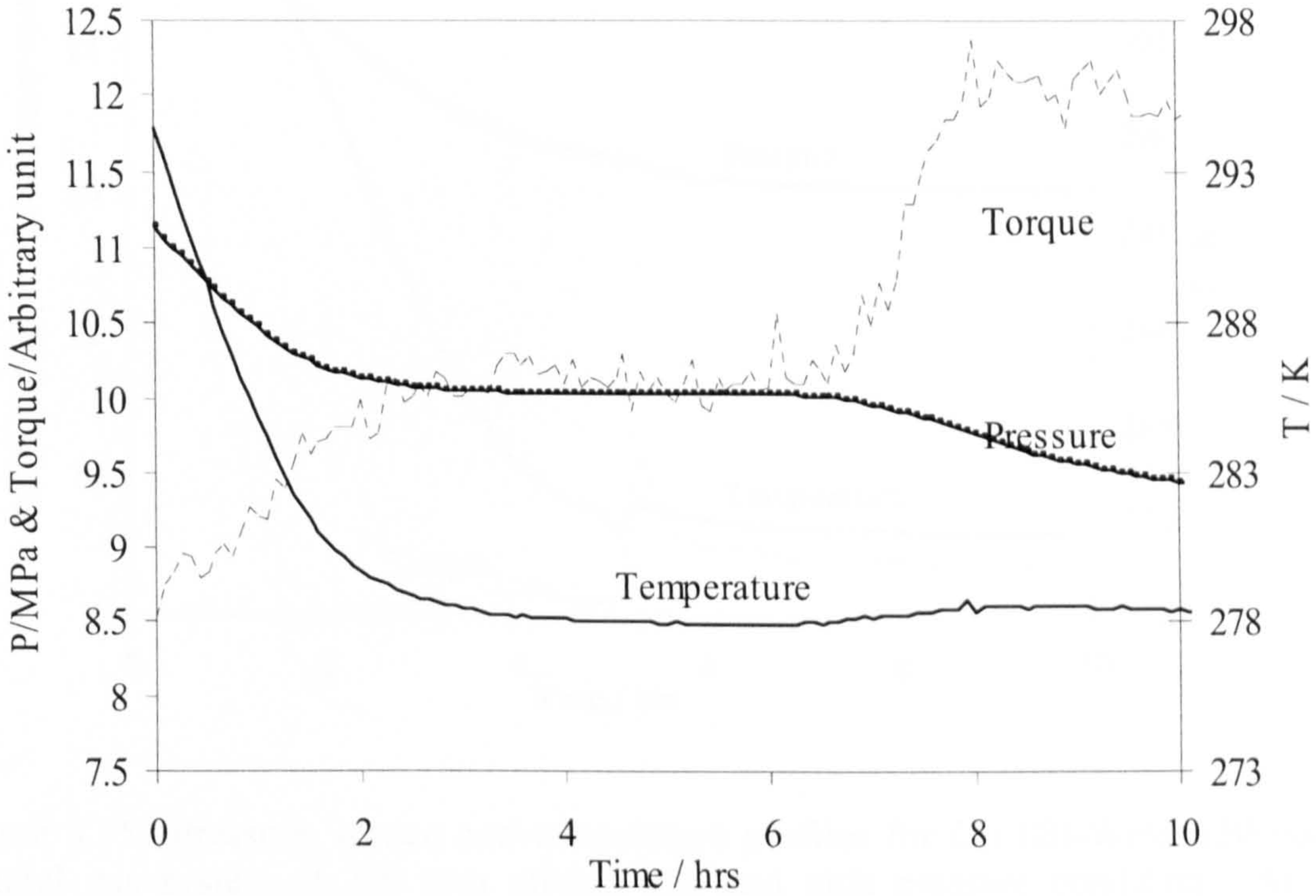

Figure 3.13 Pressure, torque and temperature profiles for Oil (B)-Water (30 vol%)-Natural gas system at 550 rpm mixing rate. The system was left at 307.15 K for 4 hours before cooling down. After formation of a stable emulsion (e.g. Figure 3.11, with 800rpm), the rate of mixing does not have significant effect on the system's induction time.

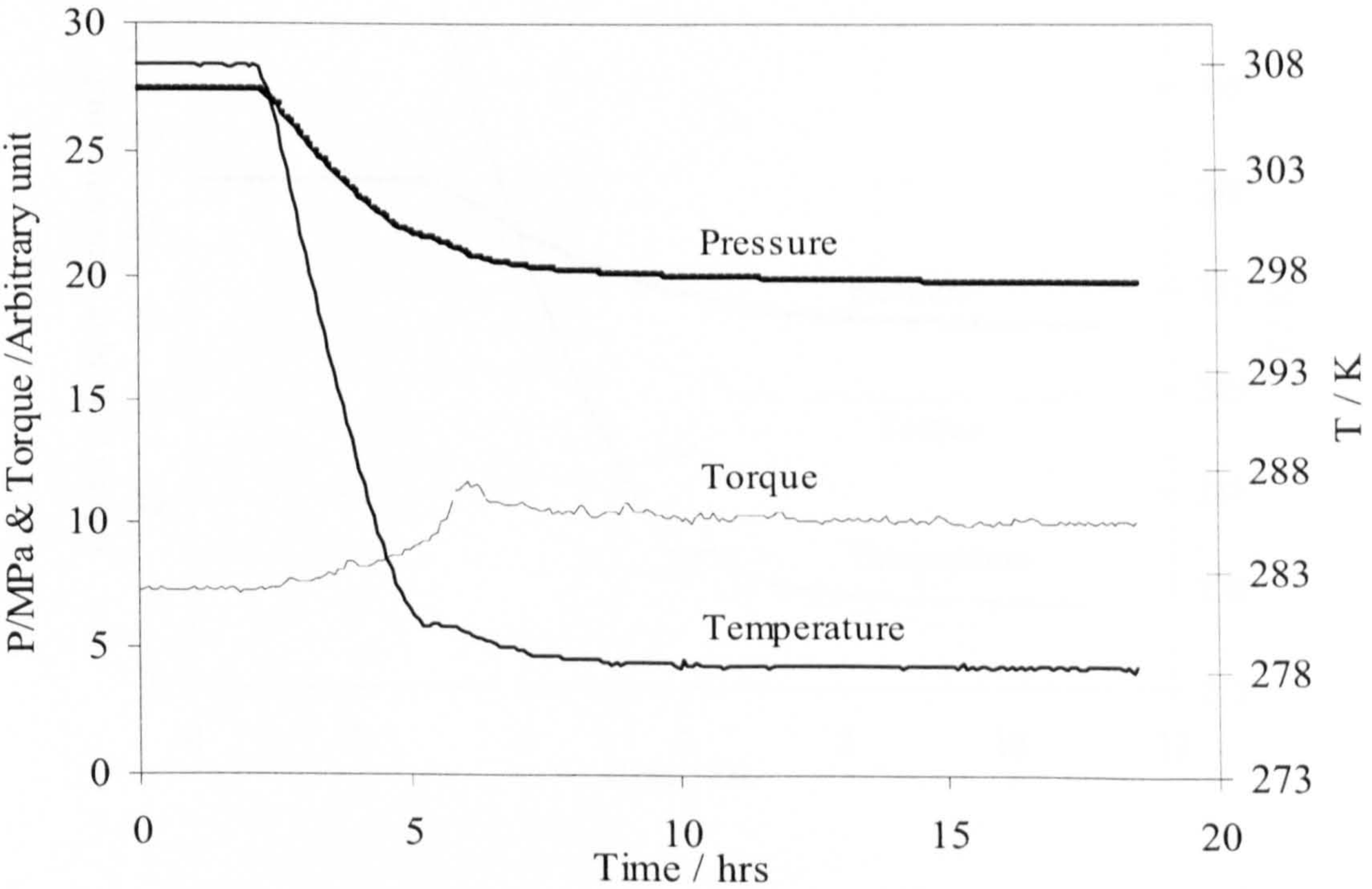

Figure 3.14 Pressure, torque and temperature profiles for Oil (B)-Water (30 vol%)-Natural gas system at 600 rpm mixing rate and high pressure condition. At high pressure conditions, no induction time before hydrate formation was observed.

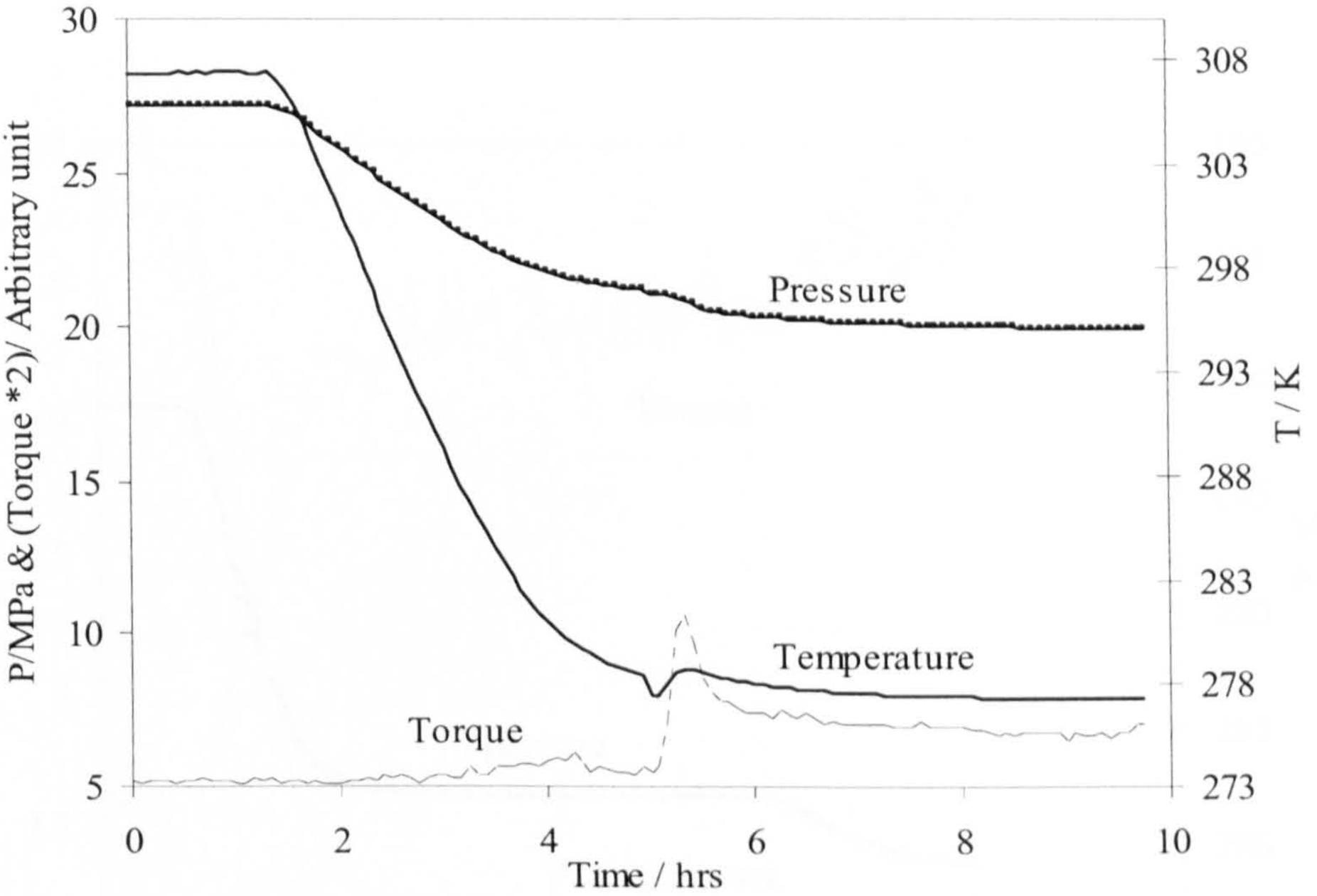

Figure 3.15 Pressure, torque and temperature profiles for Oil (B)-Water (30 vol%)-Natural gas system at 200 rpm mixing rate and high pressure condition. At high pressure conditions, no induction time before hydrate formation was observed at different rates of mixing.

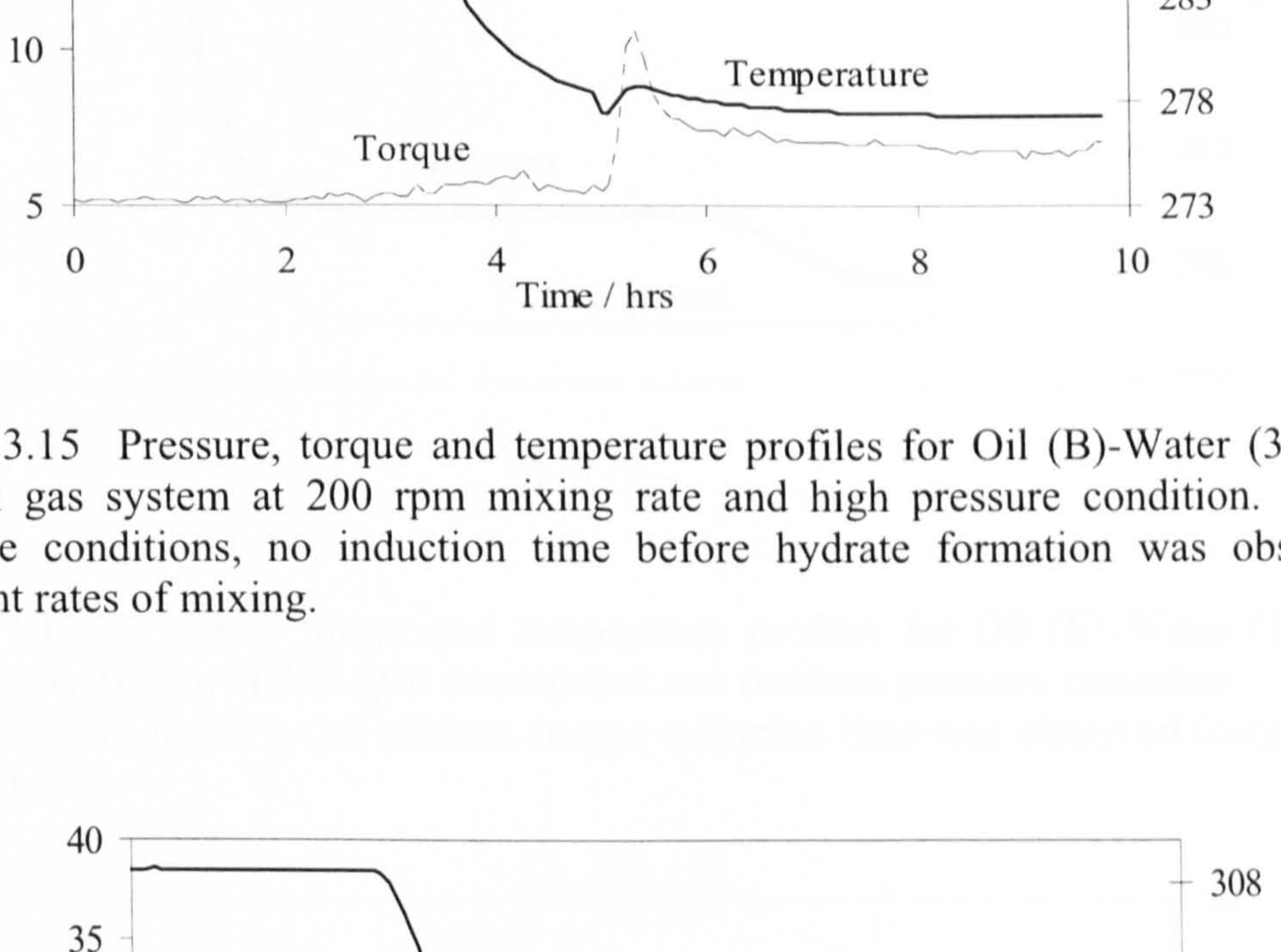

Figure 3.16 Pressure, torque and temperature profiles for Oil (B)-Water (30 vol%)-Natural gas system at 750 rpm mixing rate and high pressure condition. At high pressure conditions, no induction time before hydrate formation was observed at different rates of mixing.

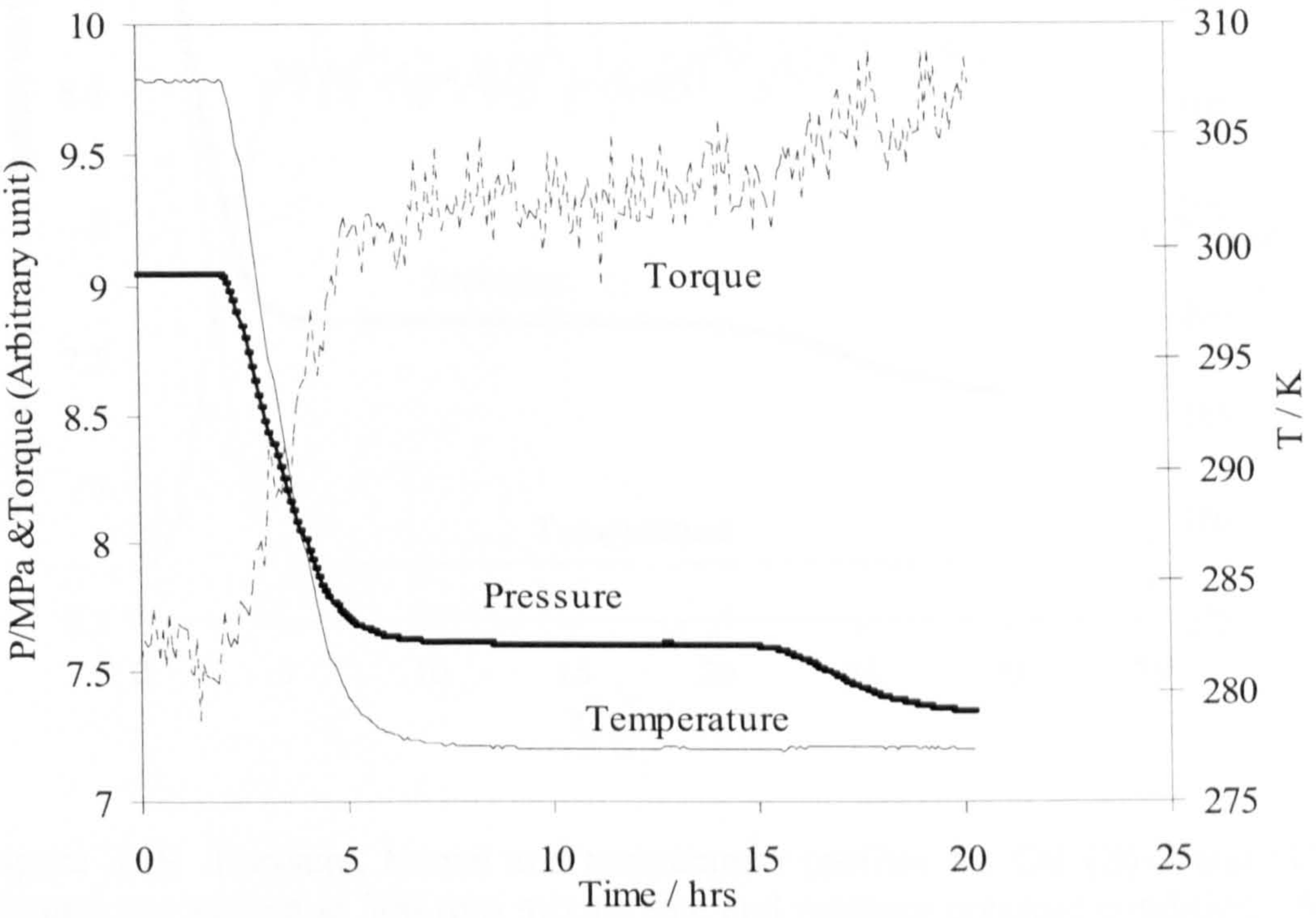

Figure 3.17 Pressure, torque and temperature profiles for Oil (B)-Water (10 vol%)-Natural gas system at 250 rpm mixing rate and medium pressure condition. At similar conditions and lower water content, longer induction time was observed (compare with Figure 3.12).

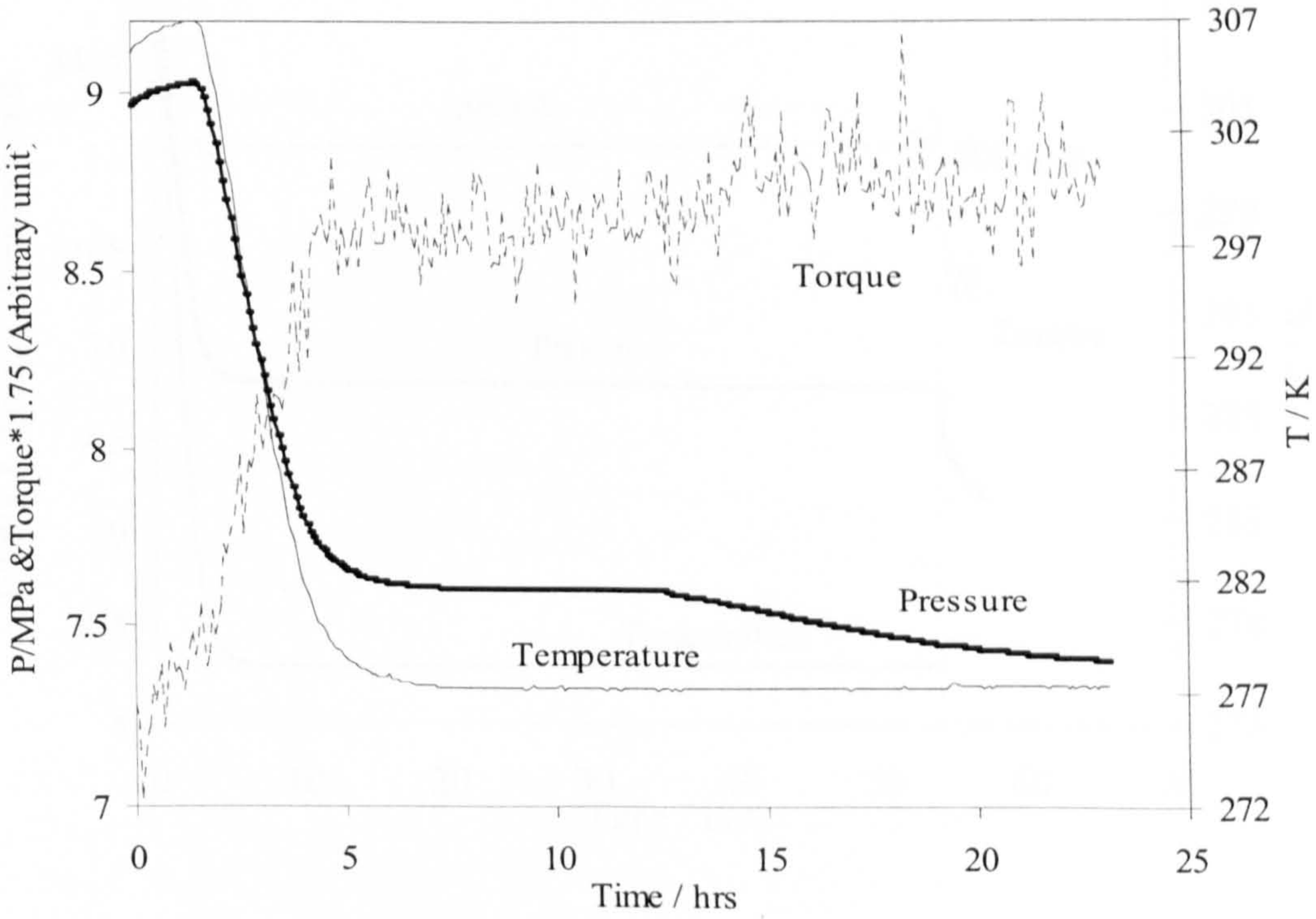

Figure 3.18 Pressure, torque and temperature profiles for Oil (B)-Water (10 vol%)-Natural gas system at 400 rpm mixing rate and medium pressure condition.

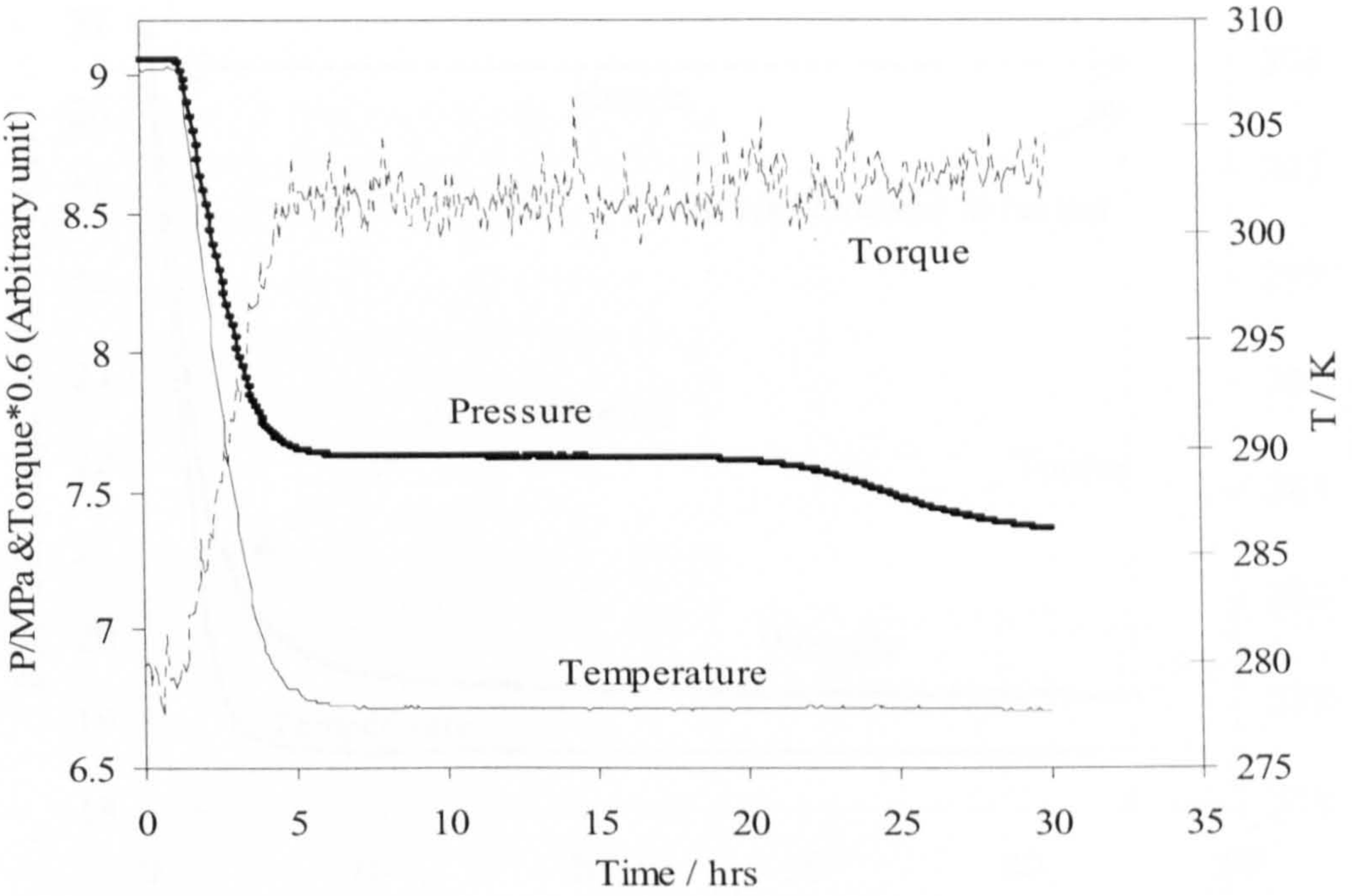

Figure 3.19 Pressure, torque and temperature profiles for Oil (B)-Water (10 vol%)-Natural gas system at 500 rpm mixing rate and medium pressure condition. At similar conditions and lower water content, longer induction time was observed (compare with Figure 3.13).

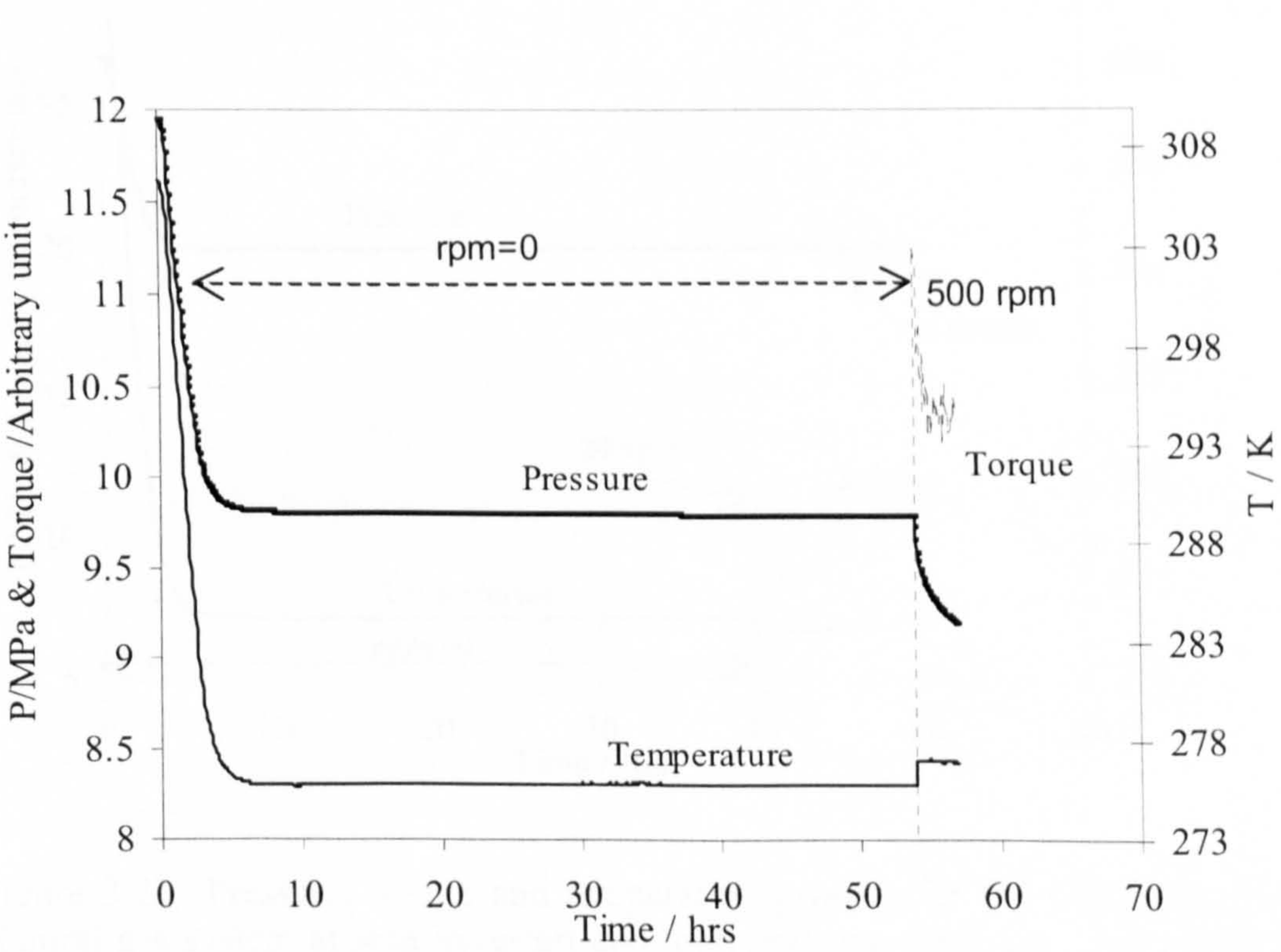

Figure 3.20 Pressure, torque and temperature profiles for Oil (B)-Water (30 vol%)-Natural gas system during shut-in/restart and medium pressure conditions. After shut-in period the stirrer was not blocked and the mixing restarted.

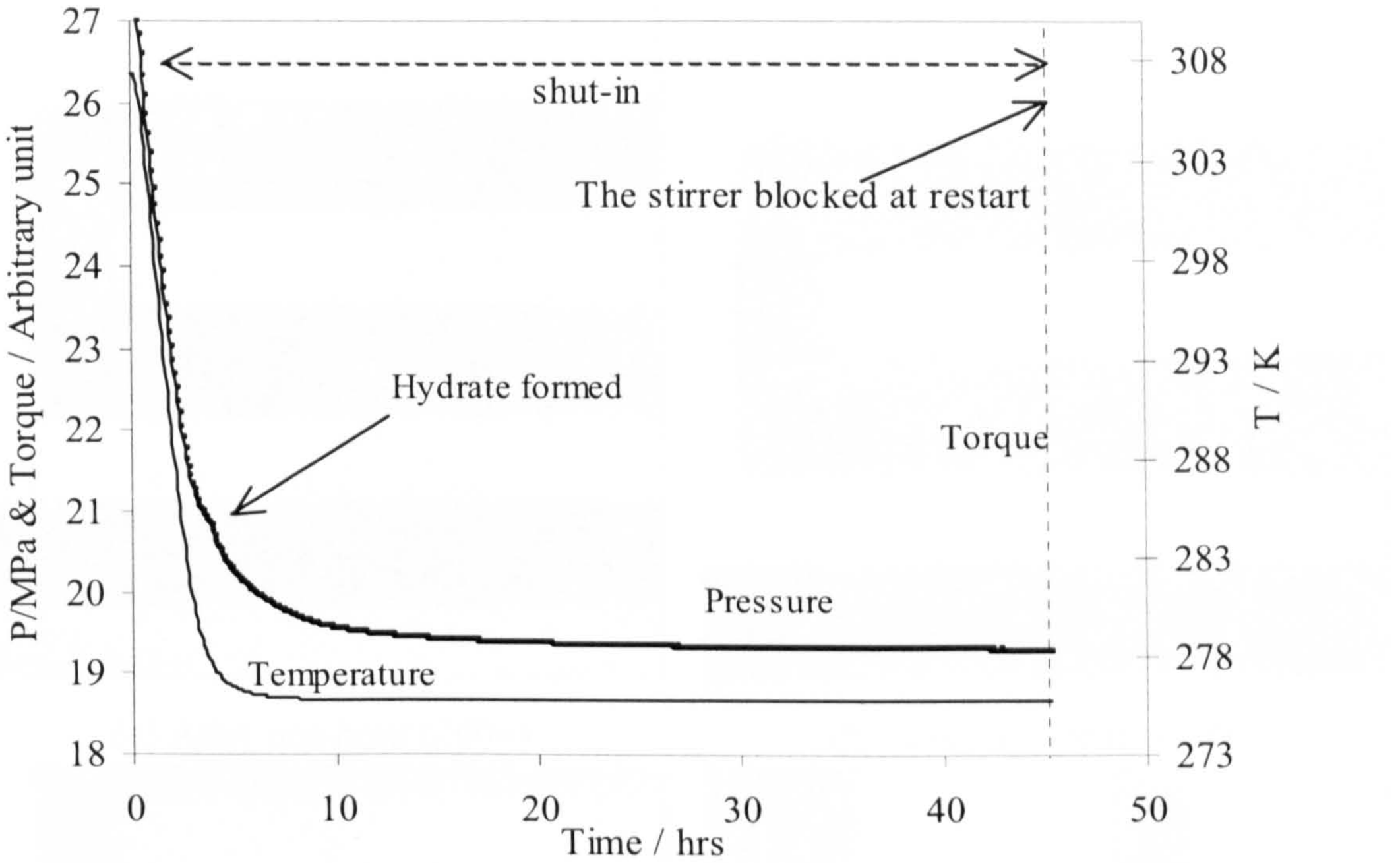

Figure 3.21 Pressure, torque and temperature profiles for Oil (B)-Water (30 vol%)-Natural gas system at shut-in/restart and high pressure conditions. After shut-in period the stirrer was blocked.

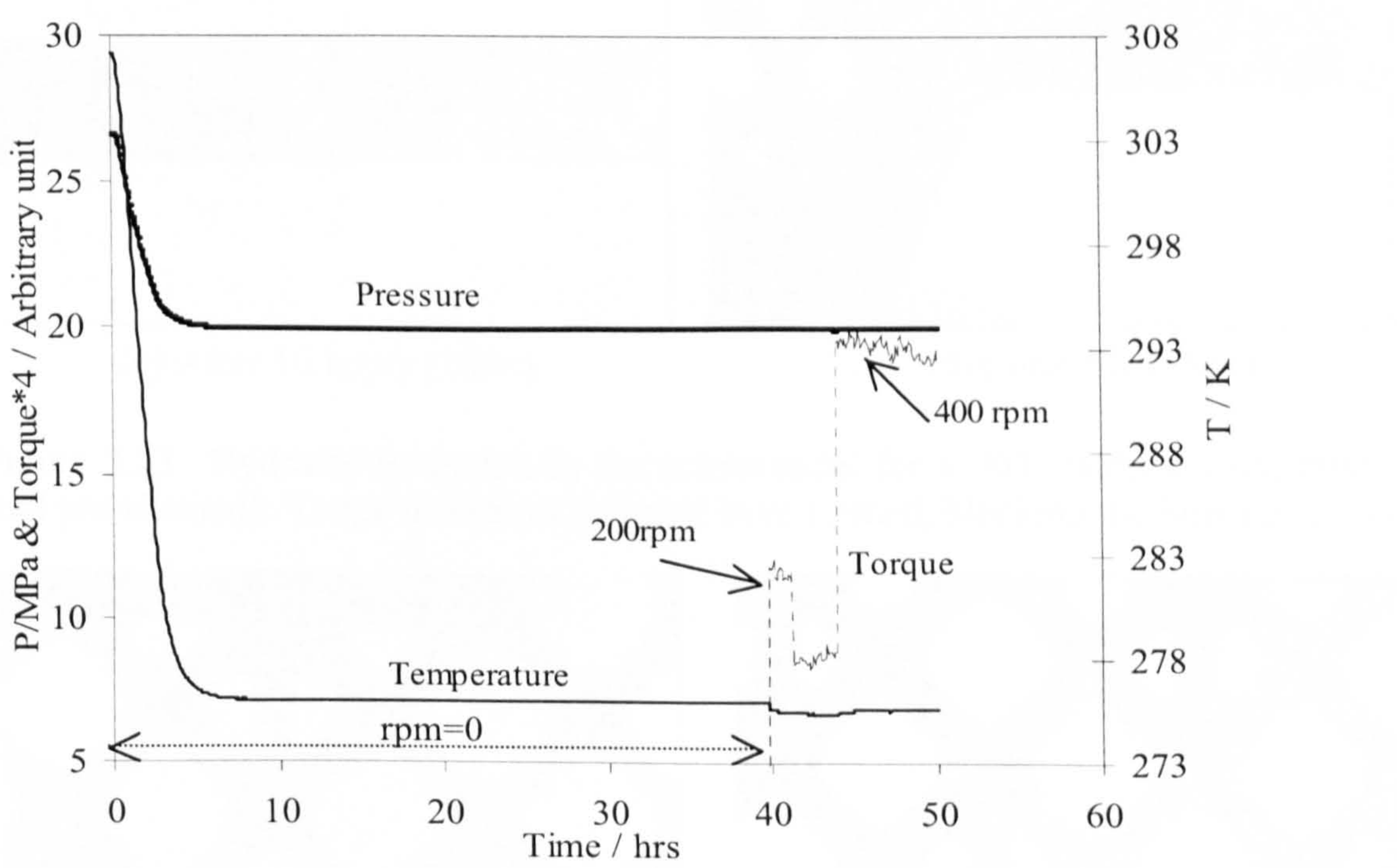

Figure 3.22 Pressure, torque and temperature profiles for Oil (B)-Water (10 vol%)-Natural gas system at shut-in/restart and high pressure condition. After shut-in period the stirrer was not blocked and the mixing restarted.

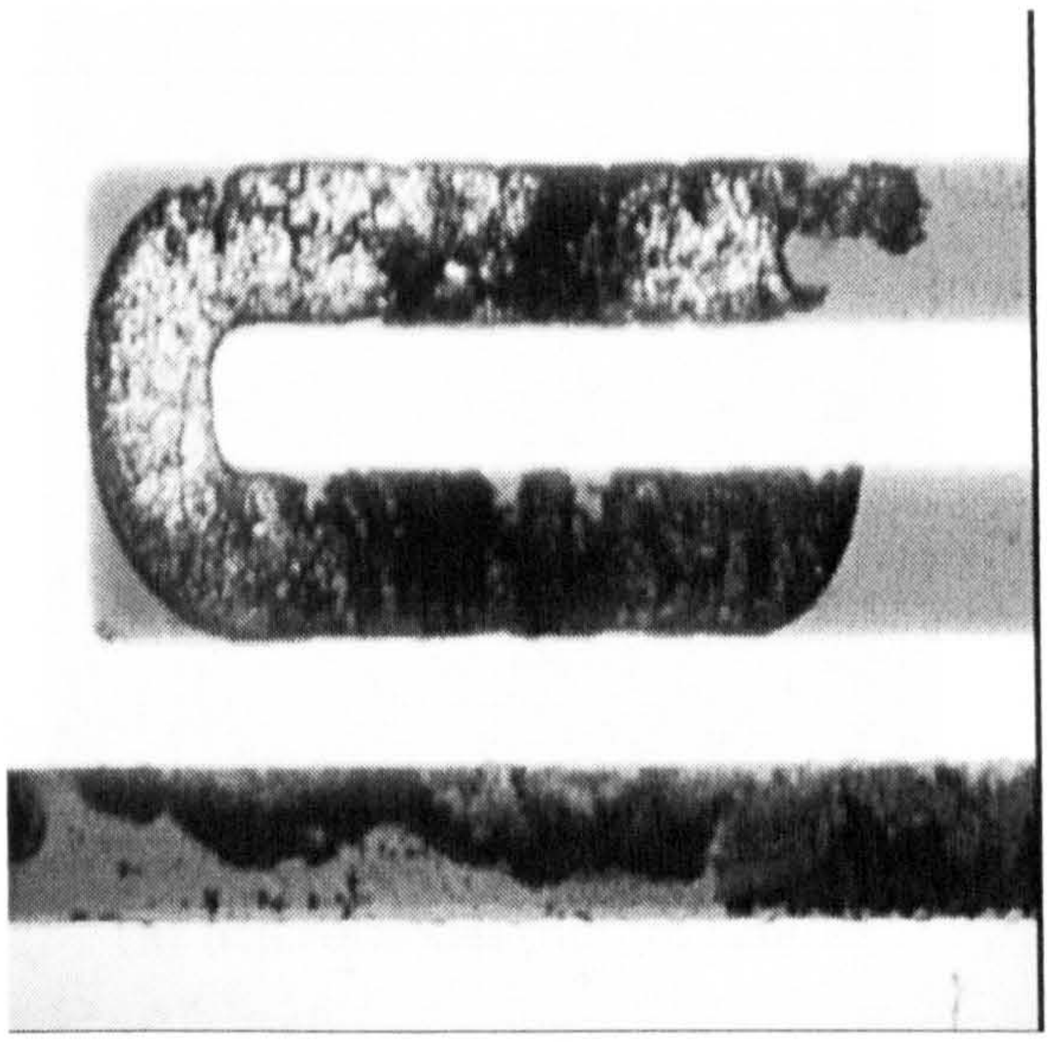

(a) After one hour (200×)

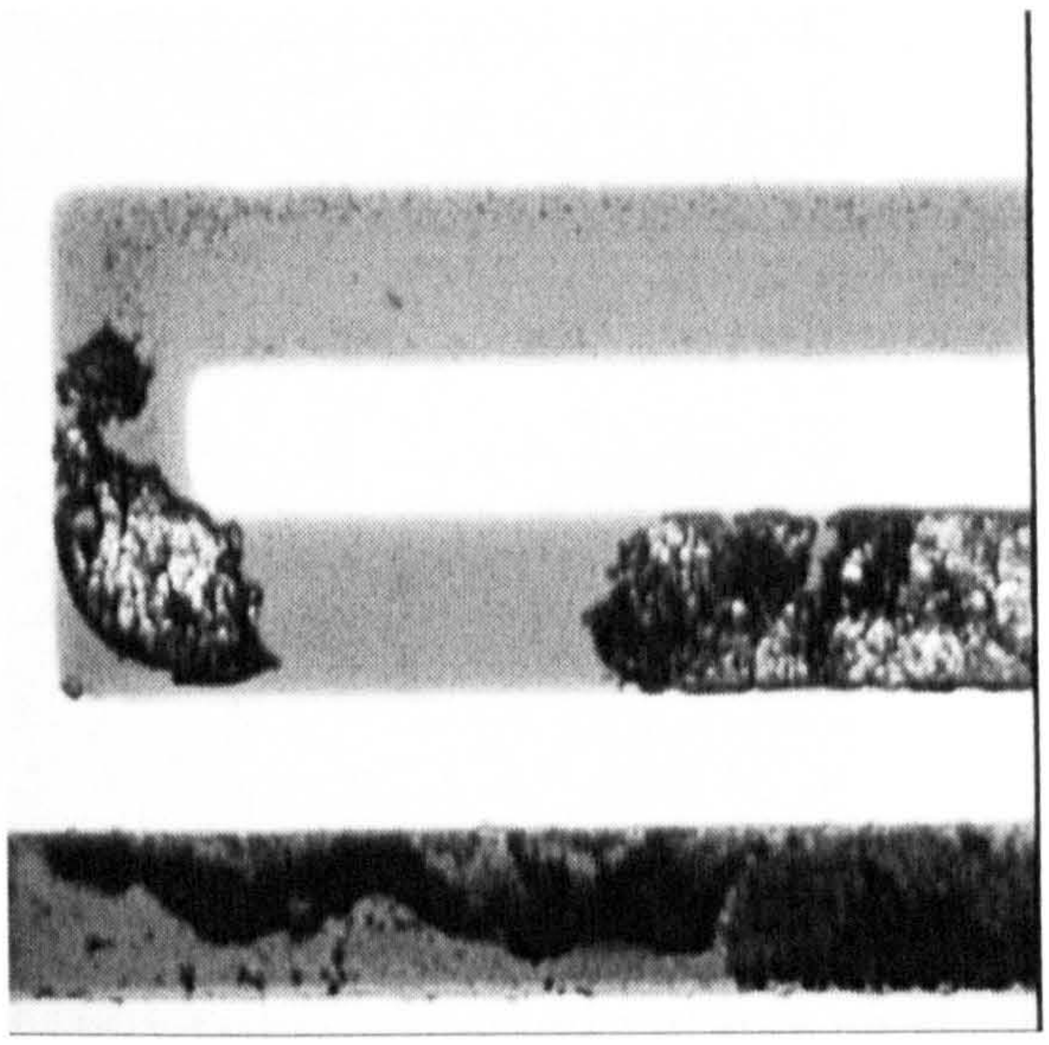

(b) After two hours (200×)

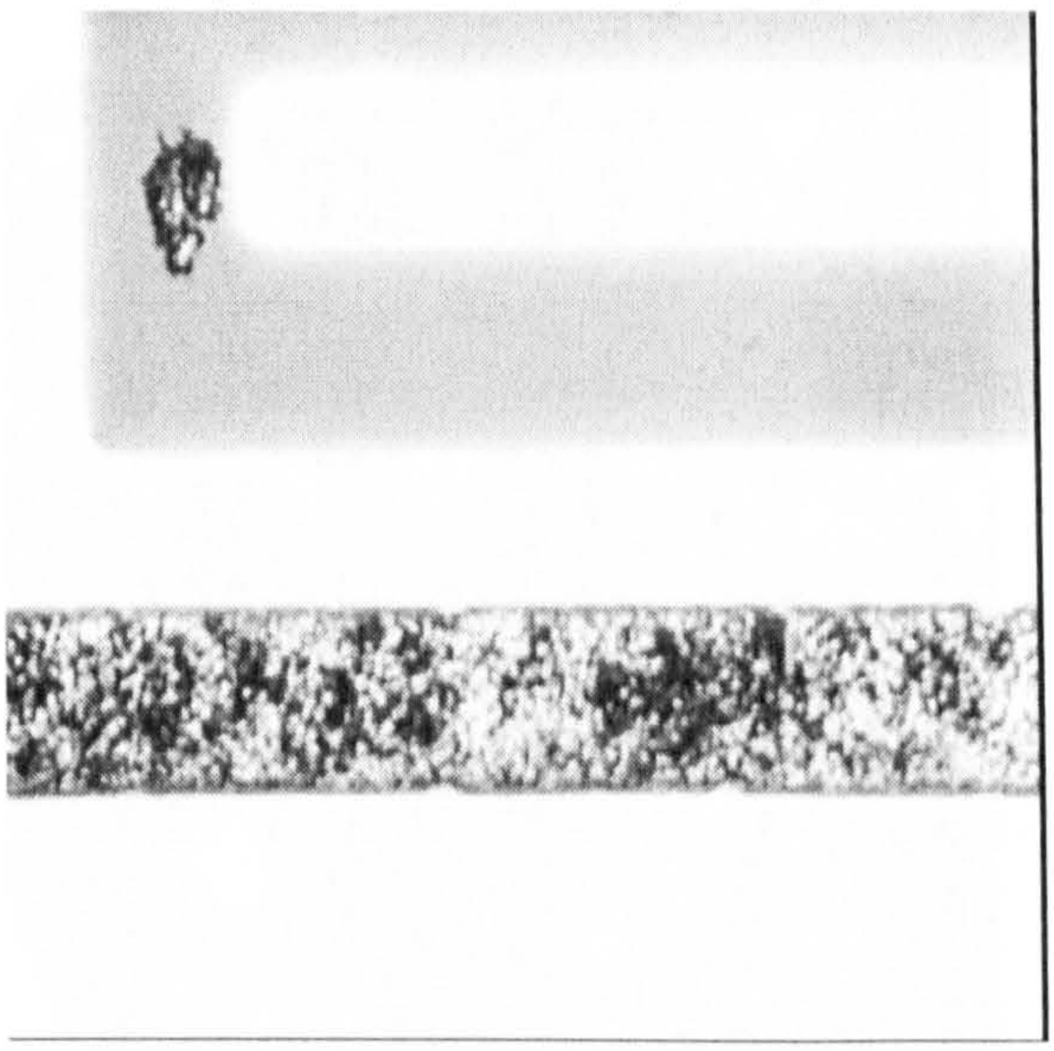

(c) After 10 hours (200×)

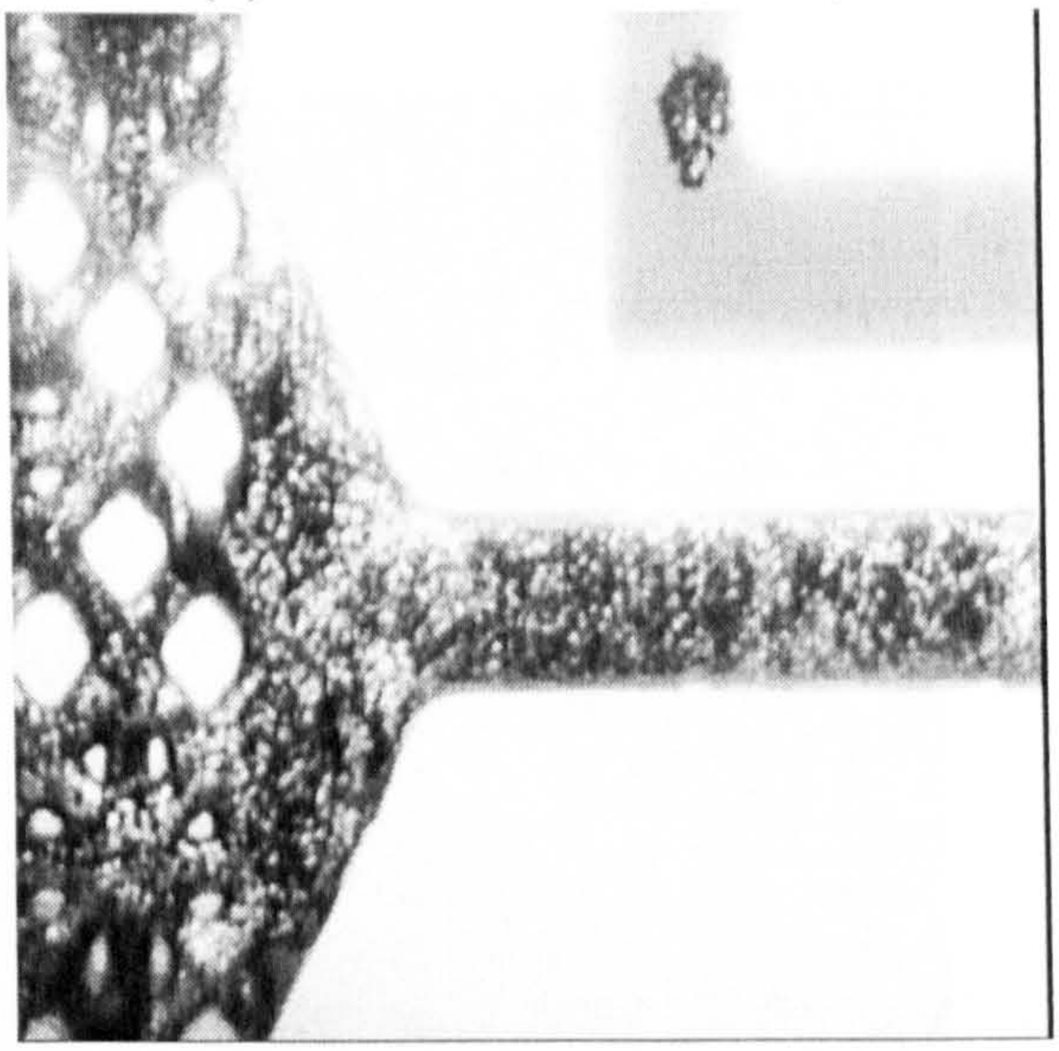

(d) After one day (150×)

Figure 3.23 Hydrates formation in the micromodel for a 30% water-oil (B) mixture (not pre-sheared). Large masses of hydrates have formed, blocking the inlet/outlet line.

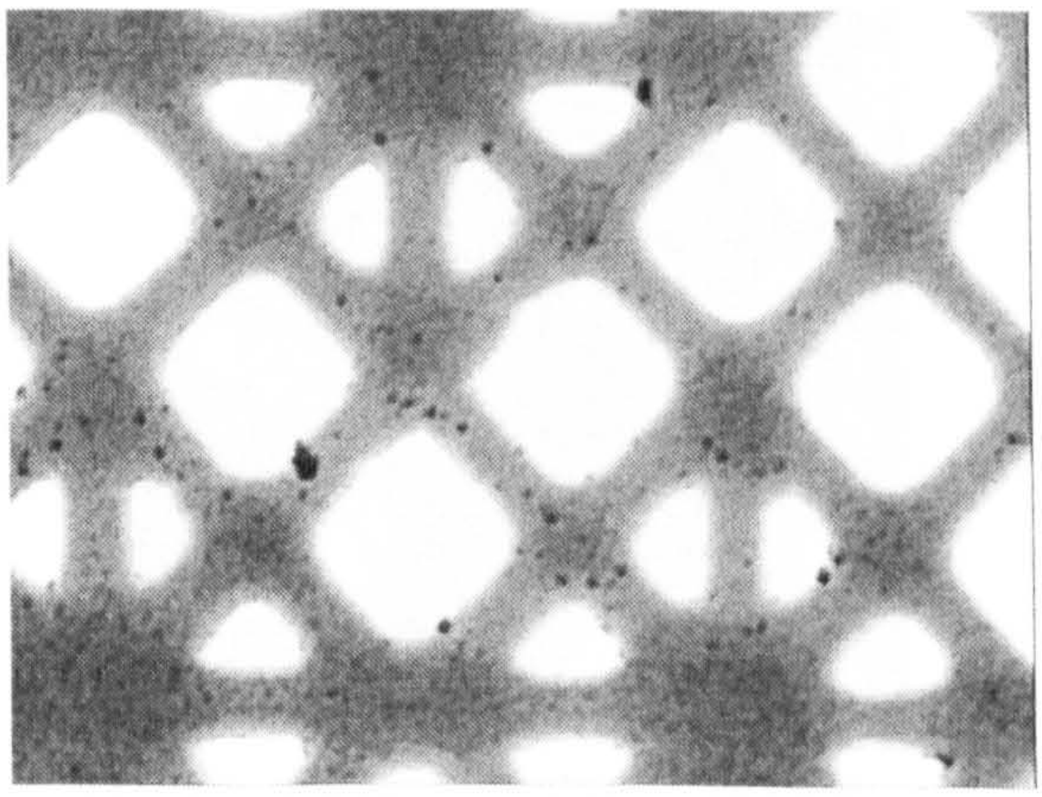

(a) T=303.15 K (200×)

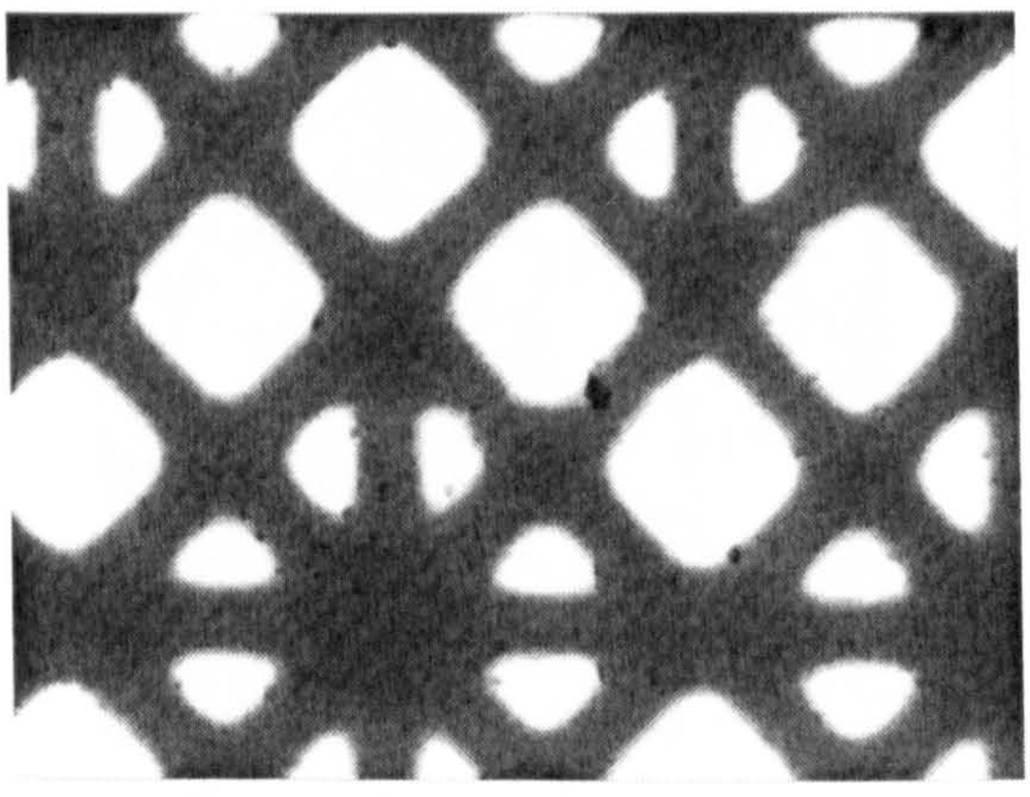

(d) T=268.35 (200×)

Figure 3.24 Oil (B)in micromodel, no dark lumps of oil heavy components formed even at subzero temperatures.

(a) Micromodel picture (200×)

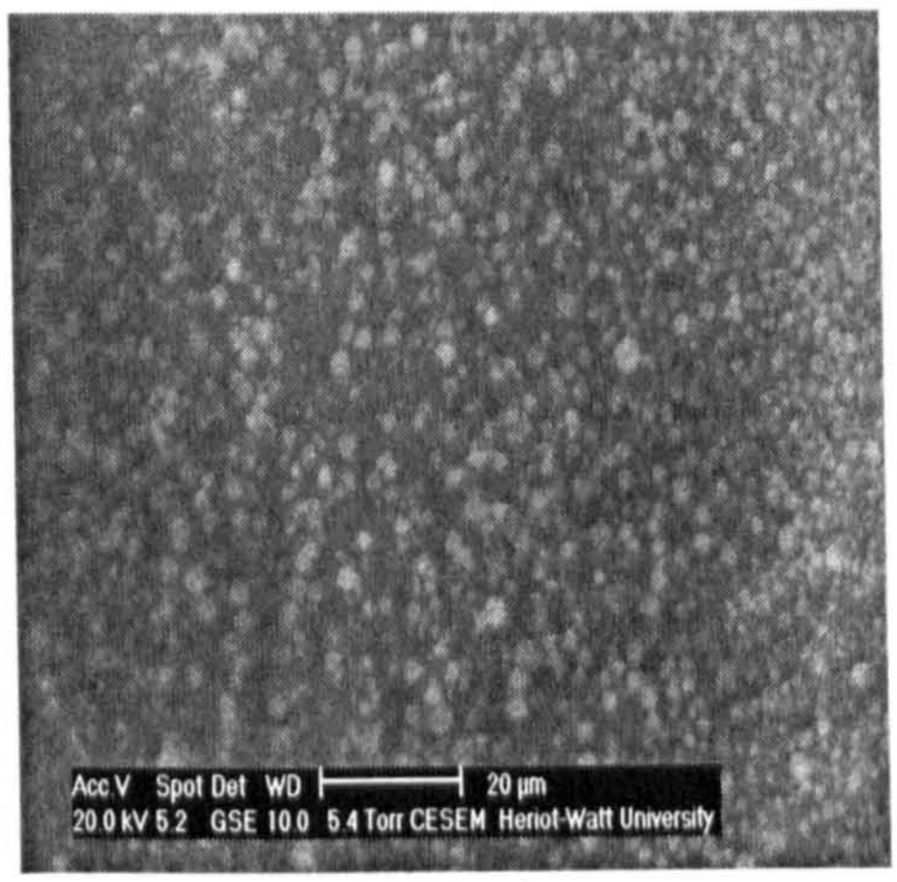

(b) SEM picture

Figure 3.25 Water (30%) in oil emulsion of Oil (B)after 15 minutes of mixing at high shear rate mixing (10,000rpm).

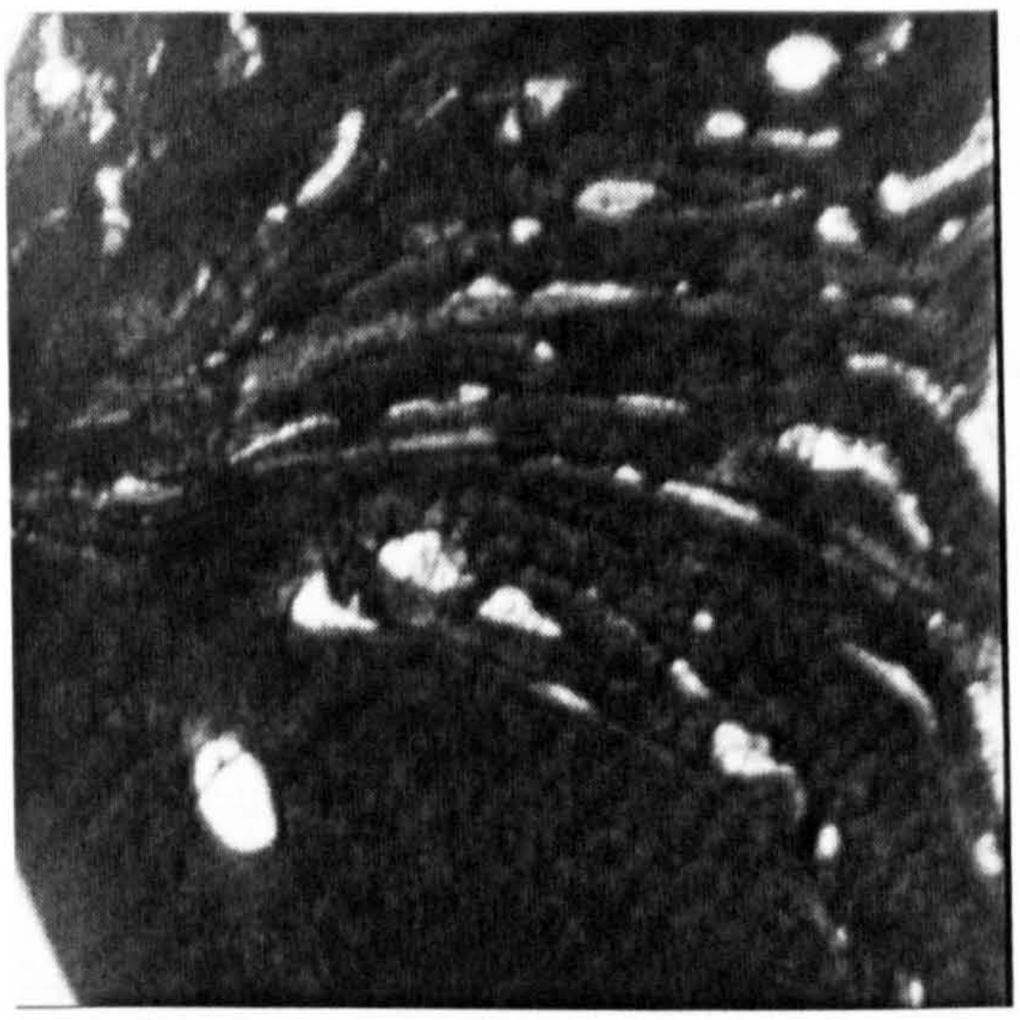

(a) Micromodel picture (150×)

(b) Micromodel picture (200×)

Figure 3.26 Hydrates formation in stable water in oil (B) emulsion at flowing conditions (P = 7 MPa, T = 269.15 K).

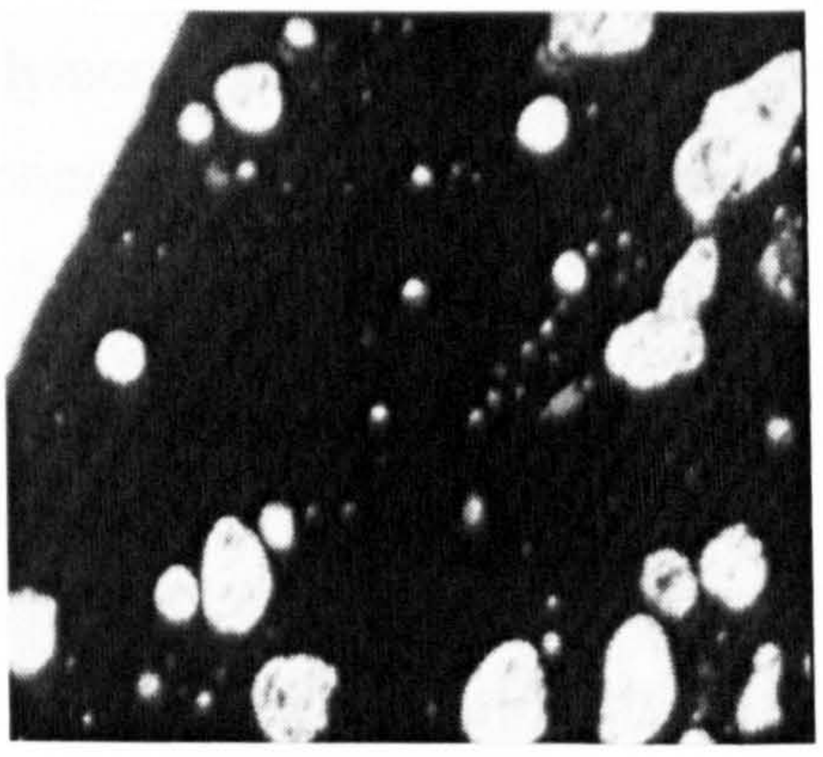

(a) After 6 hours of shut-in (300×)

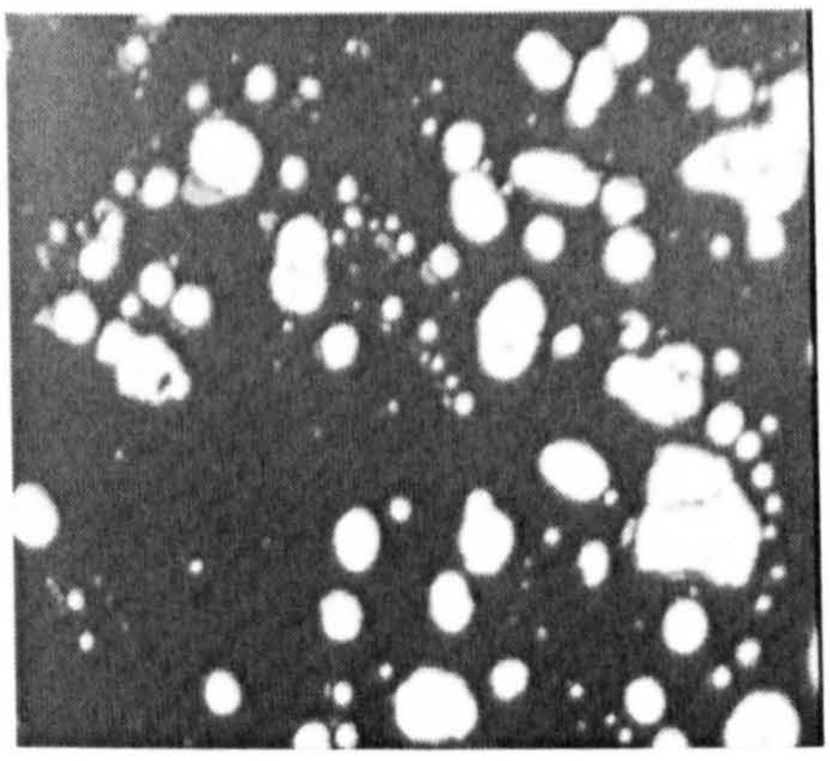

(b) After 24 hours of shut-in (200×)

Figure 3.27 Hydrate particles formed from 30% water-oil (B) emulsion prepared with 10,000 rpm pre-shearing at shut-in conditions. Some of the hydrate particles agglomerated after 18 hours.

CHAPTER 4

RATIONAL DESIGN AND TESTING OF LOW DOSAGE HYDRATE INHIBITORS

4.1 INTRODUCTION

In the past decade, a new group of non-thermodynamic chemical hydrate inhibitors has been developed which has received considerable attention from the industry. The search for novel Kinetic Hydrate Inhibitors (KHI) was driven by the need to reduce chemical costs and logistical issues, especially those associated with thermodynamic inhibitors (e.g. methanol, ethylene glycol etc.). Some of the early inspiration came from the occurrence of natural inhibitors in the plant and animal world. In particular, it is known that some fish produce so-called anti-freeze proteins (AFPs), which allow them to function at low temperatures and high pressures without freezing solid. The background to the development of kinetic hydrate inhibitors is well documented (Sloan, 1998). Initially, alkylarysulfonic acid and its salt, alkyl glycosides, tyrosine derivatives, and some surfactants have been patented as kinetic inhibitors. The finding of polymeric materials, such as polymers with an amide group (-N-C=O), has made the so-called first generation of KHIs available for commercial applications (Sloan, 1998, Fu, et al., 2002). Polymers used in the first generation KHIs include homopolymers, such as poly vinyl pyrrolidone (PVP) and poly vinyl caprolactam (PVCAP), and their copolymers. The performance of the initial inhibitor formulation with single polymer component was not very satisfactory. Therefore, the second-generation of inhibitors have been formulated and commercialised for industrial applications. These products are mainly new formulations based on PVP and PVCAP and their derivatives to enhance product performance. Some modifications on polymer structure, molecular weights, polymerisation process, and adding good synergists have been made to increase the inhibitor performance (Cohen et al 1998, Bakeev et al, 2000). A number of successful field trials (Frostman. and Przybylinski, 2001, Fu et al., 2002, Argo et al. 2000, Lovell and Pakulski, 2002) and full field application (Wu et al., 2007, MacDonald et al. 2006, Swanson et al, 2005) of KHIs have been reported in literature.

Despite the technical achievements offered by the KHIs, the mechanism of inhibition remains unclear. It has been argued whether the polymers act on the surfaces of an already exiting hydrate crystal or whether they associate in some manner with hydrate-forming constituents while still in solution. The adsorption theory was supported by studies using small-angle neutron scattering techniques and molecular simulations (King et al., 2000, Storr et al., 2002, Makogon et al., 2002). However, whether and how the polymers delay or enhance hydrate nucleation is still not clear (Koh et al., 2002). The characterisation of the underlying mechanisms for synergism effect remains unexplored. Service companies have done a lot of research on the synergists which have not been published.

While the KHIs developed over the past decade have been applied in many oil and gas fields for controlling hydrate (Wu et al., 2007, MacDonald et al. 2006, Swanson et al, 2005), there is much scope for further development (Kelland et al 1994, Lederhos and Sloan 1996, Sloan et al. 1998). The history of the development of LDHIs has been reviewed by Kelland (Kelland, 2006). Two problems in particular arise: the extent of subcooling induced (*i.e.* how far the temperature can be lowered below the equilibrium hydrate formation temperature without risk of forming a hydrate blockage), and the environmental acceptability. The current generation of KHIs allows only 10–12 K subcooling whereas about 20 K is needed in many applications. Also, by far, the main method for identifying KHIs has been screening a large number of potential chemicals. For example Lederhos and Sloan tested and screened over 1500 chemical combinations and concentrations to obtain a class of satisfactory inhibitors (Lederhos and Sloan 1996). For these reasons, there is an urgent need to develop new classes of high performance KHIs on the basis of rational design of them.

Some leading hydrate research groups have attempted to use computer modelling techniques to model hydrate kinetic inhibitors interactions with the hydrate crystal surface (Carver et al 1996, Kvamme 1996, Makogon and Sloan 2002, Kelland et al 1998). Rodger (Kelland et al. 1998) has already developed some appropriate computer modelling methods that have led directly to one patent for a new KHI. However, significant extensions to the methodology, *e.g.* to incorporate some of the more recent methods developed by Rodger (Fidler and Rodger 1999) are still needed before the goal of tailor-designed KHIs for specific reservoir fluids can become a reality.

Computer modelling techniques are very powerful tools to investigate hydrate phenomena. Indeed, hydrate computer simulations may shortly outnumber hydrate

experimental observations, because simulations are generally easier than experiments. However, such tools investigate phenomena, which are on a much smaller dimension (hundreds to thousands of molecules) than normally observed and a limited time scale (10^{-9}seconds) (Sloan, 1998). This necessitates macroscopic techniques to validate the results from computer modelling techniques.

The above discussion was the basis of establishing a collaborative research programme between Department of Chemistry of Warwick University and Institute of Petroleum Engineering of Heriot-Watt University. The objective was to use molecular dynamics computer simulation in conjunction with carefully designed experimental tests to identify the molecular mechanisms by which low dosage hydrate inhibitors work and thereby to design and synthesise new KHIs for use in the oil and gas industry.

The new class of KHIs based on quaternary ammonium zwitterions were identified from a hydrate surface adsorption study by Storr et al (2002) as having an unusual interaction with hydrate surface. The general structure of the new kinetic inhibitors is shown in Figure 4.1(a). In Figure (4.1a), R1-R3 can be one of the propyl, butyl, pentyl, or hexyl groups attached to the nitrogen atom and R4 is methylene spacer groups between nitrogen and (SO_3^-) ion. Before that study in most surface adsorption studies it had been found that the active component of KHI binds inside the large potholes of hydrate. For new KHIs however it was found that KHI actually capped the top of potholes (shown in Figure 4.21) with strong hydrogen bonding interaction between the hydrate surface and both cationic and anionic centres (Storr et al., 2002).

This chapter details the results of the experiments conducted on fourteen newly designed and synthesised KHIs by Warwick University. A High-pressure hydrate kinetic cell was utilised to evaluate the performance of new KHIs in terms of induction time. Their performance subsequently was compared with those of a commercial kinetic inhibitor and a conventional kinetic inhibitor in different hydrate structures at pipeline conditions. The anti-agglomeration property of the new chemicals in a water-condensate-natural gas system has been explored. Finally, the primary mechanism of hydrate inhibition and the morphology of the formed hydrates in the presence and absence of one the new KHIs were studied with the glass micromodel set up.

4.2 MATERIALS, EXPERIMENTAL SET-UPS AND PROCEDURES

Fourteen synthesised low dosage hydrate inhibitors were supplied by Department of Chemistry of Warwick University. They were labelled as; KI-1: $BuMe_2NC_3S$, KI-2:

Bu_2MeNC_3S, KI-3: Bu_3NC_3S, KI-4: Bu_3NC_4S, KI-5: Pr_3NC_2S, KI-6: Pr_3NC_3S, KI-7: $BuMe_2NC_2S$, KI-8: $BuMe_2NC_4S$, KI-9: Bu_3NC_2S, KI-10: Pe_3NC_4S, KI-11: Pe_3NC_3S, KI-12: He_3NC_3S, KI-13: He_3NC_4S, KI-14: (Pr_2 NC_3 S) C_5 (Pr_2 NC_3 S), where (Pr) is propyl, (Bu) is butyl, (Pe) is pentyl, (He) is hexyl, and (C) is methylene spacer groups between nitrogen (N) and (SO_3^-) ion (S). A commercial kinetic inhibitor, Luvicap®, consisting of 40 mass percent Poly n-Vinyl Caprolactam (PVCap) (Figure 4.1c) and 60 mass percent ethylene glycol was provided by Clariant Oil Services. Poly Vinyl Pyrrolidone (PVP) (Figure 4.1b), with an average molecular weight of 10000 (gr/mol), was purchased from Aldrich Company. Natural gas (NG) and research grade pure methane gas were provided by Air Products. The natural gas composition is shown in Table 4.1. A North Sea natural condensate was provided by Clariant Oil Services. In all the experiments carried out for comparing the performance of KHIs, a solution of 0.5 mass% of KHI in deionised water has been used unless otherwise specified.

A Hydrate Kinetics Rig was used in this study. It consists of a test vessel (500 ml), a stirrer with magnetic motor and a temperature control system. The rig is mounted in an external bath for heating and cooling (Figure 4.2). The pressure capacity of the system is up to 70 MPa. The test procedure has been detailed in Chapter 3 (Section 3.2). All the tests carried out at a mixing rate of 600 rpm unless otherwise specified. The glass micromodel experimental set up described in Chapter 3 was used for studying the morphology of the gas hydrates formed in the presence and absence of the KHIs. An in-house thermodynamic (hydrate) computer model (HWHYD, detailed in Chapter 2) was used to calculate the hydrate phase boundaries for natural gas and methane in the presence of pure water. The hydrate equilibrium conditions for methane and natural gas are depicted in Figure 4.3. In different experiments carried out, the degree of subcooling in testing condition was determined from this diagram.

4.3 EXPERIMENTAL RESULTS

4.3.1 Tests on Natural Gas-Water System in the Presence of KHIs

The hydrate kinetic rig has been utilised to measure the performance of new synthesised KHIs in terms of induction time. In the experiments the time at which the temperature and pressure have been stabilised is considered as the reference point for calculation of induction time before hydrate formation (determined by the system pressure drop and temperature rise). The experiments carried out in relatively high degree of subcooling, 10.8-11 K, and moderate pressure of 6.8-7.1 MPa at a mixing rate of 600 rpm, to simulate pipeline conditions in seabed.

The results of the tests with all the synthesised kinetic inhibitors in natural gas-water system, which forms structure II hydrate, are summarised in the Table 4.2 and the pressure profiles of the tests are presented in Figures 4.4 and 4.5. From Table 4.2 and Figures 4.4-4.5, it appeared that KI-10 and KI-11 have a better performance in inhibition of natural gas hydrate than other synthesised kinetic inhibitors.

4.3.2 The Performance of Kinetic Inhibitors in Different Hydrate Structures

Usually the hydrate inhibitors are tested with natural gases that contain more than one percent of propane or butane and form structure II hydrates. However in some gas fields (e.g. Nuggets gas field in North Sea) the natural gas has more than 99 mole% of methane and less than 0.1% of propane and butane. In such a natural gas structure I hydrate is more stable. Therefore for a comprehensive testing of new inhibitors, their performance in the systems forming structure I hydrate should also be considered.

In this study, two of the synthesised kinetic inhibitors (KI-10 and KI-1) were re-tested in the system of methane and water at different degrees of subcooling. The results are summarised in Table 4.3. For methane–water system with a similar temperature and pressure condition as that with the natural gas system, the induction time achieved by KI-1 was more than 13 hours (Test No.1). This result was expected because of a low degree of subcooling (5 K) in the methane system at the similar conditions (refer to Figure 4.3). To reach to the same degree of subcooling as that of the above system at 278.55 K, the pressure was increased to about 13.17 MPa. At 10 K subcooling, KI-1 inhibited hydrate formation for 70 minutes (Test No.2, Figure 4.6). The test results show that, at similar temperatures and degree of subcooling range, the inhibition effect of KI-1 in natural gas-water system (sII hydrate) is better than that in methane-water system (sI hydrate). The negative effect of pressure on the performance of KHIs has been discussed in Chapter 7 (7.6.2).

The performance of KI-10 in methane system was tested in different pressures (11.72 MPa and 13.03 MPa) and subcooling range of 9-10 K (Tests No.3-5). Induction times of 140-300 minutes were achieved by the KI. The results shows that KI-10 is better than KI-1 in structure I hydrate systems. Again at similar degrees of subcooling the performance of KI-10 in sII hydrate system (Test No.10 Table 4.2) is better than structure I hydrate systems (Test No.4, Table 4.3, and Figure 4.7).

4.3.3 Comparison with the Conventional Kinetic Hydrate Inhibitors

For comparison, a series of experiments were conducted with two conventional kinetic inhibitors: a commercial PVCAP-based KI (Luvicap®) and PVP, both with a concentration of 0.5mass% in water. Their performance in terms of induction time was measured in two systems of natural gas-water and methane-water. Tables 4.4 and 4.5 present the results of the tests with commercial kinetic inhibitor (Luvicap®), PVP and KI-10 at similar conditions. Figures 4.8 and 4.9 present the pressure profiles of the experiments. In natural gas systems, the performance of the KI-10 is not as good as that of commercial kinetic inhibitor and PVP in terms of induction time. However in methane gas system (structure I) its performance is better than PVP (Table 4.5). It is worth to note that although the degree of subcooling in the tests with methane is lower than that of natural gas system, the induction times in general are shorter.

4.3.4 Tests with Higher Concentrations of Kinetic Inhibitors

In the severe field conditions (low temperatures and high pressures), the hydrate inhibitors should be able to prevent hydrate formation for more than several hours. In order to achieve this, higher concentrations than 0.5mass% of the synthesised KHIs are needed. In this preliminary study, two tests were carried out with KI-1 and KI-11 in seabed pipelines conditions. Figure 4.10 depicts the pressure and temperature profiles for the test with methane and 1.5 mass% of KI-1 in water solution. As shown in Figure 4.10, the condition of the kinetic rig was stabilised at 12.34 MPa and 278.35 K (9.6 K subcooling). The induction time for this test was more than 3700 minutes. Subsequently, the temperature was reduced to 276.55 K (11.5 K subcooling) and after 830 minutes hydrates formed. Figure 4.11 shows the results of test with natural gas-water system in the presence of 1 mass% KI-11 in water. As shown in the figure, at the testing conditions of 10 MPa and 277.15 K (9 K subcooling) the induction time is about 1200 minutes.

4.3.5 Anti-Agglomeration Property of New KHIs

The anti-agglomeration property of the new KHIs was tested in the Kinetics Rig. A paddle type stirrer was used for mixing and torque measurement. During the experiments, the rheology of the hydrate slurry was monitored by measuring the torque applied on the stirrer shaft. After hydrate formation, torque will increase. However, if the hydrates formed are dispersed into oil/condensate phase as small particles, as expected when an anti-agglomerant is present, torque increase will be limited. Otherwise, large torque increase can be observed, which may lead to the blockage of the stirrer. In this study two aqueous systems in the presence of natural gas were

examined: a solution of water (30 volume%) and condensate (70 volume%) for blank test and another solution of 1 mass% KI-11 in water (30 volume%) and condensate (70 volume%). Figure 4.12 shows the results obtained in a test with water solution without KI-11. The profiles of pressure, temperature and torque measured in the test are illustrated. The stirring rate was maintained at 600 rpm during the test. Experiment started at 305.88 K and 11.9 MPa where the torque was around 3.9 (arbitrary unit). After cooling down the system the pressure, temperature and torque stabilised at 10.1 MPa, 276.8 K and 4.4, respectively. Three hours induction time was observed at those conditions. Large torque increase was observed (from 3.9 to 19.7) after hydrate formation, and the stirrer was blocked.

The above test was repeated at similar conditions in the presence of 1 mass% KI-11. The profiles of the test are presented in Figure 4.13. The test started at 305.5 K and 12.9 MPa where the torque was around 4.1 (arbitrary unit). After cooling down the system the pressure, temperature and torque stabilised at 10.6 MPa, 277.2 K and 4.4, respectively. Three and half hours induction time was observed at those conditions. After hydrate formation the torque was increased to 9.7 and stabilised there for 7 hours before termination of the test. The experiments results show that KI-11 has been successful in preventing agglomeration of hydrate particles, as after hydrate formation in the presence of the new KHI the stable torque was half of that in the blank test.

4.3.6 The Primary Mechanism of Hydrate Inhibition by KHI, Application of Glass Micromodel

In this study glass micromodel has been exploited to observe the effect of new KHIs on the hydrate formation process. Experiments were conducted on systems NG-water, and NG-water in the presence of KI-11. The aim of these experiments was to observe hydrate growth in the presence of the new KHI and without it to investigate the primary mechanism of KHI in hydrate inhibition. For both experiments, natural gas was left to equilibrate with distilled water and/or distilled water plus KI-11 in a pressurized reservoir vessel for 24 hours at room temperature. The equilibrated liquid was then injected into the model under pressure, and the temperature lowered to form hydrates. The testing pressure and temperature tried to be kept close to those of the experiments carried out in the kinetic Rig. Figures 4.18 and 4.19 depict the hydrate formation and growth in a chronological order (A, B, C), in the presence of KI-11 and without it. As seen in the NG-water system (Fig.4.14A) at 291.55 K and 7.14 MPa there are only liquid and gas bubbles in the micromodel. After cooling down to 279.55 K within two hours, hydrates formed from free gas bubbles (Fig.4.14 B). Hydrate growth (a moving

front in the liquid phase), agglomeration and bubble dissolution in water (shrinking bubbles) can be observed in Figure 4.14 B-C.

In the presence of the new KHIs (KI-11), following cooling down the system from 291.25 K (and 7.66 MPa) to 278.65 K hydrate formed after 22 hours. As expected for hydrate formation longer induction time was needed compared to the NG-water system. The hydrates formed from some of the gas bubbles and dissolved gas (Fig.4.15 A-B), however after five days there was no sign of agglomeration of hydrate particles. The size of the bubbles and hydrate particles already formed did not change during this period. These phenomena can be explained by the result of molecular dynamic simulations carried out in Warwick University (Storr et al., 2002). The simulations showed that the inhibitor induces significant changes into the structure of interface, particularly affecting the dynamical behaviour of water in this region, and altering the local order of the hydrate lattice. Makogon and Sloan (Makogon and Sloan, 2002) using molecular dynamic simulations explained the mechanism of inhibition by adsorption of inhibitor to the hydrate crystal. "The inhibitor forces the hydrate to grow around and between the polymer strands, with a small radius of crystal curvature. Inhibitors also sterically block non-polar solutes such as methane from entering and completing a hydrate cavity".

Figures 4.16 A-B depict massive hydrate formation in the presence of KHI (KI-11) and without it. As seen, the hydrates formed from natural gas and water (Fig.4.16A) are mainly geometrical with a smooth surface. They have also covered the pores completely in those regions. However, in the presence of inhibitor the hydrates formed are not geometric. They have a coarse surface and they did not block all the pores space. These observations are in conformation with the above explanations.

4.4 CONCLUSIONS

Fourteen new low dosage hydrate inhibitors, designed using molecular dynamic simulation techniques and synthesised in Warwick University, were screened by testing them in a hydrate kinetic rig. One of the inhibitors among them was compared with a commercial and a conventional KHI at similar conditions. In natural gas-water system the new KHI was not as successful as the other two inhibitors. However, in methane-water system it performed better than PVP. The effect of hydrate structure on the performance of new KHIs was studied. It appeared that the tested KHIs in this study were more efficient in structure II hydrates. Tests with higher concentrations (1-1.5

mass%) of the new synthesised kinetic inhibitors have demonstrated better results at seabed pipeline conditions compared to 0.5% of KHI. The anti-agglomeration property of one the KHIs was tested in condensate-water-natural gas system by torque measurement in a kinetic rig. The results of the tests showed that quaternary ammonium zwitterions have good anti-agglomerant properties for the systems investigated.

The primary mechanism of hydrate inhibition was studied by application of glass micromodel. Visual observation of hydrate formation and growth in the presence of new KHI showed that it prevents agglomeration of the hydrate particles and causes deformation of the hydrate crystals. The results of above experiments demonstrate the success of the methodology.

4.5 TABLES

Table 4.1. Composition of the natural gas used in this work.

Component	Mol %	Component	Mol %
N_2	3.86	i-C_4	0.2
CO_2	1.5	n-C_4	0.35
C_1	86.49	i-C_5	0.08
C_2	5.71	n-C_5	0.08
C_3	1.63	C_6^+	0.1

Table 4.2. The results of the experiments in the system of natural gas -water in the presence of different synthesised inhibitors.

Test	Kinetic	Testing Conditions		Subcooling	Induction Time
No.	Inhibitor	T / K	P / MPa	/ K	/ Minutes
1	KI-1	278.45	7.00	11.0	80
2	KI-2	278.55	7.01	10.9	100
3	KI-3	278.45	7.00	11.0	140
4	KI-4	278.45	7.00	11.0	160
5	KI-5	278.35	7.03	11.0	0
6	KI-6	278.35	7.03	11.0	200
7	KI-7	278.55	7.00	10.8	75
8	KI-8	278.45	7.09	11.0	0
9	KI-9	278.65	7.03	10.8	0
10	KI-10	278.30	6.85	10.9	370
11	KI-11	278.45	6.96	10.9	400
12	KI-12	278.55	7.00	10.8	80
13	KI-13	278.45	7.04	11.0	100
14	KI-14	278.35	7.03	11.0	100

Table 4.3. The results of the experiments in the system of methane-water in the presence of different synthesised inhibitors.

Test	Kinetic	Testing Conditions		Subcooling	Induction Time
No.	Inhibitor	T / K	P / MPa	/ K	/ Minutes
1	KI-1	278.15	7.17	5.0	>800
2	KI-1	278.55	13.17	10.0	70
3	KI-10	279.45	13.03	9.0	300
4	KI-10	277.45	11.72	10.0	140
5	KI-10	277.95	11.72	9.50	200

Table 4.4. Performance of KI-10 in comparison with two conventional kinetic hydrate inhibitors (0.5 mass%) in natural gas-water system.

	Kinetic	Testing Conditions		Subcooling	Induction Time
No.	**Inhibitor**	**T / K**	**P / MPa**	**/ K**	**/ Minutes**
1	KI-10	278.30	6.85	10.9	370
2	PVCap	278.15	7.24	11	950
3	PVP	278.15	6.96	11	800

Table 4.5. Performance of KI-10 in comparison with two conventional kinetic hydrate inhibitors (0.5 mass%) in methane-water system.

Test	Kinetic	Testing Conditions		Subcooling	Induction Time
No.	**Inhibitor**	**T / K**	**P / MPa**	**/ K**	**/ Minutes**
1	KI-10	277.45	11.72	10	140
2	PVCap	277.65	11.79	9.8	300
3	PVP	277.65	11.79	9.8	80

4.7. FIGURES

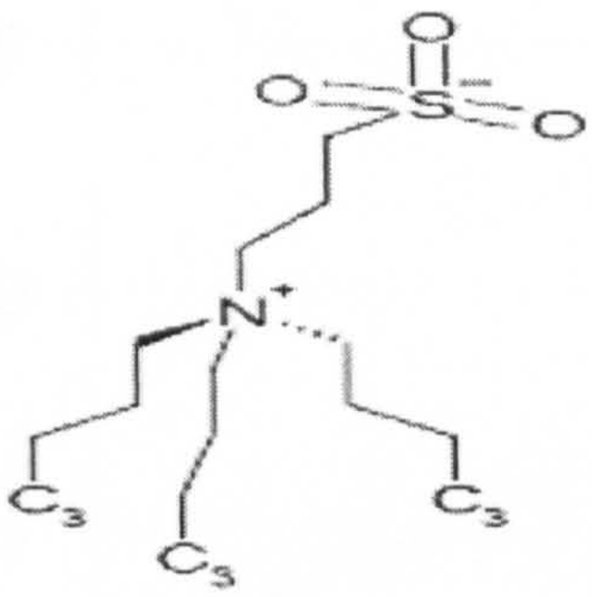

(a) Quaternary Ammonium Zwitterions

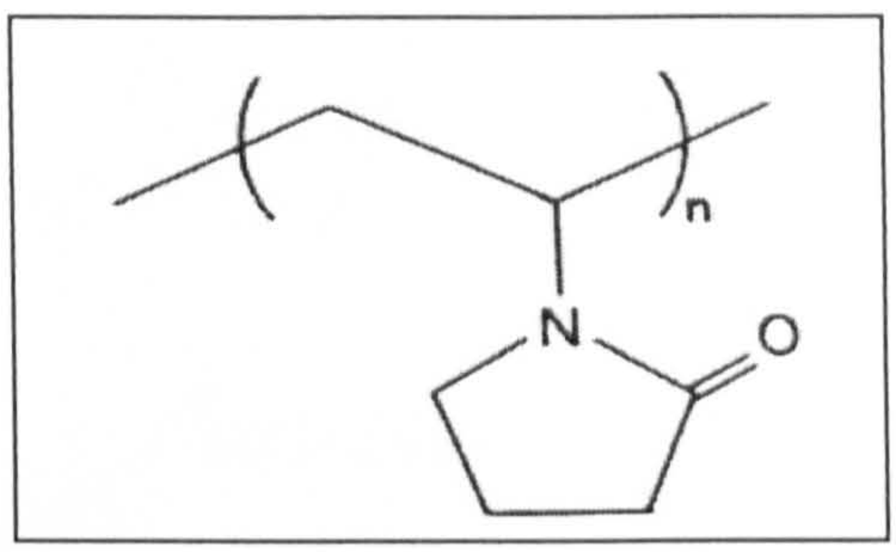

(b) Poly n-Vinyl Pyrrolidone (PVP)

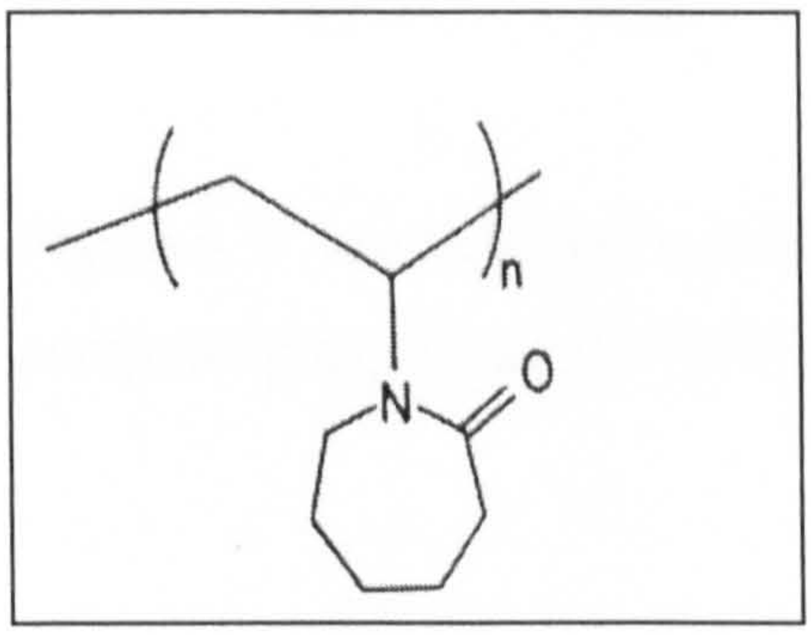

(c) Poly n-Vinyl Caprolactam (PVCap)

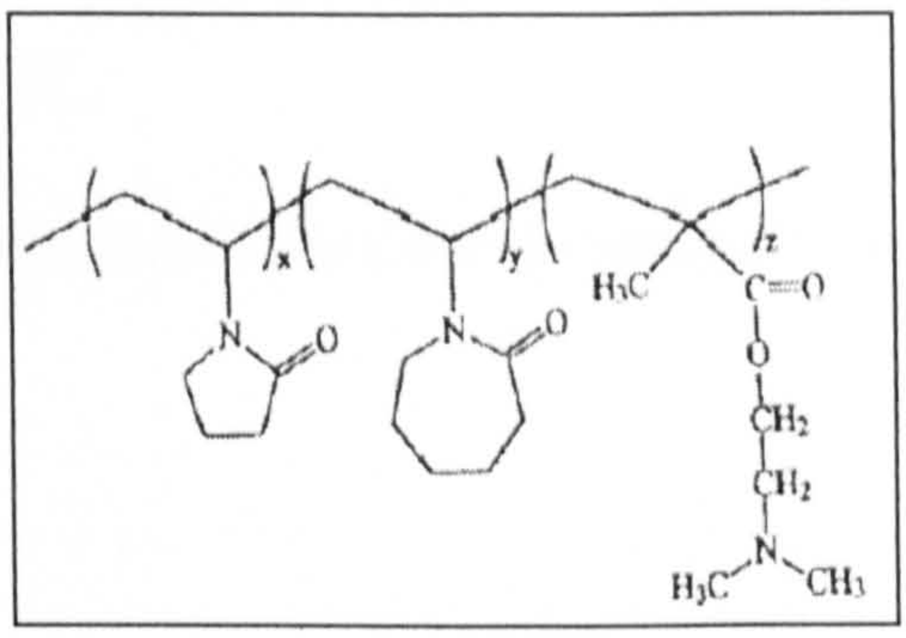

(d) VC-713 (a terpolymer of PVCap, PVP and dimethyl amino ethyl methacrylate

Figure 4.1. The structures of several kinetic hydrate inhibitors.

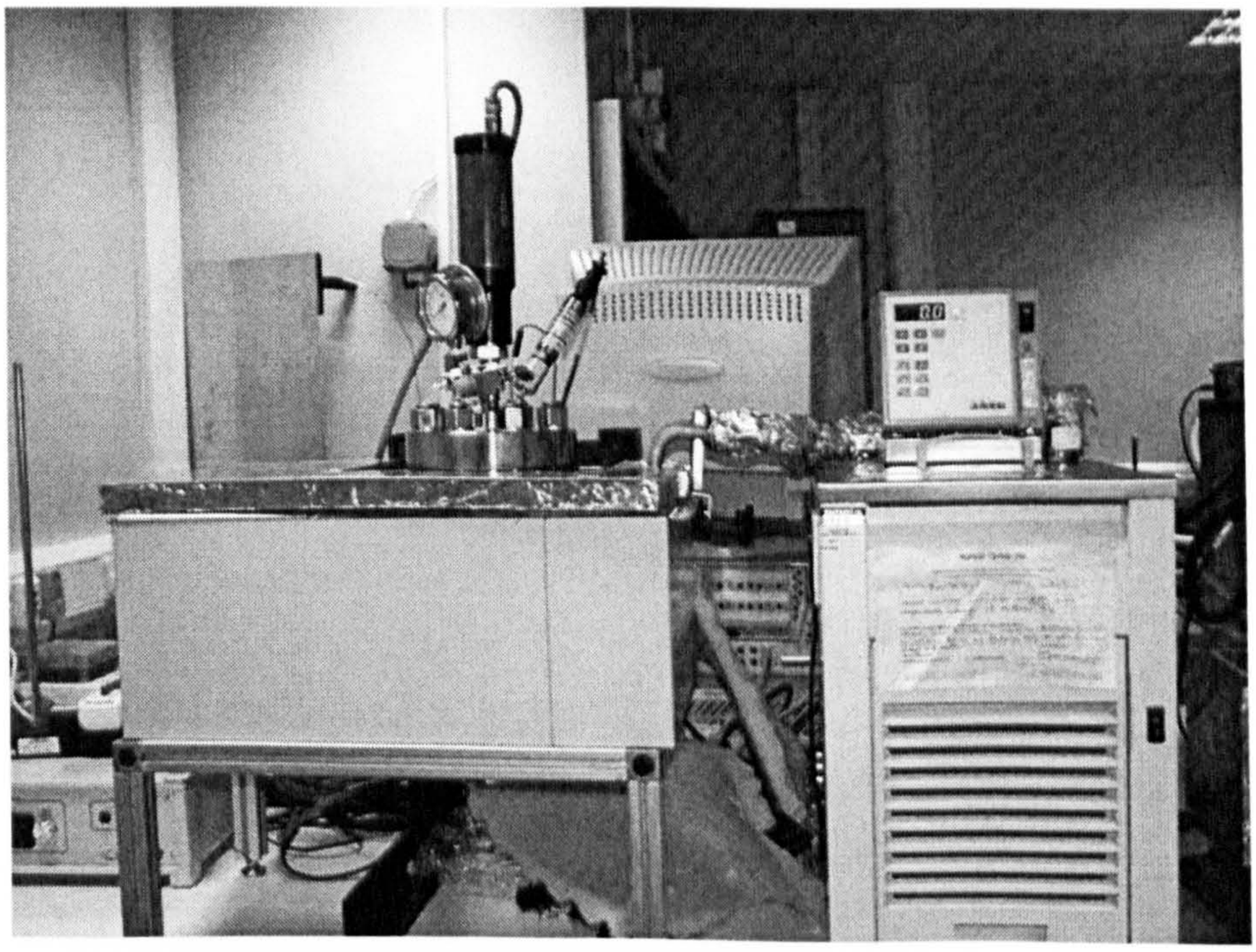

Figure 4.2. Hydrate Kinetic Rig 2 set up.

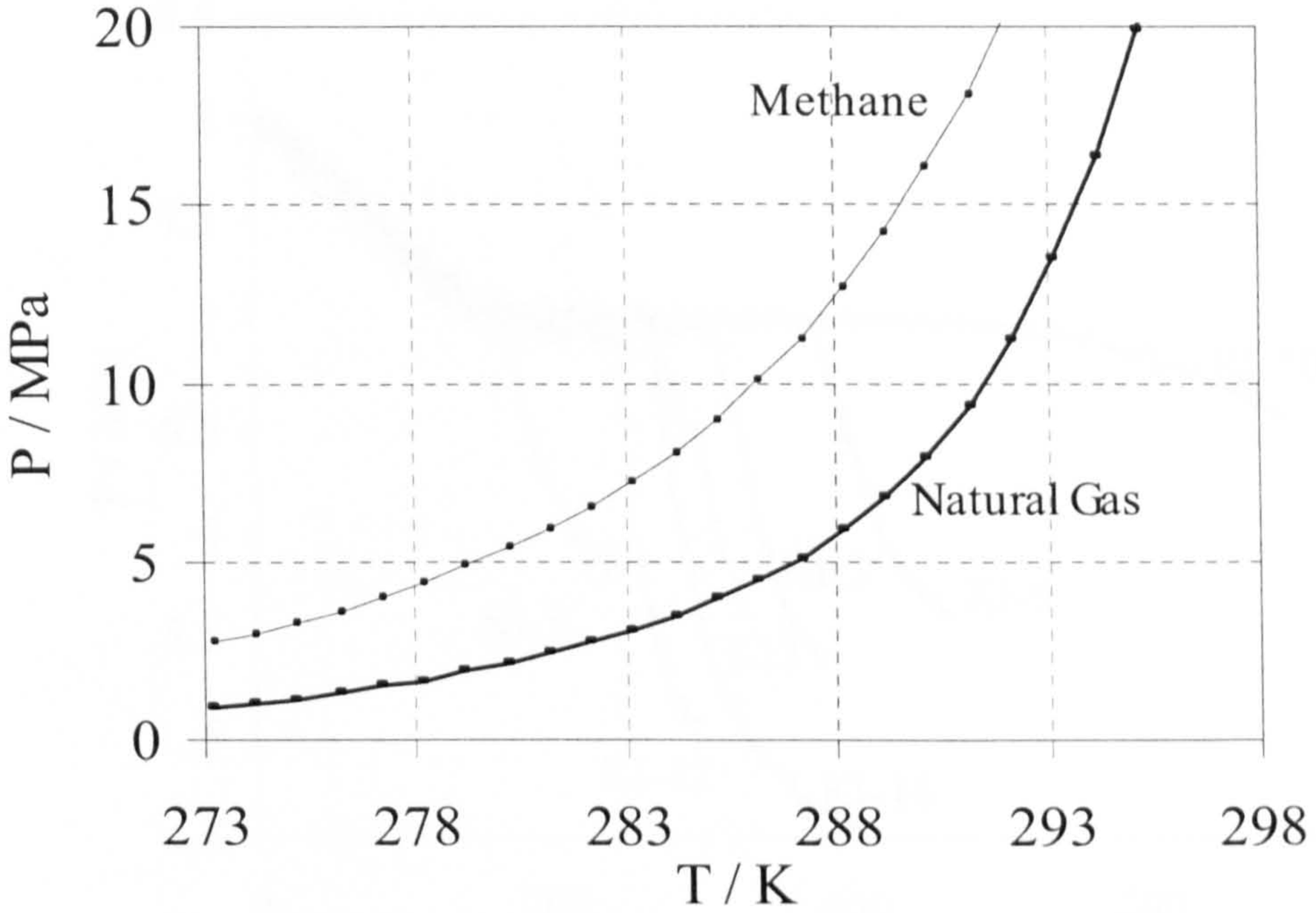

Figure 4.3. Methane and natural gas hydrate phase boundaries predicted by an in-house computer programme (HWHYD).

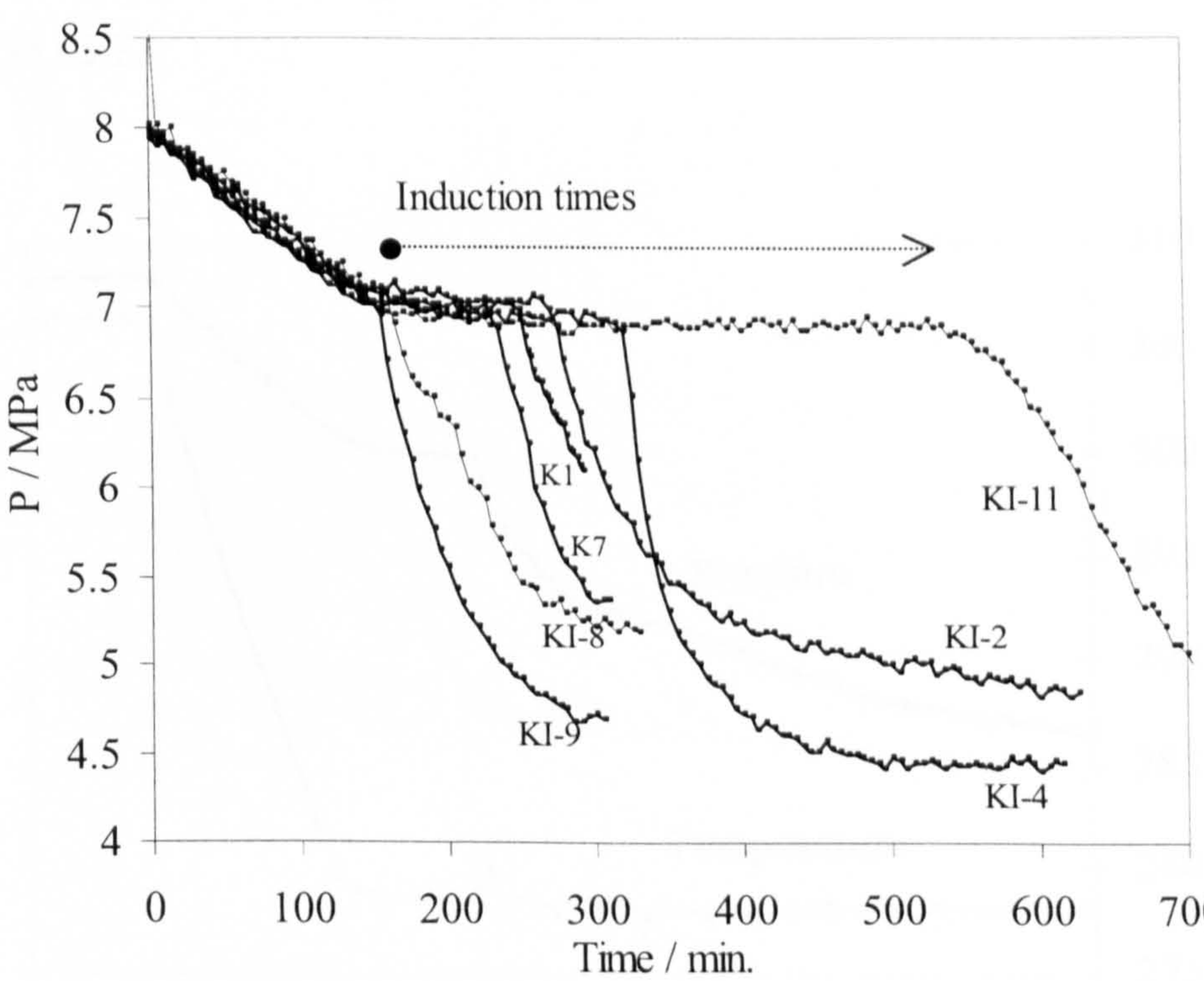

Figure 4.4. Pressure profiles of the experiments on 0.5 mass% different synthesised kinetic inhibitors in natural gas-water system. The tests stable temperatures were 278.35-278.65 K.

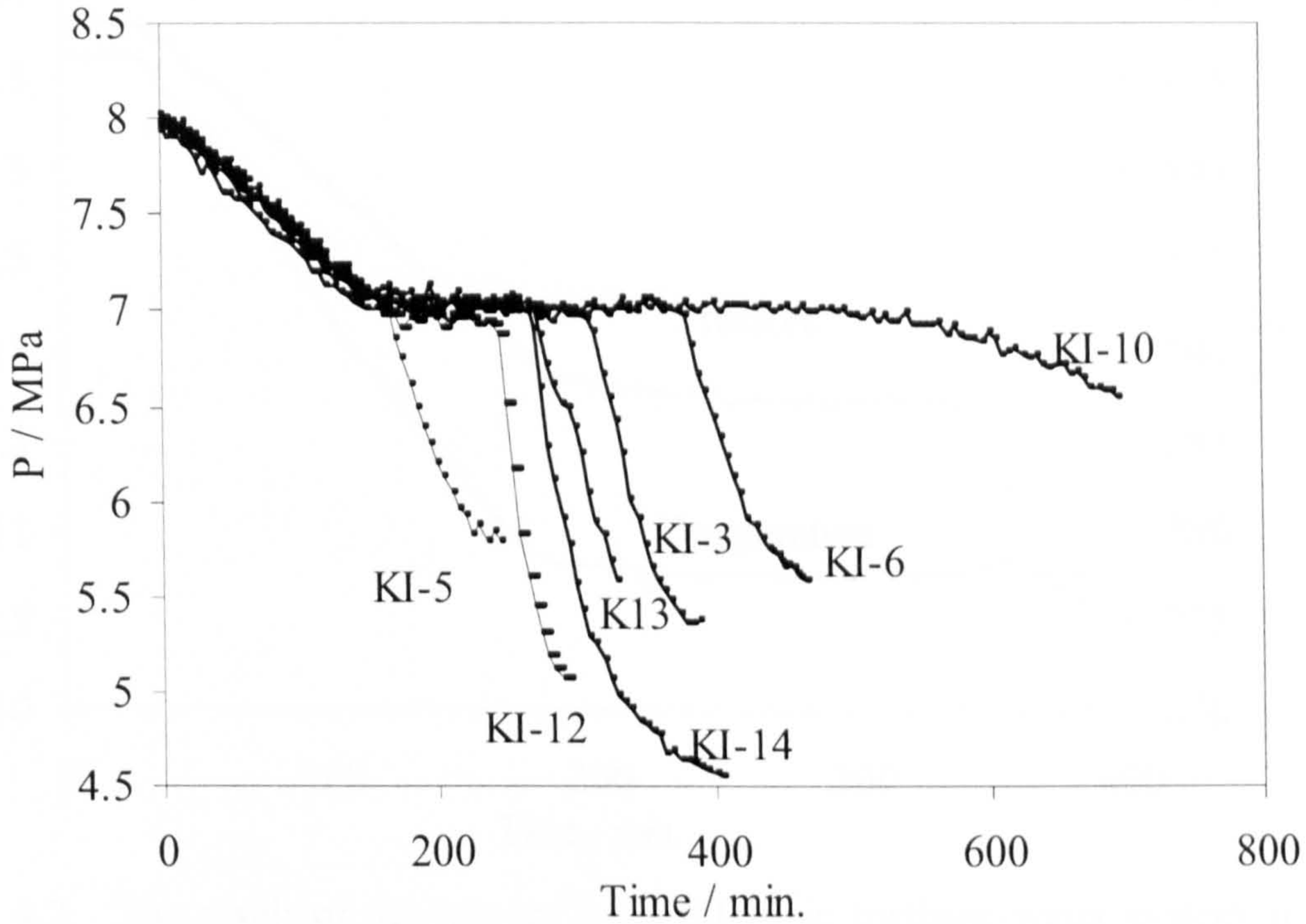

Figure 4.5. Pressure profiles of the experiments on 0.5 mass% different synthesised kinetic inhibitors in natural gas-water system. The tests stable temperatures were 278.35-278.65 K.

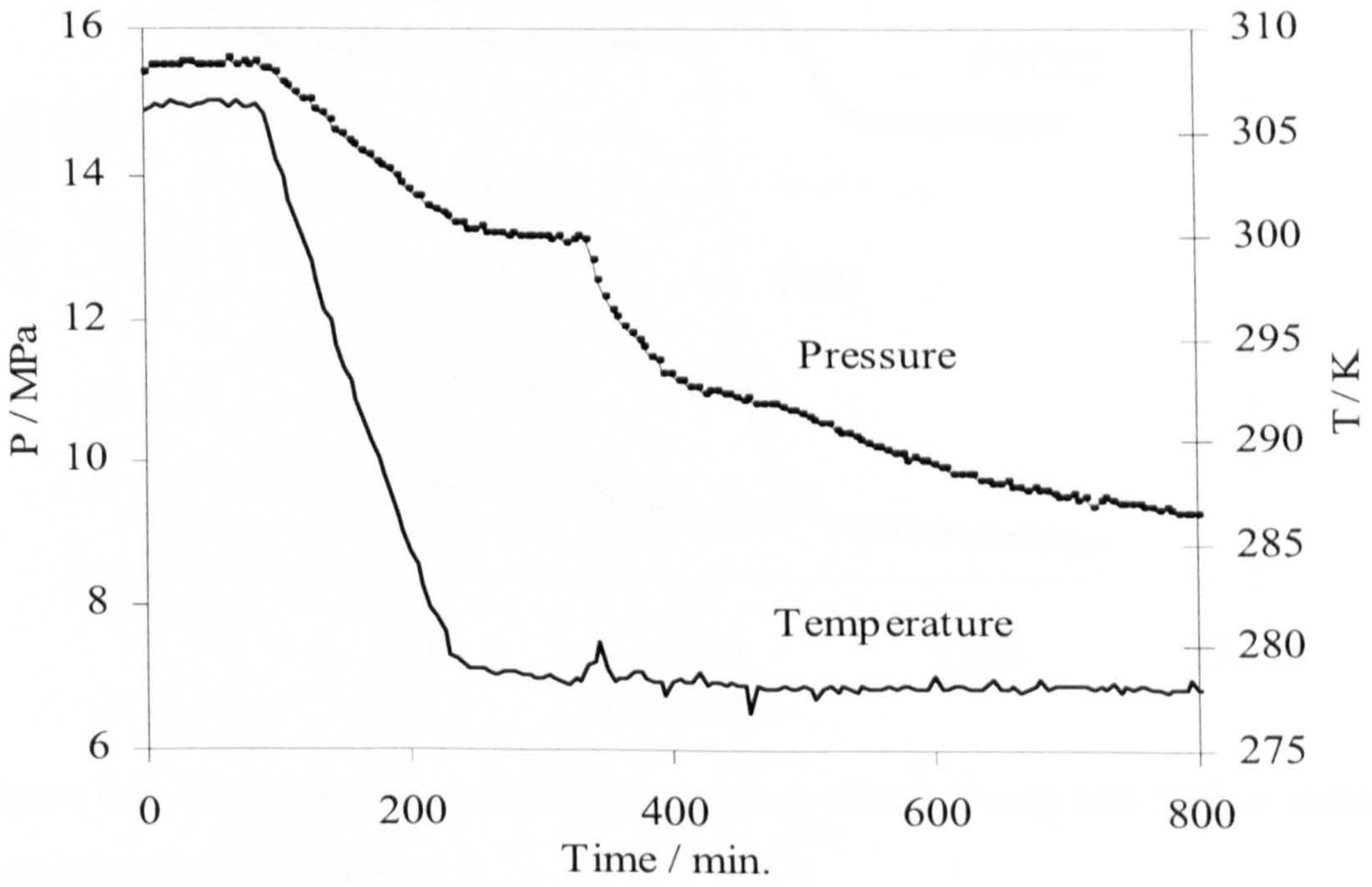

Figure 4.6. The result of the test on 0.5% KI-1 in methane-water system.

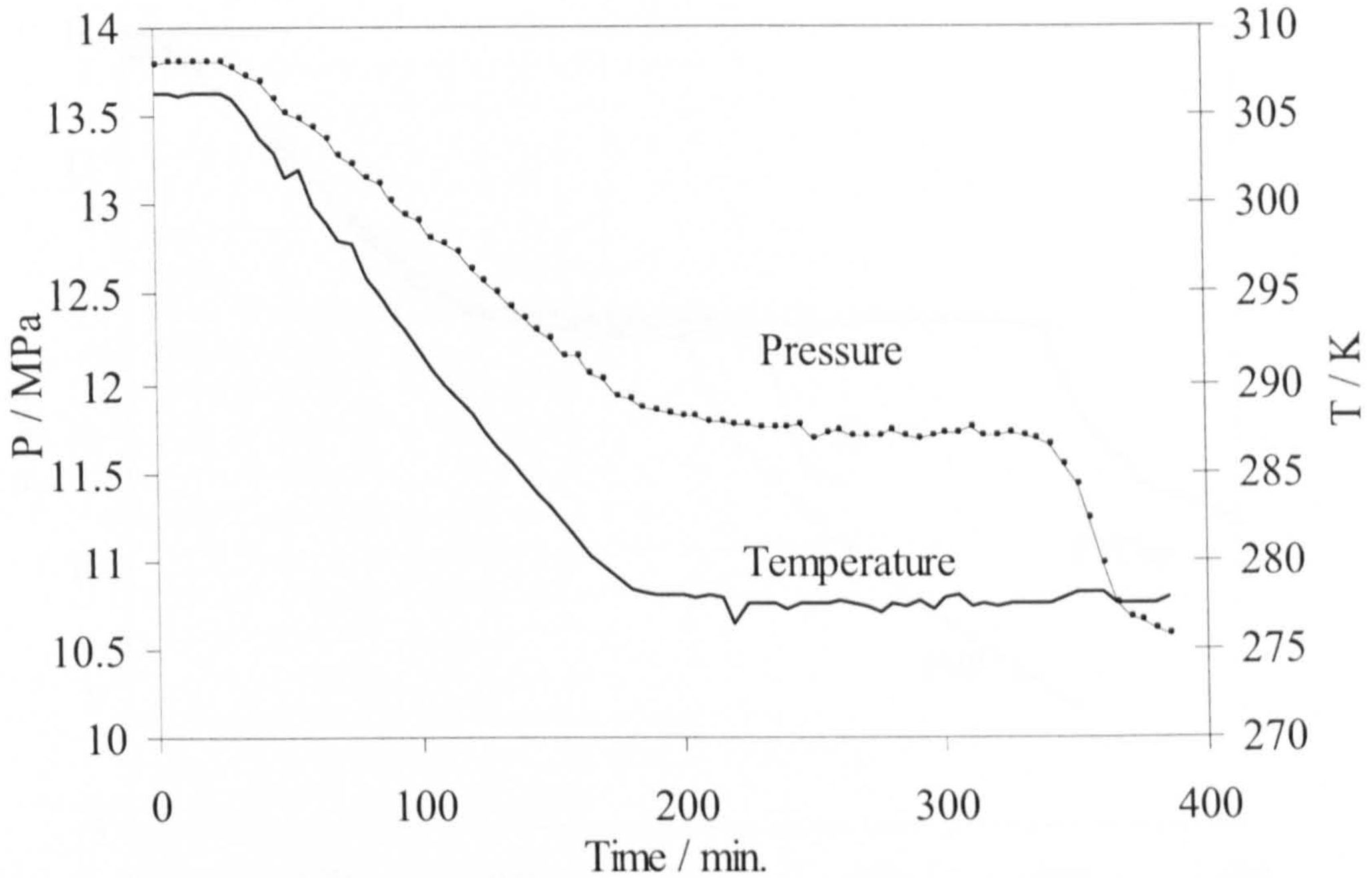

Figure 4.7. The result of the test on 0.5% KI-10 in methane-water system at 10 K subcooling.

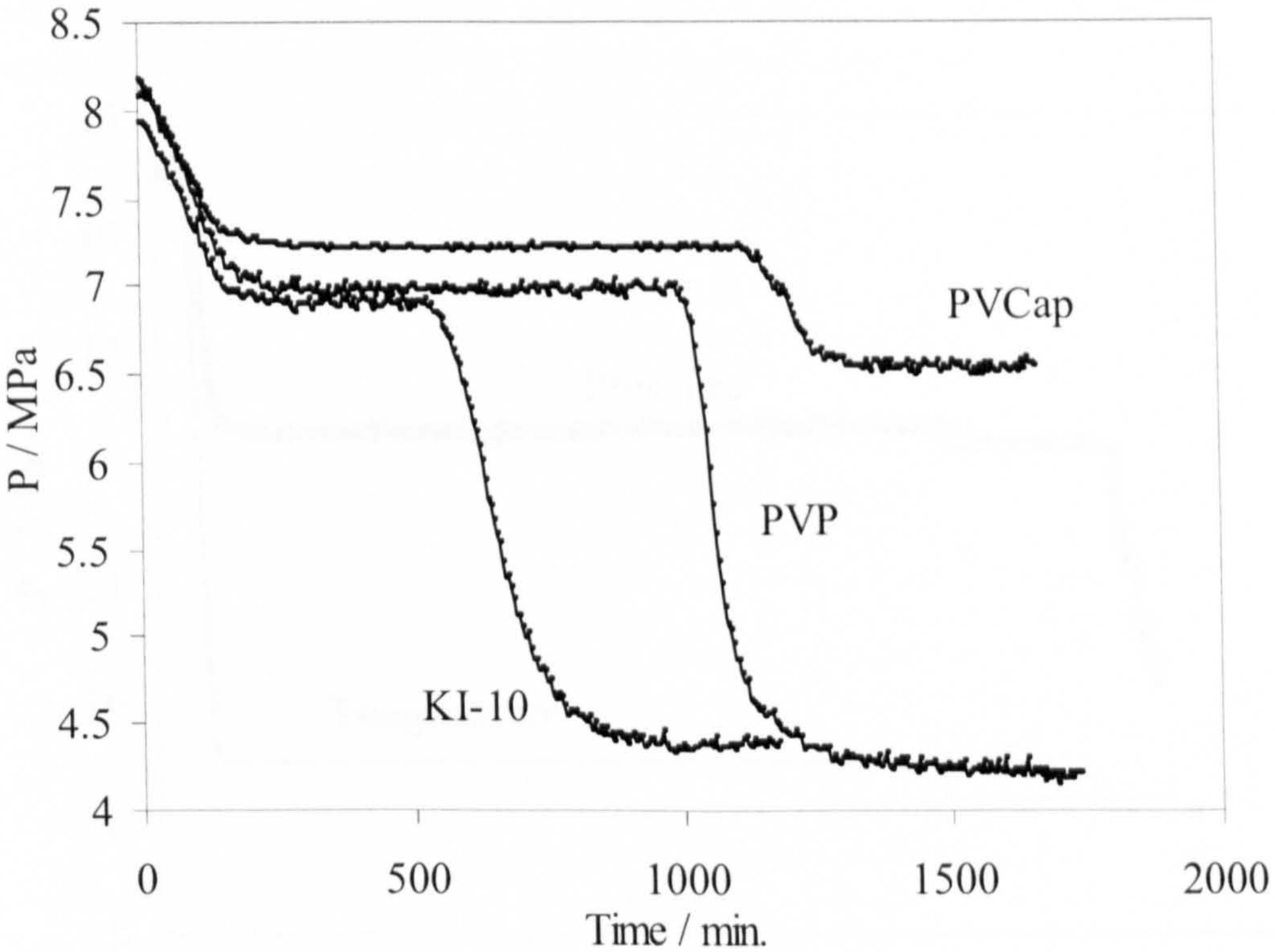

Figure 4.8. The pressure profiles of the tests on KI-10, Pvcap and PVP in Natural gas-water system (Table 4.4).

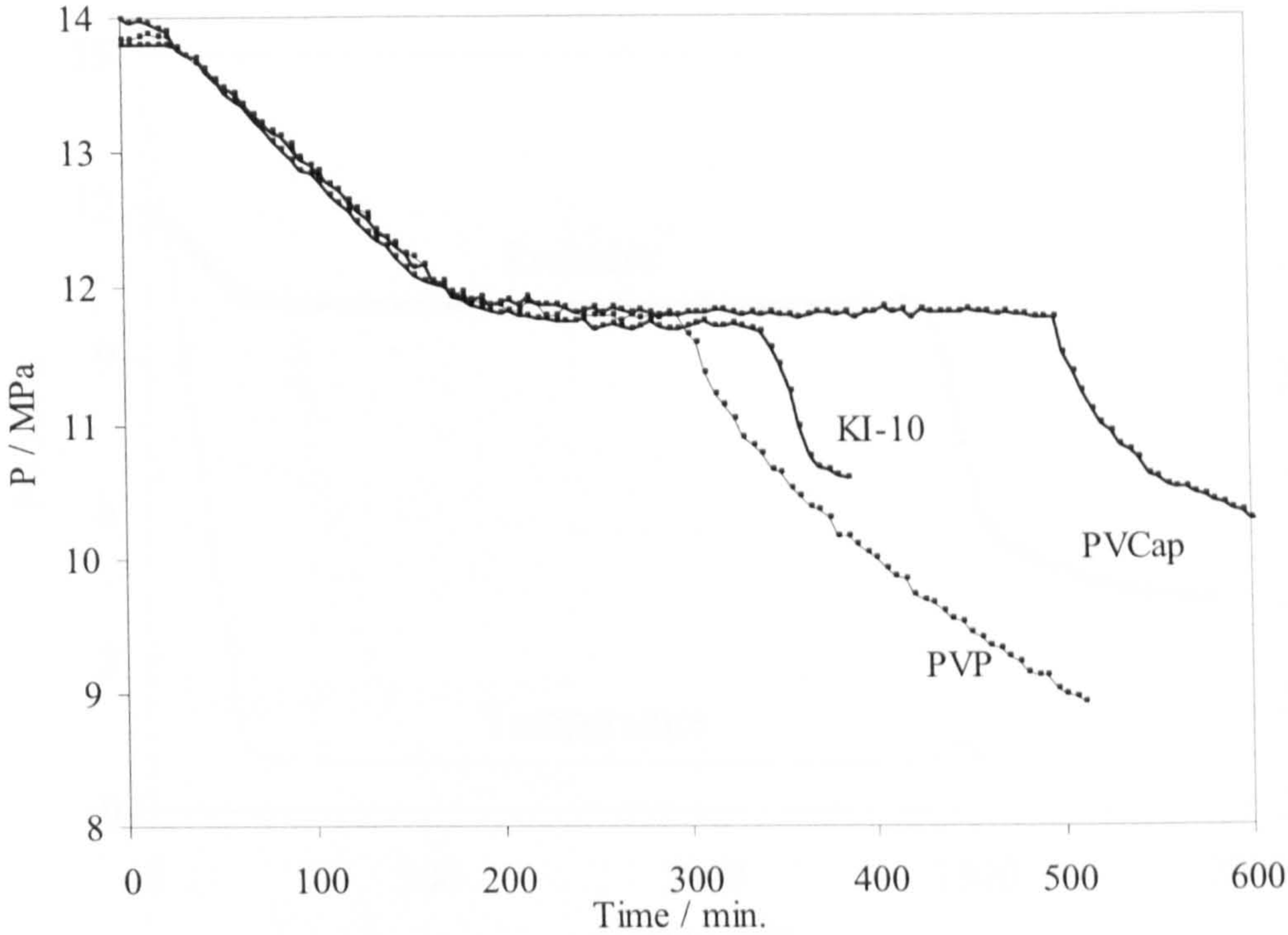

Figure 4.9. The pressure profiles of the tests on KI-10, PVCap and PVP in methane-water system (Table 4.5).

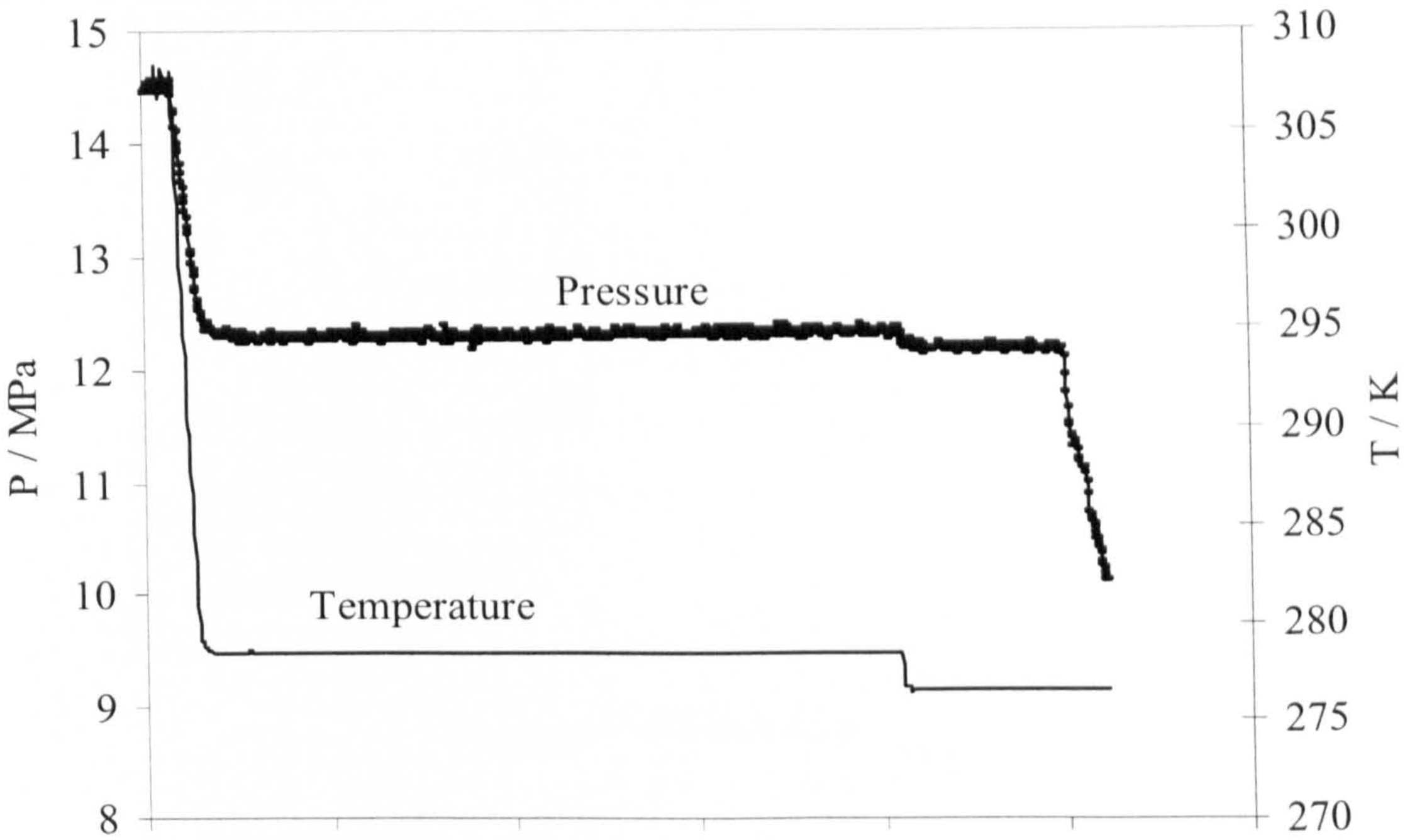

Figure 4.10. The result of the test on 1.5 mass% of KI-1 in methane-water system. An induction time of more than 60 hours at 9 K subcooling was observed.

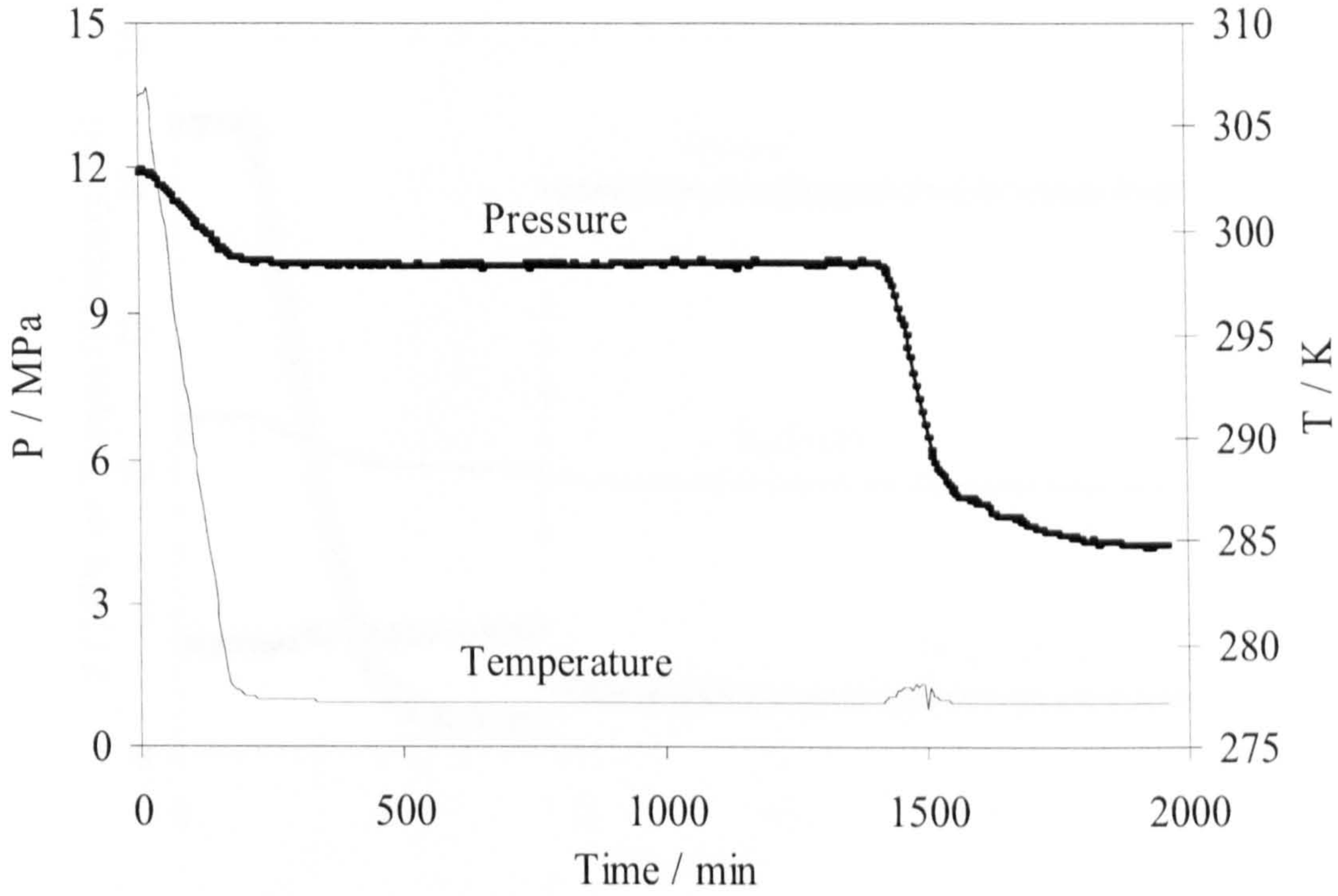

Figure 4.11. The result of test on 1mass% of KI-11 in natural gas-water system. An induction time of 20 hours at 14 K subcooling was observed.

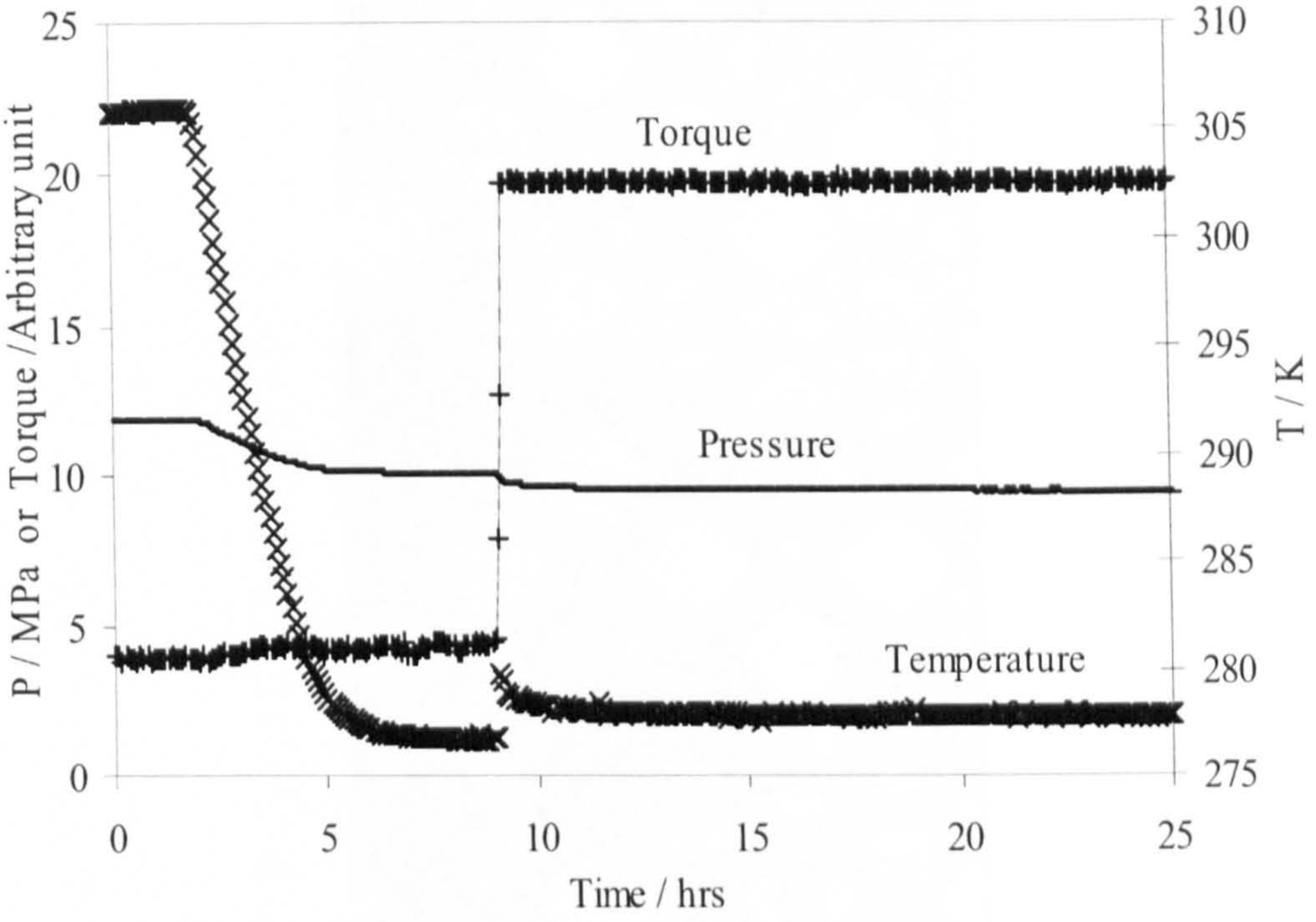

Figure 4.12. Pressure, temperature and torque profiles for blank test; water-condensate-natural gas. W/C=0.3 and 600 rpm.

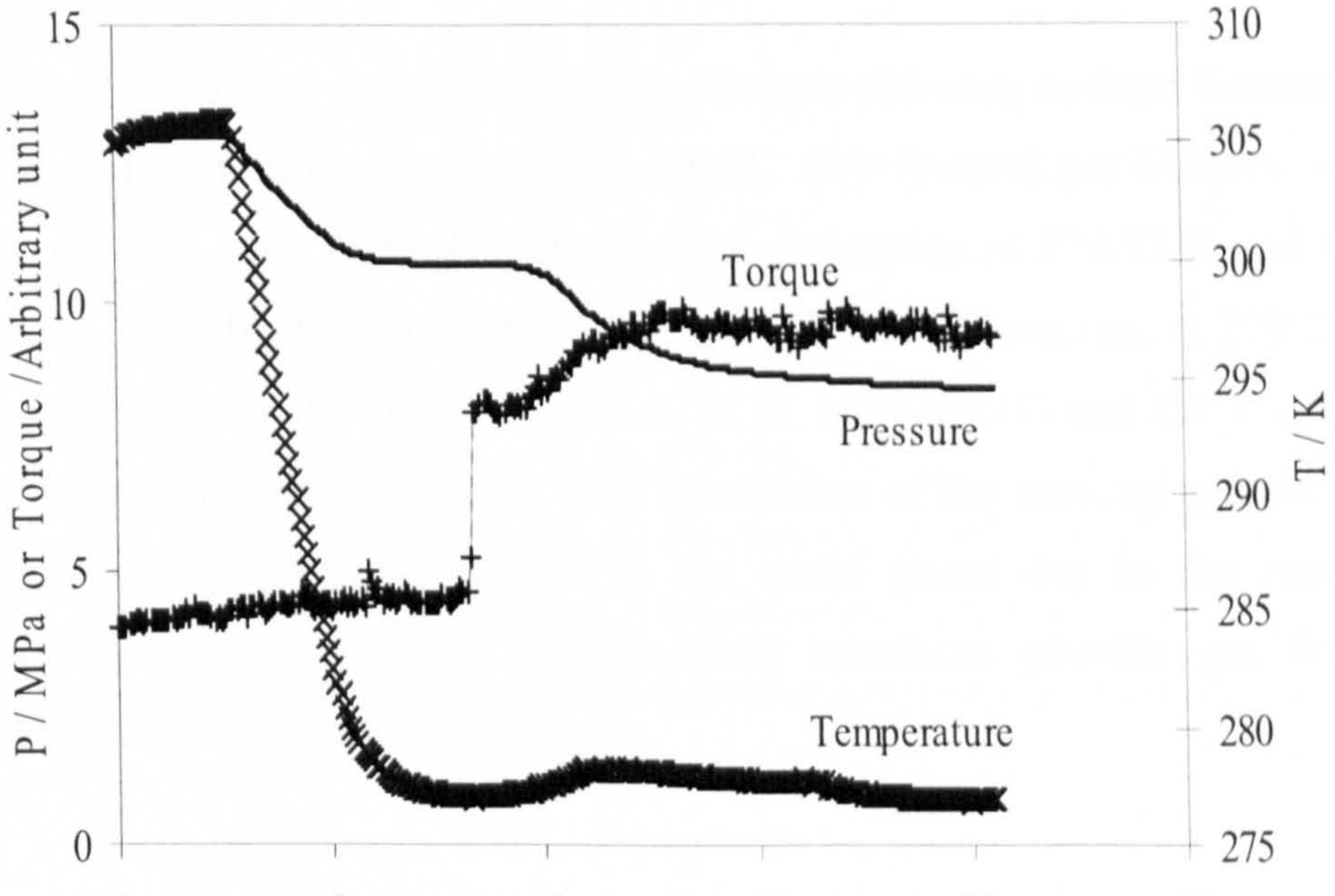

Figure 4.13. Pressure, temperature and torque profiles for the system of water-condensate-natural gas t in the presence of 1 mass% KI-11. W/C=0.3 and 600 rpm.

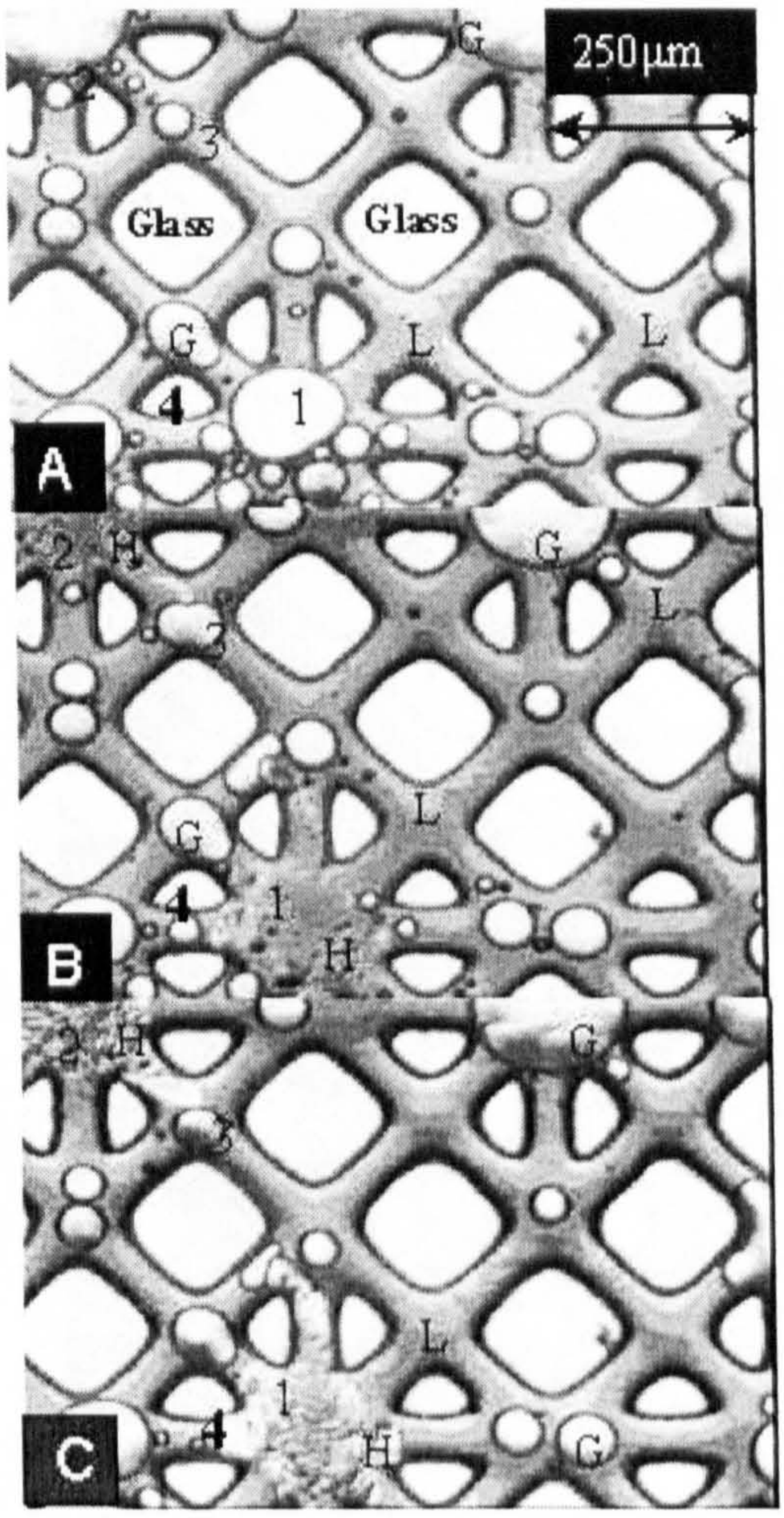

Figure 4.14. Natural gas and water system. Images showing hydrate formation in the micromodel. H = Hydrate, G = gas, L = liquid. (A): Natural gas bubbles in water at 291.55 K and 7.14 MPa, time=0. (B): Hydrate formation at 279.55 K and 6.96 MPa after 2 hours. (C): Hydrate growth 2 days after hydrate formation, at 279.25 K, 6.50 MPa. The numbers on the above images A, B, C, indicate: (1) and (2): Formation and growth of hydrate from gas bubbles. (3): Penetration of the moving hydrate front into the gas bubble. (4): Diffusion of gas in the water phase due to the concentration gradient between gas-water and hydrate-water interfaces provide gas for hydrate growth. The bubble is shrinking with time.

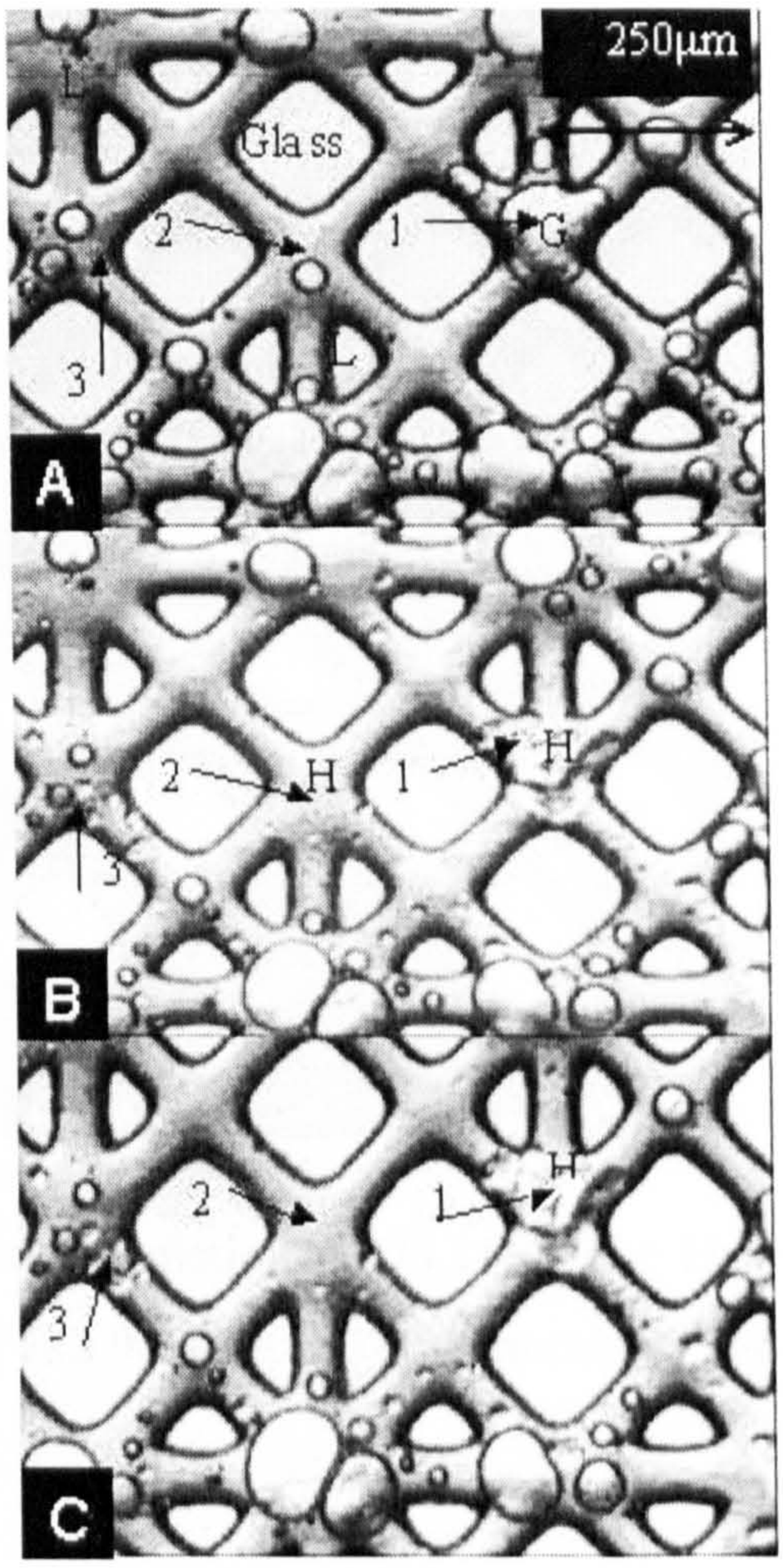

Figure 4.15. Natural gas and water in the presence of KI-11. Images showing hydrate formation in the micromodel. H = Hydrate, G = gas, L = liquid. (A): Natural gas bubbles in water+0.5mass% KI-11, at 291.25 K and 7.66 MPa, time=0. (B): Hydrate formation at 278.65 K and 7.53 MPa, after 22 hours. (C): Five days after hydrate formation, at 279.05 K, 7.26 MPa, there are no significant changes in the size of hydrate particles and gas bubbles, demonstrating the effect of KHI on the rate of hydrate growth. The numbers on the above images indicate: (1): Hydrate formation from gas bubble. (2) and (3) Hydrate formation from dissolved gas. The rates of dissolution of gas bubbles in water and hydrate particles growth are slow.

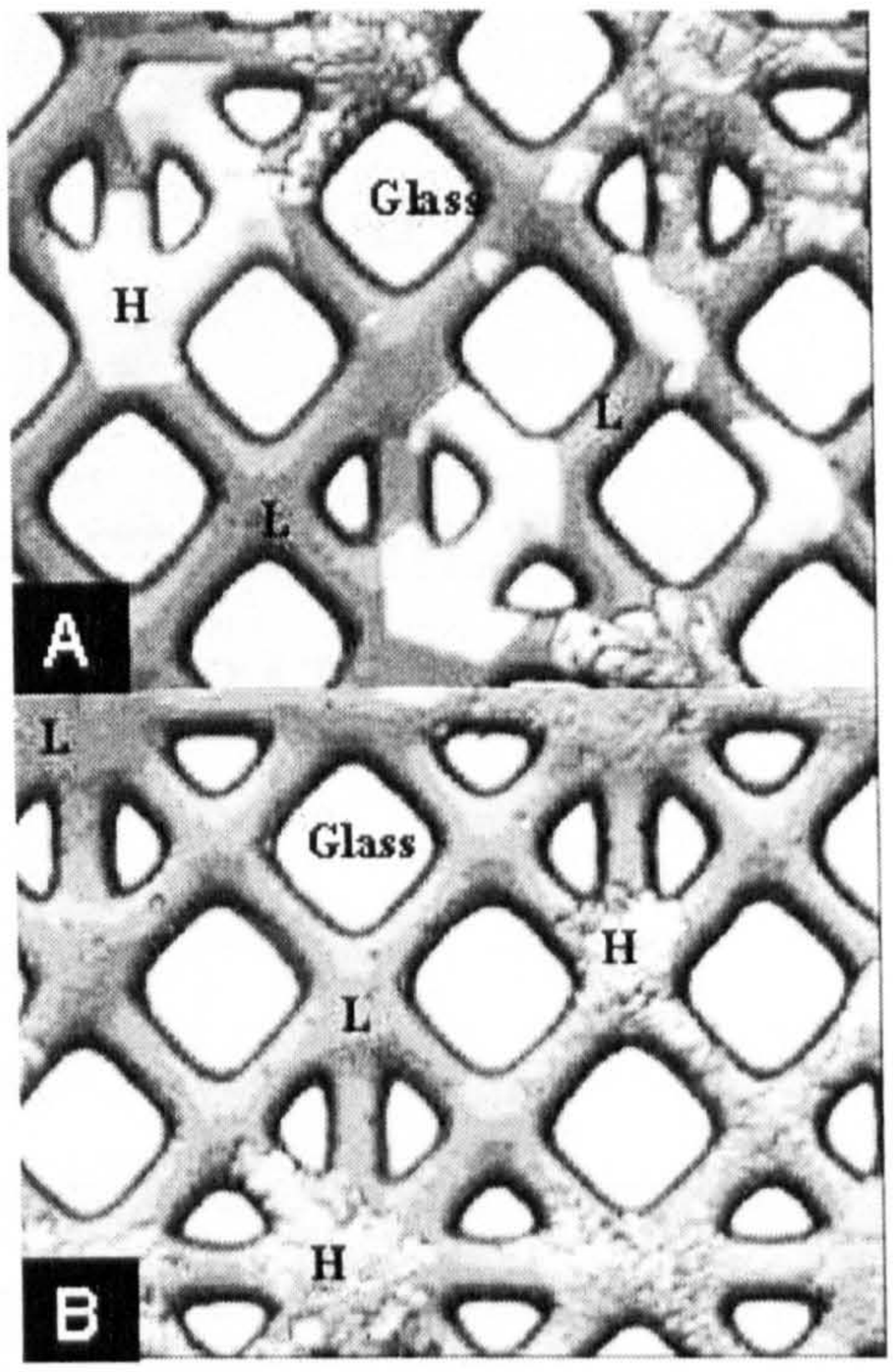

Figure 4.16. Massive hydrate formation at 274.15 K. H = Hydrate, G = gas, L = liquid. (A): Natural gas and water at 5.91 MPa. (B): : Natural gas and water in the presence of KI-11 at 7.36 MPa.

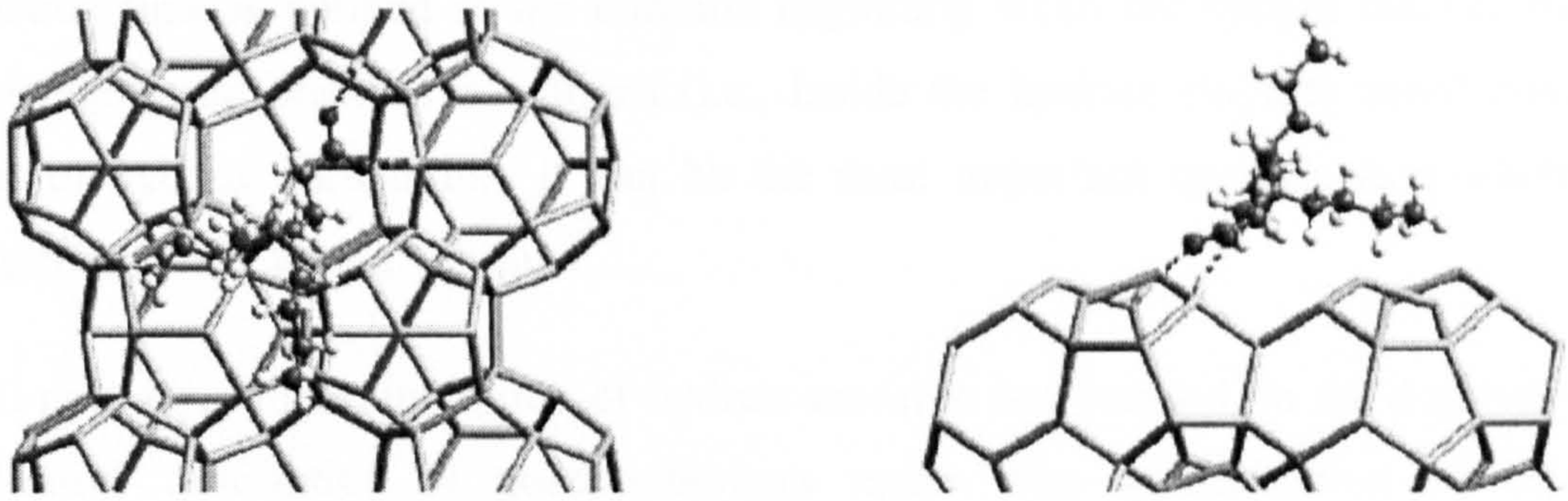

Figure 4.17.Top (left) and side (right) views of a zwitterionic LDI capping a large pothole on the static surface of a type II hydrate (Storr et al., 2002).

CHAPTER 5

PARAMETERS AFFECTING THE PERFORMANCE OF KINETIC HYDRATE INHIBITORS

5.1 INTRODUCTION

The hydrate formation process and growth is described through three different stages: nucleation (an induction period), a slow growth period prior to a final stage described by a catastrophic fast growth rate. It is speculated that the effect of a kinetic inhibitor is to interfere the nucleation process and/or prevent the crystal growth after its nucleation (Sloan, 1998, King, et al., 2000, Koh, et al., 2002, Storr, et al., 2002, Makogon, et al., 2002). Therefore, effective kinetic inhibitors should either delay/prevent hydrate nucleation, and/or delay the catastrophic growth of hydrates and provide a hydrate induction time exceeding the water residence time in the pipeline. In this work, the induction time is defined as the duration beginning when the system reaches the set temperature and pressure conditions (i.e., inside the hydrate stability zone) until the onset of hydrate formation. It can be the most important quantity to evaluate the performance of a kinetic inhibitor.

Until recently, kinetic inhibition of hydrate research has focused on the discovery and qualitative description of good inhibitors rather than quantification of inhibitor performance. Identification of the parameters affecting the performance of KHIs is not only useful in elucidation of inhibition mechanism by kinetic inhibitors but also is crucial for effective design, screening and deployment of them in deepwater applications.

The objective of this work is to investigate some of the influential parameters on the performance of kinetic hydrate inhibitors experimentally by application of a kinetic rig and a visual rig. In all the experiments either PVCap or PVCap in a solvent, Luvicap® (supplied by Clariant Oil Services), were used. The effect of shut-in versus flowing conditions, pressure, polymer molecular weight, the solvent and different gas hydrate structures on the performance of PVCap as one the most efficient kinetic hydrate

inhibitors (Cohen et al., 1998) have been investigated. In another part of the study the compatibility PVCap with other inhibitors such as a corrosion inhibitor was investigated. Finally, the effect of subzero conditions on the performance of PVCap has been studied. The details of test procedure in the kinetic rig and composition and phase boundary of the natural gas used in the experiments have been presented in Chapter 4.

5.2 EFFECT OF SHUT-IN VERSUS FLOWING CONDITIONS

It has been reported that shut-in / start up conditions in the pipelines are the worst case in terms of hydrate formation and blockage (Urdahl, et al., 1997, Rasch et al., 2001). However, the experiments for screening and evaluation of kinetic hydrate inhibitors are usually carried out at flowing (mixing) conditions.

In this work the above-mentioned issue was addressed by studying the performance of a commercial kinetic inhibitor at shut-in versus flowing conditions. The kinetic hydrate inhibitor Luvicap® consists of 40 mass percent of active polymer (PVCap) and 60 mass percent ethylene glycol as carrier fluid.

5.2.1 Kinetic Rig Experiments

Two sets of experiments were carried out in the kinetic rig (detailed in Chapter 3) on a natural gas (composition in Table 4.1) –water system in the presence of 2.5 mass% Luvicap® (equivalent to 1mass% PVCap). The tests conducted at two different pressure ranges and at mixing and static conditions. The results of the tests are summarised in Table 5.1. As presented in Table 5.1 the first test carried out at 9.3 MPa and 14.1 K subcooling with a mixing rate of 600 rpm and 46 hour induction time was achieved by the kinetic inhibitor. The test was repeated with the same conditions in the absence of mixing and the induction time was decreased to 4 hours (Test No.2). The third test was conducted at 8.7 MPa and 12.8 K subcooling in the presence of mixing and the induction time appeared to be 80 hours. However in the absence of the mixing the induction time was 4 hours (Test No.4). The pressure profiles of the experiments are illustrated in Figure 5.1 for comparison. The experimental results showed that the induction time for shut-in case was shorter than that of flow conditions.

5.2.2 Experiments in High Pressure Visual Rig

The above results are contrary to the usual trend in hydrate work which normally shows hydrate formation is both delayed, in terms of induction time, and less efficient, in terms of the time required to reach equilibrium, when the test fluids are not mixed. As

the experimental rig used for these tests has no visual capabilities it was decided to utilise a high-pressure visual rig (The tests in the visual rig were carried out by Mr. Rod Burgass, which is gratefully acknowledged) to further investigate the observed behaviour. The high-pressure visual rig allows observations and capturing of both still and moving pictures.

A schematic of the experimental rig is shown in Figure 5.2. It is comprised of a high-pressure cylinder fitted with sapphire windows at both ends. The cell can be used at pressures up to 51.7 MPa and at temperatures between 245.15 and 325.15 K. The cell temperature is controlled by circulating water from a heater/chiller through an inbuilt jacket. A platinum resistance temperature probe monitors the cell temperature. The pressure of the cell is monitored by a strain gauge pressure transducer connected to the cell via a high-pressure line. The accuracy of the temperature and pressure measurement are ±0.1 K and ±0.03 MPa, respectively. A computer is used to log the cell pressure and temperature. The cell is mounted on a rocking mechanism in order to give mixing when required.

The hydrate formation in the presence of natural gas and two different solutions were studied: a) pure water b) 2.5 mass% Luvicap® (containing 1 mass% active polymer PVCap) in water. All the tests were conducted at static conditions. In the tests 50 ml of the liquid was injected into the cell and then natural gas was injected to the desired start point pressure. The cell was mixed to equilibrate the contents and then held in a horizontal position in order to make visual observations with the aid of a magnifying camera.

In the first test distilled water was used and the initial pressure was set to 13.1 MPa at 307.45 K. The temperature was then lowered at a constant rate to 277.25 K over a 12 hour period, and it was left at this temperature for the duration of the test (50 hours). The pressure profile of the test is shown in Figure 5.3. The pressure drop during the test was little (0.2 MPa within 48 hours) indicating small amount of hydrate formation. Hydrates were seen to form at the gas/water interface. During the test the bulk of the water phase remained hydrate free with only a few needle type hydrate crystals growing into it from the gas/water interface.

In the second test exactly the same procedure was followed but with 2.5 mass% Luvicap® present, the starting pressure was 13.0 MPa (Figure 5.3). In the presence of kinetic inhibitor, after cooling down the system to 277.25 K, the pressure drop over the

time was much greater (4 MPa within 20 hours) than the previous test, indicating much more hydrates formation. Hydrates initially were seen to form at the gas/water interface and on the cell walls in the vapour phase. Hydrates forming at the gas/water interface are shown in Figure 5.4. These hydrates then appeared to dissociate and hydrate formation was seen to take place in the upper part of the cell. The water phase appeared to be drawn upwards leaving no water in the lower part of the cell. Figures 5.5 through 5.7 show the sequence of events. This sequence of events was seen to happen over a period of around 20 minutes commencing at the time when the cell temperature was reduced to 4.1°C. There was no great pressure drop (about 0.3 MPa) during this time indicating that the amount of gas bonded in hydrates was small although the mass appeared significant. During the next 20 hours, hydrate formation continued and more bulk and more solid looking masses of hydrate formed.

The observations in visual cell show that at static conditions and in the presence of Luvicap®, the mechanism of hydrate growth is different with that of natural-water system. The results of above experiments in the kinetic rig and visual rig denote the importance of mixing on the performance of the commercial kinetic inhibitor used in this study in delaying the hydrate formation. In testing KHIs for field application, both static and flow conditions need to be considered.

5.3 EFFECT OF HYDRATE STRUCTURE

Studying the performance of kinetic hydrate inhibitors in different hydrate structures is important for two reasons. Firstly, as mentioned in Chapter 4 (Section 4.3.2) while in most of the oil and gas fields structure II hydrate is likely to form, in some gas fields (e.g. Nuggets gas field in North sea), because of high concentration of methane (>98%) in the gas mixture structure I hydrate is dominant and the performance of kinetic inhibitors in other hydrate structures becomes important. Secondly, it helps understanding the hydrate inhibition mechanism by the kinetic inhibitors. For example the results of molecular dynamic simulation have shown that some kinetic inhibitors interact with large cages of structure II hydrate (Storr et al. 2004). It was speculated that some kinetic inhibitors perform better in systems with s-II hydrates than s-I. In Chapter 4 (Section 4.3.3), the performances of three hydrate kinetic inhibitors were studied in a series of experiments in a natural gas (s-II) and methane (s-I) systems. The data showed that all the three inhibitors performed better in the natural gas system than that in methane system at a similar degree of subcooling and temperature range (Tables

4.4 and 4.5). However, in those tests, the effect of pressure was not excluded since at the same degree of subcooling in the two mentioned systems the pressures are different.

In this study, using an in house hydrate model (HWHYD, detailed in Chapter 2), two systems were designed in such a way that they have very similar hydrate phase boundaries while different hydrate structures will form at the same pressure and temperature conditions. Therefore the two systems can be tested at same degrees of subcooling and at the same temperature and pressure conditions. The mixtures of methane-ethane was selected as structure I hydrate former and methane-propane as structure II hydrate former. Using HWHYD, the composition of the gas mixtures were selected to be C_1 (97 mol%)-C_3 (3 mol%) for sII hydrate former and C_1 (68.6 mol%)-C_2 (31.4 mol%) for sI hydrate former. The phase boundaries of the two gas mixtures are presented in Figure 5.8. At any pressure, the temperature differences between two phase boundaries are between 0.2-0.3 K. The type of hydrate structure, which is dominant in the presence of the above mentioned gas mixtures were tested against the experimental hydrate dissociation data available in the literature.

The experimental hydrate dissociation data for a gas mixture containing of 97.4 mol% methane and 2.6 mol% propane reported by Deaton and Frost (Deaton and Frost, 1946) is shown in Figure 5.9. The hydrate phase boundaries for above mentioned gas mixture assuming structure I and structure II hydrate were predicted by the HWHYD model and have been shown in Figure 5.9 along with the experimental dissociation data. As can be seen in Figure 5.9 only prediction with structure II fits the experimental data, which denotes that the gas mixture forms structure II hydrate. Propane is known as a sII hydrate former, therefore a mixture of 3% propane and 97% methane, which used in the experiments (Figure 5.8), and is richer in propane than the above-mentioned gas mixture, certainly forms structure II hydrates. Figure 5.10 illustrates experimental hydrate dissociation data for a gas mixture containing of 56.4 mol% methane and 45.6 mol% ethane (Deaton and Frost, 1946) along with the predictions for hydrate phase boundaries with assumption of structure I and II hydrates. As can be seen in Figure 5.10 only structure I hydrate fits the experimental data. This shows that the gas mixture forms structure I hydrate. A mixture of C_1 (68.6 mol%)-C_2 (31.4 mol%), which was used for the experiments in this work also forms structure I hydrate because of higher concentration of methane (sI hydrate former) in comparison with mentioned C_1-C_2 gas mixture.

A solution of 2.5 mass% Luvicap® (containing 1 mass% PVCap) in water was prepared and tested with the above gas mixtures to measure the induction times at similar conditions using a kinetic rig (detailed in Chapter 4). The results of the tests have been summarised in Tables 5.2 and 5.3. The tests in both systems carried out at the pressure range close to 9.7 MPa. From Table 5.2 it can be seen that for sII hydrate former system, at 17.9-18.7 K subcooling, the induction times is about 30-16 hours. However in sI hydrate former system (Table 5.3) at the same pressure range, the inhibitor was not able to prevent hydrate formation even at lower degrees of subcooling (15.1-17 K). At 14.5 K subcooling only 1.5 hours induction time was observed (Test No.3-4). The results of the experiments show that gas composition or hydrate structure has a significant effect on the performance of PVCAP. It was speculated that the lactam ring of PVCAP has a better steric fit into the $5^{12}6^4$ cavities in the sII hydrate structure (Makogon, 1997).

5.4 EFFECT OF PRESSURE

As new oil production developments are moving toward deepwater, the operating pressure is expected to increase considerably. The higher operating pressures of deepwater operations have increased the concerns over pressure effect on the performance of kinetic inhibitors. It has been reported that for certain kinetic inhibitors the absolute pressure has a negative impact on performance. The effect was less pronounced at pressures lower than 9 MPa but was quite dramatic at pressures between 9 and 20 MPa (Svartaas et al. 2000). A different result was reported by Rasch and her coworkers (Rasch et al. 2002). They evaluated a kinetic inhibitor (labelled as EC6481A), which contained a low molecular weight polyvinyl caprolactam polymer and various synergistic additives for enhancing its performance. Their experiments carried out on a saline water (containing 2.5 mass% KI)-synthetic natural gas system at different pressures in the range of 7-15.2 MPa and similar degrees of subcooling. No indication of pressure influence on the performance of kinetic inhibitor was reported. However the experiments (at 7 MPa), with visual information available, showed that hydrates were formed even if the tests were classified as "no hydrate" in the system based on pressure and temperature measurements. Fu and his coworkers (Fu et. al. 2002) reported that in their experiments on some kinetic hydrate inhibitors (not disclosed) an increase in the system pressure did not lead to a decrease in the performance so long as the degree of subcooling was within the effective range of the selected KHI. They also mentioned that it remains unknown whether a noticeable

effect could exist at pressures greater than 20 MPa. They added the information is lacking because of the rareness of high-pressure test equipment.

In this study the effect of the pressure on the performance of PVCap with and without a synergist chemical in inhibition of natural gas hydrate formation is investigated. Two series of experiments carried out in the kinetic rig. In the first series of tests the induction times for hydrate formation in the presence of 1 mass% PVCap (2.5 mass% Luvicap®) in water and natural gas were measured at similar degrees of subcooling and different pressures. The results of the experiments have been summarized in Table 5.4. The results show that at 11.1 K subcooling and 10.82 MPa induction times longer than 30 hours were achieved by the kinetic inhibitor (Tests No.1-2). However by increasing the pressure to17.48 MPa at the same degree of subcooling (11.1 K) the induction time was decreased to 3.5 hours and at higher pressure of 24.34 MPa no induction time was observed (Tests No.3-5).

In the second series of the experiments the effect of pressure on the performance of PVCap in the presence of a synergistic chemical was studied. Tetra Butyl Ammonium Bromide (TBAB) was selected as synergist. Previously, TBAB was reported as hydrate anti-agglomerant (Klomp et. al. 1995). It has also been reported by several sources that an addition of anti-agglomerant improves hydrate inhibition characteristics (Pakulski 1998, Peiffer et al., 1999, Lovell and Pakulski 2002). The synergistic effect of TBAB on KHIs has been patented (Duncum et al, 1996). In the tests 0.5 mass% PVCap and 0.5 mass% TBAB in water was used in the presence of natural gas. The results of the tests are presented in Table5.5. By comparing the results the synergistic effect of TBAB on PVCap is clear. For example 1 mass% of PVCap is not able to inhibit hydrate formation in a system of natural gas-water at 24.34 MPa and 11.1 K (Table 5.4, Tests No.4-5) while 0.5 mass% PVCap and 0.5 mass% TBAB at similar pressure and higher degree of subcooling (13.5 K) inhibit hydrate formation for 7-8 hours (Table 5.5, Tests No.5-6). The negative impact of pressure on the performance of the PVCap in the presence of synergist has been shown in Table 5.5. At pressure range of 8.6-8.8 MPa and 14-17 K subcooling the system induction times are generally longer than 30 hours (Tests No.1-3), while at higher pressure range of 31.9-32.4 MPa even at lower degrees of subcooling (12-13.5 K) the induction times are shorter than 20 hours (Tests No.7-8). The above results demonstrate the negative impact of pressure on the performance of PVCap in the presence and absence of a synergist.

5.5 EFFECT OF POLYMER MOLECULAR WEIGHT AND SOLVENT

Interactions between a polymer and the solvent influence polymer chain dimensions (i.e., conformations). When the polymers are dissolved in a solution due to their large number of carbon atoms bonded together forming a long chain, they can generally adopt a lot of conformations. Synthetic polymers particularly, can display a large number of possible conformations which gives considerable flexibility to the macromolecules, and due to this flexibility, the chains do not adopt a linear form in solution, but a very characteristic conformation, known as *random coil*. The shape or magnitude of the random coil would depend not only on the type of solvent employed, but also on the temperature, and the molecular weight. The polymer-solvent interactions play an important role in this case, and its magnitude, from a thermodynamic point of view, will be given by the solvent quality. Thus, a good solvent is one whose solubility parameter (defined as $\delta = (\Delta E/V)^{1/2}$, where, ΔE is Heat of vaporization and V is molar volume) is similar to that of the polymer, the attraction forces between chain segments are smaller than the polymer-solvent interactions; the random coil adopts then, an unfolded conformation. In a poor solvent, the polymer-solvent interactions are not favoured, and therefore attraction forces between the chains predominate, hence the random coil adopts a tight and contracted conformation (Challa, 1993).

In adsorption theory, the mechanism of hydrate prevention by kinetic inhibitors is explained by adsorption of kinetic inhibitor on the surface of hydrate (Makogon et al. 1997). In that context, the polymer conformation in water is speculated to play a role on the performance of kinetic inhibitor.

In this work the effects of two parameters, which affect the polymer conformation in solution; polymer molecular weight and polymer solvent, on the performance of the PVCap as a kinetic hydrate inhibitor are investigated.

Three PVCap polymers with different molecular weights (5000, 50000, and 1000000) were supplied by BASF. To compare the performance of the inhibitors, the induction times for hydrate formation in a system containing 1 mass% of each of the PVCaps in water in the presence of natural gas was measured. The tests carried out in mixing conditions (600 rpm) in the pressure range of 9.5-10.6 MPa. The results of the tests are presented in Table 5.6. As shown in Table 5.6, PVCap with low molecular weight (5000) could prevent hydrate formation for more than 20 hours at 14-14.9 K subcooling (Tests No.1-2). However at similar pressure conditions and lower degrees of

subcooling (15.6-15.9 K) there was no induction time in the presence of PVCap with medium molecular weight (Tests No.3-4). In order to achieve induction time longer than 20 hours the subcooling was needed to be reduced to 12.7 K (Test No.5). The PVCap with high molecular weight (1000000) failed to prevent hydrate formation even at 11.7 K subcooling (Tests No.7-8).

The above results show that the performance of PVCap as hydrate inhibitor decreases with increasing its molecular weight. Because higher molecular weight of polymer is associated with longer length of polymer chain it is likely that it adopts random coil shape in the solution and provides less active sites to interact with hydrate nuclei.

In another series of experiments the effect of ethylene glycol as PVCap solvent/carrier fluid on its performance was studied. A total of four experiments carried out in the kinetic rig with 1 mass% pure dried PVCap polymer and 2.5 mass% Luvicap® (containing 60 mass% ethylene glycol and 40 mass% PVCap) at similar conditions. The results of the tests are summarised in Table 5.7 and the pressure profiles of the tests are presented in Figure 5.11. The experiments carried out at the pressure range of 10 MPa and 12.9-13.3 K degrees of subcooling. As shown in Table 5.7 and Figure 5.11 the induction times before catastrophic growth of hydrate are similar, however in the presence of 1.5 mass% ethylene glycol the rate of slow growth is slightly higher compared to dry polymer tests. The results of the tests suggest that low concentrations of ethylene glycol as a solvent does not have a significant effect on hydrate inhibition.

5.6 COMPATIBILITY WITH OTHER INHIBITORS

In deepwater oil and gas exploration and production operations, hydrate, wax, scale and corrosion are four important flow assurance concerns. Specialty chemicals, including low dosage oilfield corrosion, scale, wax and hydrate inhibitors may be used to overcome these problems to some extend. However, compatibility of various chemicals is an important issue, when using two or more chemicals, as the interaction among chemicals may influence chemical performance and in some cases exacerbate at least one of the undesirable phenomena. Therefore, it is necessary to examine the performance of each chemical in the presence of other chemical that may be used under operating conditions. For example, it has been shown that different scale inhibitors improve the performance of PVCap based kinetic hydrate inhibitors (Masoudi and Tohidi, 2005). However the interaction is not always synergistic and the balance between competitive and synergistic effects can be difficult to predict.

Some corrosion inhibitors are reported to interfere with LDHIs (Frostman et al., 2003), however no experimental evidences have been reported. In this study the effect of a commercial corrosion inhibitor (labelled as Corrtreat 799, and provided by Clariant Oil Services) on the performance of Luvicap® (40 mass% PVCap and 60 mass% ethylene glycol), in terms of induction time was investigated. A total of six experiments carried out in a kinetic rig in different testing conditions in the presence of natural gas-water and mixture of above-mentioned inhibitors. In the tests a solution of 1 mass% PVCap and 500 ppm (as suggested by Clariant Oil Services) of the above corrosion inhibitor in water was used. The summary of the tests is presented in Table 5.8. As shown in Table 5.8, the tests conducted in pressure range of 7.0-7.3 MPa. The first two experiments conducted in the absence of corrosion inhibitor on natural gas-water-1 mass% PVCap system at 11.6-11.8 K subcooling (Tests No.1-2). The induction times were found to be longer than one day. In the subsequent experiments the same system with addition of 500 ppm of corrosion inhibitor was tested at similar conditions. In the presence of corrosion inhibitor and at 11.2-11.5 K degrees of subcooling, the induction times were less than 5 hours (Tests No.3-4). In order to achieve longer induction times than one day, the degree of subcooling was needed to be decreased to less than 10.7 K (Tests No.5-6). The temperature and pressure profiles of Test No.2 (in the absence of corrosion inhibitor) and Test No.4 (in the presence of corrosion inhibitor) are shown in Figures 12 and 13, respectively. The results of the above experiments show the negative impact of corrosion inhibitor tested in this study, on the performance of PVCap.

5.7 THE PERFORMANCE OF KHI IN SUBZERO CONDITIONS

Onshore pipelines could be subjected to subzero conditions; hence thermodynamic and/or kinetic hydrate inhibitors are needed to prevent hydrate and ice formation. In this study the inhibition effect of PVCap in natural gas-water system below the ice point was evaluated. In order to prevent ice formation, and providing similar degrees of subcooling at the same pressure range but different temperatures, ethylene glycol (20 mass% on the free water basis) was added to the system. It should be mentioned that methanol was not used for this purpose as it has been reported to have adverse effect on the performance of PVCap (Sloan et al, 1998).

The presence of ethylene glycol was taken into account in calculation of degrees of subcooling (Figure 5.14) in the experiments. A total of four tests were conducted in a kinetic rig charged with natural gas and a solution of 20 mass% ethylene glycol and 1

mass% PVCap in water. The tests carried out in a pressure range of 9-9.6 MPa at different degrees of subcooling. The results of the tests have been summarised in Table 5.9. As shown in the table, the experiments were started with test at 271.85 K and 9.0 MPa (13.4 K subcooling) where induction time longer than 30 hours was observed (Test No.1). In the subsequent tests the degree of subcooling was increased step by step to 15.5 K, where no induction time was observed.

For comparing the performance of PVCap at subzero and above ice point conditions, an experiment was conducted on a natural gas-water system in the presence of 2.5 mass% Luvicap® (1 mass% PVCap and 1.5 mass% EG) at 277.35 K and 9.0 MPa (13.3 K subcooling). The test pressure and subcooling were similar to Test No.1 of Table 5.9 (20 % EG), but different temperature (above ice point). The pressure profiles of the mentioned experiments and Tests No.1-2 of Table 5.9 have been shown in Figure 5.15 for comparison. As shown in Figure 5.15, at similar degrees of subcooling (13.3-13.4 K), in the presence of 20 mass% EG, longer induction time and lower rate of growth compared to 1.5 mass% EG are observed. Similar pressure profile was observed by increasing the subcooling to 15 K. The results show that 20 mass% ethylene glycol has a positive effect on the performance of PVCap and subzero conditions does not have any significant adverse effect on the performance of PVCap.

5.8 CONCLUSIONS

The experimental results detailed above demonstrated the effect of different factors such mixing conditions, gas hydrate structure, pressure, and corrosion inhibitor on the performance of kinetic hydrate inhibitors.

Mixing / flowing condition versus shut-in condition appeared to improve the performance of PVCap as in mixing condition the hydrate could only form in the gas/water interface and bulk of liquid. However, in static conditions the micro porous hydrate structure formed in the interface could stick to the wall and grew in the gas phase by sucking up the water into the gas phase, which lead to shorter induction times.

The effect of gas hydrate structure on the performance of PVCap at same pressure and degree of subcooling was studied. Two gas mixtures (one sI and the other sII hydrate formers) were designed and used in the experiments in such a way that similar temperature and pressure conditions in the tests lead to similar degrees of subcooling for sI and sII hydrate systems. The results of the tests revealed that PVCap is more

successful in inhibiting structure II hydrates compared to inhibition in structure I hydrates.

The impact of pressure on the performance of PVCap in the presence and absence of a synergist (TBAB) at similar degrees of subcooling was studied. It was shown that for both cases pressure decreases the efficacy of the KHI and/or synergist tested. PVCaps with different molecular weights were tested and it was shown that low molecular weight polymers perform superior to medium and high molecular weights polymers in preventing gas hydrate formation.

The experiment on dried PVCap polymer in the presence and absence of low concentration of ethylene glycol (1.5%) as polymer solvent/carrier fluid revealed that ethylene glycol has not significant effect on the performance of PVCap.

The compatibility of PVCap with a commercial corrosion inhibitor was studied. The result of the experiments showed the adverse effect of the tested corrosion inhibitor on the performance of PVCap.

Finally the performance of PVCap at subzero conditions in the presence of ethylene glycol (20%) was evaluated and compared with its performance at above ice point conditions. The results showed that PVCap can inhibit hydrate formation at subzero conditions in the presence of ethylene glycol and 20 % ethylene glycol improves its performance.

5.9. TABLES

Table 5.1. Induction times in natural gas-water system in the presence of 1 mass% PVCap, with and without mixing.

Test	Mixing	Testing Conditions		Subcooling	Induction Time
No.	**rate / rpm**	**T / K**	**P / MPa**	**/ K**	**/ hours**
1	600	277.05	9.3	14.1	46
2	0	277.25	9.5	14	4
3	600	277.85	8.7	12.8	80
4	0	277.95	8.8	12.7	4

Table 5.2. The results of the tests on 1mass% PVCAP in water in the presence of 97 mole % methane and 3 mole% propane.

Test	Mixing	Testing Conditions		Subcooling	Induction Time
No.	**rate / rpm**	**T / K**	**P / MPa**	**/ K**	**/ hours**
1	600	274.15	9.9	17.9	30
2	600	273.95	9.7	18.1	26
3	600	273.35	9.7	18.7	16

Table 5.3. The results of the tests on 1mass% PVCAP in water in the presence of 68.6 mole% methane and 31.4 mole% ethane.

Test	Mixing	Testing Conditions		Subcooling	Induction Time
No.	**rate / rpm**	**T / K**	**P / MPa**	**/ K**	**/ hours**
1	600	275.05	9.7	17.0	0
2	600	276.95	9.7	15.1	0
3	600	277.35	9.7	14.7	1.5
4	600	277.35	9.7	14.7	1.5

Table 5.4. The performance of 1mass% PVCAP in water in the presence of natural gas at similar degrees of subcooling and different pressures.

Test	Mixing	Testing Conditions		Subcooling	Induction Time
No.	**rate / rpm**	**T / K**	**P / MPa**	**/ K**	**/ hours**
1	600	280.9	10.82	11.1	>30
2	600	281.0	10.86	11.0	42
3	600	283.4	17.48	11.1	3.5
4	600	285.2	24.34	11.1	0
5	600	285.2	24.34	11.1	0

Table 5.5. The performance of 0.5 mass% PVCap in the presence of 0.5 mass% TBAB in a natural gas-water system at different pressures.

Test	Mixing	Testing Conditions		Subcooling	Induction Time
No.	rate / rpm	T / K	P / MPa	/ K	/ hours
1	600	276.85	8.82	14.1	>32
2	600	275.35	8.72	15.5	>40
3	600	273.75	8.62	17.0	>40
4	600	284.05	25.16	12.6	13
5	600	283.05	24.82	13.5	8.3
6	600	283.05	24.82	13.5	7.5
7	600	286.15	32.40	12	18
8	600	284.45	31.92	13.5	5

Table 5.6. The performance of PVCap with different molecular weights (1 mass%) in the presence of natural gas-water system and at 600 rpm mixing rate.

Test	PVCap	Testing Conditions		Subcooling	Induction Time
No.	MW	T / K	P / MPa	/ K	/ hours
1	5000	276.75	10.62	14.9	21
2	5000	277.65	10.62	14.0	25
3	50000	277.55	10.24	13.9	0
4	50000	277.85	10.27	13.6	0
5	50000	278.75	10.27	12.7	>30
6	1000000	278.15	9.55	12.9	0
7	1000000	279.35	9.55	11.7	0
8	1000000	279.35	9.55	11.7	0

Table 5.7. The performance of pure dried PVCap (1 mass%) in the presence and absence of ethylene glycol as solvent in natural gas-water system and at 600 rpm mixing rate.

Test	Ethylene	Testing Conditions		Subcooling	Induction Time
No.	Glycol%	T / K	P / MPa	/ K	/ hours
1	0	278.15	10.1	13.1	26
2	0	277.95	10	13.3	28
3	1.5	278.35	10	12.9	28
4	1.5	278.05	10	13.2	27

Table 5.8. The impact of corrosion inhibitor (500 ppm of Corrtreat 799) on the performance of PVCap (1 mass%) in the presence of natural gas-water system and at 600 rpm mixing rate.

Test	Corrosion Inhibitor	Testing Conditions		Subcooling	Induction Time
No.	Conc./ppm	T / K	P / MPa	/ K	/ hours
1	0	278.15	7.34	11.6	>24
2	0	277.95	7.34	11.8	>30
3	500	278.15	7.20	11.5	2
4	500	278.45	7.10	11.2	5
5	500	279.05	7.00	10.6	>36
6	500	279.15	7.15	10.5	>36

Table 5.9. The performance of PVCap (1 mass%) at subzero conditions in the presence of natural gas-water system and at 600 rpm mixing rate. Ethylene glycol was added to prevent ice formation.

Test	Ethylene	Testing Conditions		Subcooling	Induction Time
No.	Glycol%	T / K	P / MPa	/ K	/ hours
1	20	271.65	9.0	13.4	>30
2	20	270.15	9.2	15	>30
3	20	269.95	9.0	15.1	>20
4	20	269.85	9.6	15.5	0

5.10. FIGURES

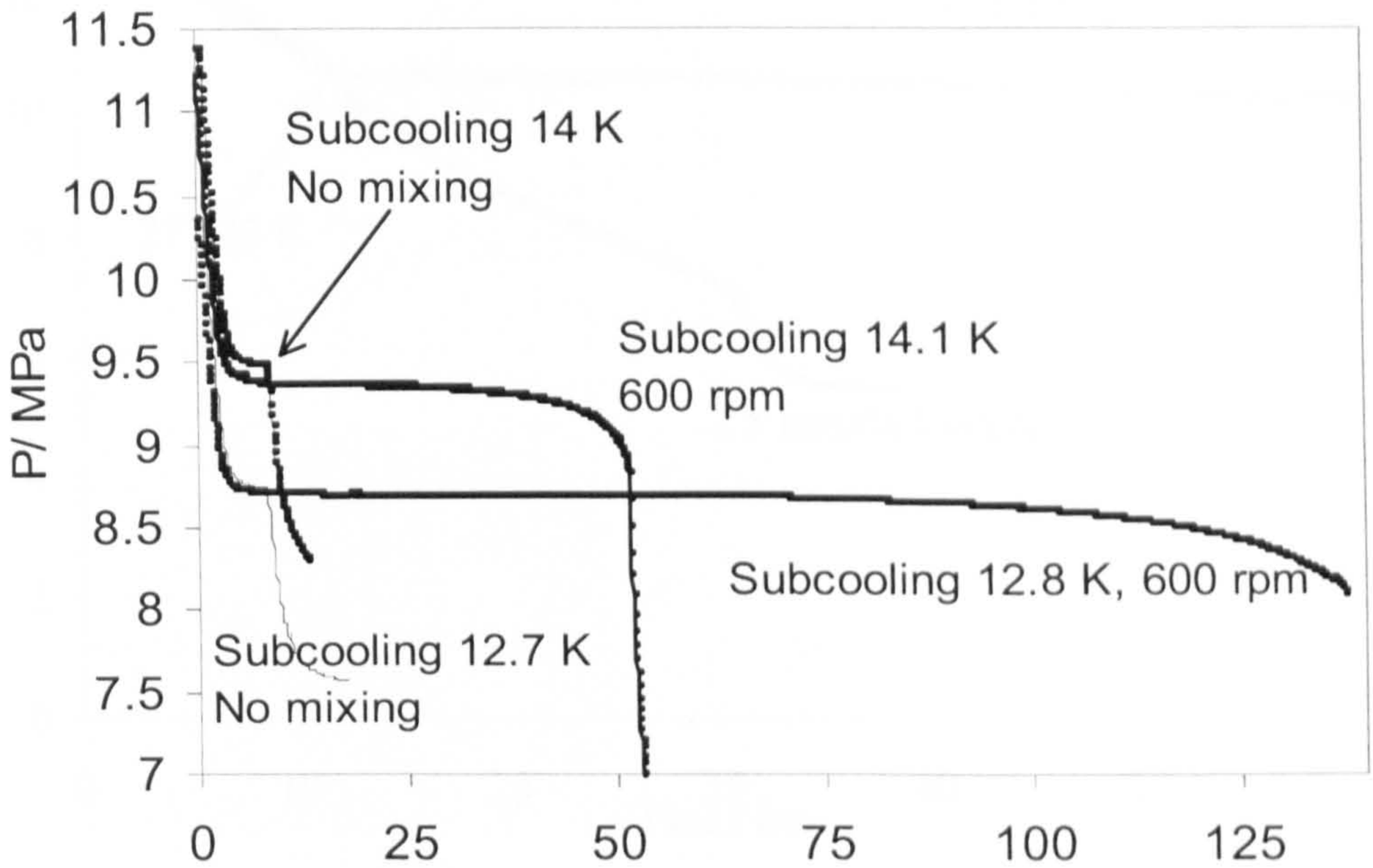

Figure 5.1. Pressure profiles of the experiments on natural gas-water-2.5 mass% Luvicap® system. The summary of the tests is in Table5.1.

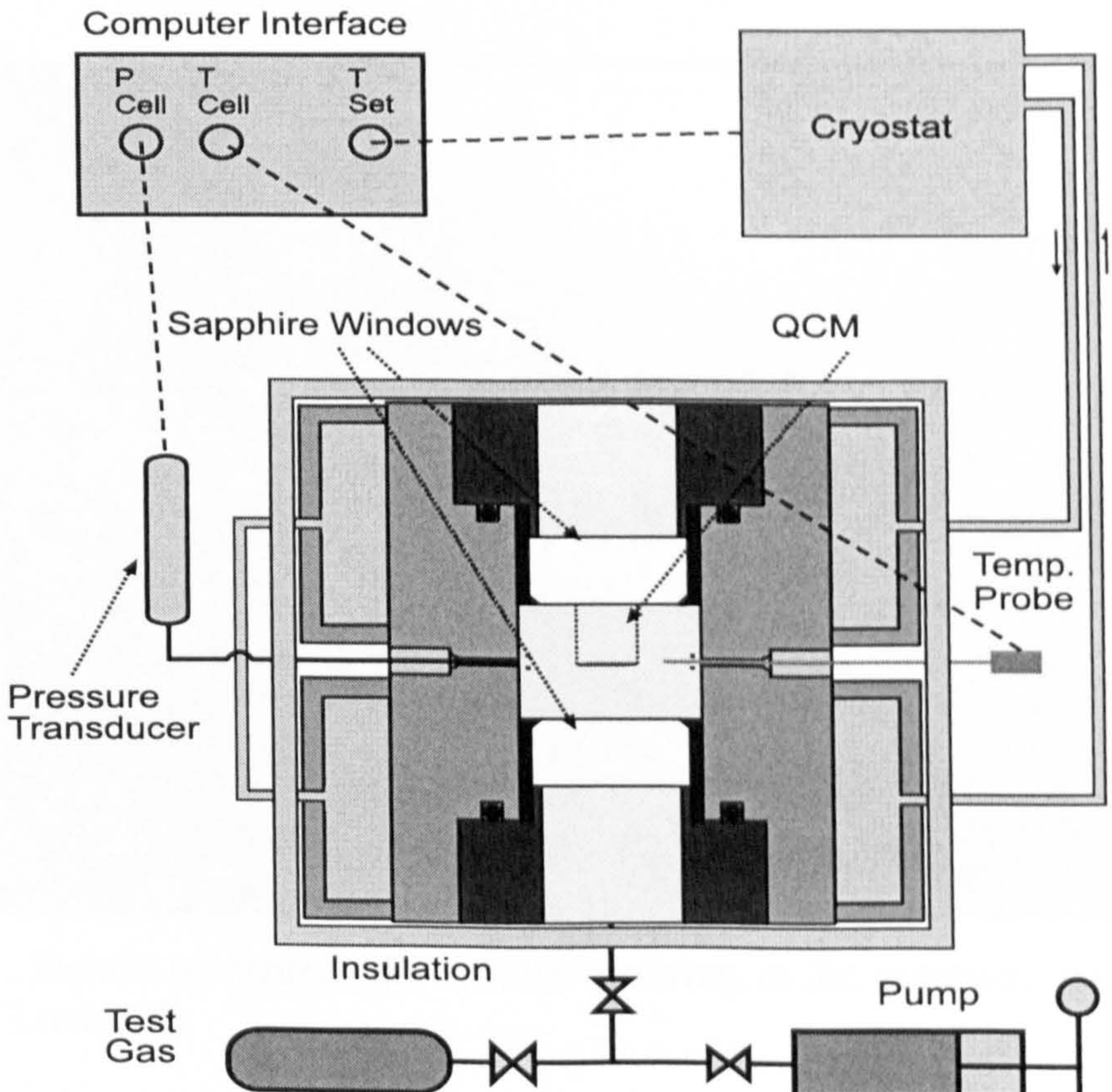

Figure 5.2. Schematic of high pressure (51.7 MPa) visual cell.

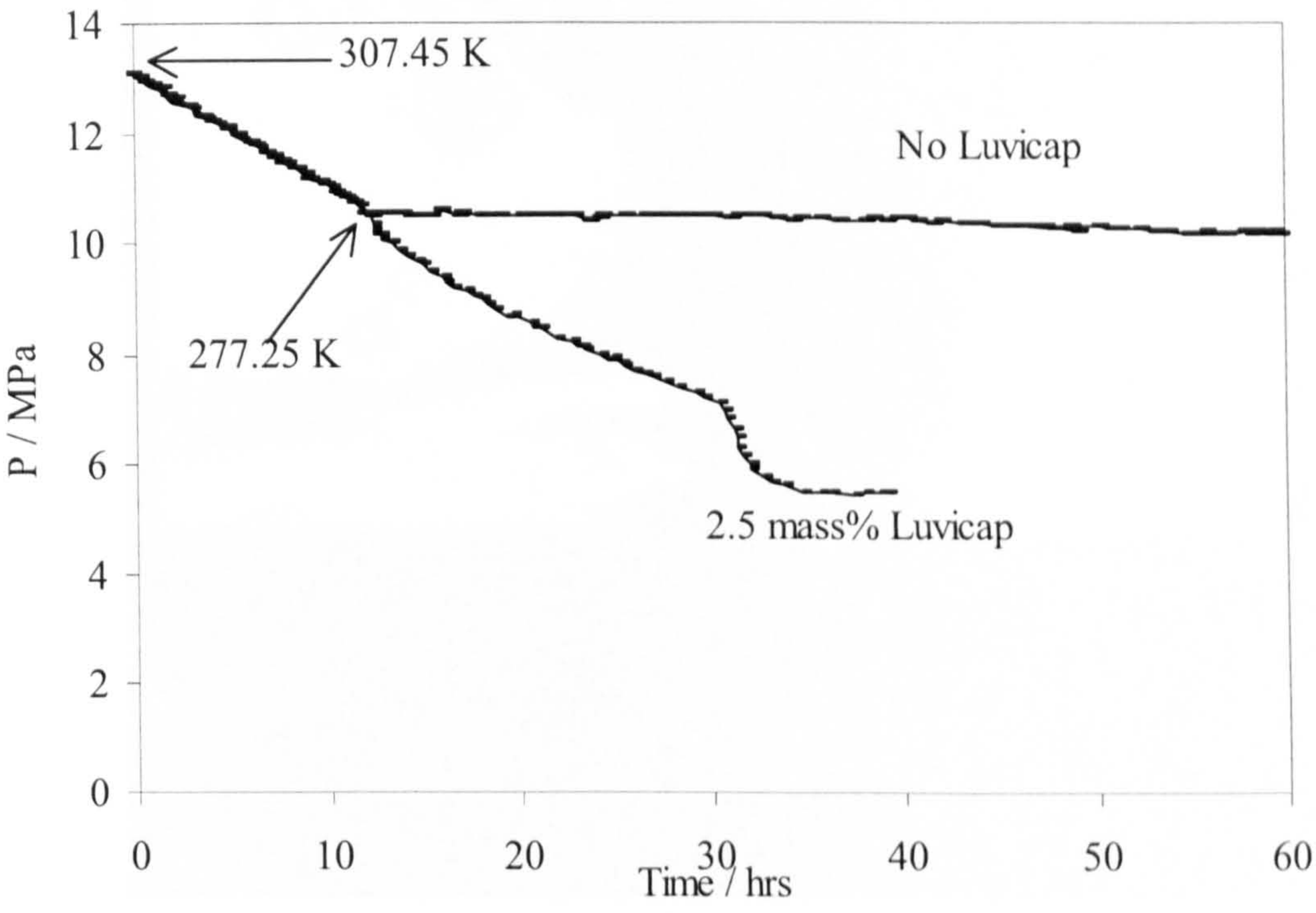

Figure 5.3. Plot of pressure vs. time data for two tests with natural gas hydrates in static conditions without and with Luvicap® (2.5 mass%).

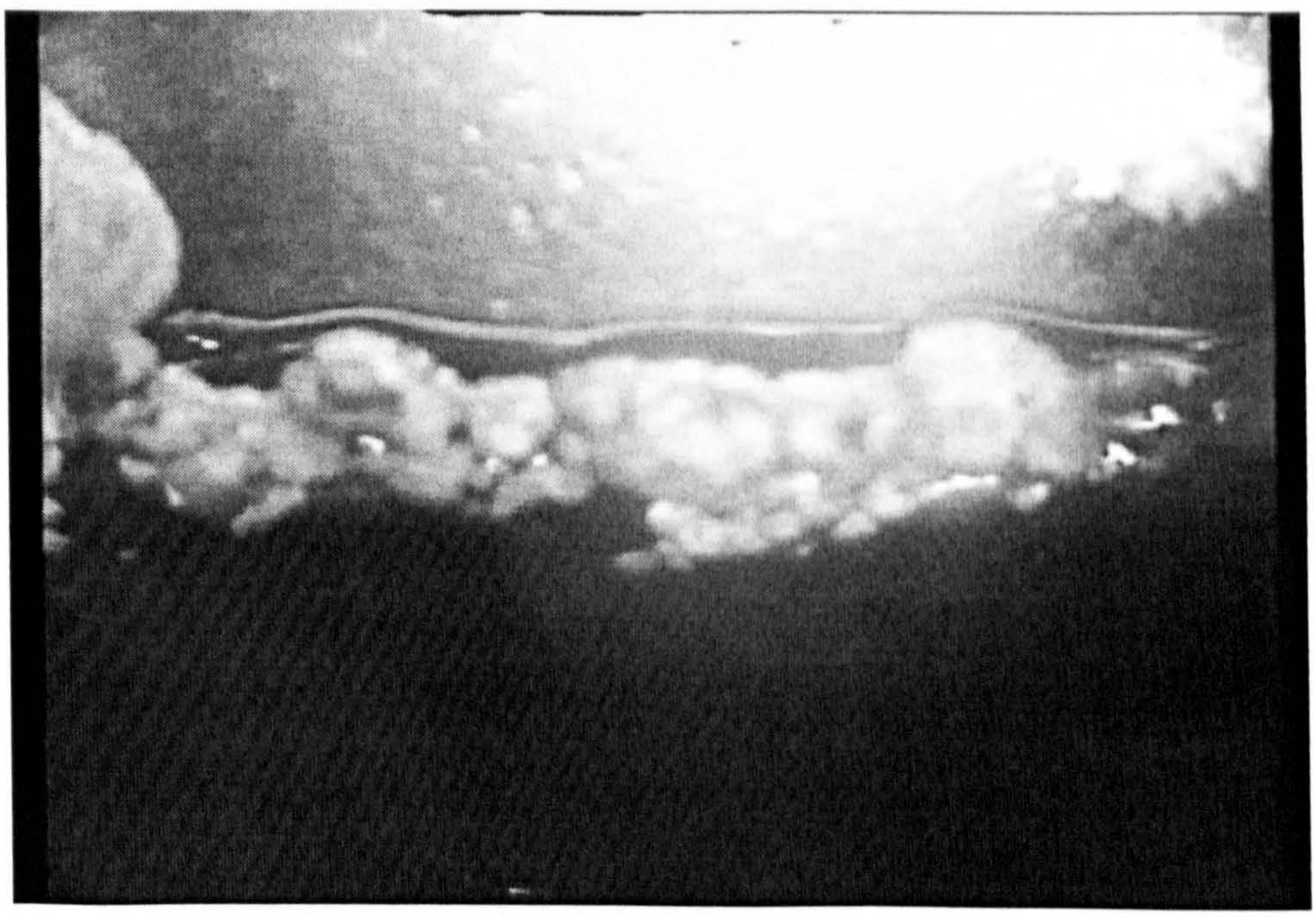

Figure 5.4. Picture of natural gas hydrates growing at the gas/water interface in the presence of Luvicap®.

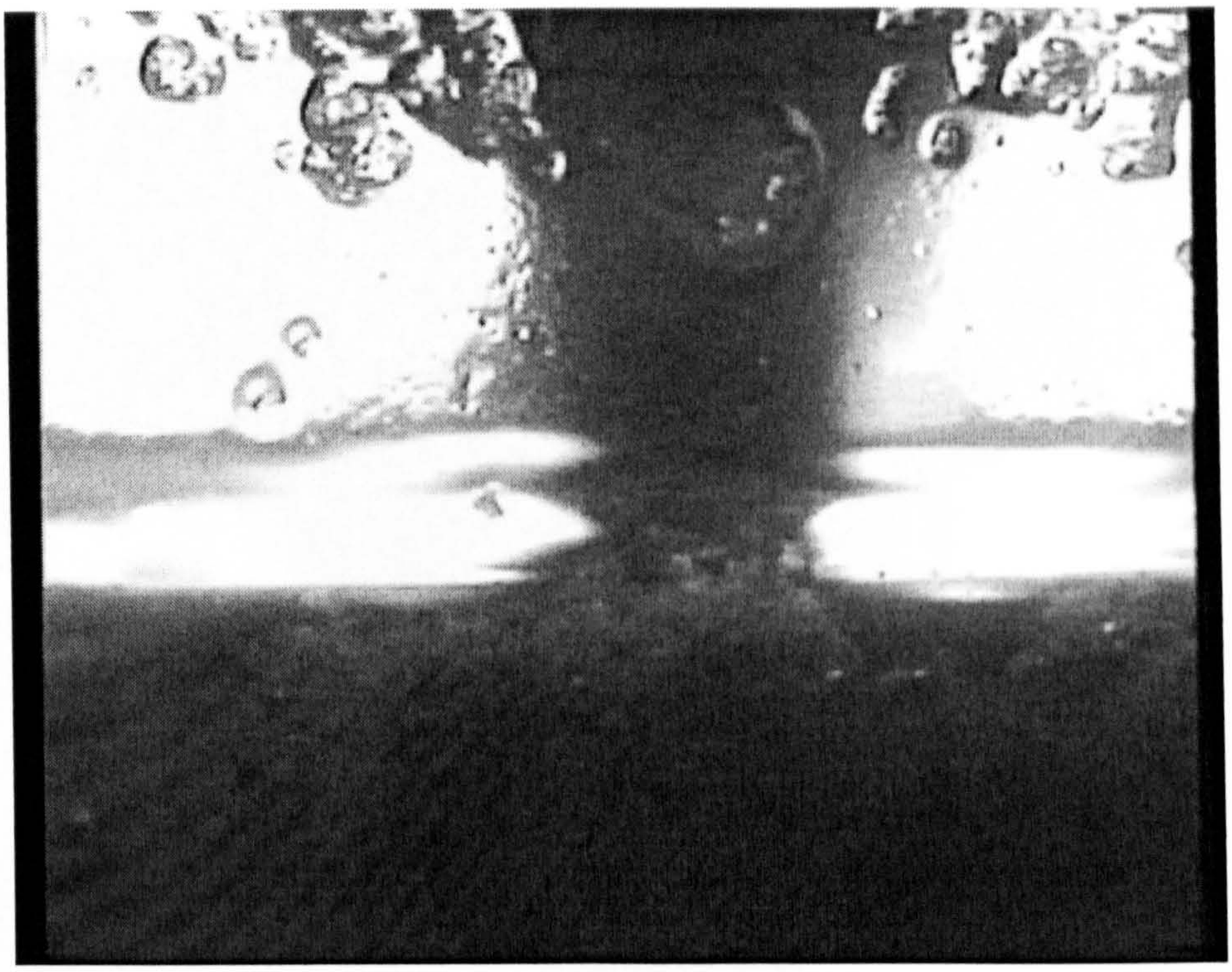

Figure 5.5. In a sequence of 3. Picture of natural gas hydrates formed in the presence of Luvicap®, water phase being drawn from the lower part of the cell

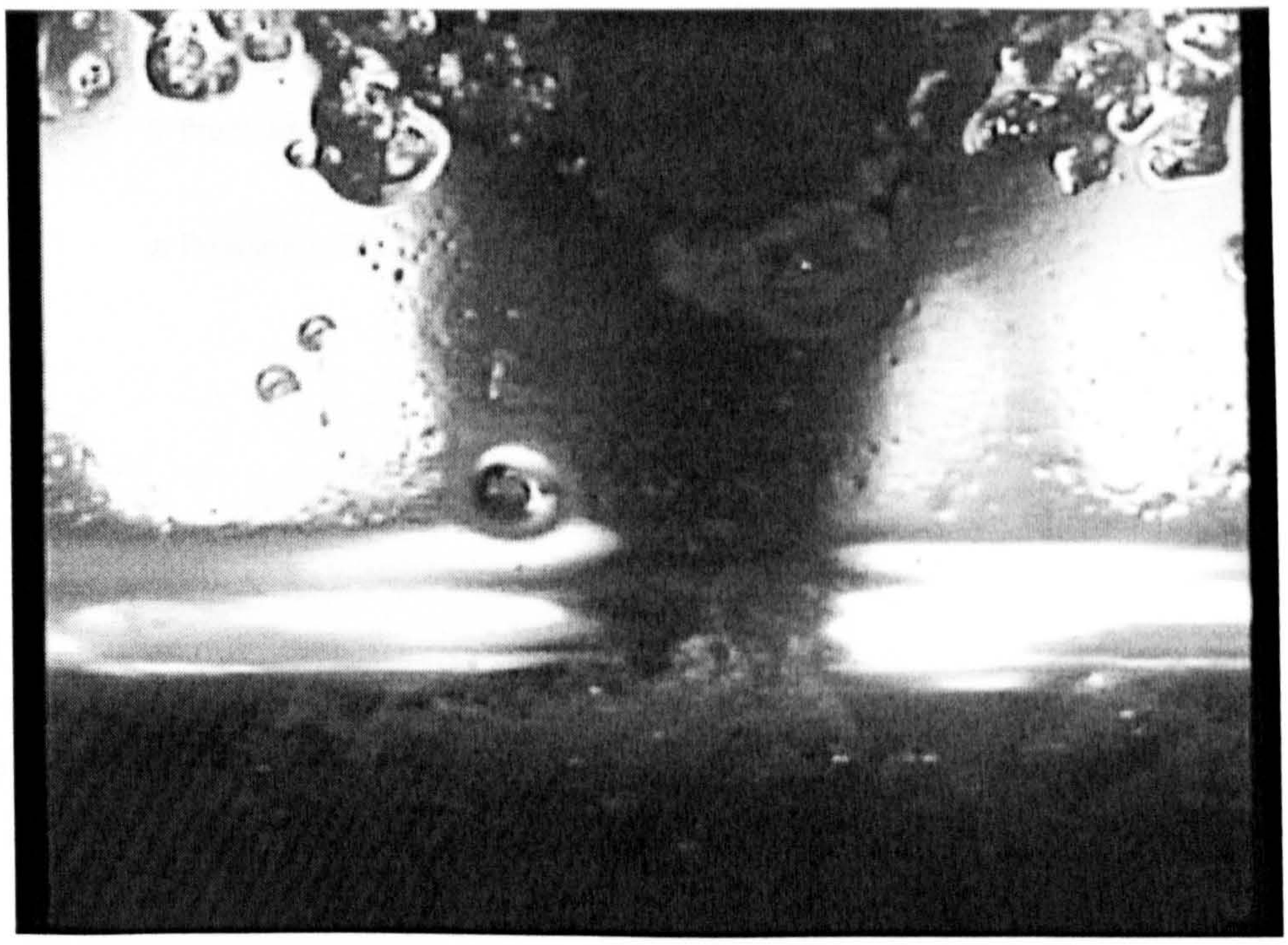

Figure 5.6. In a sequence of 3. Picture of natural gas hydrates formed in the presence of Luvicap®, water phase being drawn from the lower part of the cell.

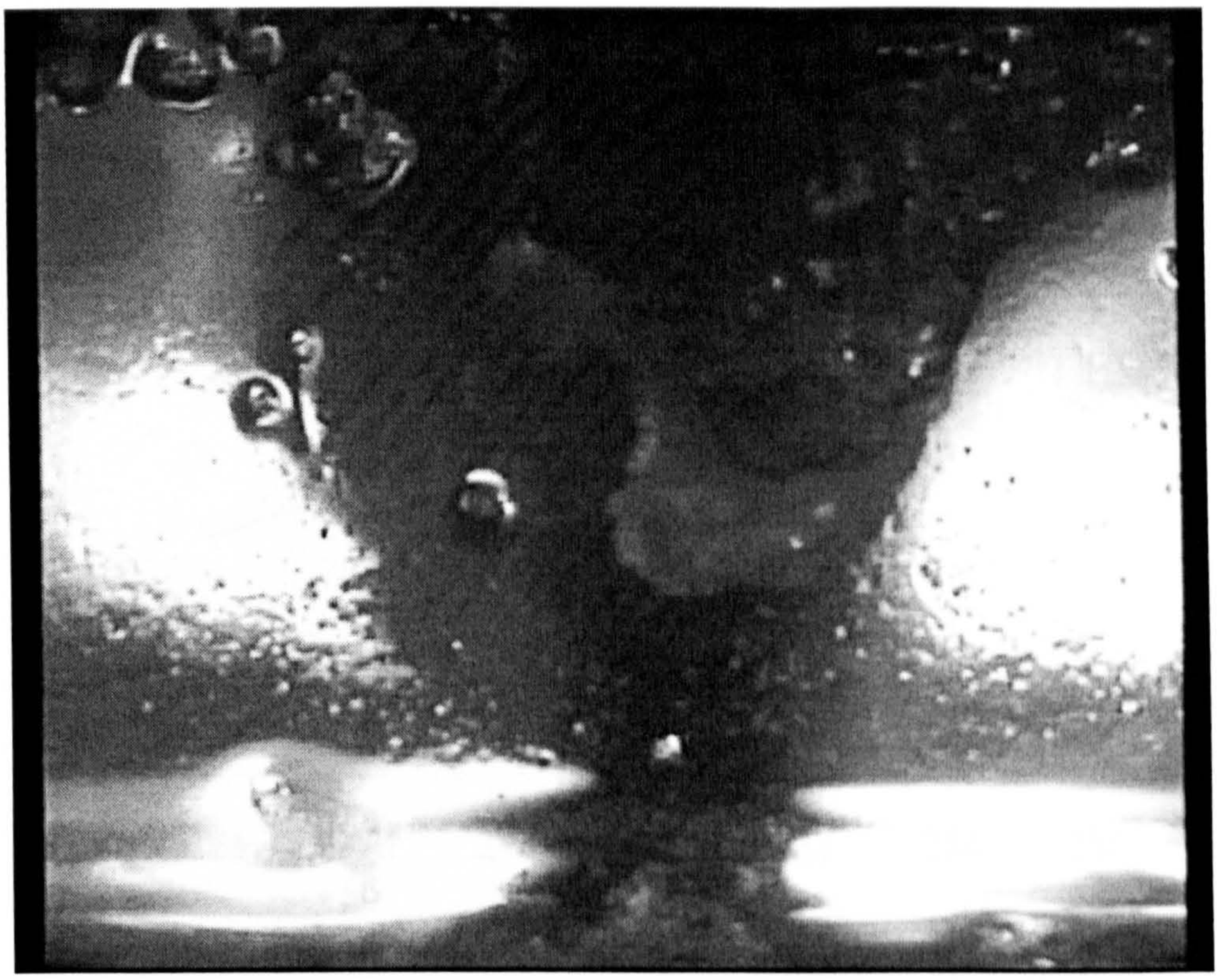

Figure 5.7. In a sequence of 3. Picture of natural gas hydrates formed in the presence of Luvicap®, water phase being drawn from the lower part of the cell.

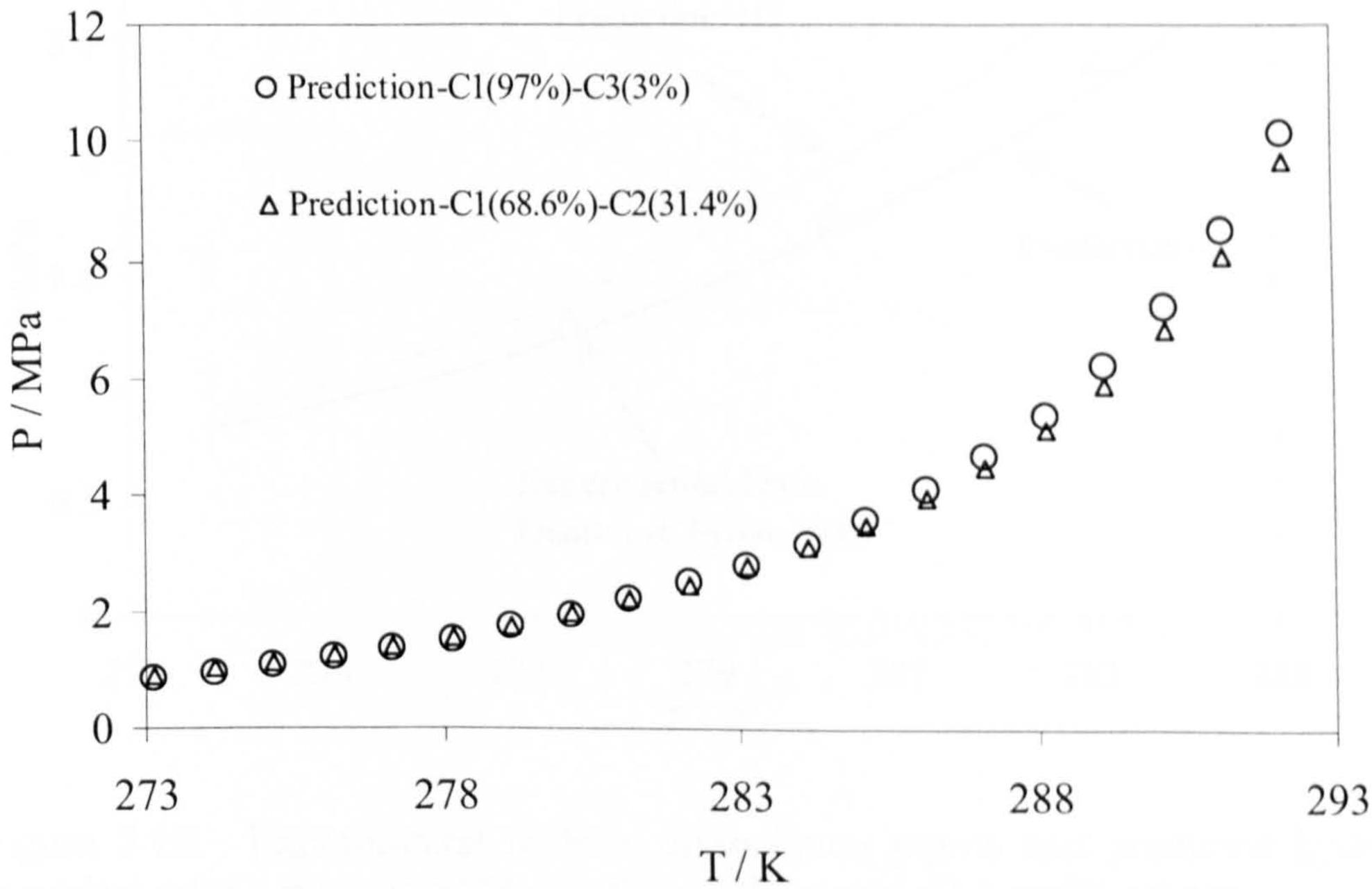

Figure 5.8. Gas mixtures-water hydrate phase boundaries predicted by HWHYD.

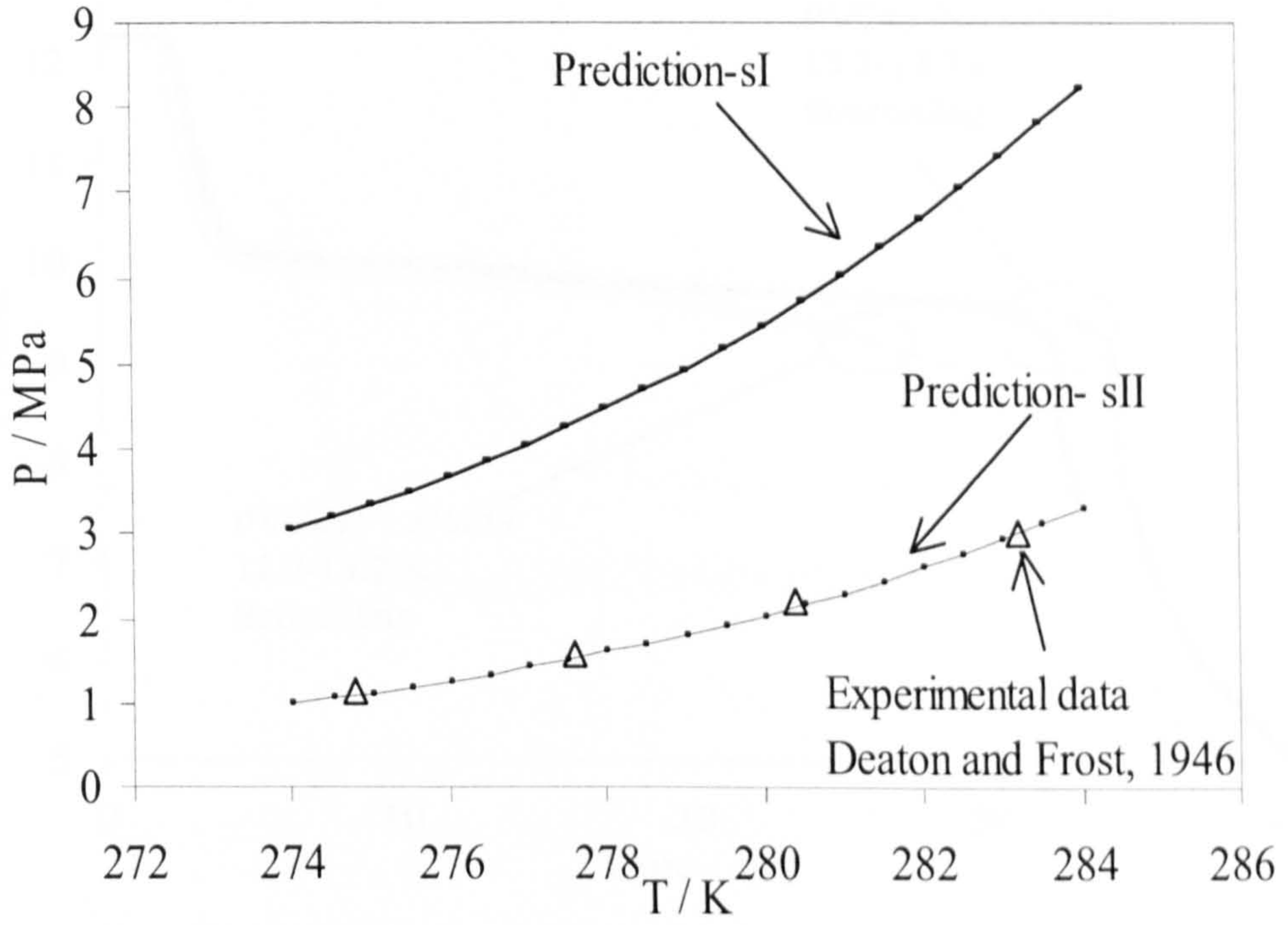

Figure 5.9. Experimental hydrate dissociation points and predicted hydrate phase boundaries for a mixture of 97.4 mol% methane and 2.6 mol% propane.

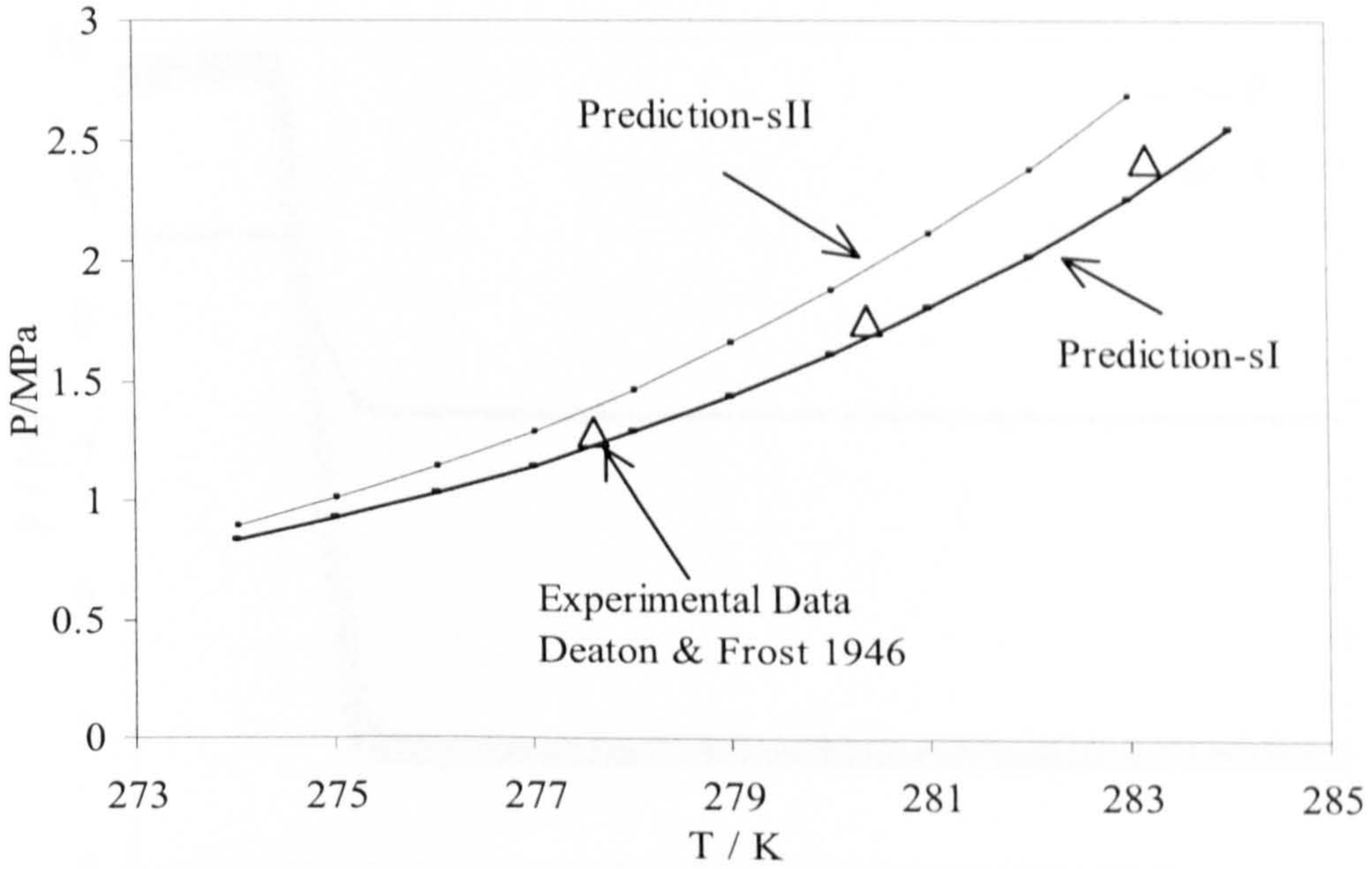

Figure 5.10. Experimental hydrate dissociation points and predicted hydrate phase boundaries for a mixture of 56.4 mol% methane and 43.6 mol% ethane.

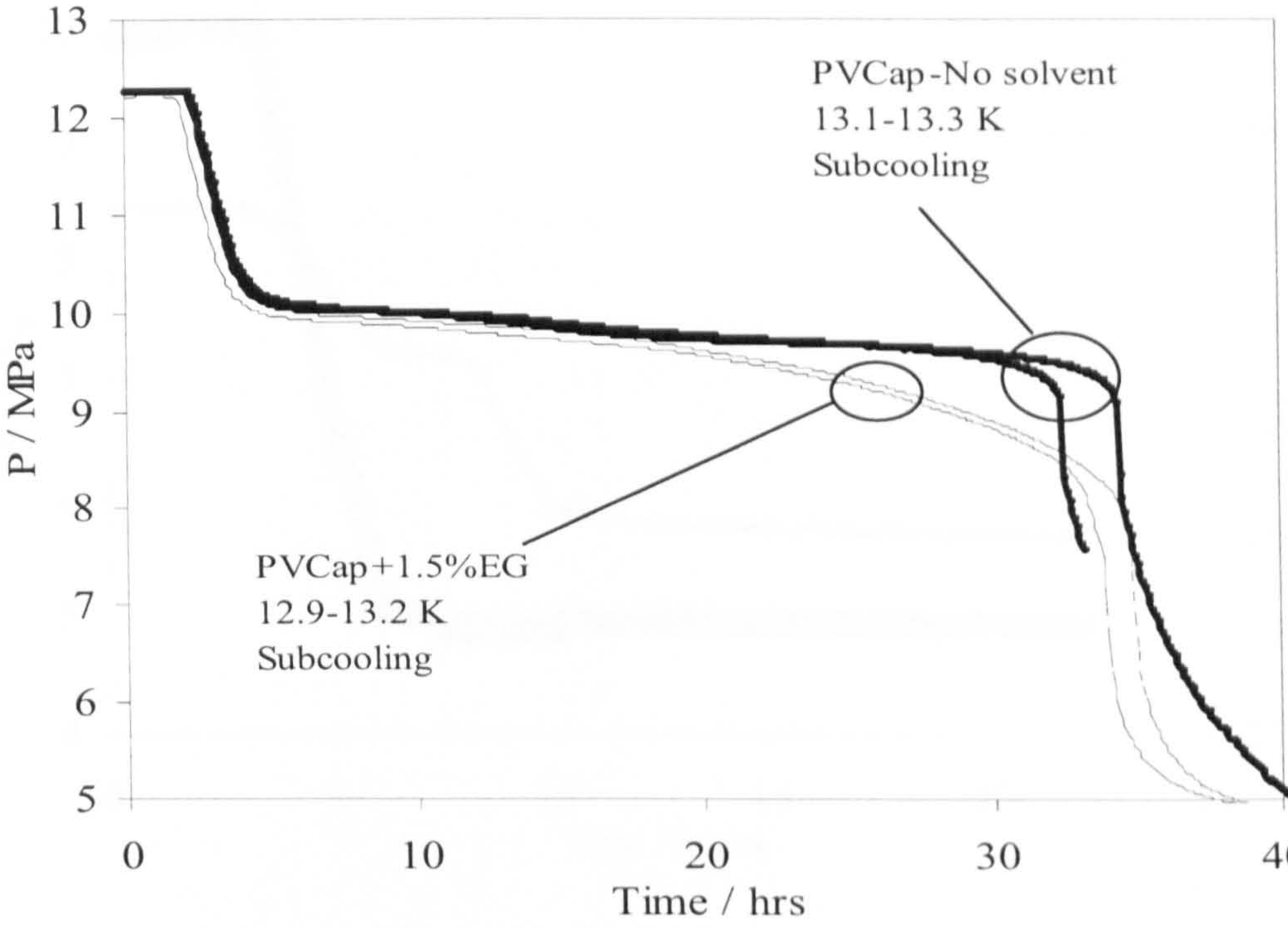

Figure 5.11. The pressure profiles of the tests carried out on PVCap in the presence and absence of ethylene glycol in natural gas-water system and at 600 rpm mixing rate.

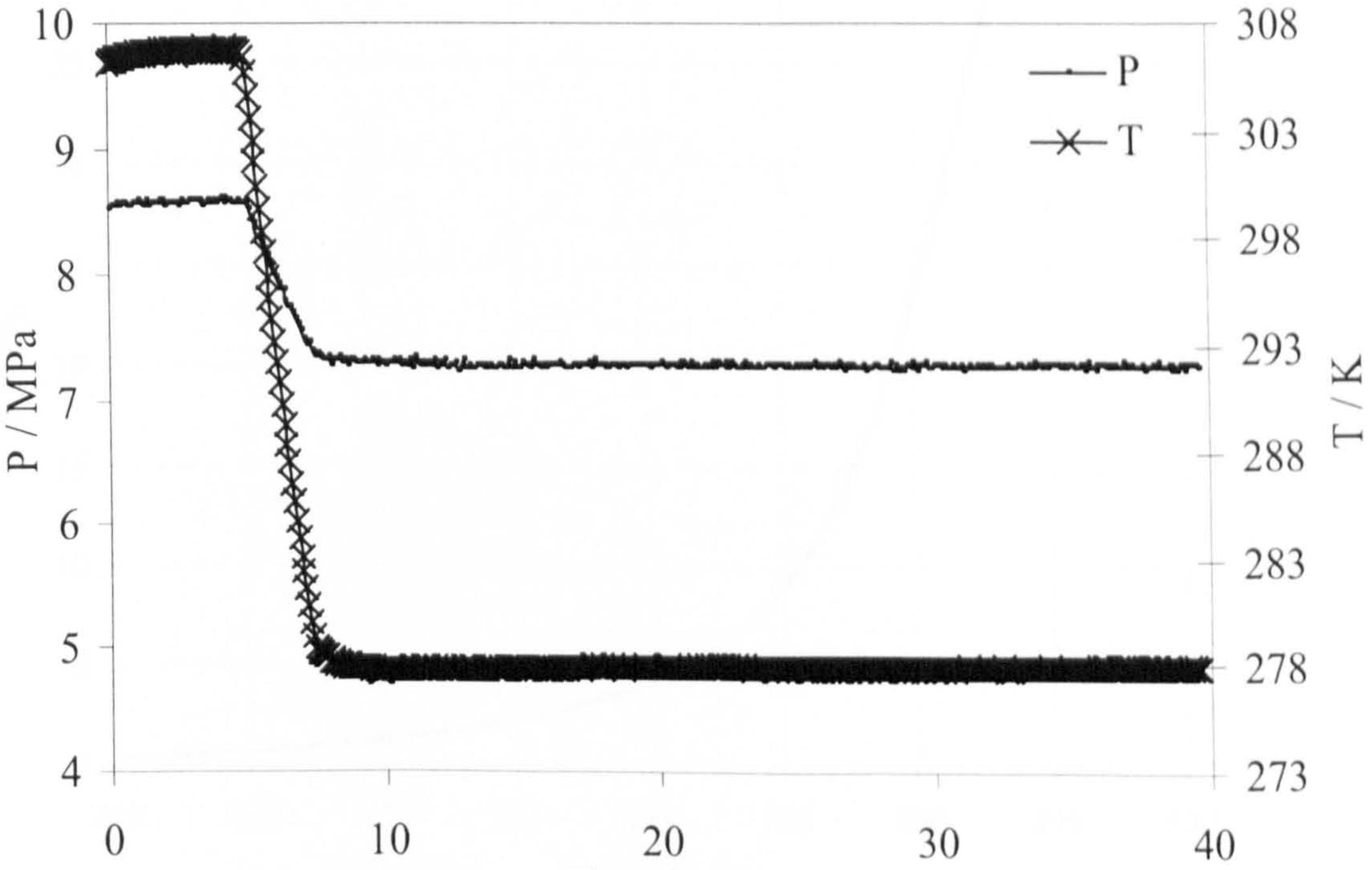

Figure 5.12. The pressure and temperature profiles of the tests carried out on 1 mass% PVCap in the presence of natural gas-water system and at 600 rpm mixing rate.

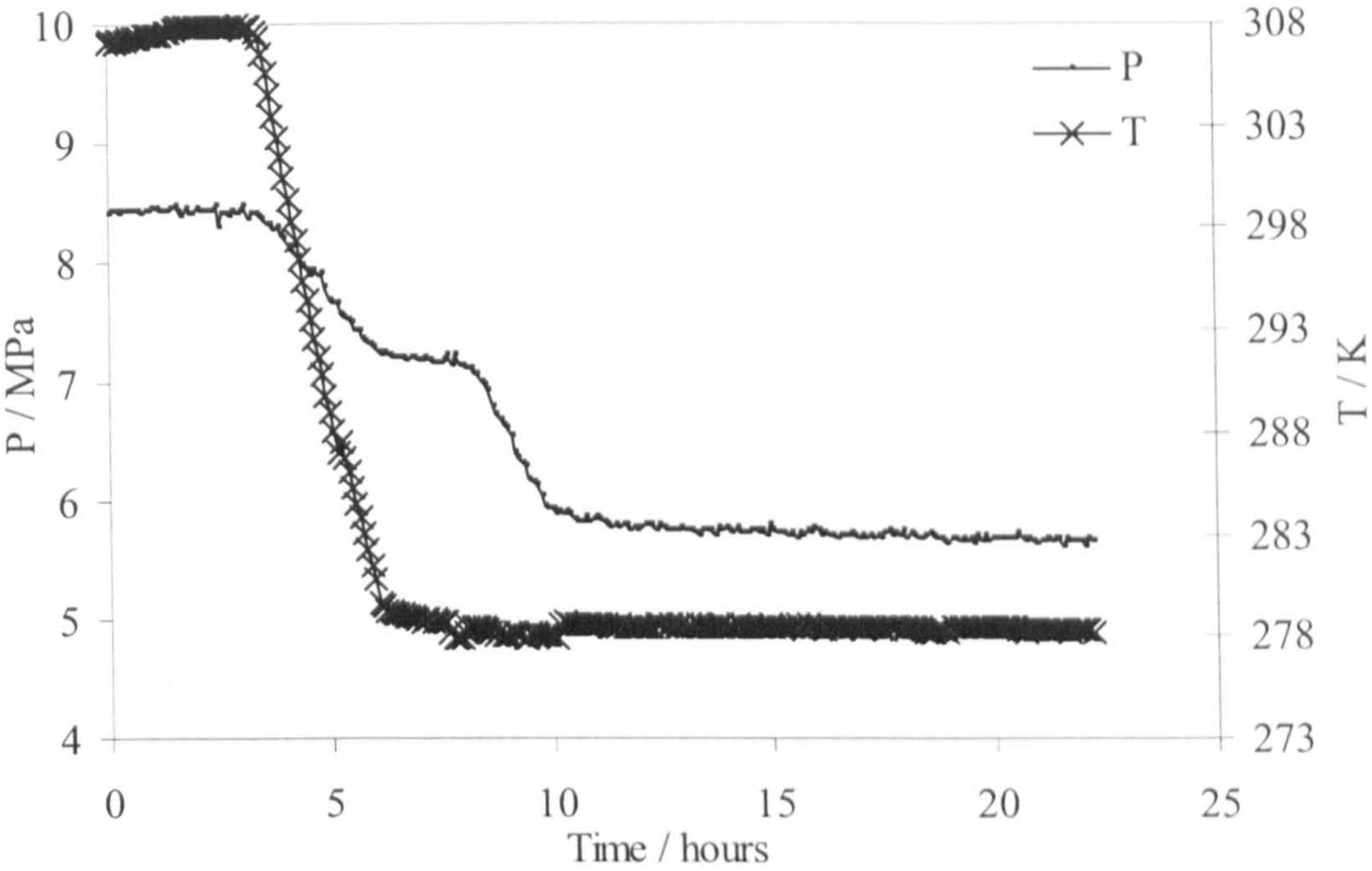

Figure 5.13. The pressure and temperature profiles of the tests carried out on 1 mass% PVCap and 500 ppm corrosion inhibitor (Cortreat799) in the presence of natural gas-water system and at 600 rpm mixing rate.

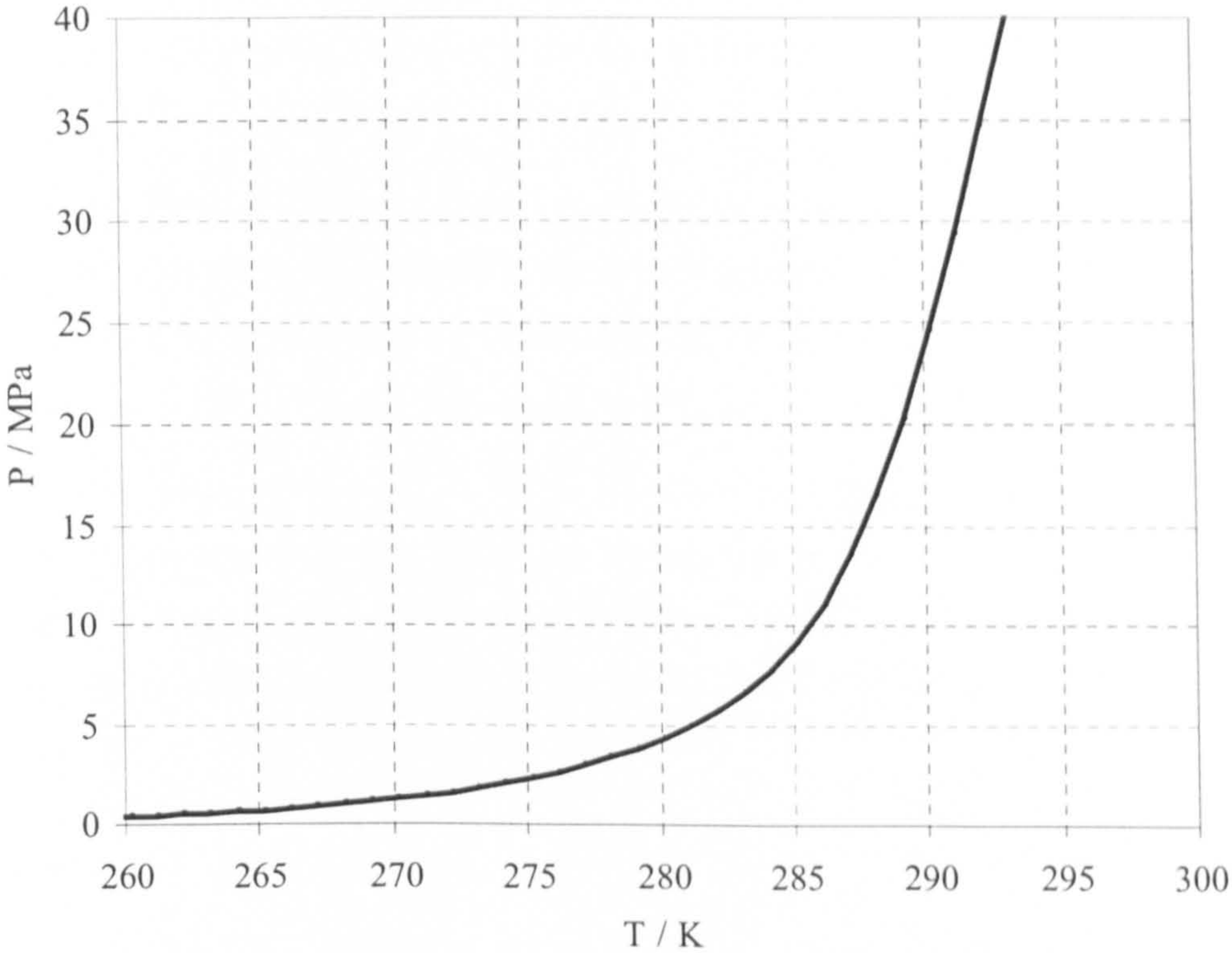

Figure 5.14. Hydrate phase boundary for natural gas-ethylene glycol (20 mass%)-water system predicted by HWHYD hydrate model.

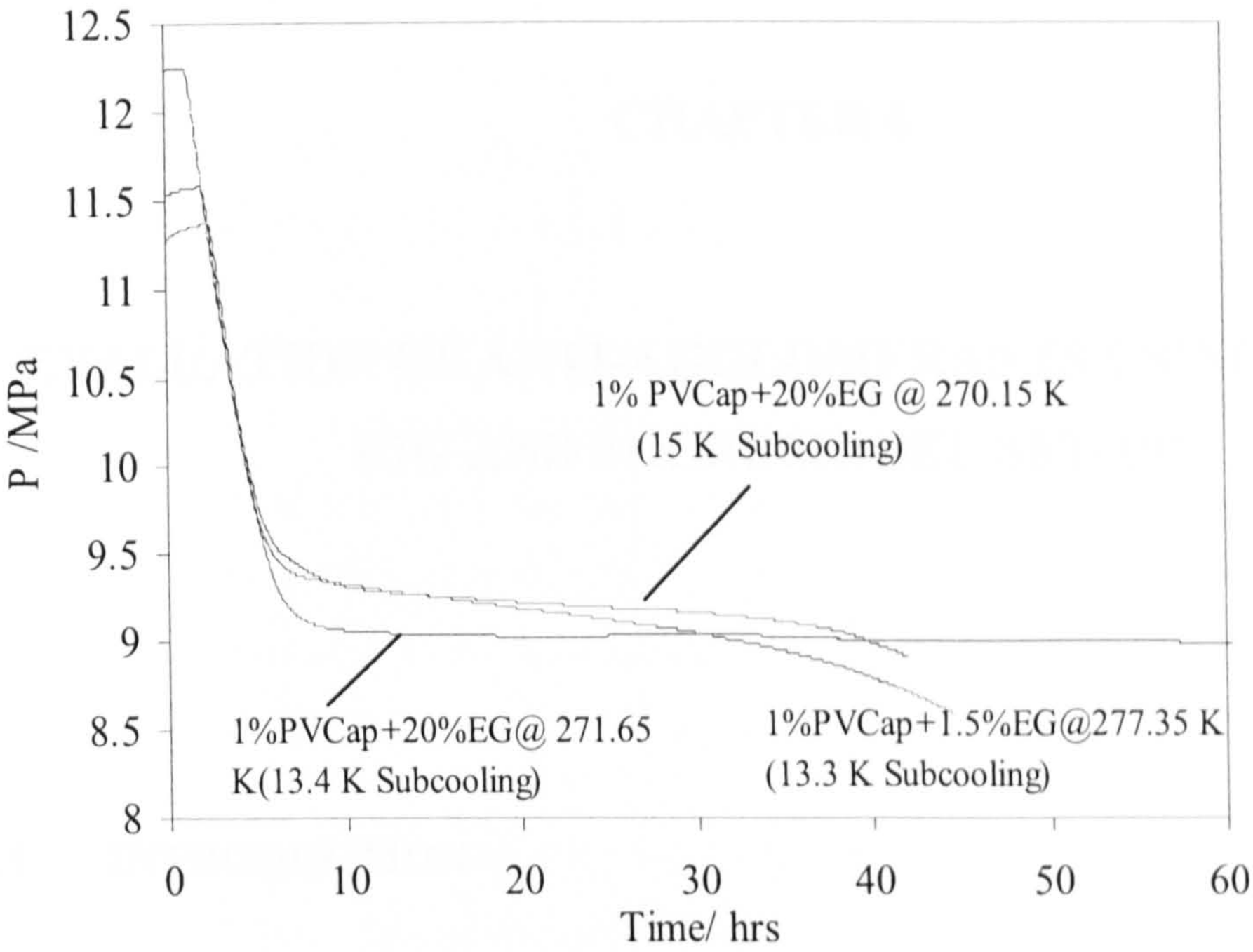

Figure 5.15. Pressure profiles of the experiments in natural gas-1 mass% PVCap in water system at temperatures above and below 273.15 K.

CHAPTER 6

EVALUATION OF ANTI-AGGLOMERANTS USING KINETIC RIG AND MICROMODEL SET-UP

6.1 INTRODUCTION

Anti-Agglomerants (AA) are another class of Low Dosage Hydrate Inhibitors (LDHI) developed over the last decade, which are fundamentally surfactants, that prevent hydrates from agglomerating and depositing in pipelines (Mehta et al., 2002). The action of AAs is based on having a "hydratephilic" head incorporated within the hydrate crystals and a "hydratephobic or oleophilic" tail that disperses the hydrates into a liquid hydrocarbon phase. AA LDHIs allow hydrates to form and have no intended effect on hydrate nucleation/growth kinetics. However, they keep the particles small and well dispersed in the hydrocarbon liquid, and the fluid viscosity remains low. This allows the hydrates to be transported along with the produced fluids. The main advantage of AAs over kinetic hydrate inhibitors (KHIs) is that they are effective even at subcooling higher than 12 K. Hence, they have a much wider range of pressure-temperature applications. However, known AAs only appear to work in the presence of a hydrocarbon phase and are limited to low water cut systems. Their performance is also affected by the type of oil/condensate and the salinity of the water (Kelland et al., 1995 (b)).

In this work, a brief description and literature survey on the development and testing of AA chemicals is presented. Some preliminary experiments have been carried out in this study to develop the methodology for testing AAs using the Kinetic Rig and the Glass Micromodel set up.

6.2 ANTI-AGGLOMERANT CHEMICALS

The anti-agglomerant method was begun by Behar and co-workers in 1987 (Behar et

al., 1988). In the late 1980s and early 1990s, many patents were filed for the use of surface-active agents as AAs. These include: organic phosphates, polyacrylamides and polyacrylates (Matthews et al., 1989), non-ionic diethanolamide, ethoxylated carboxylic acids and polyol esters (Sugier *et al*, 1990).

Kelland and his co-workers tested several chemicals, including various polysaccharides and alkyl glycosides, but they were unsuccessful (Kelland et al., 1995). Urdahl and his co-workers tested many of the commercially available surfactants including alkyl-phenylethoxylates (Urdahl et al., 1995). It was found that the efficiency of many of the available chemicals was inadequate, e.g. sodium dodecylsulphonate (SDS), polyacrylamides, and tyrosine.

In 1995, Klomp and his co-workers patented the use of highly branched quaternised alkyl ammonium or phosphonium compounds (usually with accompanying bromide/chloride ions) (Klomp et al., 1995). The compounds used to demonstrate the effectiveness of this system included, tetrapentyl-ammonium-bromide, tributyl-hexadecyl-phosphonium-bromide, and tributyl-decyl-ammonium-bromide. They extended their work by testing other AAs using a flow loop, such as dibutyl-dicocoyl-ammonium bromide) (Klomp et al., 1995, 1997). Up to now, these have been the most effective AAs available in the industry. Since then, there have been also many patents filed on new chemicals, including quaternised polyether amines (Pakulski, 2000), and novel quaternary amine polymers with increased solubility (Milburn *et al*, 2002). Huo and his co-workers tested the effectiveness of various commercially available AAs, and other potential compounds (Huo et al. 2001). They discovered a new effective AA; dodecyl-2-(2-caprolactamyl) ethanamide. The reason put forward to test the effectiveness of this type of chemicals was the nature of the caprolactamyl group. Polyvinylcaprolactam (PVCap) was found to be an effective KHI, which is due to the steric fit of the lactam ring into the $5^{12}6^4$ cavity on the *s-II* hydrate structure (Makogon T.Y, 1997). This led to the idea of using the lactam ring as a surfactant head-group to adsorb onto the hydrate surface. Thus it was concluded that the main reason why most surfactants do not function as AA is because of their inability to attach to the hydrate surface.

The first patent by Nalco involving AA claims the use of ion pair amphiphiles, which is a combination of cationic and anionic surfactants. This system has been claimed to work at higher water-cuts than other dispersant AAs (even up to 80 vol % water in condensate, Spratt 2005). In the last few years other oilfield service and chemical

companies including Champion (Panchalingham *et al.* 2005, Panchalingham *et al.* 2006) and Clariant (Dahlmann *et al.* 2004, Dahlman *et al.* 2005) have patented their own variations on the existing quaternary ammonium salt technology, including blends and different quaternary ammonium salt molecules.

6.3 FIELD APPLICATIONS

Anti-agglomerants have been found to be suitable for hydrate control in many situations encountered in offshore and onshore oil and gas productions. They are currently being tested and used in several field applications in deepwater and onshore systems. These AAs can be deployed with the existing methanol/glycol injection systems at much lower rates, thus requiring smaller pumps, small storage facilities, and less frequent supply trips (Frostman and Przybylinski, 2001). Some successful field/lab testing and implementations of AA LDHIs reported in the literature are summarised below:

1. A deepwater well in the Gulf of Mexico was producing excessive water as well as appreciable volume of gas, and a maximum methanol injection rate of 7350 gallon per day was insufficient to control hydrates in the 24 miles condensate flow lines. Baker Petrolite reported treating this well with HI-M-PACT anti-agglomerant at 0.35 gal/bbl of water, while phasing out methanol. After nine months of production there has been no hydrate problems (Baker Petrolite, 2002).

2. Shell tested their AA LDHI in the Popeye Field in the Gulf of Mexico's Green Canyon blocks, located in 2000 ft of water (Morris, 2002). To inhibit hydrates during the initial years of production, methanol was injected. Before the AA field test, the production had reached 60 MSCFD, 3000 barrel per day of condensate and 430 barrel of water per day. The methanol injection rate was 175 barrel per day. To replace methanol, AA LDHI was slowly injected over a 24-hour period until all methanol injection was stopped and the system was operating solely on LDHI. The volume of AA LDHI was 25 times less than methanol. As a part of the test, a shut in period of 24 hour was conducted, and there was no problem in the restart. Thus eliminating the need for instantaneous corrective measures during the restart operation.

3. A LDHI qualification program was performed by British Petroleum (BP) engineers to select LDHIs for a field application in a Gulf of Mexico black oil tie-back pipeline (Troika to Bullwinkle, 14 miles), which is located in 2700 ft of water (Argo et al. 2002). The main hydrate concerns in this case were hydrate formation and plugging during extended shut-ins, and the subsequent cold restarts, in which 11 K of subcooling

is encountered at 15.68 MPa. Six anti-agglomerants were pre-screened in the laboratory using a stirred autoclave reactor and a wheel flow simulator. Three of the selected AA LDHIs passed all of the tests in the presence of the field oil with up to 40-60% water cut (3.5 mass% salt solution), and 1.5 to 2 mass% chemical dosages. The hydrates formed into mobile slurry and no plugging tendency was observed. However, there has been no field test reported so far.

4. A gas well, Crimson Lake, located about 200 km northwest of Calgary, Alberta, was treated with a combined KI/AA product and an AA inhibitor by Conoco Canada (Lovell, Pakulski, 2002). The well was producing 6 SCM/D condensate, 0.1 SCM/D water and 0.5 MMSCM/D gas. During the production, the well continuously formed hydrates at depths of 500 to 300 meters. Operators were pumping between 400 to 500 litres of methanol daily and could not sustain the production for more than 16-24 hours, and up to 2 m^3 of the solvent were used in one shot to dissolve hydrate plugs when they formed.

KI/AA combination product: the combined inhibitor was diluted with methanol in a stock tank to form a 20% KI/AA solution. The solution was pumped into the well through the spaghetti tubing at the rate of 30 L/D for 30 days. This rate is equivalent to a loading 6 L/D of the undiluted inhibitor. The well did not have any freeze-ups during the test period.

AA inhibitor: The AA (GHI-7183) consists of polyether polyamines and alcohol solvents. It is significantly less expensive than the KI/AA combination product. It was started at 30 L/D as a 20% AA in methanol solution and a month later the treatment was lowered to 45 L/D of a 10% AA in methanol. The dosage 45 L/D is equal to 10% of the original ineffective methanol treatment rate and is equivalent to 4.5 L/D loading of the undiluted inhibitor. A quaternary ammonium corrosion inhibitor was co-blended at 1% to compensate for oxygen introduced into the well with solvents. After about a month, this set-up was copied to six more wells in the area and operated without any hydrate problems.

There has been no unsuccessful field-testing of AAs reported in the literature. Field experience has indicated that the following factors in the design and application of an AA LDHI should be considered:

- Correct assessment of operating conditions and produced fluid composition.
- Selection of an effective laboratory testing programme.

- Capacity of the selected AA LDHI to prevent agglomeration and suitability at higher water cut.
- Solubility of AA chemicals in water or oil phases and solvents.
- Injection and economics.
- Interaction with other chemicals used in the field, such as corrosion/scale inhibitors.
- Effect on the field production: recycling/removal issues.
- Environmental concern and safety.

6.4 LABORATORY TESTING TECHNIQUES

Laboratory testing of AA LDHIs is designed to provide a high level of confidence that a selected product will perform effectively in the field. In testing AAs the objective is to it is important to addition

There are two important issues relevant to the testing of AAs for field application. Firstly, AA inhibitors will be used in the pipelines under various flow regimes and conditions, and it is difficult to simulate geometry and flow regimes in laboratory equipment. Subsequently, caution is required during the scaling-up of laboratory results. Using similar field oils/condensates in testing AAs is not common due to difficulties in synthesising them and questionable similarity of them to the field oil/condensate. Secondly, similar to KHIs, AA inhibitors are comparatively new, and test protocols are not fully developed, or widely accepted in industry. Therefore, different testing methods and procedures should be considered.

In this section, various laboratory equipment and techniques used for LDHI testing AAs are reviewed and compared.

In general, there are three methods that can be used for AA LDHI qualification; hydrate visualisation, rheological measurement of hydrate slurry, and assessment of hydrate plugging and deposition.

Visualisation Techniques include optical cells, which are used for observation of hydrates at high pressures. The visualisation window is usually made of sapphire for high-pressure application. Turbidimetry is also used, which measures the loss in intensity of light beams that pass through the solution of forming hydrate crystals. This type of work is very useful in identifying particle nucleation and growth, which is relevant to AA LDHIs. Herri and his co-workers demonstrated this technique's

suitability for hydrate crystal systems (Herri et al., 1999). In this study, the glass micromodel set up is proposed for visualisation of hydrate particles in the presence and absence of AA. The details will be described in the next sections.

Rheological Assessment Techniques: Rheological measurement can be carried out in stirred tank type reactors, simulated flow loop equipment and other devices. A stirred tank reactor is usually equipped with accurate thermocouples and pressure gauges and temperature control systems. Hydrate formation can be detected and quantified by pressure measurement. The stirred tank with a torque measurement is particularly useful in determining the rheological properties of hydrate slurry formed. Various shapes of impeller can be used to facilitate the rheological characterisation and assessment of hydrate blockage. Hydrate formation can also be visualised in the reactor when an optical window is mounted on the reactor wall. These stirred tank reactors are used in many studies due to their relative simplicity, reproducibility, cost and versatility.

Flow Loops are used to simulate the flow in pipelines. These apparatuses consist of a temperature controlled high-pressure pipeline (usually with an ID>5 cm) with a pump used to pressurise and simulate the flow conditions encountered in field pipelines. Pressure drops across a section of the loop can be measured and used to assess the viscosity change of the fluid after hydrate formation. Different designs of flow loops exist and these will be discussed below:

Saturated Flow Loop is a conventional gas-free hydrate loop consists of a pipeline suitable of transporting water and a hydrocarbon phase saturated with a hydrate-forming gas. The decision to operate without a gas phase considerably reduces the complexity of the system in regards to pumping of the liquid. It is possible to minimise any potential damage to hydrate crystals/nuclei by the correct selection of pump such as the Moineau or screw type pumps. The advantages of this type of system stems from its simplicity, which include: the cost, the robustness of the methodology and equipment, the ability to circulate fluids without significant damage from pumps and compressors, and the minimal pressure differential across the pump as opposed to that associated with the separation and compression of multiphase loops. The disadvantage of not having a gas phase present is that the flow is not very representative of the stratified flow often found in multiphase pipelines.

Multiphase Loop is a multiphase loop involves the passing of both liquids and gases in a flow loop system. This leads to the advantage in being able to emulate the stratified

flow encountered in real pipeline conditions. The main disadvantages of this system are: cost due to the large length of the loop required to achieve meaningful stratified flow conditions, and increased pumping requirements due to the increase in differential pressure. Multiphase flow loops can either convey the liquid with a multiphase pump or by separating the gas and liquid phase and subsequently pumping the liquid and compressing the gas. In general, both multiphase systems result in greater damage of the hydrate crystals and high pressure drop than the saturated flow loop equivalent. Two examples of multiphase flow loops are as follows:

Tulsa University Flow Loop is a 3"-diameter flow loop, mounted on a 80-ft long tilt table. The flow loop is 160-ft long and has an operating pressure of 2,200 psig. A multiphase pump circulates the fluids with a velocity up to 15 ft/s and can generate the various flow patterns typically encountered in subsea pipelines. The flow loop is fully jacketed and the flow loop temperature is controlled with glycol circulating inside the annulus space. A 20-ton chilling system is used for cooling purposes and a steam heat exchanger and steam coils are used for heating. The fluid addition systems (oil, water, gas, additives, and solvents) are located inside the process equipment building. These systems are used to initially charge the flow loop with oil, water, additives and gas, as well as to add make-up gas during the hydrate formation process. The entire facility is fully automated and remotely operated from a control trailer.

Institut Français du Pétrole (IFP) Flow Loop is 140 meter long and its inside diameter is 2 inches (5 cm). It is fully temperature-controlled from 50°C down to 0°C (122°F– 32°F) and operates at pressures up to100 bar (1450 psi). It is fully instrumented to measure pressure drops, temperatures, and flow rates, with vortex or Coriolis flow meters for the gas and liquid phases. Gas balances are performed during hydrate formation thanks to pressure and temperature monitoring of the gas reserve tanks. It also includes specific equipment such as an embedded camera, gamma-ray densitometers, and a FBRM (Focused Beam Reflectance Measurement) particle size analyzer. Various flow regimes - single liquid or gas flow, stratified, slug, annular flow can be managed by accurate control of the flow rate of each phase.

Gas Lift Loop: The aim of this technology is to flow the liquid without a pump and thus remove all crystal damage associated with the pumping of liquids. To accomplish this, the differential pressure is generated by a gas-lift riser. The principle of the flowing generator is to inject methane at the base of the gas-lift riser, then to separate it from the fluid in the gas separator at the top of the riser, and using the static gravitational pressure to flow the liquid. This technology does not allow stratified flow and is not considered to be a multiphase system (only in the gas lift section). The

advantage it offers over the conventional gas-free loops is that there is no pump to damage the crystal. The main issues associated with this type of design are the flow speed limitations, and the pressure differentials associated with gas separation and injection. South West Research Institute (SWRI) and Saint Etienne School of Mines have both constructed this type of loop. The loop at SWRI consists of a 50 ft, 3 inch, gas lift type loop, rated for 1,440 psig. The loop at Saint Etienne School of Mines consists of a 50m, 2 inch, gas lift type loop (Figure 6.12).

A rolling-ball device can also be used to assess the rheological properties of hydrate slurries (Mehta et al. 2002). The device consists of a stainless steel tube with a steel ball inside, attached to a rocking system to create rock and roll movement. The velocity of the rolling ball is measured to assess the viscosity change of the hydrate slurry.

Plugging Assessment Techniques:

Hydrate plugging and blockage can be readily sensed in the stirred tank reactors and simulated flow loops. The other apparatus used for this purpose include rotating wheels and rotating tubes.

Rotating Wheel Flow Loop : high pressure rotating wheel has been used to assess the deposition of hydrate on the wall (Argo et al, 2002). The rotating wheel consists of a circular stainless steel tube attached to a motor gearbox system to create movement. The wheel rotation is in the vertical plane. The system has a torque-measuring device to sense the imbalance (or torque fluctuation) of the wheel due to hydrate deposition. It also has a window and camera for visualisation purposes at low pressure conditions. The wheel is placed into a temperature-controlled chamber to maintain the required temperature. This system is useful in testing the effect of flow regimes (laminar or turbulent) and is much less resource and labour intensive than a flow loop. The system was used effectively by Lund *et al.*(1995), Urdahl *et al.* (1995) and Vebenstad et al (2005).

Rocking Cells: (such as the rolling-ball type) can be also used to detect blockage caused by hydrates. The test tube is charged with a hydrocarbon, water, and anti-agglomerant mixture at required pressure and temperature. It then rocks back and forth until it is plugged by a hydrate formation.

Some service companies (e.g. Clariant Oil Services and Kernow Analytical Technologies) use rocking cells apparatus (Figure 6.13) for testing AAs. Each

apparatus incorporates two rocking cells maintained in a controlled temperature environment. The cells have a test volume of 40 ml with a sapphire window for visual observation of cell contents and can be pressurised up to a maximum of 2465psi (170 barg). The fluid temperature and cell pressure is logged throughout. The progress of the magnetic pellet as the cell rocks from side to side is recorded both visually and by the use of proximity sensors at either end of each vessel. As the vessel rocks, each sensor counts the pellets movement. As hydrates form, the pellet is impeded and this lead to a change in the rate of counts registered by the sensors. Point of failure for the hydrate tests is when the proximity sensor counts stop.

In this work, a blind stirred tank reactor and a glass micromodel set up (detailed in Chapter 3) are used for evaluating anti-agglomerants. The blind stirred tank reactor is used to test the effect of different AAs on the transportability of the system by torque measurements. Although those rigs can be used to simulate different flow regimes (mixing or static) in the field at bulk conditions for testing AAs, but they are not able to provide important information such as hydrate particles size, morphology and their distribution in different phases. A glass micromodel set up is used to provide that information (i.e., micro-scale information) in the presence and absence of AAs. In the micromodel set up hydrate particles in μm scale can be visualised, however, the hydrate formation were under static conditions only and in conduits with 50-100 μm diameters. The different information obtained from two set-ups is complementary for evaluation of AAs and valuable in understanding some of the mechanisms involved and designing new AAs.

6.5 EXPERIMENTAL TECHNIQUES IN THIS STUDY

6.5.1 Application of Kinetic Rig in Evaluation of Anti-Agglomerants

The kinetic rig detailed in Chapter 3 was used to evaluate the anti-agglomerants. Two different types of impeller were used in the experiments in the kinetic rig for mixing and torque measurements. The first type impeller (Figure 6.1(a)) is a specially designed paddle-shape impeller and the second impeller is a helical tube (Figure 6.1(b)) fitted into the testing cell. During the experiments, the rheology of the hydrate slurry is monitored by measuring the torque applied on the stirrer shaft. After hydrate formation, torque will increase. However, if the hydrates formed are dispersed into oil/condensate phase as small particles as expected when an AA-LDHI is present, torque increase will be limited. Otherwise, large torque increase can be observed,

which may lead to the blockage of the stirrer. In the experiments, the required amount of water and oil/condensate are first loaded into the test cell, and then gas is charged into the cell up to the required pressure. The AA inhibitor can be pre-mixed with water phase or injected into the testing cell using a metric pump at high pressures. In the following sections the results of the tests with the above-mentioned impellers for evaluation of anti -agglomerants in the kinetic rig are presented.

In the tests distilled water was used. Natural gas supplied by Air Product (Composition in Table 3.1). A commercial anti-agglomerant (AA1) was provided by Baker-Petrolite. Two other commercial anti-agglomerants (labelled as AA-2, AA-3) and Natural gas condensate (East Frigg Field condensate) were provided by Clariant Oil Services.

6.5.1.1. Paddle-Shape Impeller

The first test was a blank test in the presence of condensate, water (water cut by volume (W/C)=0.33) and natural gas. The profiles of pressure, temperature and torque measured in the test are illustrated in Figure 6.2. As presented in Figure 6.2, the experiment started at 11.8 MPa and 307.4 K where the torque was at 5 (arbitrary unit). After cooling down the system, the hydrate formed at 280.3 K and 9.8 MPa before getting to stable temperature (277.2 K). A stirring rate of 600 rpm was used during the test period. Temperature and torque rises and a sudden pressure drop accompanied the hydrate formation. The torque increase was prominent (from 5 to 9, 180% rise). The torque dropped with time afterward from 9 to 5.7. The reduction of torque with time after hydrate formation may be attributed to the impeller centrifugal force, which pushes the hydrates toward the kinetic rig wall and thus leaves less hydrate on the impeller path. The torque was then stabilised after few hours at 5.8, as shown in Figure 6.2.

The second test was carried out on a system of water, condensate (W/C=0.33) and natural gas in the presence of 2.5%vol of an anti-agglomerant (AA-1) in water. The results are shown in Figure 6.3. As presented in Figure 6.3, the experiment started at conditions similar to blank test conditions (11.5 MPa and 306.3 K, 600 rpm), where the torque was at 5 (arbitrary unit). After cooling down the system, the hydrate formed at 283.7 K and 10 MPa before getting to stable temperature (277.4 K). After hydrate formation, the pressure drop and temperature rise during hydrate formation were prominent, however there were slight changes in the torque profile. During the test time, the torque variation was between 5-6.1 (less than 25% change) while in the

absence of anti-agglomerant the torque variation was about 180%, which denotes efficacy of the used anti-agglomerant. As shown in Figure 6.3, further reduction in the system temperature after 10 hours did not lead to more hydrate formation / pressure drop.

6.5.1.2. Helical Tube Impeller

In the experiments with paddle type impeller in some tests after hydrate formation the torque decreases with time because of impeller centrifugal force on hydrate particles which pushes them towards the kinetic rig wall. In order to avoid that problem, the impeller was changed with a helical cupper tube (ID= 7.7mm), (Figure 6.1(b)). In addition, the flow of fluid in the helical tube is more representative of pipeline conditions than turbulence caused by paddle type impeller in the cell. The applied torque is a function of the shear force due to fluid flow inside and outside of the helical tube stirrer.

Three blank tests were conducted on the natural gas-water system at different rates of mixing to study the torque sensitivity in different rates of mixing (rpm) after hydrate formation. In all the experiments, the test started at around 12 MPa and 306.15-307.15 K and the system was cooled down to 276.15-277.15 K to form hydrates. After hydrate formation, the system was left for some time and then it was heated up to 306.15 K to dissociate the hydrates. Pressure, temperature and torque profiles were recorded during the test. Figure 6.4 presents the results of test at 100 rpm. As shown in the figure, at 305.92 K the torque value is 1.06 (arbitrary unit), by cooling down the system to 276.73 K, hydrate started to form at around 10.1 MPa and 278.58 K (13 K subcooling). The rate of hydrate growth was slow (as seen from slow pressure drop) and the torque was increased to 1.46. After one day, the pressure dropped to 8.68 MPa and the torque was fluctuating between 1.8-1.96. The slow rate of hydrate growth is believed to be due to relative poor mixing of the system. After heating the system up to 306.3 K, the hydrate dissociated and pressure increased to 12 MPa and torque decreased to its primary magnitude 1-1.09. The above test was repeated with 200 rpm and the resulted profiles are presented in Figure 6.5. In that test because of higher rate of mixing, hydrate formed at lower degree of subcooling (10 MPa and 280.15 K equivalent to 11.5 K subcooling) than that of test with 100 rpm. In addition more hydrate formed (pressure dropped to 4.2 MPa) with higher rate of growth. After hydrate formation the torque increased from 1.5 to 5.9 and after one hour it was dropped to 2.6. The torque stabilised at 2.6-2.85, where no more hydrate was formed for 11 hours. By heating up

the system to 306 K the torque decreased to its primary magnitudes 1.5-1.6 again. In the test with 400rpm (Figure 6.6), after hydrate formation at around 10.5 MPa and 284.5 K (7 K subcooling), the torque increased from 1.8 to 8.4 and stabilised there for three hours. During the next 9 hours, after increasing the system temperature to 306, the torque decreased slowly to 6.5. By comparing the torque profiles of above tests it appears that rate of mixing of 100 rpm results in more stable torque profile. However at 100 rpm the mixing is poor and hydrate formation is very slow. Rates of mixing higher than 400 rpm led to vibration of mixer motor, which could damage the mixer. Therefore the rate of mixing of 400 rpm was selected for the next experiments in the presence of condensate and anti-agglomerant.

In the second series of experiments, which was a repetition of the above-mentioned test procedure with a mixing rate of 400 rpm, a mixture of 33 volume % water in a natural gas condensate was used in the presence and absence of anti- agglomerants (AA-2 and AA-3). The first test was carried out in the absence of AA. The profiles of the first test are shown in Figure 6.7. As shown in the figure, the test started at 11.7 MPa and 306.65 K, where torque was about 1.8. The system was then cooled down and when hydrate formed at about 283.45 K and 10 MPa (8.2 K subcooling with respect to natural gas-water hydrate phase boundary), torque was increased to 10.2 and after one hour it was stabilised at 10. By increasing the temperature to 307.4 K, torque was reduced to 1.8.

The above test was repeated in the presence of 2.5 volume % of AA-2 and AA-1. The results of the test in the presence of AA-2 are shown in Figure 6.8. As shown in the figure, after hydrate formation (at 284 K and 10 MPa bar equivalent to 7.6 K subcooling with respect to natural gas-water hydrate phase boundary) torque increased to 8.9 and then decreased to 7.5 within few hours. Then the system was heated up to dissociate the hydrates. As expected, in comparison to the test without AA (Figure 6.7), in the presence of AA, after hydrate formation, the maximum torque was decreased by 25% (Figure 6.8).

The test was repeated in the presence of another anti-agglomerant (AA-3). The profiles of test are shown in Figure 6.9. As illustrated in the figure, after hydrate formation (at 284.25 K and 10 MPa) the torque was increased from 1.9 to 5.6 and after being at 5.6 for about 2 hours the torque was reduced to 1.9 again. The maximum torque in the presence of AA-3 (5.6, Figure 6.9) is around 60 % less compared to the maximum torque in the presence AA-2 (8.9, Figure 6.8) denoting better performance of AA-3

compared to AA-2.

The above results show that the new helical tube mixer can successfully be used for screening anti-agglomerants using a kinetic rig. However, torque measurement technique may not show how effective is an AA for field application, especially for the system where blank test do not fail catastrophically. Information such as hydrate particles size, their agglomeration and distribution in different phases, in the presence and absence of an AA is also needed along with information from torque measurement tests for selection of an AA for field application.

6.5.2 Application of Glass Micromodel Set-Up in the Evaluation of Anti-Agglomerants

Another experimental set-up, which was used for the first time in the evaluation of anti-agglomerants, was glass micromodel (detailed in Chapter 3). A micro pump was used for fluid injection in to the micromodel. The size, morphology and location of hydrate particles formed in the presence of AA inhibitors have been visualised as well as the movement of hydrate particles between the oil and water phases.

The first test in micromodel was a blank test (natural gas-water-condensate) in order to visualise hydrate formation in the absence of anti-agglomerant. To charge the micromodel with the testing fluids, water was first injected, followed by condensate (dyed with Sudan Red), and then gas was charged to achieve a system pressure of 8.2 MPa. The system was left over night to achieve equilibrium. The system was then cooled to 273.45 K for hydrate formation. The images of distribution of different phases before and after hydrate formation have been presented in Figure 6.10. As shown in Figure 6.10(b) after hydrate formation, lumps of hydrates blocked some of the micromodel pores. By opening the outlet valve and establishing a pressure gradient, no flow was observed in the model due to the hydrates blockage in the micromodel pores.

Further evaluation of AA-1 was carried out in the next experiment in order to visualise the size, morphology and distribution of hydrate particles formed in a condensate/water/natural gas mixture in the presence of 2.5 volume % AA-1. In this test, it was not possible to dye the condensate with Sudan Red as it reacted with the anti-agglomerant and deposited in the pores. After injection of water and condensate phases the pressure of the model was increased to 7.38 MPa by charging natural gas. The system was then cooled to 273.15 for hydrate formation. Hydrates were formed overnight. Figures 6.11 (a) and (b) show the micromodel images taken before and after

hydrate formation, respectively. Hydrate formation was taken place at static conditions, but local fluid movement was observed in the micromodel, probably induced by pressure changes due to gas consumption. The size and distributions of hydrate particles formed in the presence of AA-1 are shown in Figures 6.11(b). Small hydrate particles formed all over the micromodel, most were around 5-10 μm and all were less than 20 μm. It is interesting to observe that, after hydrate formation, many hydrate particles were in the condensate phase, or being surrounded by the condensate phase. The hydrates formed have some affinities toward the condensate, and it would be readily dispersed into the oil phase under flowing conditions, as shown in the kinetics rig tests. By opening the micromodel outlet valve, the movement of hydrate slurry in the condensate phase was observed which showed the transportability of the hydrate slurry. The experimental results obtained from the kinetics rig (Figure 6.3) and the micromodel have clearly demonstrated the excellent performance of AA-1 as an effective anti-agglomerant.

6.6 SUMMARY AND CONCLUSIONS

In this section, the development of AA LDHI chemicals was briefly reviewed. The most effective AAs up to date appeared to be quaternised alkyl ammonium or phosphonium compounds. There are several commercial AAs available in the market from various suppliers. The current AAs need to operate in the presence of a liquid hydrocarbon phase, and have a limitation on the water cut.

There have been several successful field-testing and implementations of AA LDHIs reported in the literature. Most of them were in the Gulf of Mexico. In most cases, AAs were deployed for treatments during shut-in and restart to replace methanol. There was also a case where excessive water was involved, and the use of methanol was impossible due to limited injection rate and cost. AAs are suitable for systems with limited water cut (less than 50% or 30%) in multiphase transportations. There is no report on adverse effect of AAs on other aspects of field operations. AA has been proven to be an economically viable alternative to conventional inhibitors for deepwater pipelines, due to its low dosage, fewer requirements on injection and storage.

Laboratory testing of AAs involves three basic techniques: hydrate visualisation, rheological measurement of hydrate slurry, and assessment of hydrate plugging and deposition. Rocking cells and flow loops, with and without optical windows, are the most popular laboratory equipment used for AAs selections.

In this study, for evaluating the performance of the AAs, a blind kinetics rig, with two specially designed stirring impellers for torque measurement and a Glass Micromodel set-up were utilised. The Kinetics Rig was used for rheological characterisation and blockage detection of the AA systems. The torque measurement was improved by using a helical tube instead of paddle impeller. It was shown that the information obtained from torque measurement technique can be used for screening AAs, however it is not sufficient for selection of an AA for field application. It was shown that complementary information such as hydrate particles size, morphology and their distribution in different phases can be obtained from Glass Micromodel set-up. Preliminary experiments, using a proven AA chemical in comparison with another similar compound and an un-inhibited system, have shown that the techniques developed in this study are suitable and effective for the testing of AAs.

Current practice for selection of an AA for field application is primary testing/screening of AAs in rocking cells and then testing them in a flow loop. In the rocking cell the hydrate slurry and/or blockage is detected visually and/or by a magnetic pellet and the proximity sensors. The new method (kinetic rig and glass micromodel) can also be considered as a method for primary testing of AAs before flow loop test. The rheological characterisation of the system containing AA can be studied by torque measurement in the kinetic rigs and the hydrate particles size and morphology can be observed in the micromodel.

6.7 FIGURES

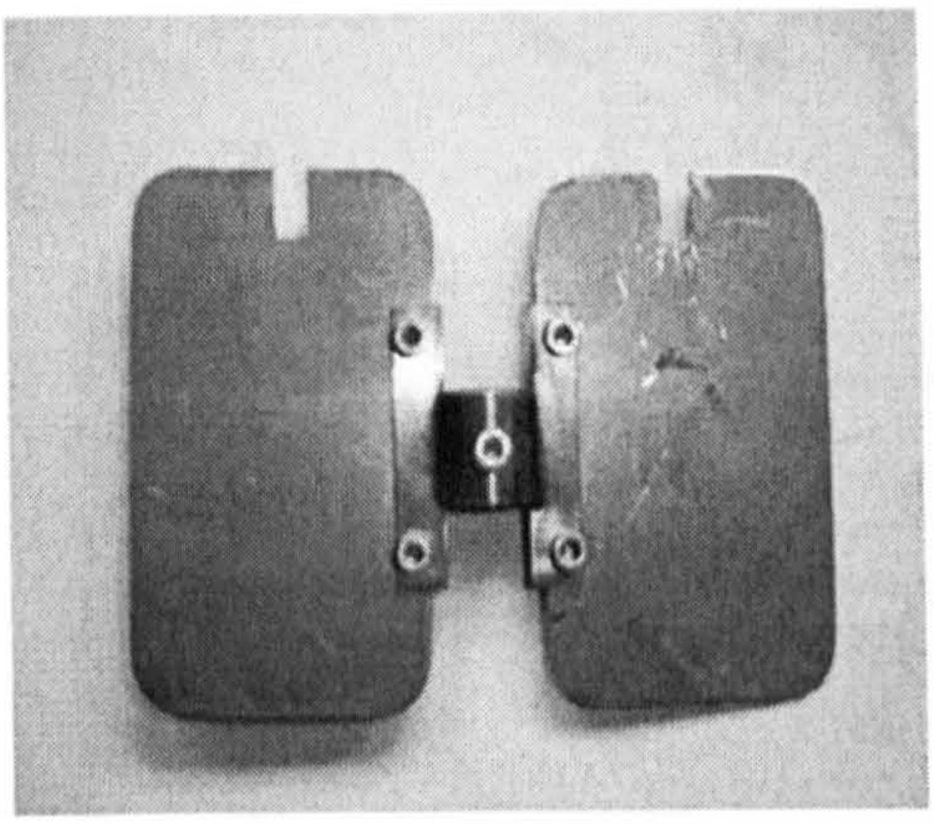

(a) Paddle-Type impeller

(b) Helical Tube impeller

Figure 6.1. Different types of impeller used in the kinetic rig for evaluation of anti-agglomerants.

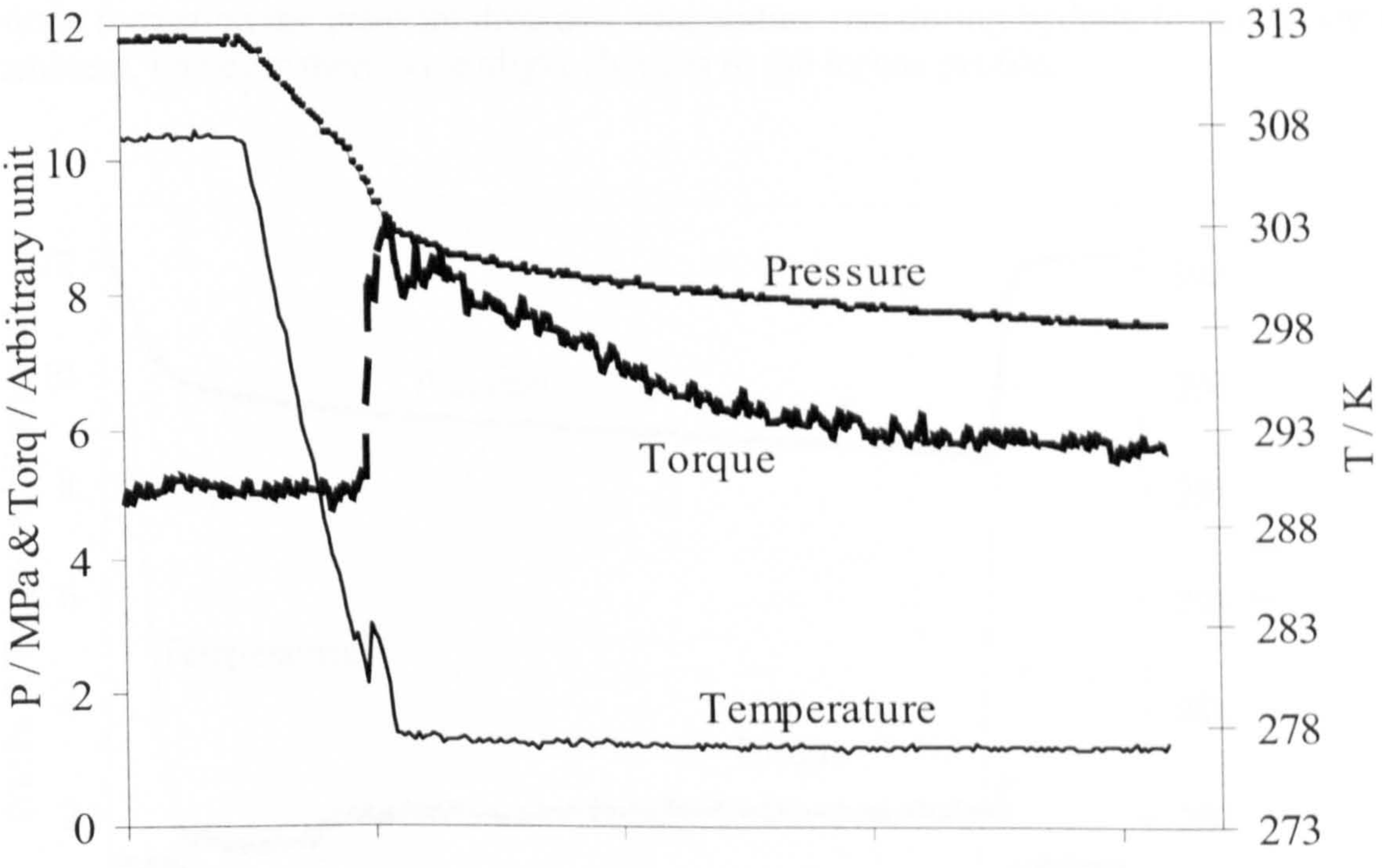

Figure 6.2. Pressure, temperature and torque profiles for NG-water-condensate, W/C=0.33, paddle type impeller, rpm=600. After hydrate formation the torque increase was prominent. The reduction of torque with time after hydrate formation can be attributed to the impeller centrifugal force on hydrate particles.

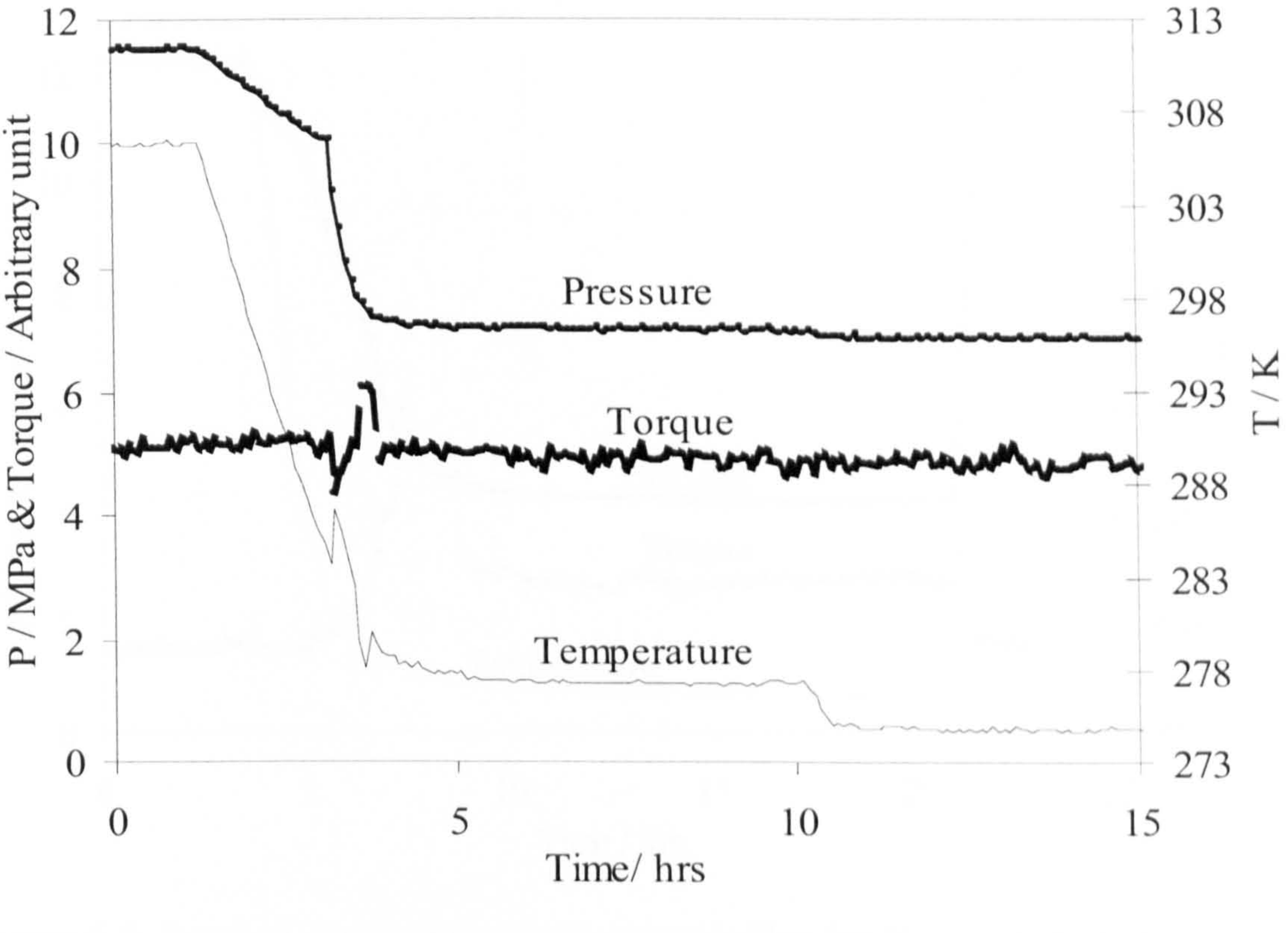

Figure 6.3. Pressure, temperature and torque profiles for NG-water-condensate, W/C=0.33, 2.5 vol% AA-1 in water phase, paddle type impeller, rpm=600. After hydrate formation the pressure drop and temperature rise during hydrate formation were prominent, however there were slight changes in the torque profile.

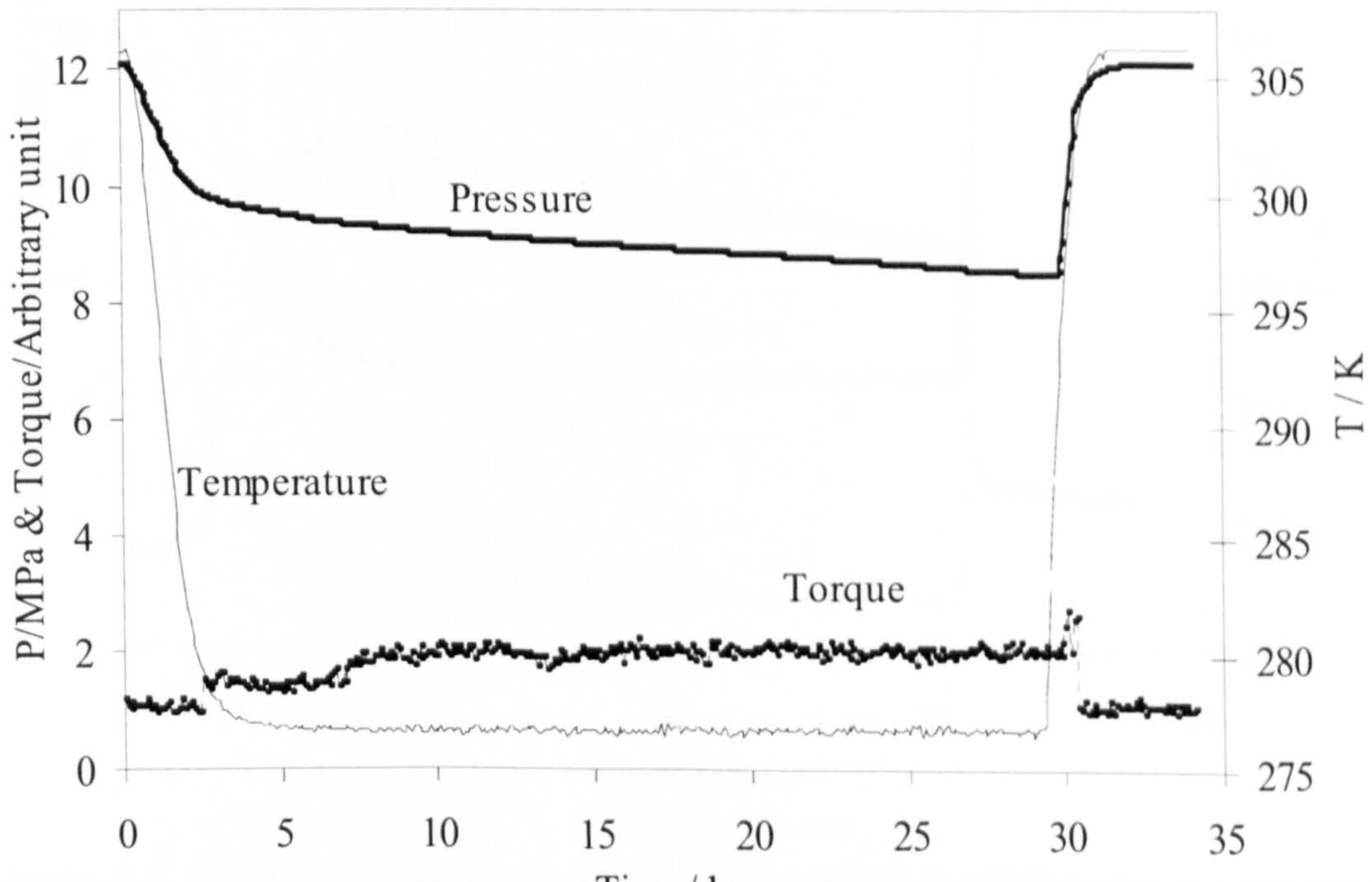

Figure 6.4. Pressure, temperature and torque profiles for NG-water system stirred with helical tube impeller, rpm=100. The slow rate of hydrate growth (pressure drop) at 100 rpm mixing rate is believed to be due to poor mixing.

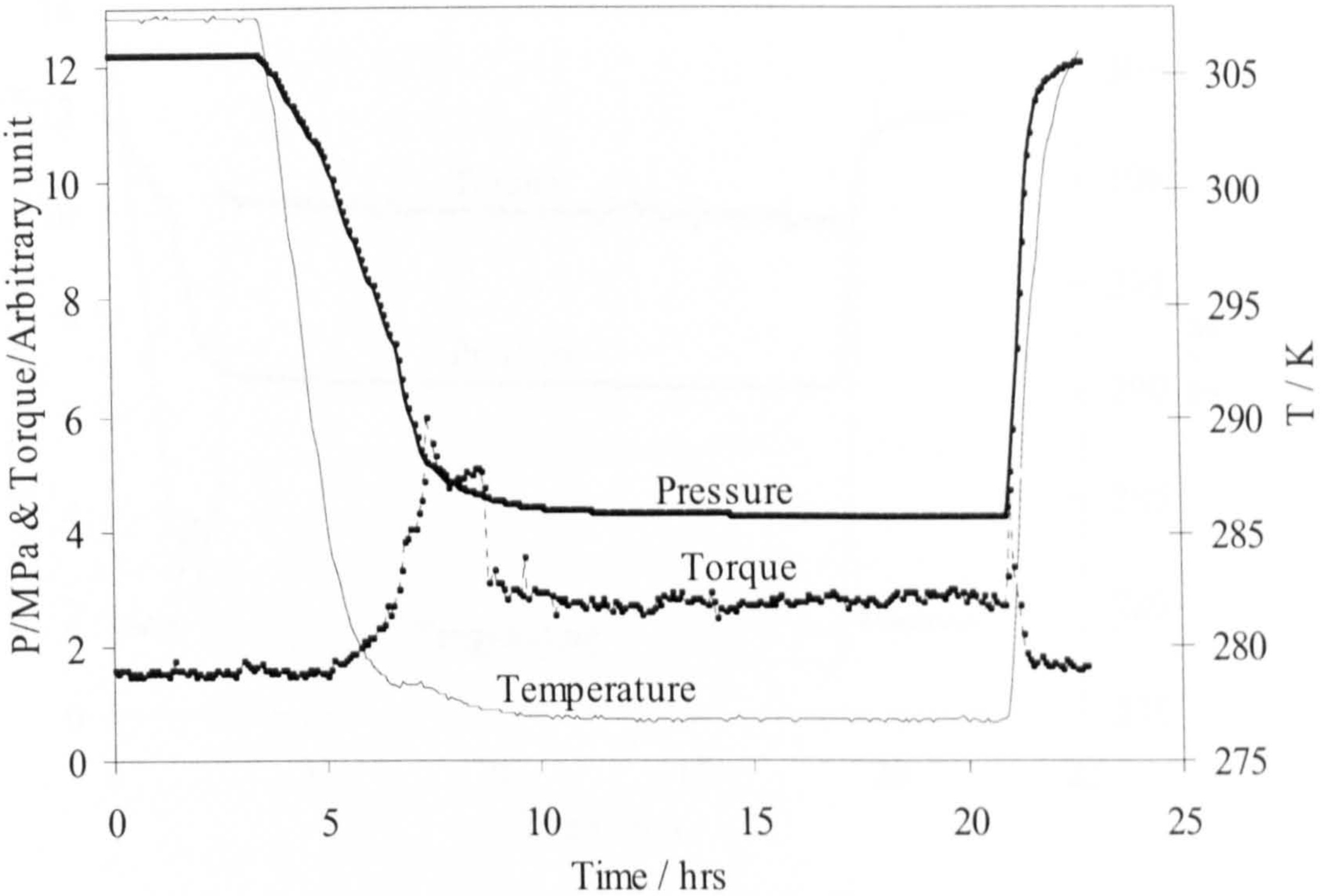

Figure 6.5. Pressure, temperature and torque profiles for NG-water system stirred with helical tube impeller, rpm=200. In comparison with the test at 100 rpm, more hydrate formed with higher rate of growth and after hydrate formation the torque is less stable (compare with Figure 6.4).

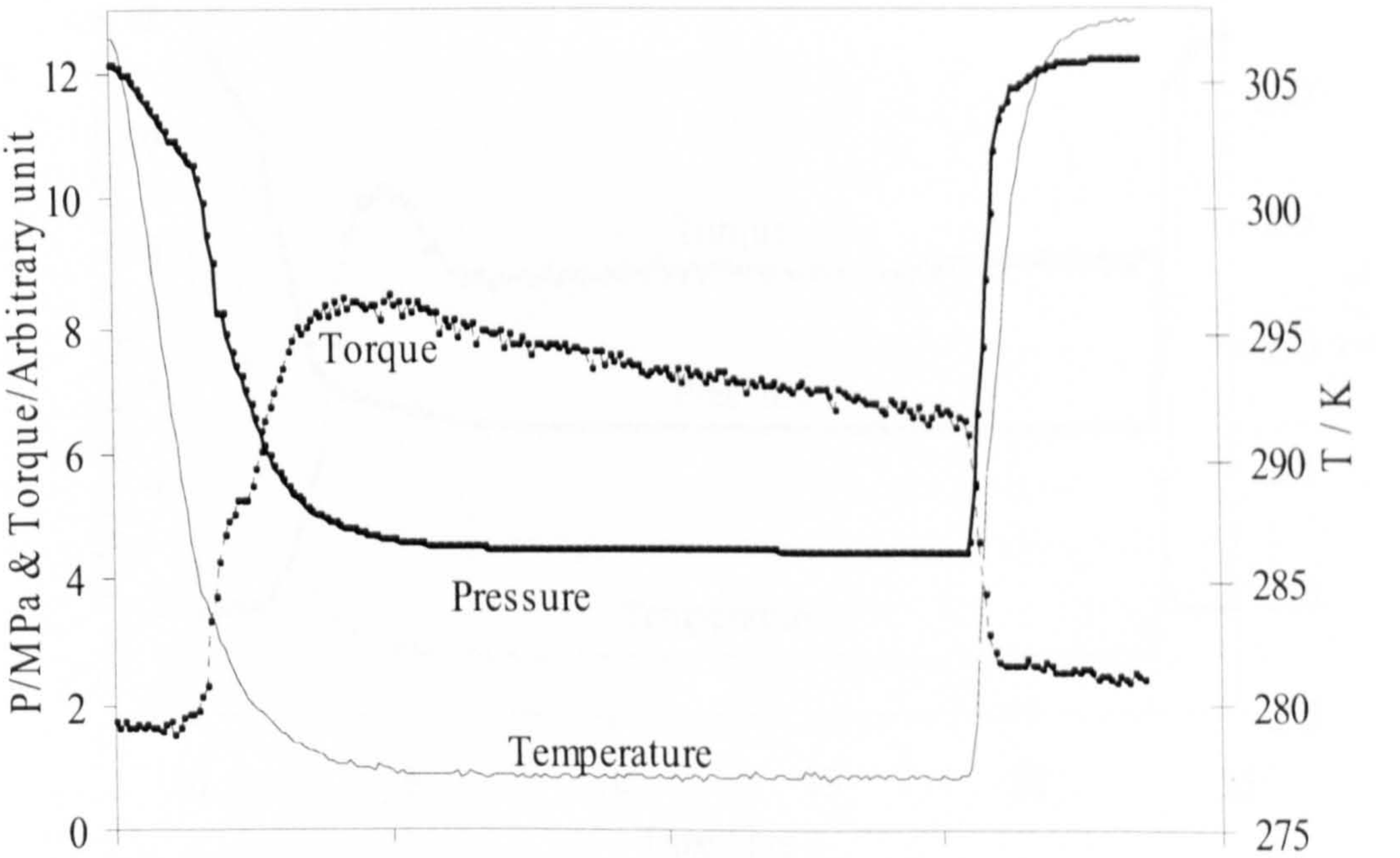

Figure 6.6. Pressure, temperature and torque profiles for NG-water system stirred with helical tube impeller, rpm=400. At 400 rpm, the stability of the torque profile was better than the test at 200 rpm (Figure 6.5).

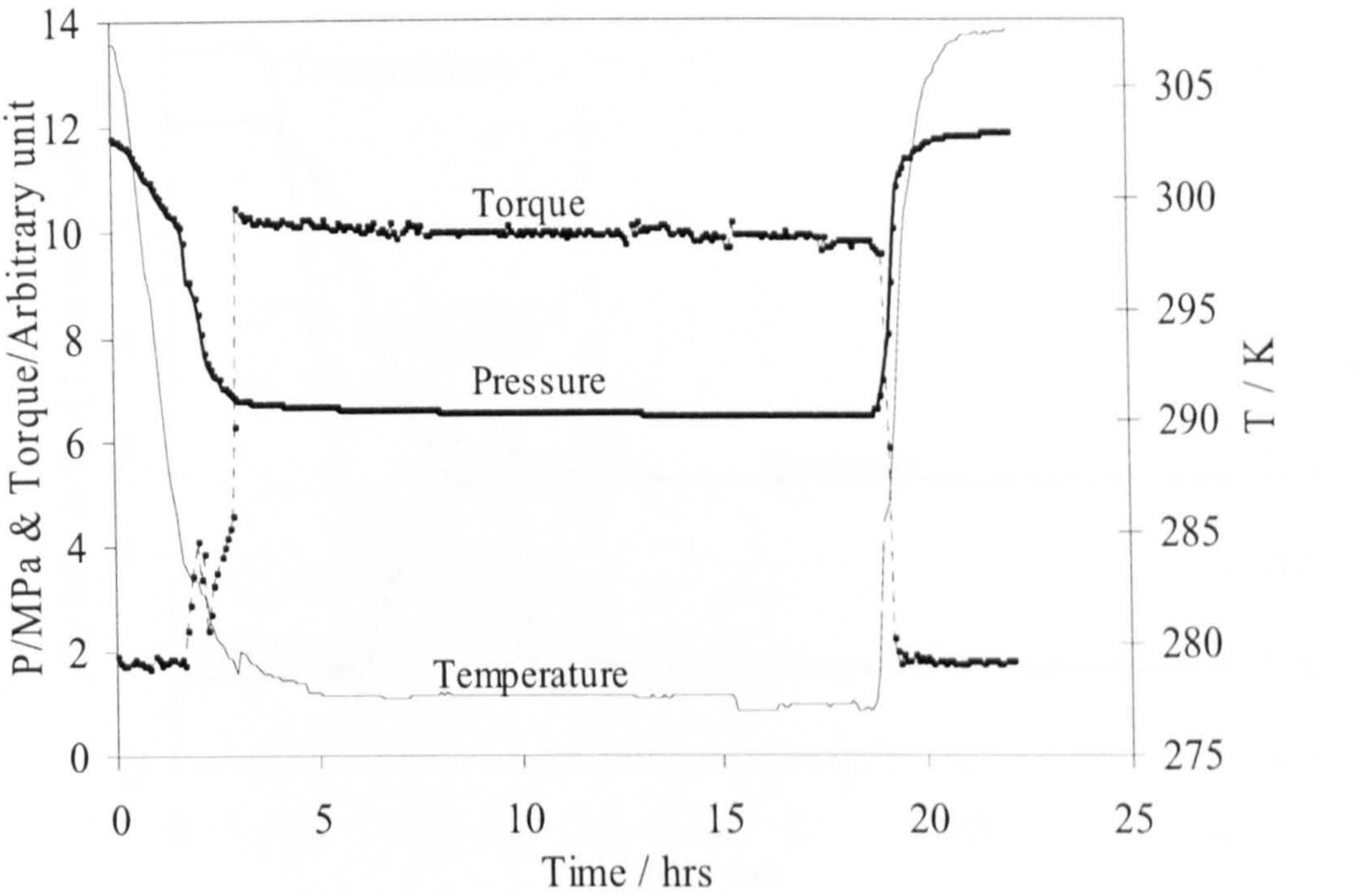

Figure 6.7. Pressure, temperature and torque profiles of the blank test on NG-water-condensate system (W/C=0.33), stirred with helical tube impeller at 400 rpm.

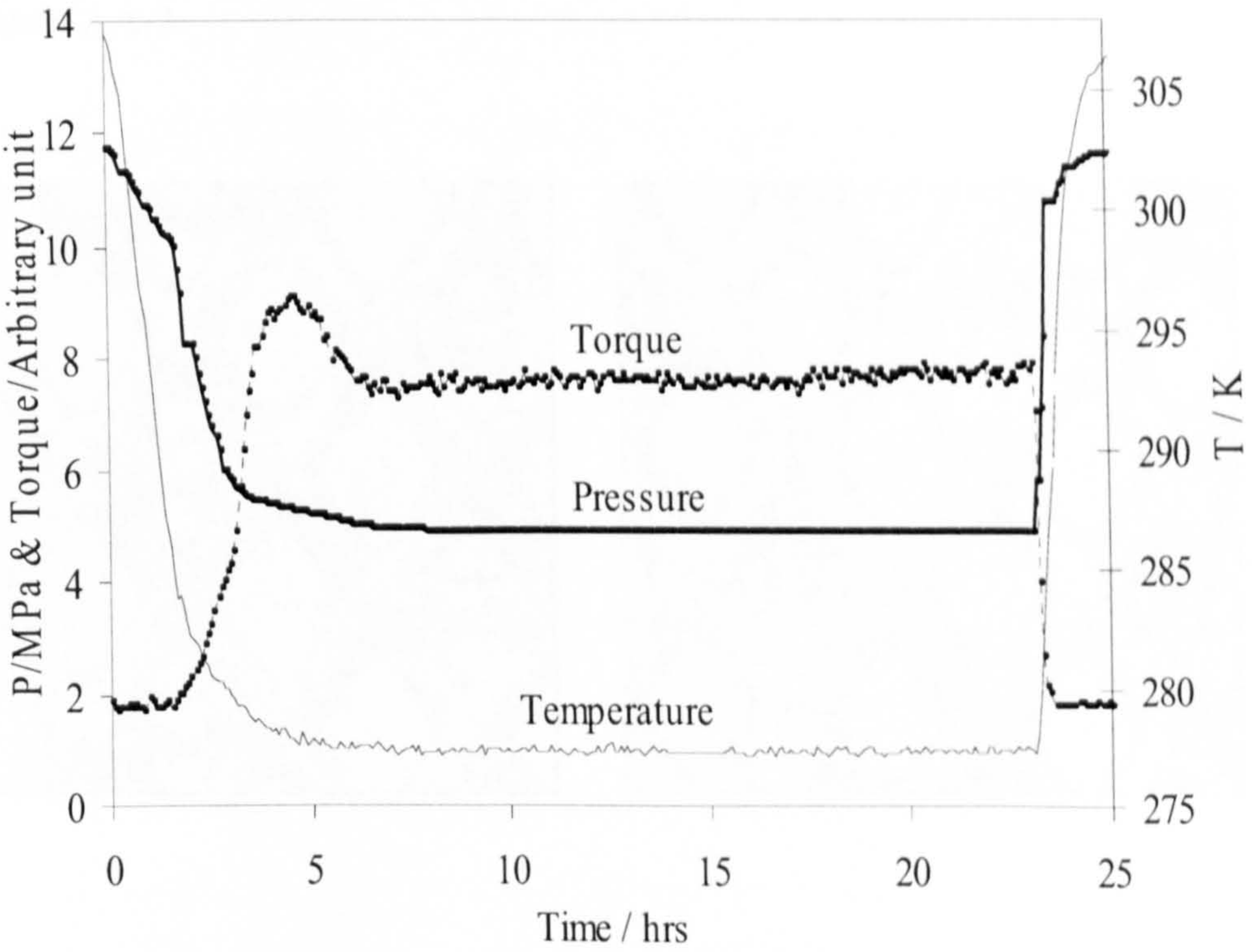

Figure 6.8. Pressure, temperature and torque profiles of the test on NG-water-condensate system (W/C=0.33), in the presence of 2.5 vol% AA-2 in water phase, stirred with helical tube impeller at 400 rpm. The torque after hydrate formation was less than that of blank test (Figure 6.7).

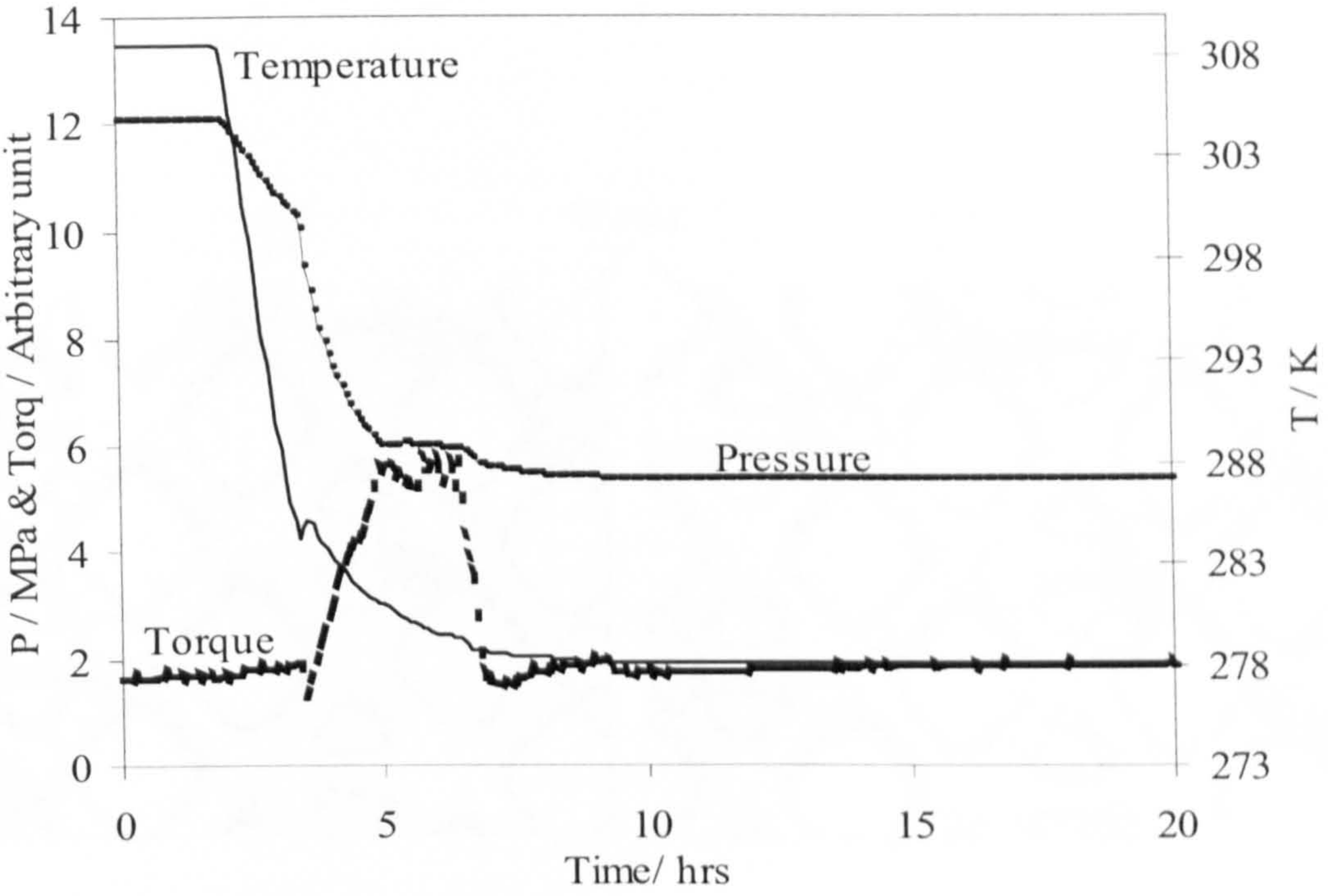

Figure 6.9. Pressure, temperature and torque profiles of the test on NG-water-condensate system (W/C=0.33), in the presence of 2.5 vol% AA-3 in water phase, stirred with helical tube impeller at 400 rpm. The torque after hydrate formation was less than that of the test with AA-2 (Figure 6.8), demonstrating better performance of AA-3 than AA-2.

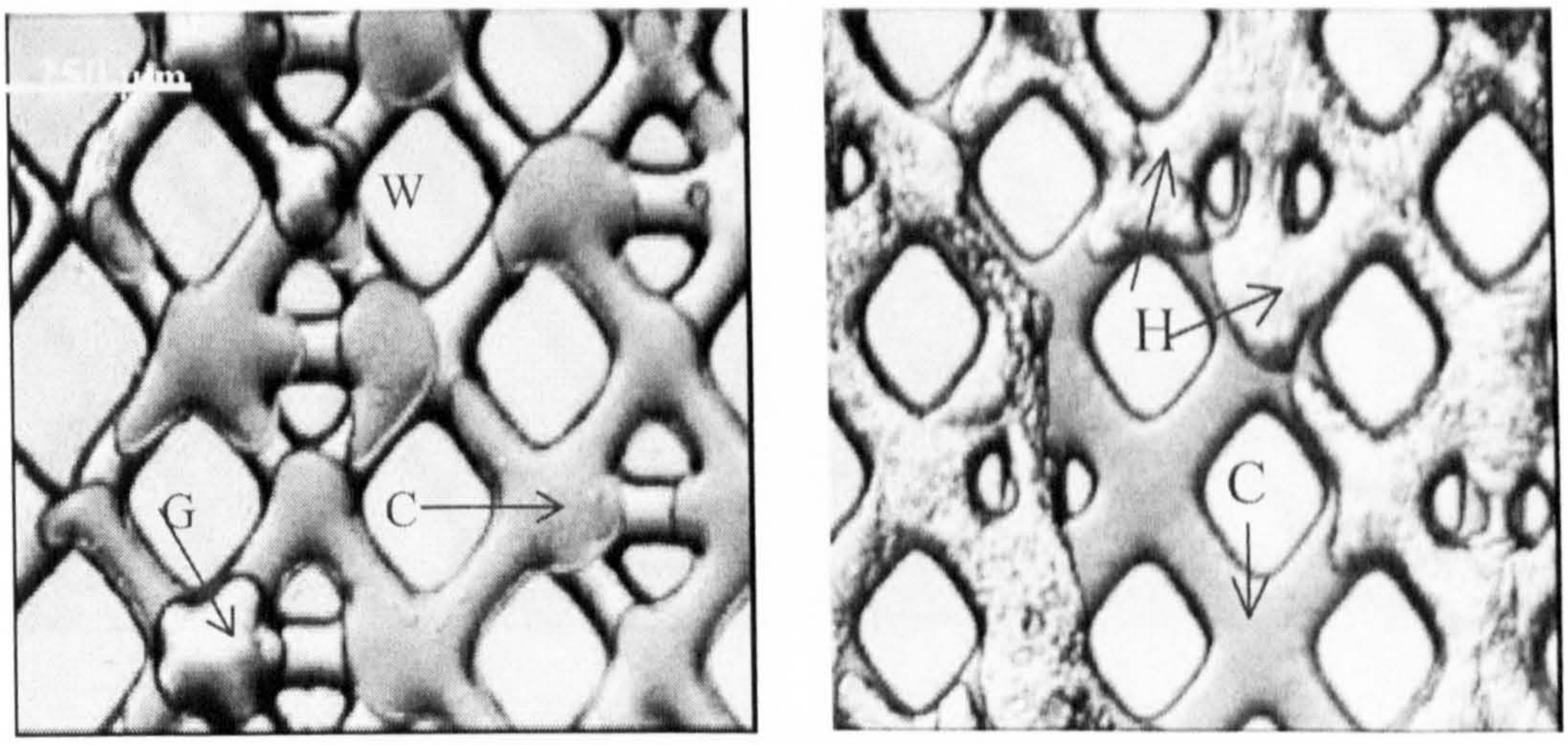

(a) Before hydrate formation (b) After hydrate formation

Figure 6.10. Water, condensate and natural gas phases in the micromodel before and after hydrate formation. W (water), G (gas), C (condensate). After hydrate formation, lumps of hydrates blocked some of the micromodel pores.

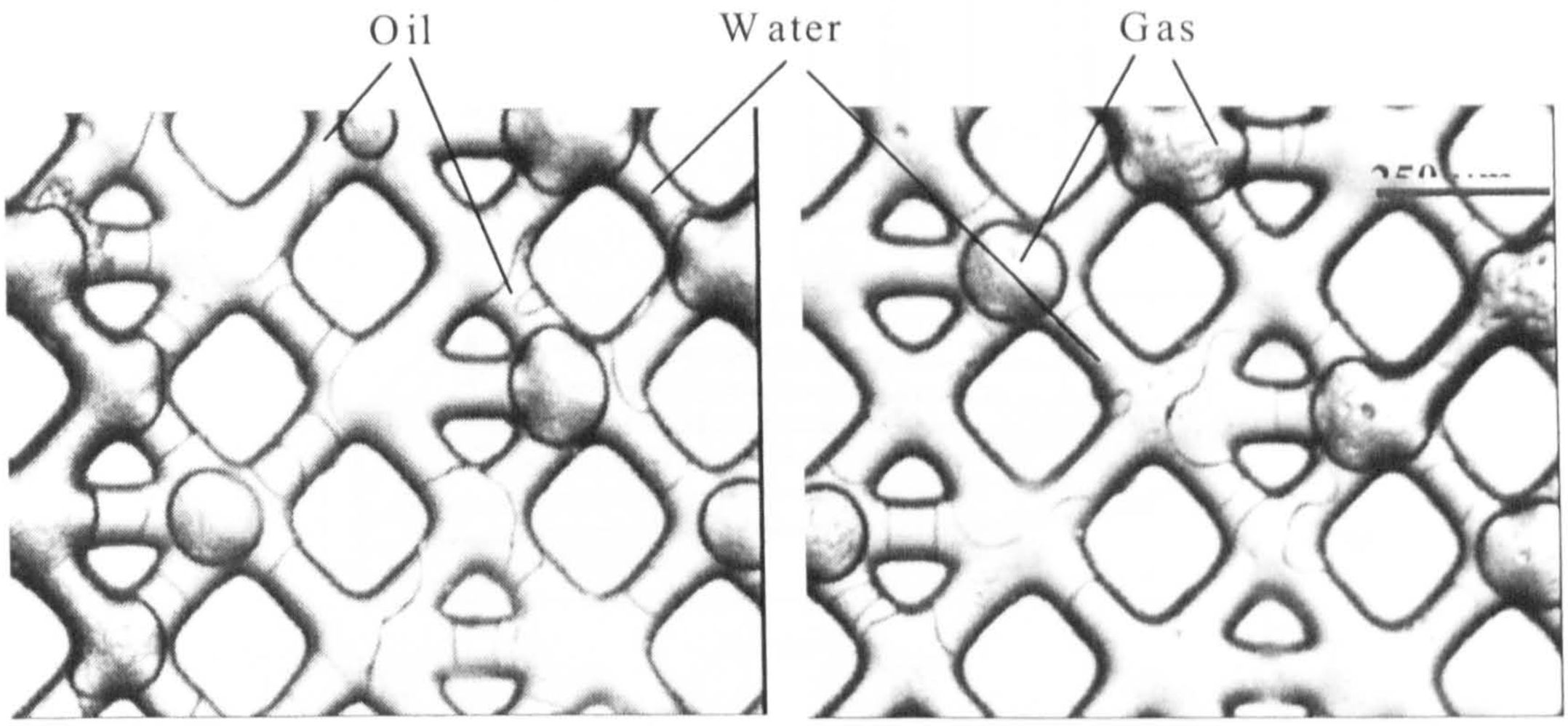

(a). Condensate-water-natural gas phases before hydrate formation in the presence of AA-1 in micromodel.

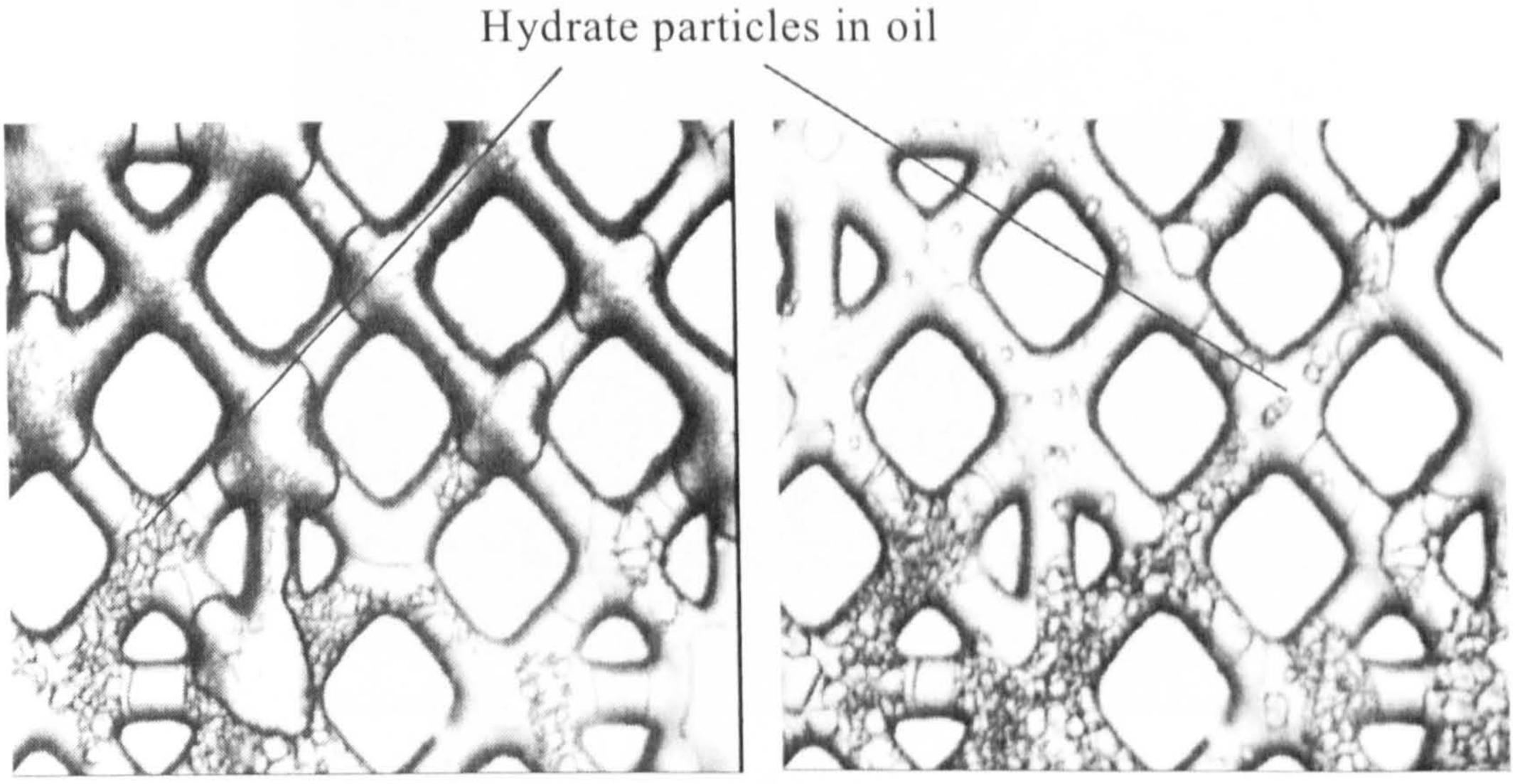

(b). Hydrate particles formed in the continuous condensate phase in micromodel pores.

Figure 6.11. Images of distribution of phases before and after hydrate formation in condensate-water-natural gas system in the presence of AA-1 in micromodel. The hydrates particles were not agglomerated.

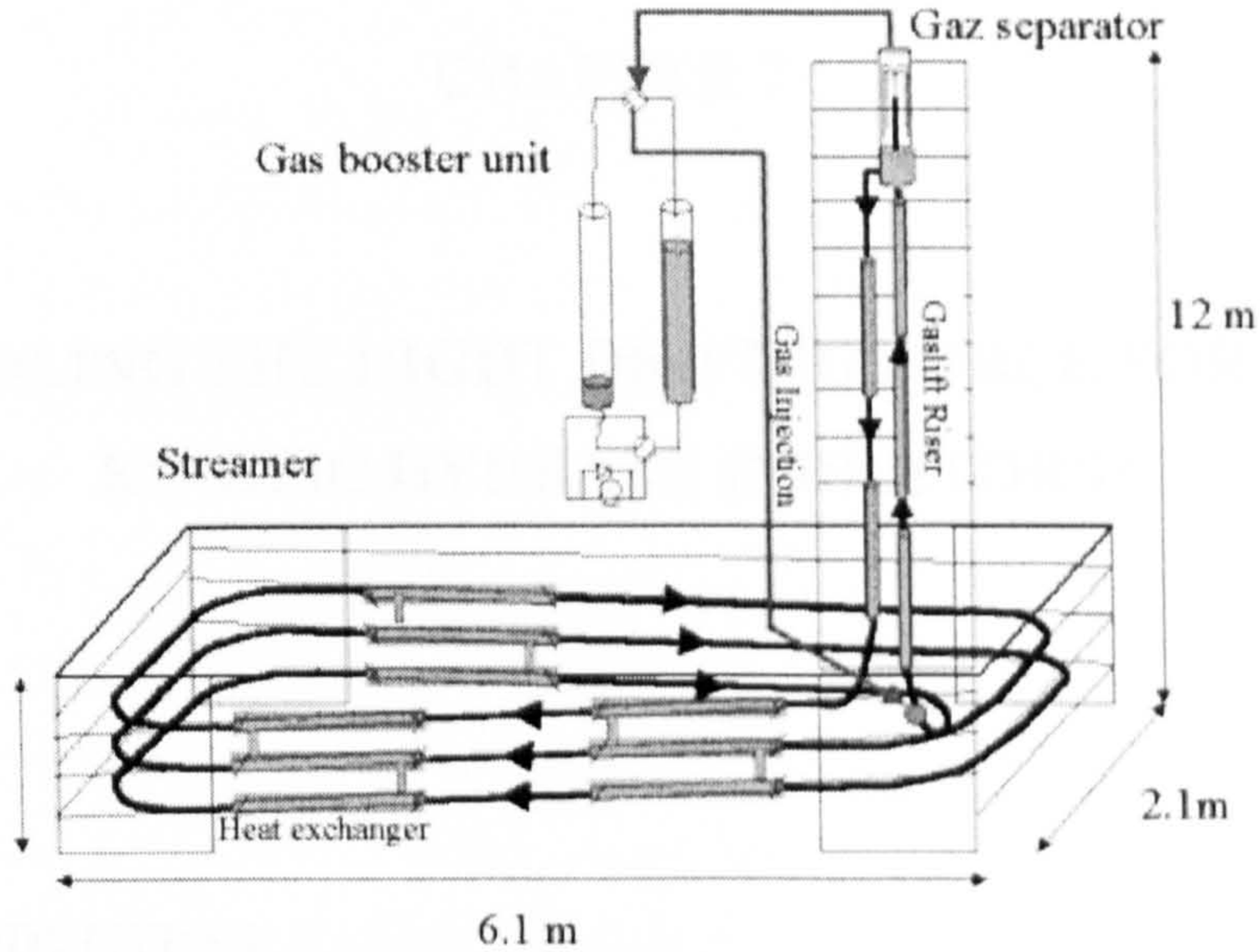

Figure 6.12. Schematic of Saint Etienne School of Mines'gas lift flow loop.

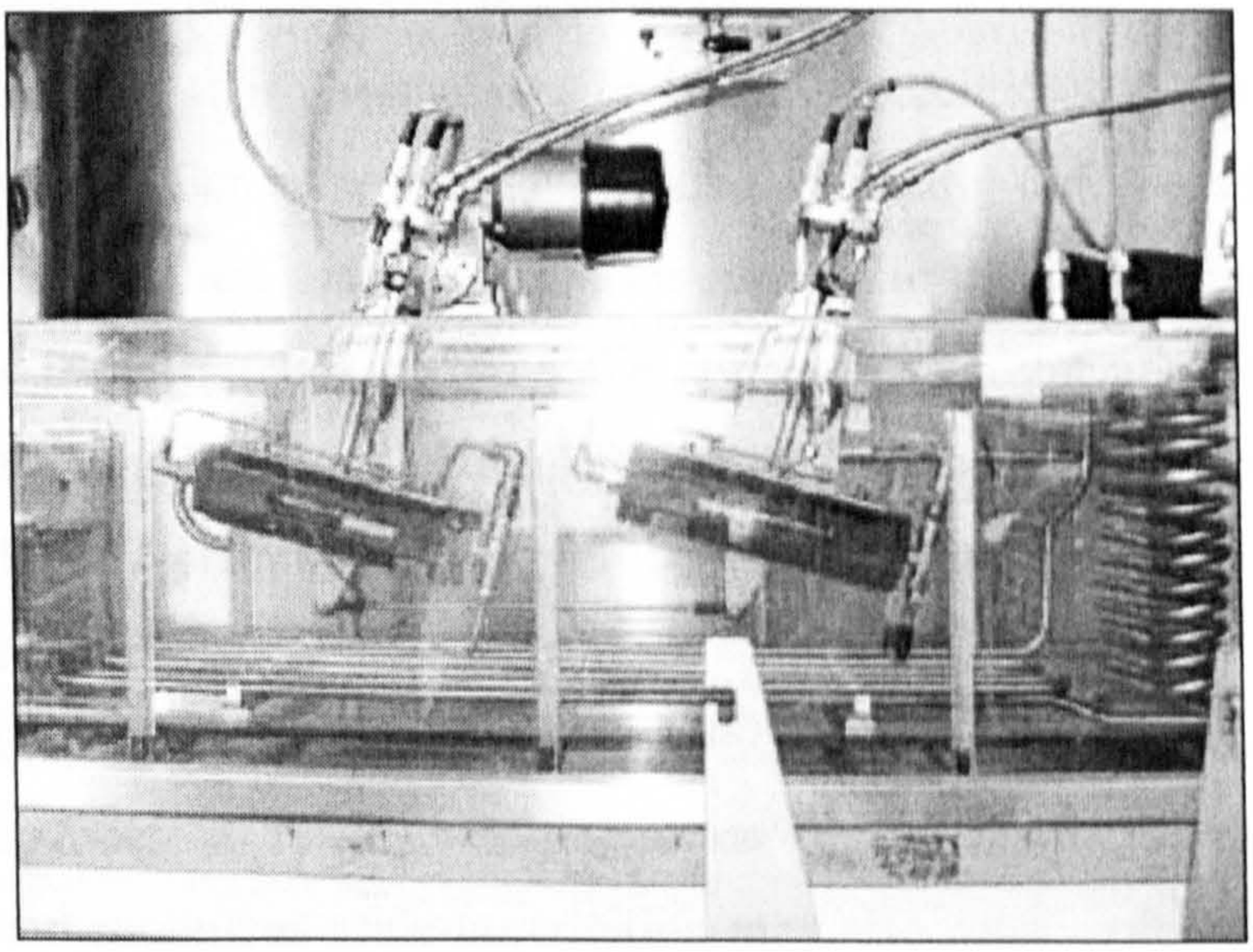

6.13. Rocking cells used for evaluation of AAs.

CHAPTER 7

IS SUBCOOLING THE RIGHT DRIVING FORCE FOR TESTING KINETIC HYDRATE INHIBITORS?

7.1 INTRODUCTION

The performance of kinetic inhibitors is usually evaluated in autoclaves and /or flow loops in terms of the induction time. The induction time is defined as the elapsed time from the start of the experiments to the onset of hydrate formation. The experiments are usually conducted at isothermal and/or isobaric conditions to simulate the field operating conditions. For such tests, subcooling is usually considered as the driving force for hydrate formation and a criterion for simulating field conditions. Subcooling is calculated as the difference between the system temperature and the equilibrium temperature (on the hydrate phase boundary) at the system pressure. In many cases, it is a routine industrial practice to scale up the experiments conducted at low-pressure conditions to high pressures based on some similarity principles. Application of subcooling as the driving force and scale-up criterion may be reliable in some cases, while in other cases it may overestimate or underestimate the pressure effect. Application of subcooling as scale-up criterion may also cause potential complications such as changes of phase (in oil systems), or shifting the test conditions to sub-zero temperatures and ice formation.

A comprehensive driving force for the description of the appearance and growth of gas hydrates is of great importance in the investigations associated with gas hydrates. A number of driving force expressions for hydrate formation have been reported in the literature. Vysniauskas and Bishnoi (Vysniauskas and Bishnoi, 1983) introduced subcooling as the driving force for hydrate formation. Skovborg and Rasmussen (Skovborg et al., 1992) defined it as the difference of water chemical potentials in the hydrate crystal and liquid water phase. Natarajan and Bishnoi (Natarajan et al., 1994) considered ($f_i^{exp}/ f_i^{eq} - 1$) as the driving force, where f_i^{exp} and f_i^{eq}, are fugacity of

component 'i' in the bulk and in the hydrate interface, respectively. Christiansen and Sloan (Christiansen and Sloan, 1995) presented the total molar change in Gibbs free energy in hydrate formation reaction, Δg^{exp}, as the driving force for hydrate formation. Sloan (Sloan, 1998) has shown that, the driving force derived by Christiansen and Sloan, Δg^{exp}, is the general case for all driving forces presented by the previous investigators. The fundamental driving force for crystallization is defined as the difference between chemical potential of the given substance in the transferring and the transferred state, e.g. in solution and in the crystal (Mullin, 1997; Garside et al., 2002). Kashchiev and Firoozabadi (Kashchiev and Firoozabadi, 2002) considered the hydrate formation as a crystallization reaction and derived the driving force, supersaturation, for hydrate formation in a pure gas- water system on the basis of the difference between chemical potentials of the old phase (aqueous water with dissolved gas) and the new phase (hydrate). A comprehensive driving force for hydrate formation in a gas-water system, derived on the basis of thermodynamics principles, should be applicable to any system in the presence of low dosage hydrate inhibitors. This is because the inhibitors are present in very low concentrations in the aqueous phase, and their effect on the hydrate phase boundary can be ignored.

In this study, first a brief description of the two latest driving force expressions for hydrate formation (Christiansen-Sloan, and Kashchiev-Firoozabadi) is presented. The former method is applied to calculate the variation of driving force with pressure at isothermal conditions, and its relationship with subcooling for methane and natural gas hydrates. The latter is used for calculating the variation of driving force with temperature at isobaric conditions. Next, the effect of pressure on the driving force at a constant degree of subcooling for methane and natural gas hydrate is calculated to find out the conditions where subcooling alone can be considered as a driving force index for up-scaling means. Finally, the results of the experiments in relation to the effect of pressure on the induction time of natural gas –water systems in the presence and absence of kinetic inhibitor are presented.

7.2 BACKGROUND

7.2.1 Christiansen and Sloan Approach

Christiansen and Sloan (Christiansen and Sloan, 1995) derived the driving force for hydrate formation on the basis of molar changes of the total Gibbs free energy of the system when hydrate crystal forms from water and gas. With the application of the

isothermal path, Figure 7.1, for calculating ΔG of hydrate formation, they obtained the following equation for multi-component systems:

$$\Delta G^{exp} = n_w(v_w - v_h)\,(P^{eq} - P^{exp}) + RT\,\Sigma\,(n_i)\,\ln[\,f_i^{eq}/\,f_i^{exp}] \qquad (7.1)$$

$$\Delta g = \Delta G^{exp} / n_w \qquad (7.1a)$$

where ΔG^{exp} is the change in Gibbs free energy at operating conditions, Δg change in specific Gibbs free energy at operating conditions (The total changes of Gibbs free energy in the isothermal path shown in Figure 7.1, per mole of water consumed), n_w the number of moles of water consumed (hydration number); v_w and v_h the molar volumes for water and hydrate respectively, and f_i^{eq}, f_i^{exp} the fugacity of component 'i' in the gas mixture at equilibrium and experimental conditions, respectively.

For isobaric conditions, Sloan (Sloan, 1998) applied the Gibbs-Helmholtz relation to obtain:

$$\Delta g = (-s)\,\Delta T \qquad (7.2)$$

where (-s), the entropy term, relates the Gibbs free energy to the temperature change.

7.2.2 Kashchiev-Firoozabadi Approach

They derived the driving force for formation of gas hydrate for a system of one gas component and water (Kashchiev and Firoozabadi, 2002). The system was considered at constant pressure and temperature and hydrate formation was assumed to be analogue to a solid precipitation reaction in a solution:

$$G + n_w\,H_2O \Leftrightarrow G.\,n_w\,H_2O \qquad (7.3)$$

One molecule of dissolved gas and n_w (hydrate number) water molecules of the solution form one building unit (G. n_w H_2O) of the hydrate crystal. By defining μ_{gs} and μ_w as the chemical potentials of gas and water molecules in the aqueous solution, the chemical potential of a hydrate building unit (one gas molecule and n_w water molecules) in solution, μ_{hs}, we obtain:

$$\mu_{hs} = \mu_{gs} + n_w\,\mu_w \qquad (7.4)$$

By definition, the driving force for the new phase formation is the difference between the chemical potentials of the old and new phases. This difference is called super saturation Δμ and can be calculated by:

$$\Delta\mu = \mu_{hs} - \mu_h = \mu_{gs} + n_w \mu_w - \mu_h \quad (7.5)$$

where μ_h is the chemical potential of a hydrate building unit in the hydrate crystal. Nucleation and/or growth of hydrate crystals are possible only when $\Delta\mu>0$: then $\mu_{hs} > \mu_h$ and the solution is supersaturated.

With expansion of relevant chemical potential terms in Equation 7.3 and with assuming chemical equilibrium between the solution and the gas phase, they derived the driving force at isothermal and isobaric conditions. For isothermal conditions the driving force was found to be:

$$\Delta\mu = kT \ln[\varphi(P,T)\, P / \varphi_e(P_e,T)\, P_e] + \Delta v_e(P-P_e) \quad (7.6)$$

where, k is the Boltzmann constant, P_e is the hydrate equilibrium pressure at T, and φ is the fugacity coefficient of gas at given P,T. Δv_e is the difference between the volume of n_w water molecules in the solution and the volume of a hydrate building unit in the hydrate crystal at the equilibrium pressure:

$$\Delta v_e = n_w(P_e,T)\, v_w(P_e,T) - v_h(P_e,T) \quad (7.6a)$$

v_h can be calculated from : $v_h = v_{cell} / n_g$, (7.7)

where n_g is the number of gas molecules per unit cell of hydrate crystal lattice and v_{cell} is the volume of the unit cell of hydrate crystal lattice.

For isobaric conditions, by applying some approximations in the derivations, they determined the driving force as:

$$\Delta\mu = \Delta s_e(T-T_e) = \Delta s_e\, \Delta T \quad (7.8)$$

where ΔT is subcooling and Δs_e is given by:

$$\Delta s_e = n_w(P,T_e)\, s_w(P,T_e) - s_h(P,T_e) + s_{gg}(P,T_e) \quad (7.8a)$$

s_{gg}, s_w and s_h are the entropies per gas molecule in the gas phase, per water molecule in the water phase, and per hydrate building unit in the hydrate crystal, respectively. Δs_e, is the hydrate dissociation entropy per hydrate building unit at equilibrium temperature, i.e. the entropy change in the transfer of one gas molecule and n_w water molecules from the hydrate crystal into the gas phase and the water-rich liquid phase at the given P and T.

By comparing equations 7.1 with 7.6, it appears that both approaches for calculation of driving force are similar with different basis for derivation; one molecule of gas and n_w molecules of water in Kashchiev-Firoozabadi approach and one mole of gas and n_w mole of water in Christiansen-Sloan approach. The calculated driving force for a pure gas-water system by Equation 7.6 would be similar to that of Equation 7.1, if it is multiplied by Avogadro number thus:

$$\Delta G^{exp} = N_{av} . \Delta\mu$$

Since Christiansen-Sloan method can be applied for multicomponent gases, their approach (Equation 7.1) was adopted for calculating the driving force in the following sections. At isobaric conditions, derivation of driving force by Kashchiev-Firoozabadi, Equations 7.8 is more clear and applicable than Equation 7.2. Some of the subroutines of an in-house hydrate programme, HWHYD, (detailed in Chapter 2) (Avlonitis et al., 1994; Tohidi et al. 1995), were used for calculating the driving force from Equation 7.1.

7.3 DRIVING FORCE FOR SIMPLE HYDRATES

Hydrates formed from a single hydrate former are known as simple hydrates. In this section the driving force for these systems are discussed.

7.3.1. Changes of Driving Force at Isothermal and Isobaric Conditions

Consider an isothermal operating line on the methane hydrate phase boundary (Figure 7.2), by increasing the pressure the subcooling will increase. If the changes (increasing) in subcooling and the calculated dimensionless driving force ($-\Delta G/RT$) are plotted against pressure in the same diagram, by adoption of an appropriate scale for the subcooling axis, the two curves almost match (Figure 7.3). Thus, from Figure 7.3, at a constant pressure, one can read the degree of subcooling and the driving force at the same time from different axes and relate them to each other. The driving force for hydrate formation in methane-water system is found to be proportional to the degree of subcooling at isothermal conditions. Comparing the axes of Figure 7.3, for methane the following relationship between driving force and subcooling can be concluded.

$$-\Delta G/RT \cong 0.08\ \Delta T \qquad \text{at constant temperature; } T=273.2\text{ K and given P} \qquad (7.9)$$

The above discussion is true for all pure gases. For example, the driving force and subcooling versus pressure diagrams for ethane and propane at 273.15 K are presented in Figures 7.4 and 7.5 respectively. Again by adoption of an appropriate scale for the subcooling axis, the two curves almost match. It should be mentioned that the

subcooling coefficient in Equation 7.9 changes for different gases. At isobaric conditions, Equations 7.2 and 7.8 show that the driving force is also proportional to subcooling.

Using Equation 7.1, the variation of driving force with subcooling at different isobars for methane has been calculated and shown in Figure 7.6. As expected by Equation 7.8, all of the isobars are linear, demonstrating a linear relationship between the driving force and subcooling with a slope of $\Delta s_e/RT_e$. Furthermore, there is an increase in the slope with reduction in the system pressure. It is worth noting that the main decrease in the slope of the lines (12.5%) occurs from 5.36 MPa to 19.4 MPa, afterwards up to 43 MPa there is only 7% decrease in $\Delta s_e/RT_e$.

From the above discussions it can be concluded that for hydrate formation from a single compound, the driving force is proportional to subcooling. At isothermal and isobaric conditions, the changes of driving force with pressure or temperature can be followed by the change of subcooling.

7.3.2 Changes of Driving Force with Pressure at Constant Degrees of Subcooling

At constant degree of subcooling, an increase in the system pressure will result in an increase in the system temperature, as shown in Figure 7.7. For methane-water system, the changes of driving force with pressure at constant degrees of subcooling have been calculated and presented in Figure 7.8. In general, at constant degrees of subcooling, the driving force decreases as pressure increases. However, the magnitude of driving force decrease as a function of pressure is not considerable (7%-15% decrease after increasing the system pressure from 10 to 75 MPa). It should also be noted that the main reduction in driving force occurs at pressures lower than 20 MPa, above this limit the driving force is practically constant. Therefore, in pure gas–water systems, for practical applications, where the operation pressure is higher than 20 MP, subcooling alone can be representative of the driving force for hydrate formation.

7.4 DRIVING FORCE FOR DOUBLE HYDRATES

When two compounds take part in hydrate formation the resulting hydrate is called double hydrates. In this section the driving force for these systems is discussed. A natural gas system has been chosen for this purpose due to availability of experimental data, but the approach is applicable to any multi-component system.

7.4.1 Isothermal and Isobaric Conditions

As shown in Figure 7.9, if the degree of subcooling and the calculated driving force for natural gas are plotted against the system pressure (by adoption of an appropriate scale for the subcooling axis), it is not possible to get a good match at all pressures (unlike pure gas system as shown in Figure 7.3). The composition of this natural gas 2 (NG2) is presented in Table 7.1. As demonstrated in Figure 7.9, at some pressure ranges, the degree of subcooling could be a good measure of the driving force. However, at P=4-20 MPa the subcooling underestimate the driving force which calculated from the mentioned model. It should be mentioned that the deviation in the driving force curve changes with the composition of the natural gas. Figure 7.10 shows that for a different natural gas (NG1) with a lower concentration of propane and butane, the deviation in the driving force curve is less than that of high propane content natural gas (NG2). The composition of NG1 is also presented in Table 7.1.

The reason for such changes in the driving force with pressure in multi-component systems can be found from studying different terms in the driving force equation (Equation 7.1). Figure 7.11 presents the plot of different terms of Equation 7.1 (all the terms are divided by RT to be dimensionless) for Natural Gas 2 (NG2). As shown in the figure, the fugacity term in Equation 7.1 causes the deviation in the driving force curve for the natural gases.

Plotting the logarithm of the fugacity ratios for each component of natural gas versus pressure (Figure 7.12) shows that the variation of logarithm of fugacity ratios for propane and butane with pressure is more than other components. The equilibrium composition of the components in the hydrate structure (n_i in Equation 7.1) can increase or decrease the effect of each component in the overall driving force curve. At isobaric conditions, and applying Equation 7.1, the changes of driving force with subcooling can be calculated, as presented in Figure 7.13. As shown in the Figure 7.13, the isobars are almost linear and in the pressure range of 0-20MPa the slope of isobars decrease at higher pressure values. However at pressures higher than 20MPa, the isobars coincide. Despite that Equation 7.8 has been derived for pure gas and water systems only, by analogy it may also be used in multi-component systems and the slope of the lines in Figure 7.13 may be considered as $\Delta s_e/RTe$ for natural gas.

When comparing Figures 7.6 and 7.13, it can be seen that in 0-20MPa pressure range the changes in the slope of isobars in the natural gas case is more pronounced than that

of methane, however for both cases at isobaric conditions the changes of driving force can be followed by changes of subcooling with a good approximation.

7.4.2 Constant Degree of Subcooling Condition

The variation of driving force with pressure at different degrees of subcooling for Natural Gas 2 (NG2) is presented in Figure 7.14. As shown in the Figure 7.14, up to 20 MPa, by increasing the pressure the driving force decreases (approximately 20 % drop in the driving force). Above that the driving force is not a strong function of the system pressure (e.g., 1-2% increase in driving force within 20-55 MPa). In other words, for the natural gas in the pressure range of P>20 MPa, with a good approximation, constant degree of subcooling is equivalent to constant driving force (Figure 7.7).

7.5 SUBCOOLING AS DRIVING FORCE CRITERION IN DIFFERENT SYSTEMS

It is a common practice to test a low dosage hydrate inhibitor in different laboratories to assure its performance and the repeatability of the tests. Different natural gases with different compositions may be used in the laboratories for testing the same inhibitor. The results of the tests are comparable only when the reported driving forces for hydrate formation are comparable. In practice, the degree of subcooling is generally reported with little attention to the potential effects of pressure and gas composition.

Since the experiments are usually conducted at isothermal conditions, Equation 7.1 can be used for calculation of the driving force. In Figure 7.15 the changes in driving force with the degree of subcooling at different isobars for the two above-mentioned natural gases have been illustrated. It shows that the compositions of the natural gases have a negligible effect on the isobars and subcooling is representative of real driving force. At constant degree of subcooling, as expected from the discussion in Section 7.4.1, the effect of pressure on the driving force is mainly between 5-20MPa (about 20% decrease) for both natural gases.

In the case of testing a low dosage hydrate inhibitor with two different synthesised gas mixtures (e.g. methane–ethane or methane–propane), again the driving forces for the systems must be similar. Considering two different systems, using Equation 7.2, and by analogy the driving force for hydrate formation in each system at isobaric conditions may be written as:

$$\Delta G_1^{exp} = \Delta s_{e1}\, \Delta T_1 \qquad (7.10)$$

$$\Delta G_2^{exp} = \Delta s_{e2}\, \Delta T_2 \qquad (7.11)$$

If $\Delta G_1^{exp} = \Delta G_2^{exp}$, then:

$$\Delta T_2 = [\Delta s_{e1}/\Delta s_{e2}]\, \Delta T_1 \qquad P=constant \qquad (7.12)$$

In addition we know that: $\Delta s_e = \Delta h_e/T_e$, where Δh_e is the enthalpy of dissociation of one mole of hydrate, by substitution we reach to:

$$\Delta T_2 = [\Delta h_{e1}/\Delta h_{e2}]\, [T_{e2}/T_{e1}]\, \Delta T_1 \qquad @ \qquad P=constant \qquad (7.13)$$

From the above equation, at isobaric conditions, the subcooling in System 2, which will lead to the identical driving force as that of System 1 with ΔT_1 subcooling can be calculated. The enthalpies of dissociations can be obtained from phase equilibria via the Clapeyron equation.

7.6 INDUCTION TIME AND PRESSURE EFFECT

In the light of the above analysis we shall now consider the impact of pressure on the induction time in the absence and presence of a kinetic inhibitor when the driving force ($-\Delta G/RT$) for hydrate formation or subcooling is constant. Two series of experiments were conducted to study the pressure effect, which will be discussed in the following sections.

7.6.1. In the Absence of Kinetic Inhibitors

A total of 4 experiments were carried out in the kinetic rig to measure the induction times for hydrate formation in the Natural Gas 1 (NG1)–water system, at similar degrees of subcooling and different pressures to investigate the effect of pressure on the induction time. The kinetic rig set-up and the test procedure have been detailed in Chapter 4.

Two sets of experiments were carried out in two different pressure ranges but at the same degree of subcooling. As shown in Table 7.2, Tests No. 1-2 were conducted at 17.4 MPa and Tests No.3-4 at 6.3 MPa. The change in the system pressure had no significant effect on the induction times at constant degree of subcooling. Yousif (Yousif, 1994) has reported the results of the tests conducted on the Natural Gas 2 (NG2)-water system. The result of the tests, which were carried out at similar degrees of subcooling and different pressures, have been presented in Table 7.3. As shown in Table 7.3, at similar degrees of subcooling, the pressure does not have a significant impact on the driving forces and induction times. This is an expected result and in line with the trend predicted in Figure 7.14.

7.6.2. In the Presence of Kinetic Inhibitor

The induction times for hydrate formation in the system of Natural Gas 1 (NG1) and 1.25 mass% of a kinetic inhibitor (containing 40 mass% poly vinyl caprolactam (PVCap) and 60 mass% ethylene glycol as solvent) in water were measured in the kinetic rig. Two series of tests were conducted in two different pressure ranges and the summaries of the tests have been presented in Tables 7.4 and 7.5. Table 7.4 shows the results of the tests in the pressure range of 6.3-6.9 MPa. As shown in that pressure and at 14.2 K subcooling hydrate formed without any induction time. By decreasing the degree of subcooling to 13.7 K, 17 hours induction time was observed. At 12.5 K subcooling the induction time was longer than 60 hours. Table 7.5 shows the results of the tests in pressure range of 30-31 MPa. As shown in the table, at high-pressure conditions, even at 11 K subcooling, there was no induction time for hydrate formation. For observing 60 hours induction time the degree of subcooling needed to be reduced to 9.5 K. With comparison of the driving forces and the induction times in the Tables 7.4 and 7.5 it can be seen that for the tests carried out at high pressure conditions, in spite of lower driving forces than those in low pressure tests, shorter induction times are observed. This shows that the performance of the kinetic inhibitor tested, at constant driving force conditions, is affected by pressure.

The induction time for hydrate formation in a system is related to driving force (thermodynamic property) and kinetic barriers (e.g activation energies for hydrate formation reaction) for hydrae formation in the system. In the above mentioned tests, the significant effect of pressure on the induction time for hydrate formation in the presence of a KHI denotes the impact of pressure and KHI on the kinetic barriers for hydrate formation in a system.

The results of the tests also show the importance of considering the full operational envelope of the production system (e.g. initial high pressure operation with depletion to low pressure) for testing KHIs.

7.7. CONCLUSIONS

In this work, the driving force models for hydrate formation in the literature were reviewed. Two of the latest approaches for derivation of the driving force were applied for further analysis in pure gas and multi-component gas systems. The relationship between the driving force and the degree of subcooling for methane, ethane and propane demonstrated that subcooling is a good representative of the driving force for

pure compounds at a wide pressure range. For natural gas systems at isothermal conditions, between 5-20 MPa, subcooling underestimates the real driving force for hydrate formation, however, above 20 MPa, the variation in driving force with pressure can be estimated by subcooling. The analysis showed that a constant degree of subcooling is an appropriate criterion for up-scaling the tests for pure and natural gases. A relation was developed for calculating the required degree of subcooling in various hydrocarbon systems to achieve identical driving forces, when determining the induction time for LDHIs. For natural gas –water systems at constant driving force/ subcooling conditions the induction time does not seem to be a function of pressure, while in the presence of the kinetic inhibitor tested in this study, increasing the system pressure had a negative effect on the induction time. This was attributed to the effect of KHI and pressure on the kinetic barriers for hydrate formation in a system. Therefore, testing KHIs at similar field conditions was recommended.

7.8 TABLES

Table 7.1 Composition of the natural gases used in this work.

Component	NG1	NG2*
	mol%	mol%
C_1	86.49	87.26
C_2	5.71	7.57
C_3	1.63	3.1
n-C_4	0.35	0.79
i-C_4	0.2	0.49
n-C_5	0.08	0.2
i-C_5	0.08	0.2
C_6^+	0.1	-
N_2	3.86	0.39
CO_2	1.5	-

* Natural gas used by Christiansen (Christiansen and Sloan, 1995) and Yousif; (Yousif, 1994).

Table 7.2 Summary of the tests with natural gas 1 (NG1)-water system.

Test	Testing T/P	Subcooling	Induction Time	-ΔG/RT
No.	K / MPa	/ K	Minutes	
1	287.35 / 17.4	7.1	60	0.586
2	287.35 / 17.4	7.1	65	0.586
3	281.65 / 6.3	7.1	60	0.651
4	281.65 / 6.3	7.1	65	0.651

Table 7.3 The induction times for natural gas 2 (NG2)-water system reported by Yousif (Yousif, 1994).

Test No.	Testing T/P	Subcooling	Induction Time	-ΔG/RT
	K / MPa	/ K	Minutes	
1	280.46 / 6.89	13	17.5	0.987
2	282.47 / 9.65	13.2	25	0.932
3	283.71 / 6.89	9.7	32	0.679
4	286.05 / 9.65	9.6	43.5	0.615

Table 7.4 Summary of the tests with Natural Gas 1 (NG1)-water system-0.5 mass% PVCap at 6.3-6.9 MPa pressure range.

Test No.	Testing T/P	Subcooling	Induction Time	-ΔG/RT
	K / MPa	/ K	hours	
1	275.15 / 6.9	14.2	0	1.34
2	274.65 / 6.3	14.2	0	1.35
3	275.65 / 6.9	13.7	17	1.29
4	275.75 / 6.9	13.6	>12	1.28
5	276.15 / 6.9	13.2	>36	1.24
6	276.15 / 6.9	13.2	>36	1.24
7	276.85 / 6.9	12.5	>60	1.18

Table 7.5 Summary of the tests with Natural Gas 1 (NG1)-water system-0.5 mass% PVCap at 30-31 MPa pressure range.

Test No.	Testing T/P	Subcooling	Induction Time	-ΔG/RT
	K / MPa	/ K	Hours	
1	284.35 / 30	13.3	0	1.05
2	286.45 / 30.8	11.2	0	0.9
3	286.65 / 30.3	11.0	5	0.88
4	286.55 / 30	10.9	6	0.88
5	288.4 / 31	9.5	60	0.76

7.9 FIGURES

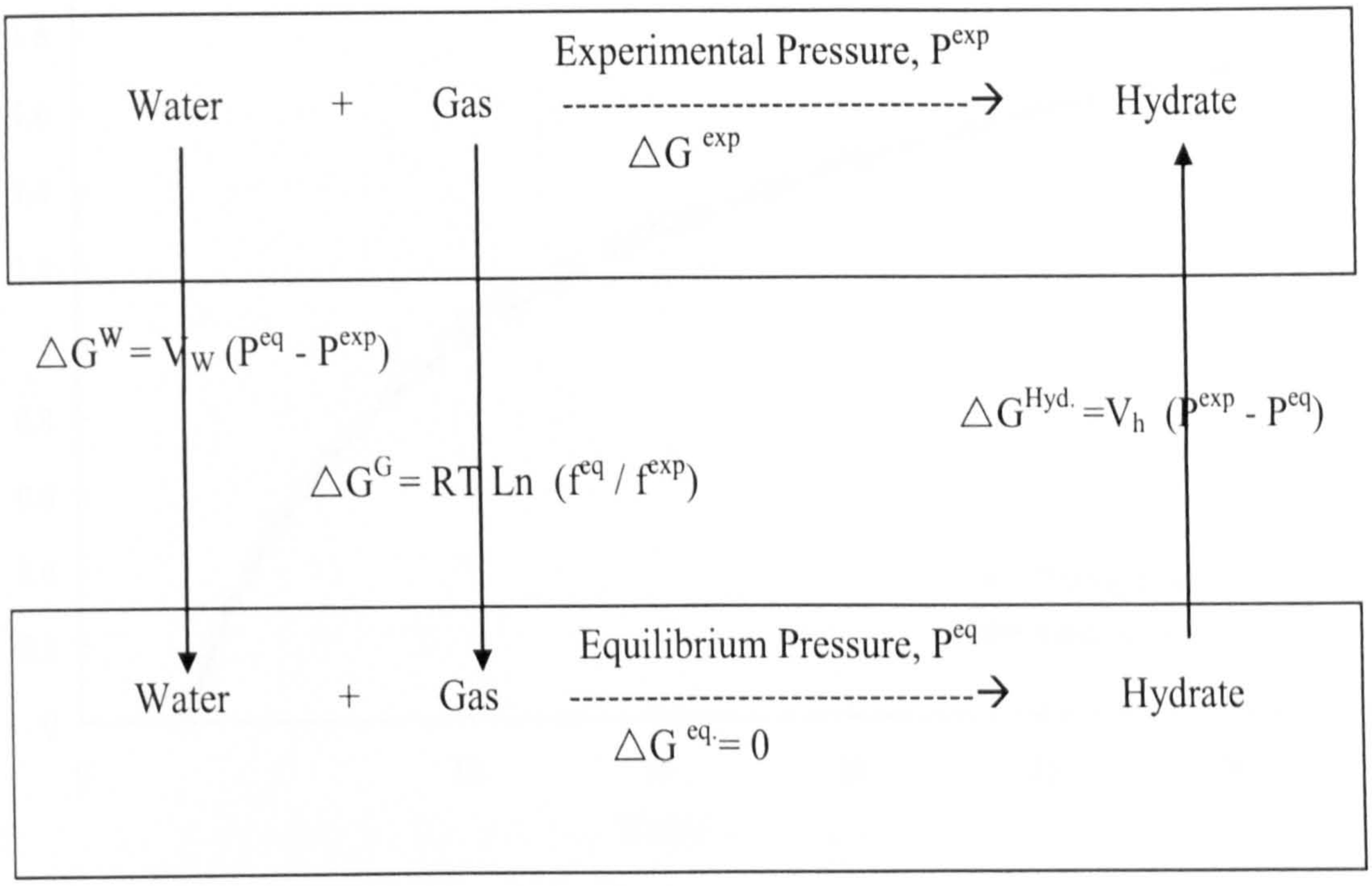

Figure 7.1 Isothermal path for calculating driving force for hydrate formation.

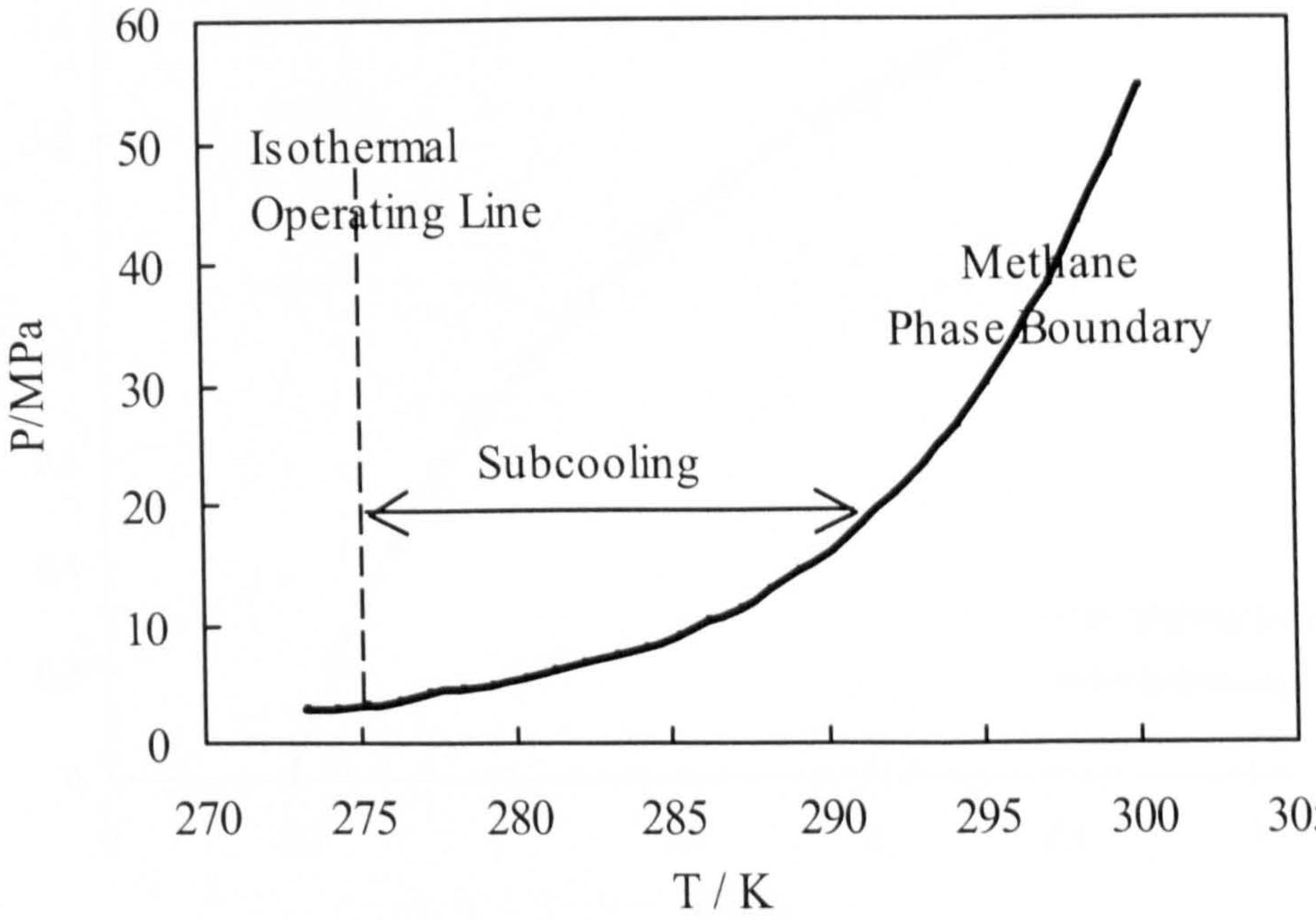

Figure 7.2 Changes in subcooling with pressure at isothermal conditions.

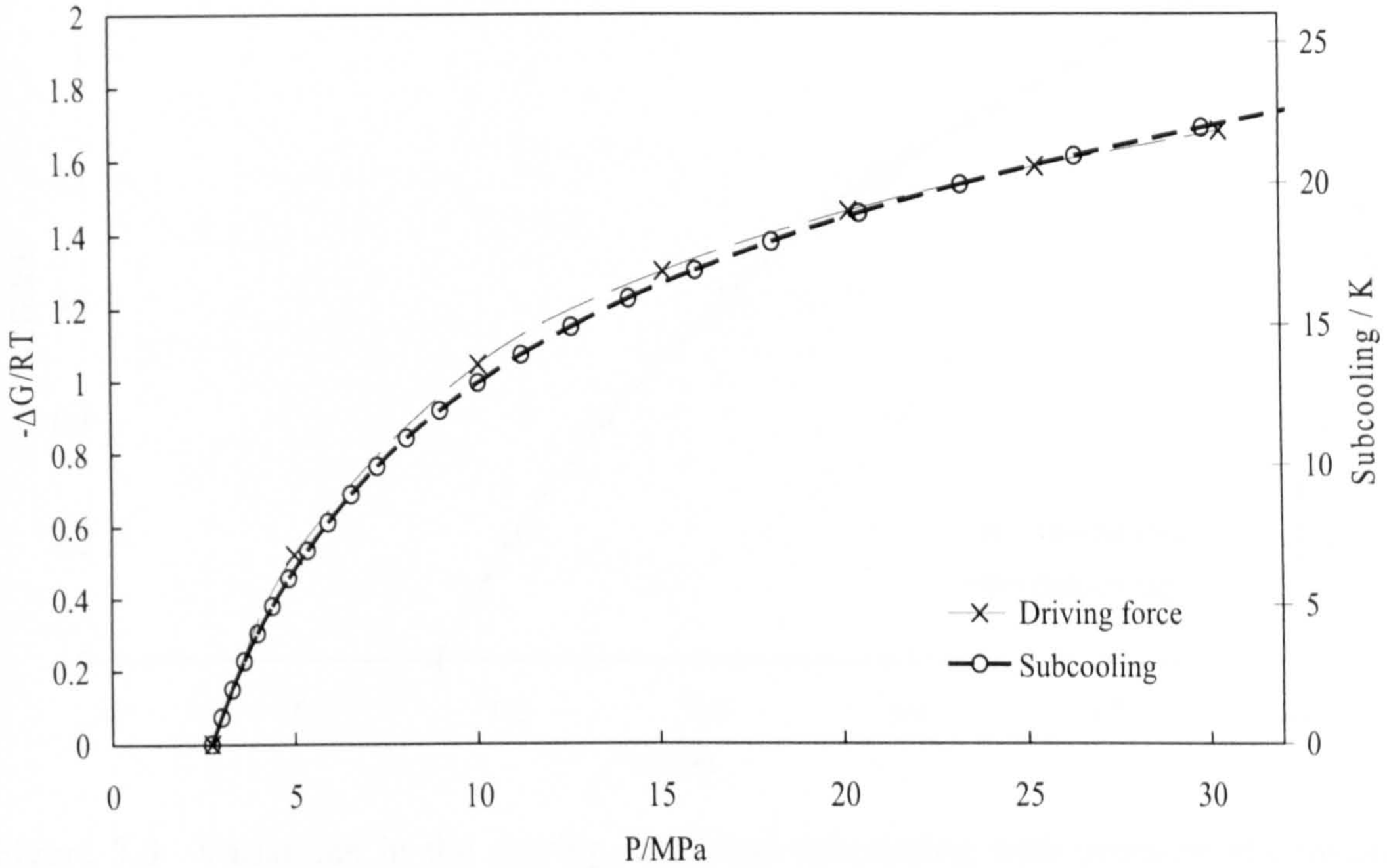

Figure 7.3 Variations in the driving force and subcooling with pressure at constant temperature, T=273.2 K, for methane-water hydrate system.

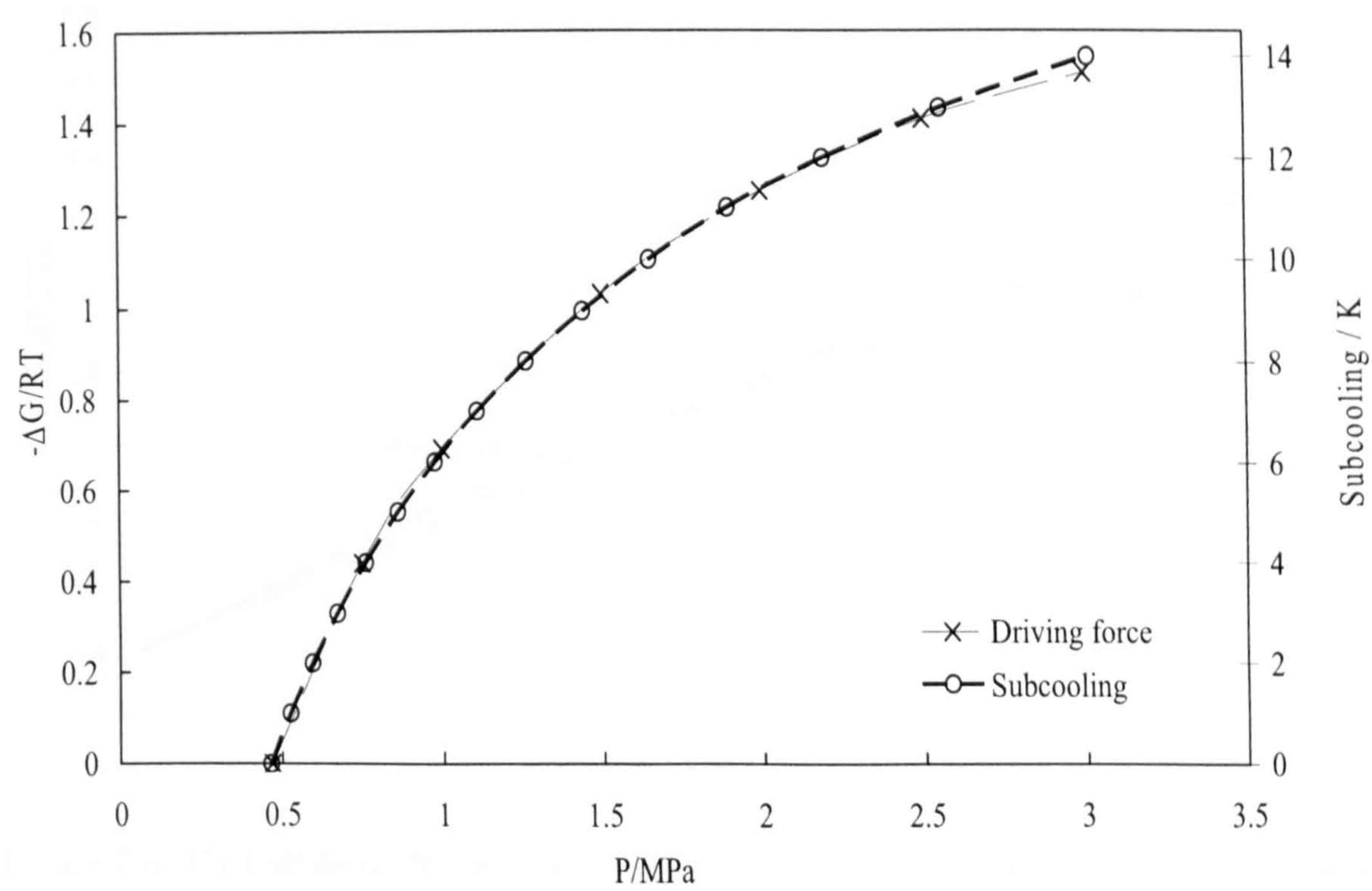

Figure 7.4 Variations in the driving force and subcooling with pressure at constant temperature, T=273.2 K, for ethane-water hydrate system.

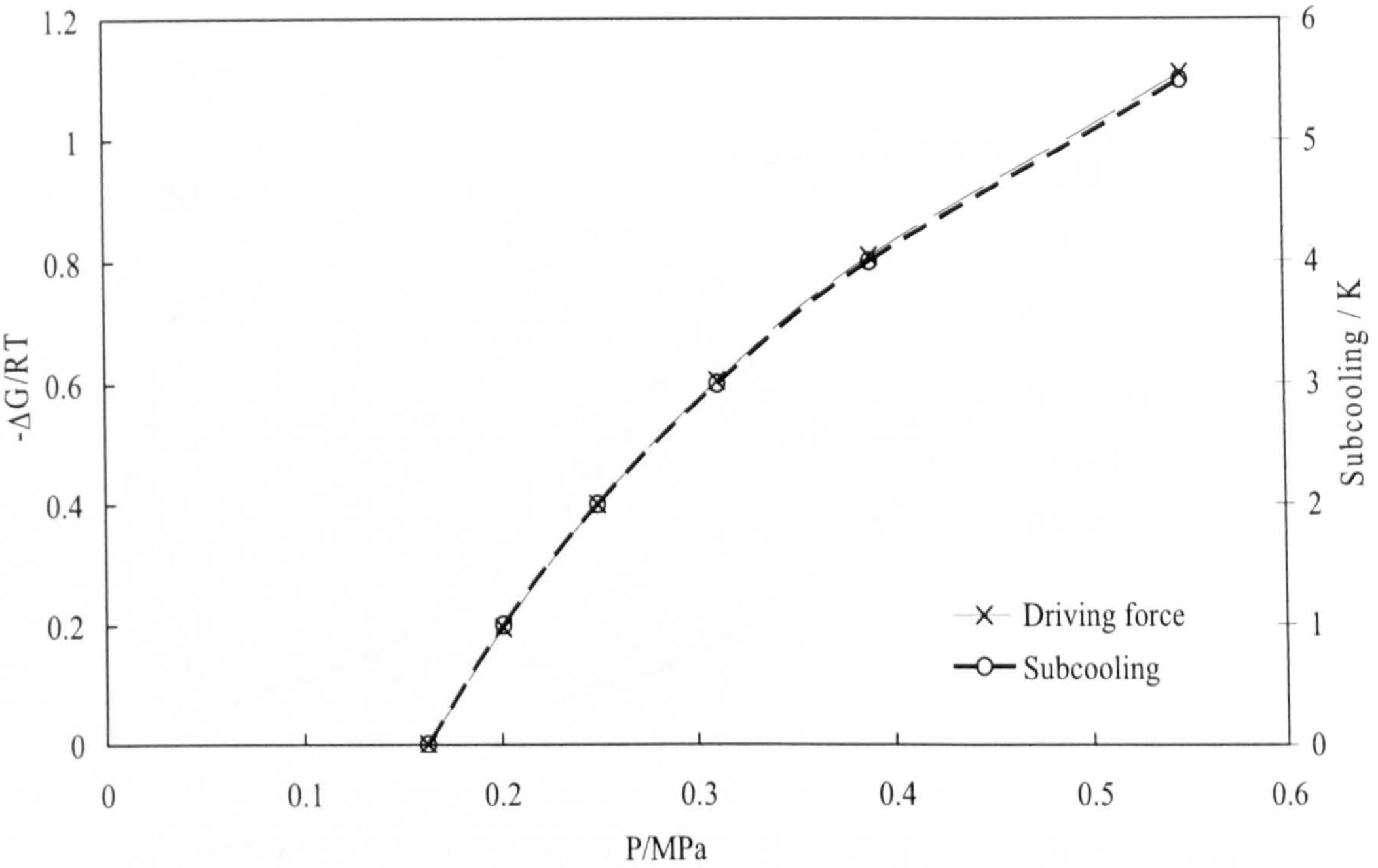

Figure 7.5 Variations in the driving force and subcooling with pressure at constant temperature, T=273.2 K, for propane-water hydrate system

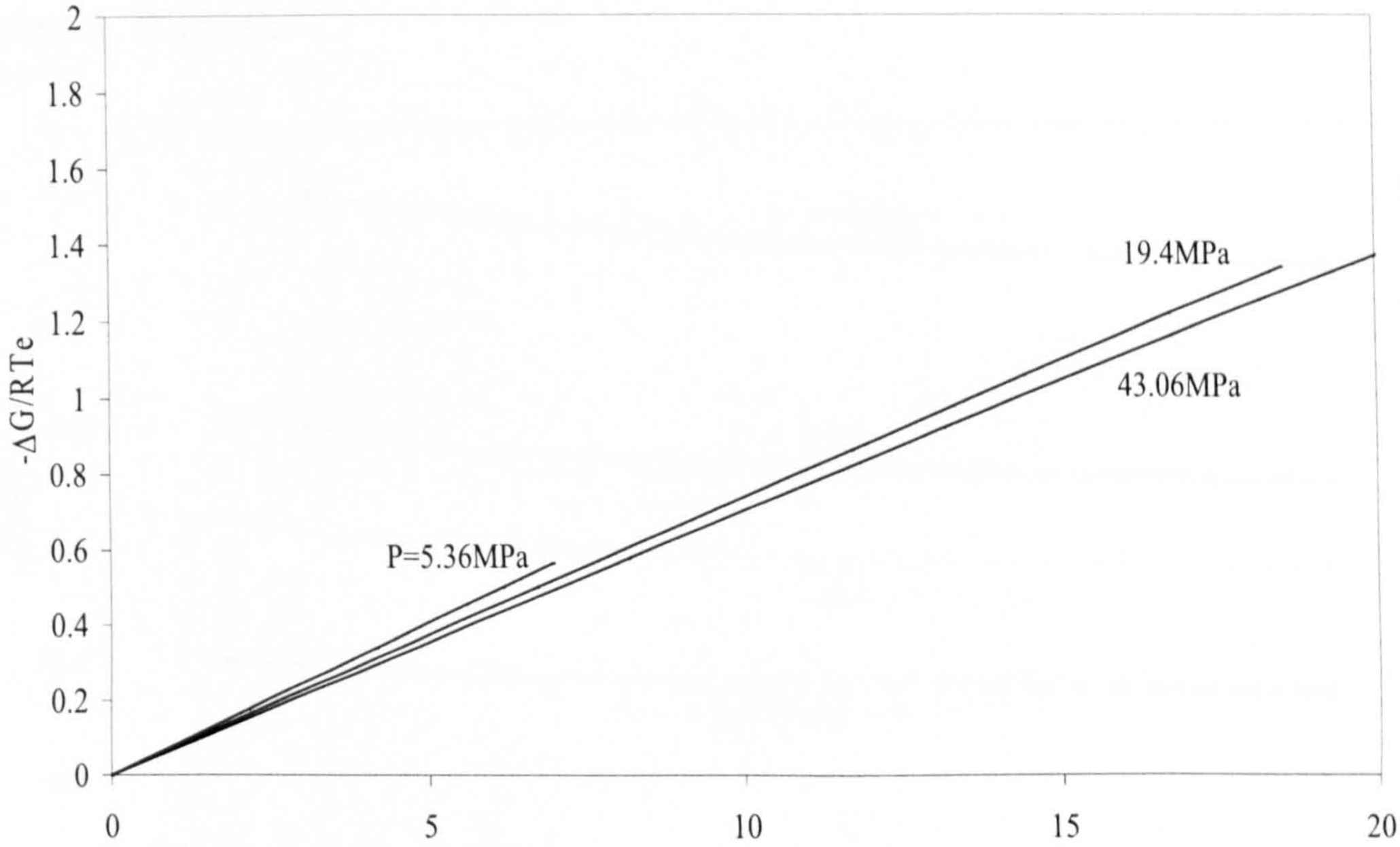

Figure 7.6 Variations in driving force with subcooling at different isobars for methane-water hydrate system

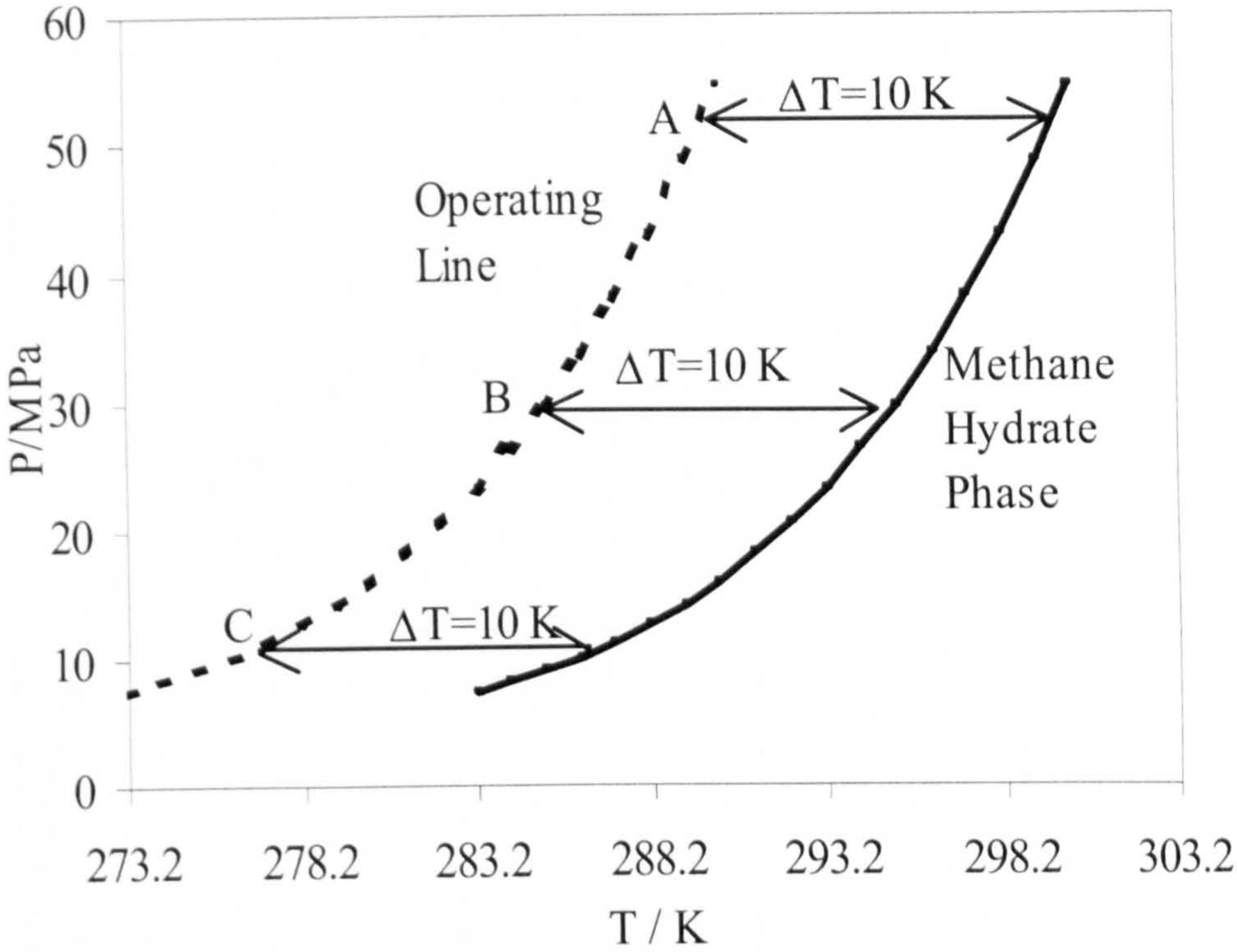

Figure 7.7 Constant degrees of subcooling at different pressures and temperatures; points A, B and C.

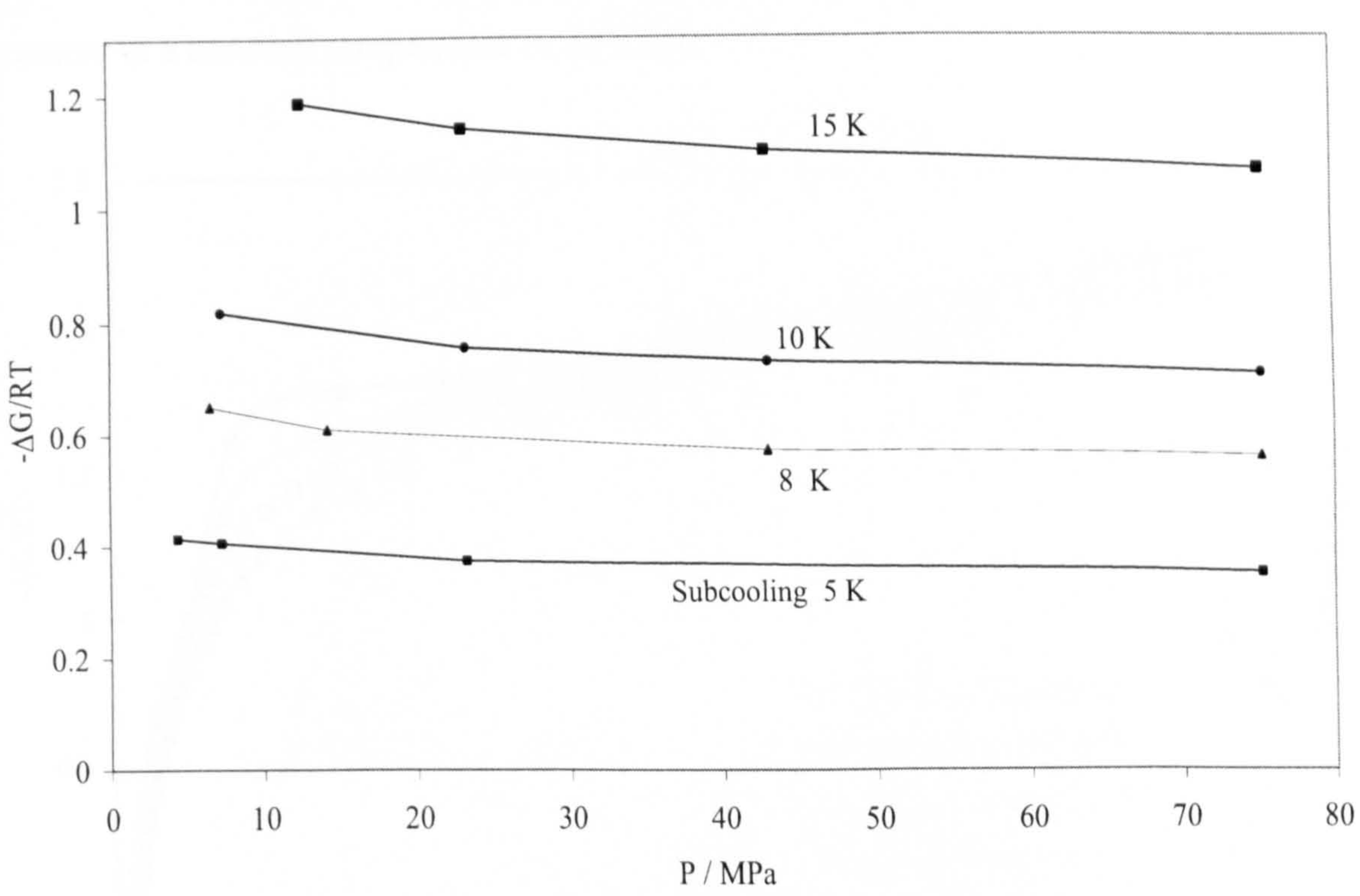

Figure 7.8 Driving force versus pressure in methane –water system at various constant degrees of subcoolings.

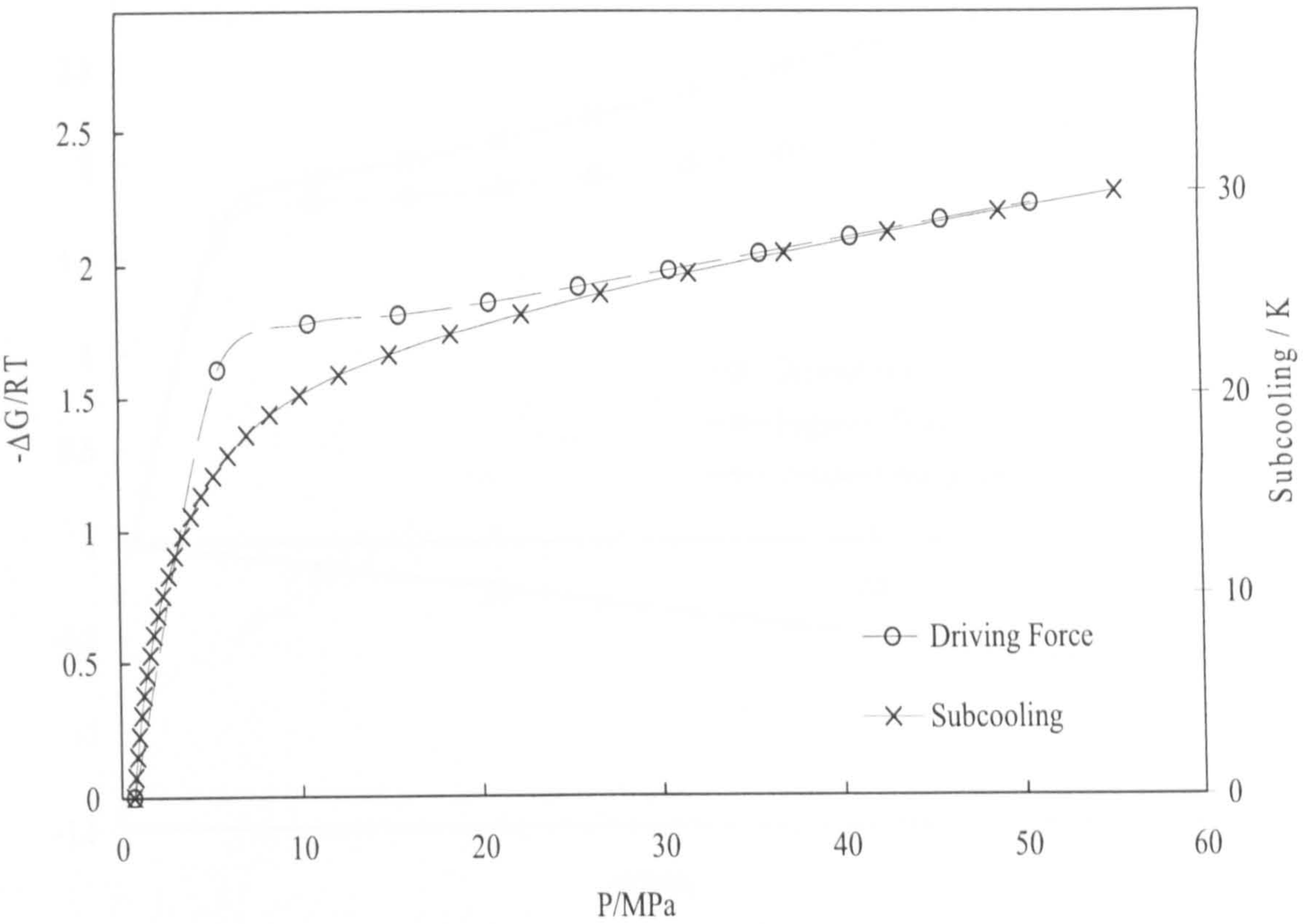

Figure 7.9 Driving force and subcooling for natural gas 2 (NG2) as a function of pressure at a constant temperature of 273.2 K.

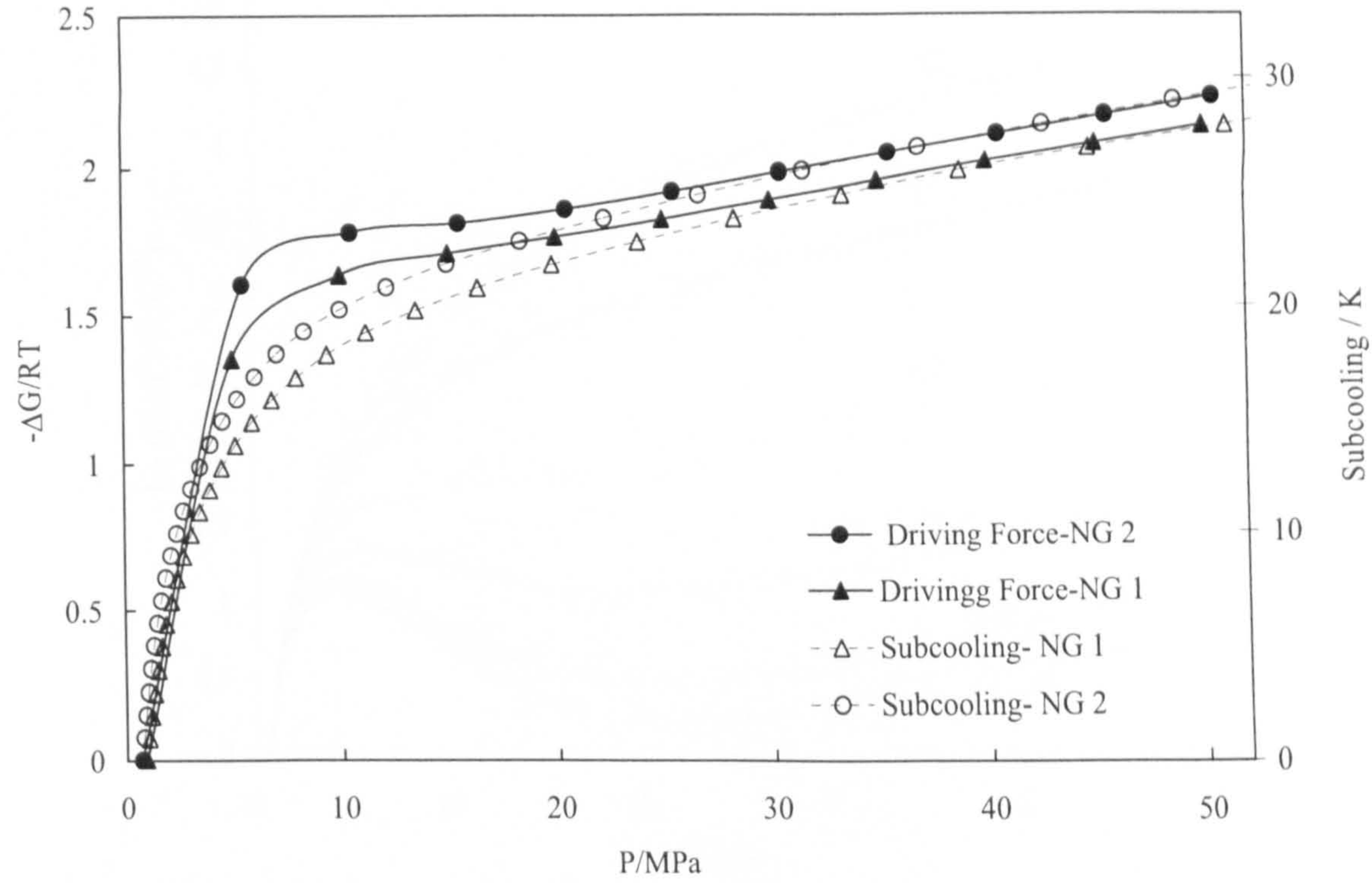

Figure 7.10 Driving force as a function of pressure for two different types of natural gases at a constant temperature of 273.2 K.

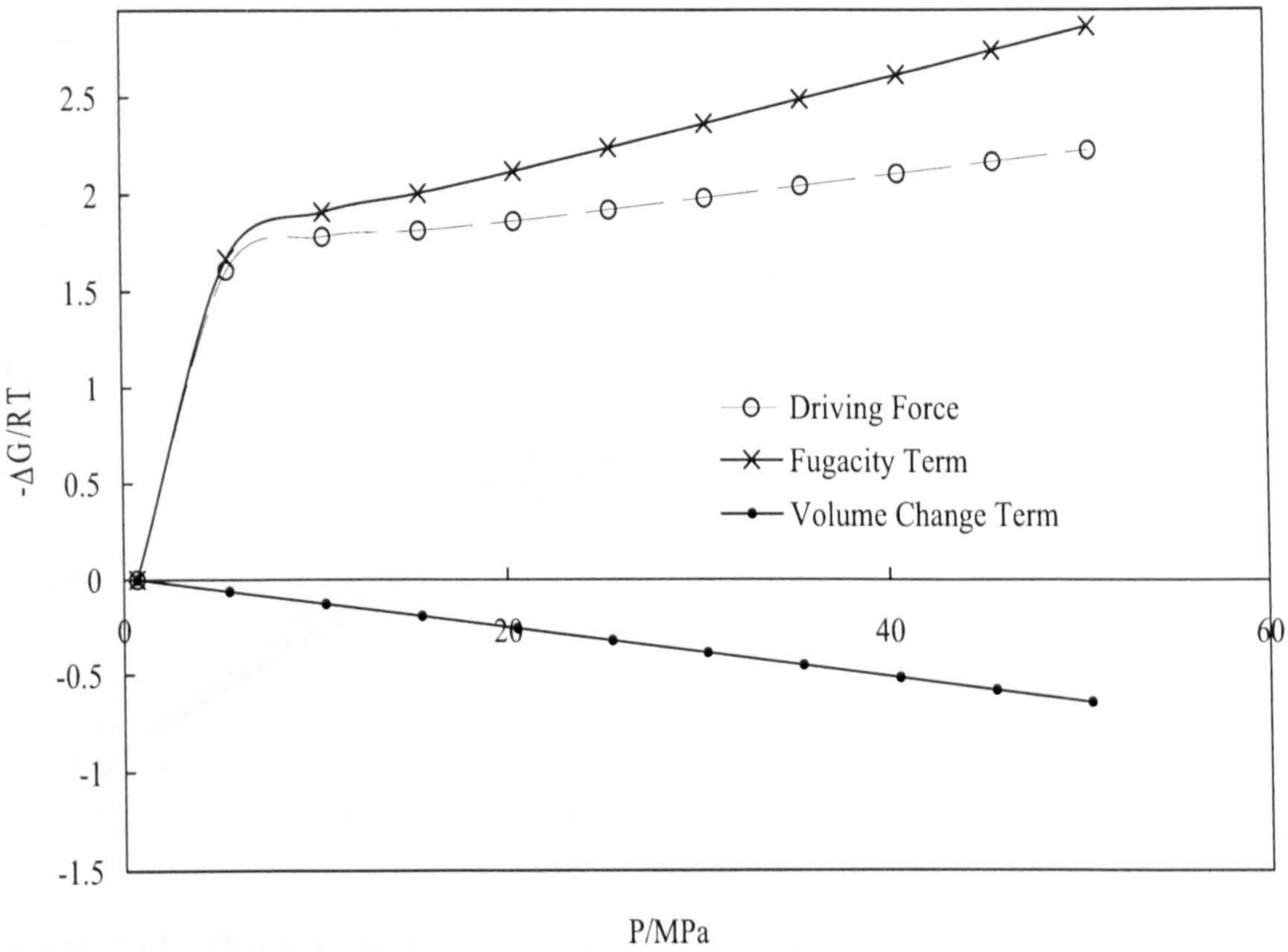

Figure 7.11 The changes of different terms in Eq.1 as a function of pressure for natural gas 2 (NG2) at constant temperature of 273.2 K.

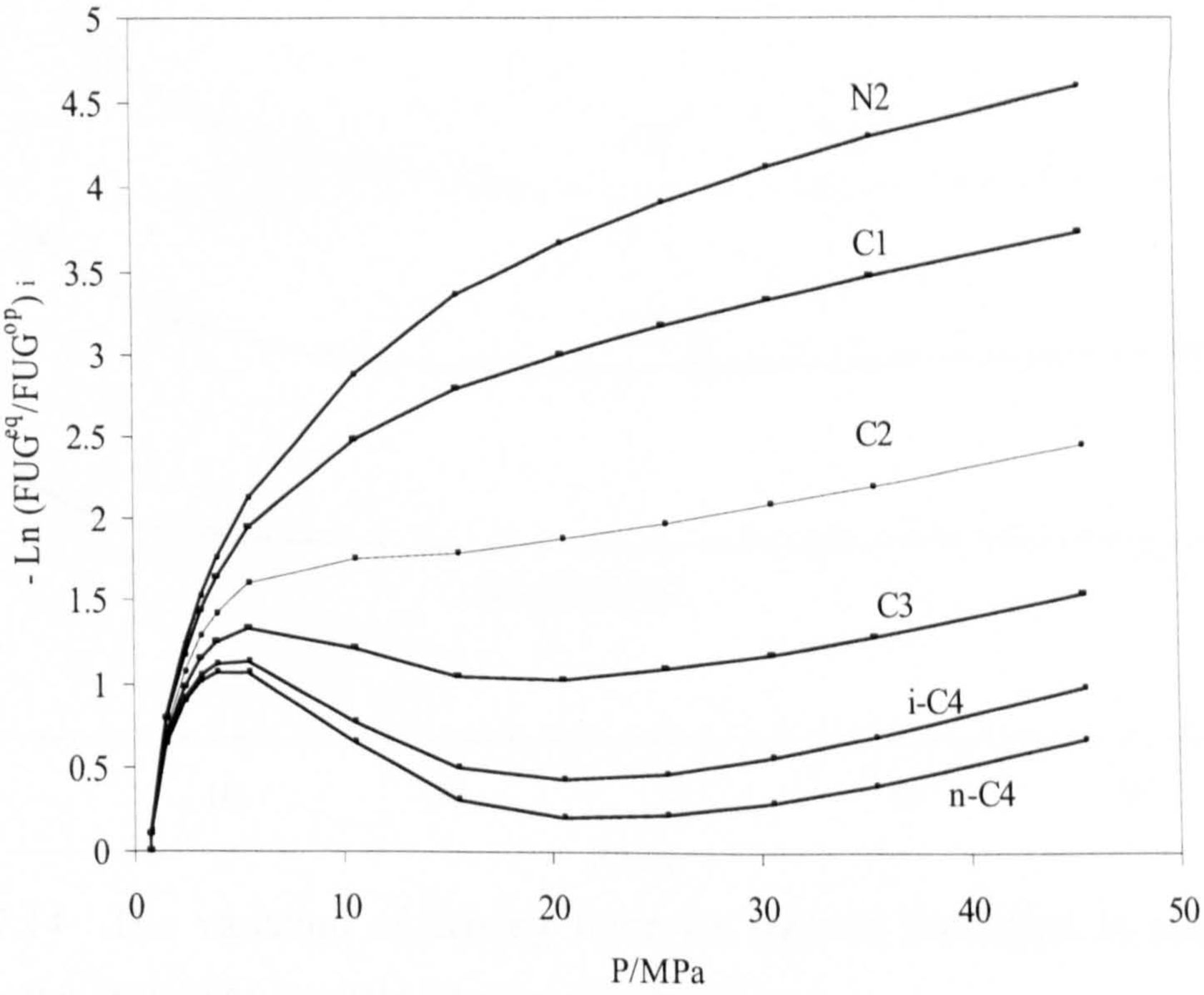

Figure 7.12 The logarithm of fugacity ratios as a function of pressure at 273.2K for different components in natural gas 2 (NG 2).

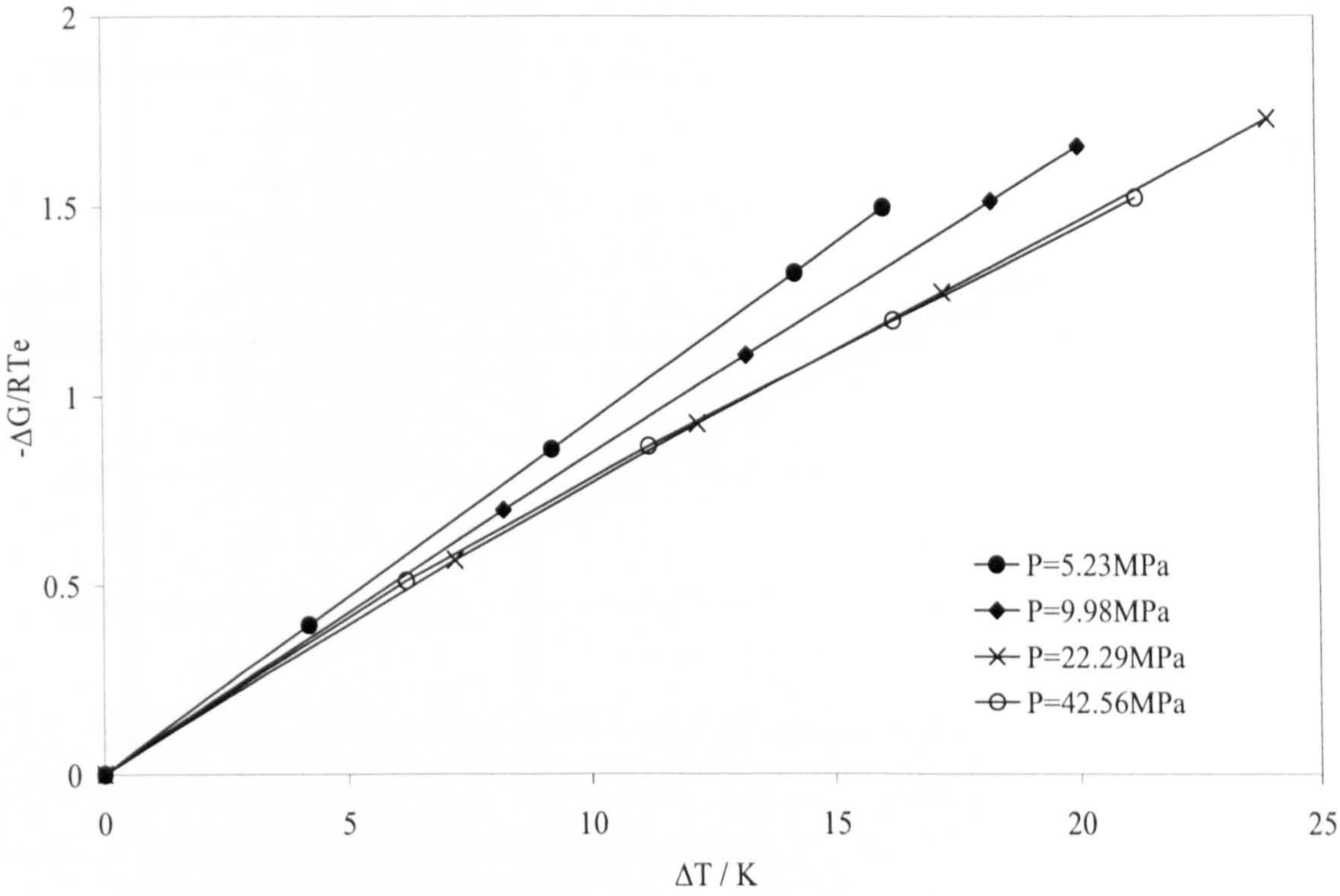

Figure 7.13 Driving force versus subcooling at isobaric conditions for natural gas2 (NG2).

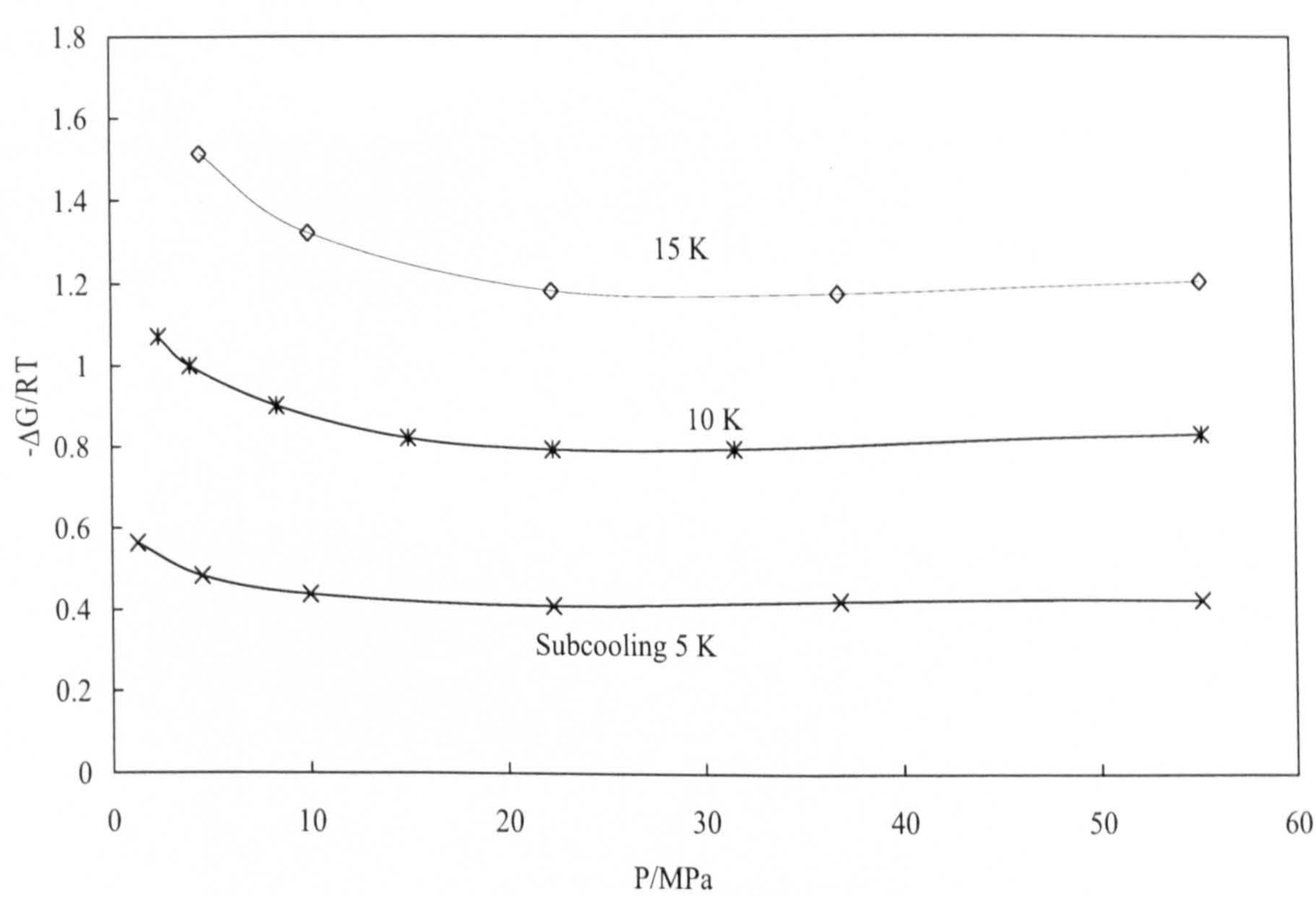

Figure 7.14 The variation of driving force for hydrate formation in natural gas 2 (NG2)-water system at constant degrees of subcooling.

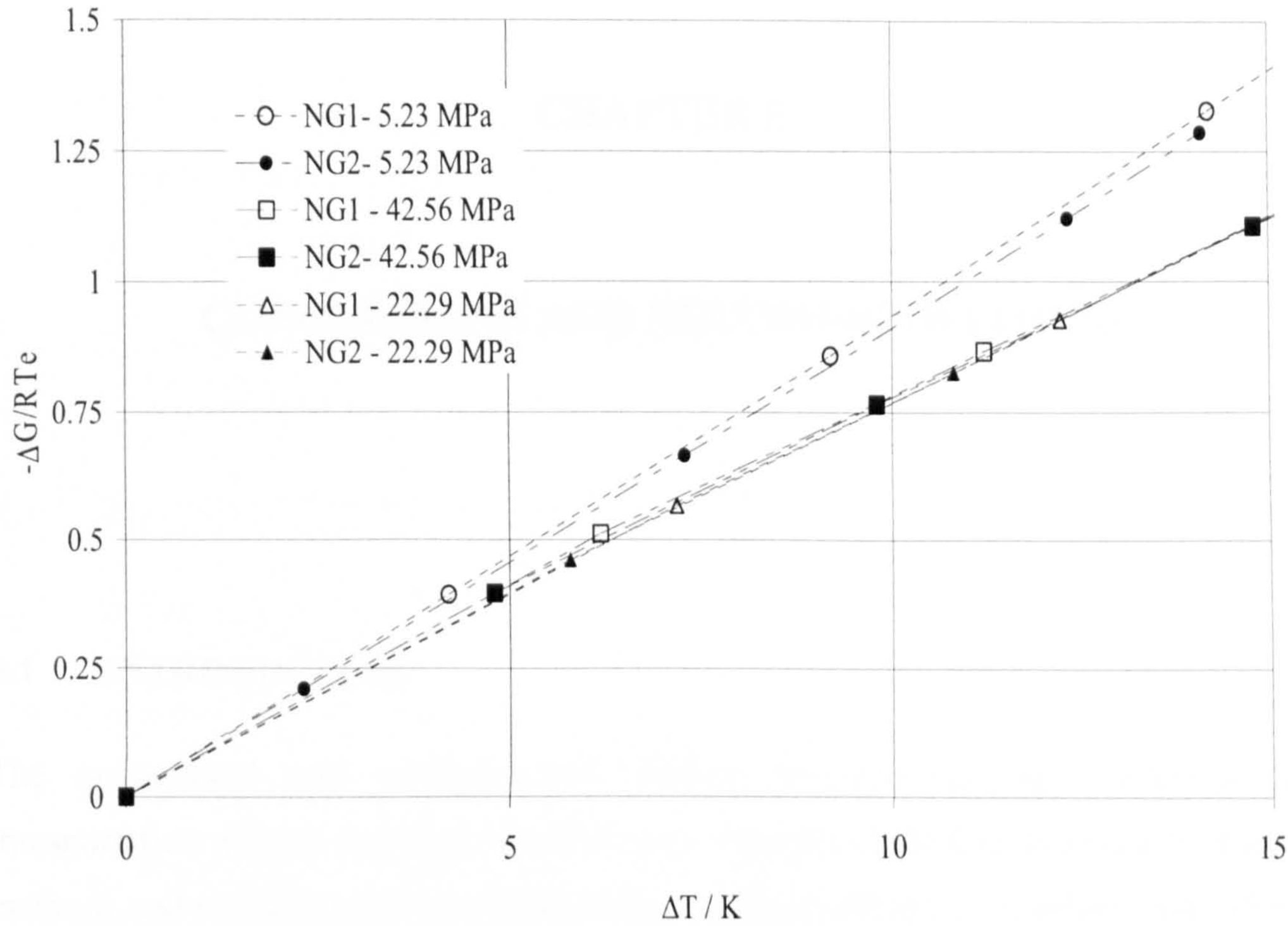

Figure 7.15 The comparison of driving forces for hydrate formation in the two different natural gas systems (NG1 and NG2) at different degrees of subcooling and pressures.

CHAPTER 8

CONCLUSIONS AND RECOMMENDATIONS

8.1 INTRODUCTION

The economical and environmental factors involved in the production and transportation of oil and gas demand cost effective and environmentally friendly methods and techniques for providing flow assurance solutions. Onshore and offshore pipelines are used for transportation of unprocessed or processed oil and gas. A major concern with these pipelines and production facilities is the possibility of flow restriction and blockage due to hydrates formation, which can lead to serious operational and safety problems.

In this thesis preventing gas hydrate problems in oil and gas industries by exploiting the oil natural hydrate inhibitors and application of low dosage hydrate inhibitors were investigated. The study involved:

(1) Presenting a simplified model for electrolyte solution-gas equilibria (Chapters 2).

(2) Applications of novel experimental techniques to study the primary mechanism of hydrate formation and inhibition by low dosage hydrate inhibitors (Chapters 3, 4, 5 and 6).

(3) Investigating the mechanism of hydrate formation and inhibition in oil systems and parameters affecting natural hydrate inhibitors in these systems (Chapter 3).

(4) Investigating the mechanism of hydrate inhibition by low dosage hydrate inhibitors and application of a new methodology for designing and testing them (Chapter 4).

(5) Investigating the parameters, which affect the performance of kinetic hydrate inhibitors (Chapter 5).

(6) Thermodynamic analysis of driving force for hydrate formation in the presence of KHIs (Chapter 7).

The main conclusions and recommendations of this thesis, and suggestions for future work, are detailed here.

8.2 SUMMARY AND CONCLUSIONS

8.2.1 A Simplified Model for Phase Equilibria in Electrolyte Solutions

The thermodynamic formulation used in this thesis for prediction of hydrate phase boundaries in different systems, which were used for calculation of degree of subcooling in different experiments in this work, was outlined in Chapter 2. General multi-phase equilibria flash calculations have been briefly discussed. The model includes an equation of state (EoS) based fluid phase model and a statistical thermodynamics hydrate model. The numerical model considers the thermodynamic equilibria between all possible phases, namely vapour, liquid hydrocarbon, water-rich phase (with the possible presence of hydrate organic inhibitors and/or salts), ice, and gas hydrates (structure-I, II, and H). In summary, the Heriot-Watt hydrate model uses the Valderrama modification of the Patel and Teja equation of state (VPT EoS) together with a Non-Density Dependent (NDD) mixing rules for fugacity calculations in all fluid phases. Hydrate phases (structure-I, II, and H) have been modelled by the ideal solid solution theory, and ice has been treated as a sub-cooled liquid.

In addition, a new approach in modelling phase equilibria and gas solubility in saline solutions has been proposed. Salts were introduced as components in the EoS by calculating their EoS parameters from corresponding cation and anion parameters. A non-density dependent mixing rule was used for calculating a, b, and c parameters of the EoS. The inclusion of salts in the EoS resulted in the omission of Debye-Huckel electrostatic contribution term in the fugacity coefficient calculations. Water-salt binary interaction parameters were optimised using freezing point depression and boiling point elevation data of aqueous electrolyte solutions. Gas solubility data in aqueous electrolyte solution were used for optimising salt-gas BIPs. The predictions of the model have been compared with independent experimental data, demonstrating the reliability of the approach.

8.2.2 Natural Hydrate Inhibition in Oil Systems

In Chapter 3, hydrate formation and natural hydrate inhibition in oil-water-natural gas systems were investigated. Two different types of oils were used in this study. A kinetic rig was used to study the effect of different factors affecting the natural hydrate inhibition of oils by measuring the induction times before hydrate formations at pipeline conditions. The torque measurements on the stirrer before and after hydrate formation at different conditions were used to determine the transportability and/or blockage of the system and the effect of different parameters on them. The flowing and shut-in/restart conditions were simulated in the kinetic rig by switching on and off the stirrer in the kinetic rig.

The parameters playing a role in reducing hydrate blockage risk in oil systems were identified to be oil properties, mixing rate and mixing history, water content, and operational conditions (e.g. pressure).

A micromodel set up was used to visualise hydrate formation and distribution of different phases in oil-water emulsion in the presence of natural gas. The size and morphology of the hydrate particles and their agglomeration were shown in the mircomodel.

The main conclusions of this section are as follows:

(1) Formation of water in oil emulsions play an important role in natural hydrate inhibition and the transportability of hydrocarbon systems. This can be attributed to the dispersion effect of oil on hydrate particles formed in flowing conditions, which prevents the formation of massive hydrate blocks and stop hydrate sticking on the wall.

(2) Oil properties, mixing rate and mixing history, water content, and operational conditions (e.g. pressure) were shown to play significant role in diminishing hydrate blockage risks in oil/water systems.

(3) The effect of mixing rate on the induction time before hydrate formation appeared to be a function of system mixing history (degree of emulsification of water in oil). Before formation of stable emulsion, the induction time increases with mixing rate. However after formation of stable water/oil emulsion induction time is not a strong function of the mixing rate.

(4) Water content is believed to be the most important factor in controlling the risk of hydrate blockage and assuring the transportability of the system. The lower the water content the less the risk of hydrate blockage and the more transportable the hydrate slurry.

(5) At constant temperature the induction time (i.e., time before hydrate formation) decreases at high-pressure conditions (> 10 MPa). Furthermore, the risk of hydrate blockage increases with system pressure at constant temperature.

(6) Micromodel set up provides valuable visual information regarding the state of water oil emulsion, size of water droplets in the emulsion, hydrates particle size and morphology and distribution of different phases in the system

(7) In micromeodel set-up it was observed that gas hydrate particles formed in a water /oil emulsion adsorb oil heavier components.

(8) At static condition the agglomeration of hydrate particles appeared to be easier than in flow conditions in the Micromodel set-up. This is in line of the results obtained from the kinetic rig tests (where long shut-in times resulted in stirrer blockage).

8.2.3 Rational Design and Testing of Low Dosage Hydrate Inhibitors

In Chapter 4, a new methodology was proposed for design and testing low dosage hydrate inhibitors. In the framework of a joint project, fourteen new KHIs, based on quaternary ammonium zwitterions, were designed by molecular dynamic simulation and synthesised in Warwick University. The performance of the new KHIs was evaluated in a high pressure Kinetic Rig at subsea pipeline conditions. On screening the new KHIs in natural gas-water system, two of them appeared to perform better than others. The performance of one of the best inhibitors among them was compared with a commercial (Luvicap®) and a conventional hydrate inhibitor (PVP) in structure II hydrate former system (natural gas-water) and structure I hydrate former system (methane-water) at similar conditions.

The anti-agglomeration property of that KHI was also tested in a natural gas-condensate-water system in the kinetic rig. Micromodel set up was used for investigating the primary mechanism of hydrate inhibition by new KHIs.

The main conclusions of this work are as follows:

(1) The new synthesised KHIs showed mild hydrate inhibition effect in natural gas–water and methane water systems at the conditions which the experiments were carried out.

(2) In natural gas-water system, their performance was not as good as PVCap and PVP, however in methane water system, one of them performed better than PVP.

(3) In general the performance of the KHIs tested in this study including PVCap and PVP appeared to be better in structure II hydrate systems compared to structure I hydrates, at similar degrees of subcooling and temperatures.

(4) Tests with higher concentrations (1-1.5mass%) of the new synthesised kinetic inhibitors have demonstrated promising results in seabed pipeline conditions.

(5) The new KHI showed good hydrates anti-agglomeration effect in water-condensate-natural gas system.

(7) Visual observation of hydrate formation and growth in the presence of new KHI showed that it prevents agglomeration of the hydrate particles and cause deformation of the hydrate crystals.

8.2.4 Parameters Affecting the Kinetic Hydrate Inhibitors Performance

Identification of the parameters affecting the performance of kinetic hydrate inhibitors is not only useful in elucidation of inhibition mechanism by kinetic inhibitors but also is crucial for effective design, screening and deployment of them in deepwater applications. The impact of different parameters on the performance of a typical kinetic hydrate inhibitor (PVCap) was studied by experiments carried out in a kinetic rig and a visual rig (Chapter 5). Physical parameters such as mixing, pressure, temperature (subzero conditions), and chemical parameters such as polymer molecular weight, polymer solvent/carrier fluid, gas composition (different gas hydrate structures), and compatibility with other chemical inhibitors (e.g. corrosion inhibitor) were studied. From the results of the experiments the following conclusions can be drawn:

(1) Mixing versus shut-in conditions appeared to improve the performance of the kinetic inhibitor. In mixing conditions hydrates formed slowly in the gas/water interface and bulk of liquid. However, in static conditions a micro porous hydrate structure formed in the interface, which stuck to the wall and grew in the gas phase by sucking up the water into the gas phase, which lead to shorter induction times.

(2) Two gas mixtures, which form different hydrate structures and have the same hydrate phase boundaries were designed and synthesised to test the effect of different hydrate structures on the performance of the PVCap at same temperature and pressure conditions. The experimental results showed that PVCap is more successful in inhibiting structure II hydrates compared to inhibition in structure I hydrates at same temperature and pressure conditions (i.e. same subcooling).

(3) The performance of PVCap decreases with increasing the pressure while the subcooling in the system is kept constant (by increasing the temperature). Addition of Tetra Butyl Ammonium Bromide (TBAB) enhanced the performance of PVCap, however the adverse effect of pressure (at same subcooling) was also observed in the experiments on PVCap and TBAB mixture.

(4) Three different molecular weights of PVCap polymer (5000, 50000 and 1000000) were used for inhibition of hydrates at similar conditions. The results of the experiments showed that the lowest molecular weight of polymer used in the tests is the most successful one.

(5) The effect of polymer solvent/carrier fluid on the performance of PVCap was studied. The hydrate inhibition effect of dried PVCap polymer in the presence and absence of low concentration of ethylene glycol (1.5%) as polymer solvent/carrier fluid was tested at similar conditions. The test results showed that ethylene glycol does not have significant effect on the performance of PVCap.

(6) The compatibility of PVCap with a commercial corrosion inhibitor was studied. The result of the experiments showed the negative impact of the tested corrosion inhibitor on the performance of PVCap.

(7) The performance of PVCap at subzero conditions in the presence of ethylene glycol (20% EG, to prevent ice formation) was evaluated and compared with its performance at above ice point conditions and similar degrees of subcooling. The results showed that PVCap can inhibit hydrate formation at subzero conditions in the presence of ethylene glycol. Furthermore, 20 % ethylene glycol enhances PVCap performance.

8.2.5 Evaluation of Anti-Agglomerants Using Kinetic Rig and Micromodel

In Chapter 6, the development of anti-agglomerant (AA) chemicals, their reported field deployment in the literature, and different laboratory testing techniques for their

evaluation were reviewed. Subsequently, a new methodology for assessing anti-agglomerants, using torque measurement technique along with visual observation method was presented. Here are the main aspects of the method and conclusions:

(1) A blind stirred tank reactor was used to test the affect of different AAs on the transportability of the system by torque measurements. The torque measurement was improved by using a helical tube instead of paddle-shape impeller. It was shown that the information obtained from torque measurement technique can be used for screening AAs, however it is not sufficient for selection of an AA for field application

(2) It was shown that the complementary information such as hydrate particles size, morphology and their distribution in different phases can be obtained from Glass Micromodel set-up.

(3) Preliminary experiments, using a proven AA chemical in comparison with another similar compound and an *un-inhibited* system, showed that the techniques developed in this study are suitable and effective for the testing of AAs.

(4) The new method (kinetic rig and glass micromodel) can be considered as a method for primary testing of AAs before flow loop test.

8.2.6 Is Subcooling the Right Driving Force for Testing Low Dosage Hydrate Inhibitors?

In testing the performance of low dosage hydrate inhibitors, subcooling is usually considered as the driving force for hydrate formation and a criterion for simulating field conditions. In many cases, it is a routine industrial practice to scale up the experiments conducted at low-pressure conditions to high pressures based on some similarity principles. However, subcooling does not encompass the effect of pressure. A comprehensive driving force for hydrate formation is a function of pressure, temperature, and gas composition; however, its calculation is not as simple as that of subcooling. Application of subcooling as driving force and scale-up criterion may be reliable in some cases, while in other cases it may overestimate or underestimate the effect of pressure.

In this work (Chapter 7), by applying two of the latest driving force expressions for hydrate formation, the relationships between subcooling and the calculated driving force at different conditions for pure gas–water and natural gas–water systems were analysed. The variations of driving force with pressure at isothermal conditions for

methane and natural gas hydrates were shown and related to subcooling. Next, the effect of pressure on the driving force at constant degree of subcooling for methane and natural gas hydrates was calculated to find out the conditions where subcooling alone can be considered as a driving force index for up-scaling. Finally, the results of the experiments in relation to the effect of pressure on the induction time of natural gas–water systems, at similar driving forces, in the presence and absence of kinetic inhibitor were presented. The main conclusions are as follows:

(1) The relationship between the driving force and the degree of subcooling for methane, ethane and propane demonstrated that subcooling is a good representative of driving force for pure compounds over a wide pressure range.

(2) For natural gas systems at isothermal conditions, between 5 and 20 MPa, subcooling underestimates the calculated driving force for hydrate formation; however, above 20 MPa, subcooling is a good representative of real driving force.

(3) Constant degree of subcooling is an appropriate criterion for up-scaling the tests with pure gas and natural gas.

(4) A relation was developed for calculating the required degree of subcooling in various gas systems to achieve identical driving forces, when determining the induction time for KHIs.

(5) For natural gas–water system at constant driving force/subcooling conditions, the induction time does not seem to be a function of pressure, while in the presence of the kinetic inhibitor tested in this study, increasing the system pressure had a negative effect on the induction time. This was attributed to the effect of KHI and pressure on the kinetic barriers for hydrate formation in a system. Therefore, testing KHIs at similar field conditions is recommended.

.

8.3 RECOMMENDATIONS FOR FUTURE WORK

8.3.1 New Method for Design and Evaluation of KHIs

In this thesis a new methodology for designing and testing low dosage inhibitor was presented. The new inhibitors, designed by molecular dynamic simulation technique (Warwick University) and tested in a hydrate kinetic and transportability rig, showed promising results in inhibition of hydrates. The visual observations in micromodel set

up revealed the effect of KHIs on the morphology of hydrates, distribution of phases and particle sizes in the presence and absence of KHIs. Furthermore, by exploitation of above-mentioned experimental technique and an in-house thermodynamic model the parameters playing role on the performance of KHIs were investigated.

The above approach can be further used for investigating several topics:

- Green Inhibitors
- Inhibitor performance in oil systems and effect of salts
- Designing KHIs for structure-I hydrates

The areas of research are described in more detail in below.

Green Inhibitors: The environmental impact of hydrate inhibitors is a major concern. As the amount of inhibitor used is a function of the amount of water cut, the high water cut conditions (e.g. water-flooded oil reservoirs) means larger quantities of hydrate inhibitors should be disposed. Although the concentration of low dosage hydrate inhibitors in the water phase is generally less than 1 mass%, the large quantity of water cut in water-flooded oil reservoirs could result in severe environmental impact. It is proposed to extend the investigation to environmentally friendly chemical to minimise the impact on the environment. An environmentally friendly base chemical formulation has recently been developed (BASF Company), however, the initial results show that the performance of this chemical is not as good as other existing formulations. The above mentioned approach for design and testing new KHIs can be used to improve the formulation of the base chemical and/or finding suitable synergic compounds.

Inhibitor performance in oil systems and effect of salts: Most existing Kinetic Hydrate Inhibitors (KHI) are developed for gas systems where the aqueous phase has low or nil salinity. Therefore, the existing formulations may not be as effective in the presence of produced water. Also, gas reservoir may produce formation water at their late life. The presence of salts may have an adverse effect on the performance of KHIs. Similarly, the presence of oil/condensate phase may affect the performance of KHIs. Depending to KHI formulation, it may partially dissolve in oil phase and lead to a decrease in its concentration in water phase.

Anti-Agglomerants (AA) are generally used when a liquid hydrocarbon phase is present. However, in almost all cases the amount hydrocarbon phase is larger than the aqueous phase, resulting in a water in oil emulsion and/or hydrate slurry in a continuous

oil phase. However, in water-flooded oil reservoirs, the amount of water phase could be much higher than the liquid hydrocarbon phase. Therefore, the application of AAs should result in the formation of oil in water emulsion. Upon hydrate formation, the vapour phase may disappear, resulting in dispersed hydrate and oil in a continuous water phase. There is almost no information on such systems and how the existing AAs formulations perform under such demanding conditions.

It is proposed to conduct a systematic investigation on the effect of high water cuts and salts on the performance of KHIs and AAs.

Designing KHIs for structure-I hydrates: Almost all existing KHIs have been designed for structure II hydrates, due to tetrahydrofuran (THF) screening methods used (THF forms structure II hydrates at atmospheric conditions). However, there are very lean natural gas systems in several parts of the world (e.g., North Sea and Gulf of Mexico). It is recommended to conduct a systematic investigation on the performance of new chemicals under structure I conditions. The result may not only reduce the cost of hydrate prevention strategies for structure I systems, but also have a positive impact on the performance of structure II inhibitors.

8.3.2 Driving Force for Hydrate Formation

In this work the relationship of true driving force for hydrate formation with subcooling at different conditions was analysed. The analysis was extended to the context of *testing low* dosage hydrate inhibitors and the effect of pressure on the performance of them.

The above analysis can be further extended to the systems where in addition to KHIs, thermodynamic inhibitors (e.g. salt, methanol, glycols) are present in the system. In those cases, the fugacity of thermodynamic inhibitor needs to be taken in to account in formulation of the change of Gibbs free energy of the system at operating conditions, ΔG^{exp} (Equation 1, Chapter 7). The simplified model presented in Chapter 2 for can be used for vapour-electrolyte solution equilibria in formulation of ΔG^{exp} in the presence of electrolytes.

REFERENCES

Aasberg-Petersen, K., Stenby, E., and Fredenslund, A., 1991, "Prediction of High-Pressure Gas Solubilities in Aqueous Mixtures of Electrolytes", *Industrial & Engineering Chemistry Research*, 30 (9), 2180-2185.

Anderson, F.E., and Prausnitz, J.M., 1986, "Inhibition of Gas Hydrates By Methanol", *AIChE Journal*, **32**(8), 1321-1333.

Argo, C.B., Blain, R.A., Osborne, C.G., Priestley, I.D., 2000, "Commercial deployment of low-dosage hydrate inhibitors in a southern North Sea 69 km wet-gas sub-sea pipeline", *SPE Production & Facilities* **15** (2), 130-134.

Argo, C.B., Beger, R., Shoup, G., *Fleyfel*, F., Andersson, V and Larsen, R., 2002, "Selection of a Low Dosage Hydrate Inhibitor (LDHI) for a Gulf of Mexico Black Oil Tie-back Pipeline Application", Proceedings of the Fourth International Conference on Gas Hydrates, Yokohoma.

Avlonitis, D., Danesh, A., and Todd, A.C., 1994, "Prediction of VL and VLL Equilibria of Mixtures Containing Petroleum Reservoir Fluids and Methanol With a Cubic EoS", *Fluid Phase Equilibria*, **94**, 181-216.

Bakeev K.N., Chuang J., Drzewinski M.A. and Graham D.E., 2000, "Method for Preventing and Retarding the Formation of gas Hydrate", US Patent 6,117,929.

Barker, J.W., and Gomez, R.K., 1989, "Formation of Hydrate During Deep-water Drilling Operations", Journal of Petroleum Technology, **41**(3), 297-301.

Baker Petrolite, 2002, "HI-M-PACT Anti-Agglomerant Hydrate Inhibitor-Don't go Deep without it" ON-SPEC, March 2002, quarterly publication of Baker Petrolite Corporation.

Ballard, A.L. and Sloan, E. D., 2002, "The next generation of hydrate prediction: I. Hydrate standard states and incorporation of spectroscopy, Fluid Phase Equilibria, 194-197, 371-383.

Behar, E., Sugier, A., Rojey, A., 1988, "Hydrate Formation and Inhibition in Multiphase Flow", presented at BHRA Conference Operation Consequences of Hydrate Formation and Inhibition Offshore, Cranfield UK.

Behar, E., Delion, A-S, Sugier, A., Thomas, M., 1994, "Plugging Control of Production Facilities by Hydrates", Annals of New York Acad. Sci., 715, 94-105.

Bishnoi, P.R., Gupta, A.K., Englezos, P., and Kalogerakis, N., 1989, "Multiphase Equilibrium Flash Calculations For Systems Containing Gas Hydrates", *Fluid Phase Equilibria*, **53**, 97-104.

Byrne, P.A., and Stoessell, R.K, 1982, "Methane solubilities in multi-salt solutions", *Geochimica et Cosmochimica Acta*, **46**, 2395-2397. Also IUPAC Solubility Data Series, Volume 27/28, Methane.

Camargo, R., 2001, "Propriétés Rhéologiques de suspensions d'hydrate dans des bruts asphalteniques", *PhD Thesis*, University of Paris VI, France.

Carver, T., Drew, M., and Rodger, P. M., 1996, "Characterization of the {111} growth planes of a type II gas hydrate and study of the mechanism of kinetic inhibition by poly(vinylpyrrolidone). J. Chem. Faraday Trans. 92, 5029-5033.

Challa, G., 1993, "Polymer Chemistry: an Introduction", Ellis Horwood.

Christiansen, R.L., Sloan, E.D., 1995,"A compact model for hydrate formation", Proceedings of the 74th GPA Annual Convention. San Antonio, TX, 15–21 March.

Cohen J.M., Wolf P F. and Young; W.D., 1998, "Method for Preventing or Retarding the Formation of Gas Hydrates", US Patent 5,723,524.

Cohen J.M., Wolf P F. and Young; W.D., 1998, "Enhanced Hydrate Inhibitors: Powerful Synergism with Glycol Ethers", Energy & Fuels, 12, 216-218.

Cole, W.A., and Goodwin, S.P., 1990, "Flash Calculations for Gas Hydrates - a Rigorous Approach", *Chemical Engineering Science*, **45**(3), 569-573.

Dahlmann, U., Feustel, M., 2004, "Additives for inhibiting the formation of gas hydrates" US Patent Office 2004/0159041.

Dahlmann, U., Feustel, M., 2005, "Corrosion and gas hydrate inhibitors having improved water solubility and increases biodegradability" US Patent Office 2004/0101495.

Danesh, A., Xu, D.H., and Todd, A.C., 1991, "Comparative-Study of Cubic Equations of State For Predicting Phase- Behavior and Volumetric Properties of Injection Gas-Reservoir Oil Systems", *Fluid Phase Equilibria*, **63**(3), 259-278.

Danesh, A., Tohidi, B., Burgass, R.W., and Tod, A.C., 1994, "Hydrate Equilibrium Data of Methyl Cyclo-Pentane With Methane or Nitrogen." *Chemical Engineering Research & Design* **72**(A2), 197-200.

Davy, H., 1811, "The Bakerian Lecture: On Some of the Combinations of Oxymuriatic Gas and Oxygen, and on the Chemical Relations of these Principles to Inflammable Bodies", *Philosophical Transactions of the Royal Society, London*, **101** (Part I), 1-35.

Deaton, W. M., and Frost, E. M., 1946, "Gas Hydrates and Their Relation to the Operation of Natural Gas Pipelines", *U.S. Bur. Mines Monograph*, **8**, 101.

Dharmawardhana, P. B., Parrish, W. R., and Sloan, E. D., 1980, "Experimental Thermodynamic Parameters for the Prediction of Natural Gas Hydrate Dissociation Conditions", *Industrial & Engineering Chemistry Fundamentals*, **19**, 410-414.

Duncum, S.; Edwards, A.R.; Osborne. C.G. WO Patent Application 96/04462, 1996.

Englezos, P., N. Kalogerakis, P.D. Dholabhai and P.R. Bishnoi, 1987, "Kinetics of Formation of Methane and Ethane Gas Hydrates", *Chem.Eng. Sci.*, 42, 2647-2658.

Fadnes, F.H., 1996, "Natural hydrate inhibiting components in crude oils", *Fluid Phase Equilibria*, **117**, pp 186-192.

Fidler, J., and Rodger, P.M., 1999, "Solvation structure around aqueous alcohols" *J. Phys. Chem. B*, **103**, 7695–7703.

Frostman, L.M., 2000, "Anti-agglomerant hydrate inhibitors for prevention of hydrate plugs in deepwater systems", *SPE Annual Technical Conference and Exhibition*, Dallas, Texas, USA. *SPE* 63122.

Frostman, L.M., Przybylinski, J.L., 2001, "Successful Applications of Anti-agglomerant Hydrate Inhibitors", SPE International Symposium on Oilfield Chemistry, 13-16 February, Houston, Texas SPE 65007.

Frostman, L.,M., Thieu, V., Crosby, D. L., Downs, H. H., 2003, "Low-Dosage Hydrate Inhibitors (LDHIs): Reducing Costs in Existing Systems and Designing for the Future", presented at SPE international symposium on oilfield chemistry, Houston, Texas, SPE 80269.

Fu, B., Neff, S., Mathur, A., Bakeev, K., 2002, "Application of Low-Dosage Hydrate Inhibitors in Deepwater Operations" SPE Journal of Production & Facilities, Vol 17, No 3, SPE 78823.

Garside, J., Mersmann, A., Nyvlt, J., 2002, "Measurement of crystal growth and nucleation rates", second ed. IChemE, UK.

Gupta, A. K. 1988, *Ph.D. Thesis*, University of Calgary, Calgary, Canada.

Hall, D.L., Sterner, M., and Bodnar, R.J., 1988, "Freezing Point Depression of NaCl-KCl $-H_2O$ Solutions", *Economic Geology*, **83**, 197-202.

Hammerschmidt, E.G., 1934, "Formation of Gas Hydrates in Natural Gas Transmission Lines", *Industrial & Engineering Chemistry Research*, **26**, 851.

Herri, J. M., Gruy, F., Pic, J. S., Cournil, M. Cingotti, B., Sinquin, A., 1999,"Interest of in situ turbidimetry for the characterization of methane hydrate crystallisation: Application to the study of kinetic inhibitors". Chemical Engineering Science 54, 1849-1858.

Holder, G.D., Corbin, G., and Papadopoulos, K.D., 1980, "Thermodynamic and Molecular Properties of Gas Hydrates from Mixtures Containing Methane, Argon, and Krypton", *Industrial & Engineering Chemistry Fundamentals*, **19**(3), 282-286.

Huo, Z., Freer, E., Lamar, M., Sannigrahi, B., Knauss, D.M., and Sloan Jr., E.D., 2001, "Hydrate plug prevention by anti-agglomeration", Chemical Engineering

Science, 56, 4979-4991.

Jeffrey, G.A., 1984, "Hydrate Inclusion Compounds", Chapter 5 in: Atwood, J.L., Davies, J.E.D., and MacNichol, D.D., Inclusion Compounds, 1, Academic Press, London, 135-191.

Kashchiev, D., Firoozabadi, A., 2002, "Driving force for crystallization of gas hydrates. Journal of Crystal Growth", 241, 220–230.

Kelland, M.A., Svartaas, T.M., Dybvik, L.A., 1994, "Control of Hydrate Formation by Surfactants and Polymers", paper presented at the SPE 69th Annual Technical Conference and Exhibition, New Orleans, LA, USA, SPE 28506.

Kelland, M.-A., Svattaas T.M., Dybvik, L., 1995, "Studies on new gas hydrate inhibitors", Society of Petroleum Engineers Inc. Offshore Europe Conference, Aberdeen, UK, SPE 30420.

Kelland, M. A., Svartaas, T. M., Dybvik, L. A., 1995, "A new generation of hydrate inhibitors", SPE Paper, 30695, presented at the SPE Annual Technical Conference in Dallas.

Kelland, M. A., Rodger P.M., and Namba, T., 1998, "Composition for controlling clathrate hydrates and a method for controlling clathrate hydrate formation", (RF-Procom A/S; Nippon Shokubai Co, Ltd, Norway), Patent PCT Int. Appl. WO 98 53007 (November 26, 1998).

Kelland, M. A., 2006, "History of the Development of Low Dosage Hydrate Inhibitors", *Energy Fuels,* **20** (3), 825 -847.

King, H.E., Hutter, J. L., Lin, M.Y., and Sun, T., 2000, "Polymer conformations of gas-hydrate kinetic inhibitors: a small-angle neutron scattering study" *J. Chem. Phys.* **112**, 2523.

Kihara, T., 1953, "Virial Coefficients and Models of Molecules in Gases", *Reviews of Modern Physics*, **25**(4), 831-843.

Koh, C.A., Westcott, R.E., Zhang, W., Hirachand, K., Creek, J.L., and Soper, A.K., 2002, "Mechanisms of gas hydrate formation and inhibition", Fluid Phase Equilibria, 194, 143–151.

Klomp; U. C, Kruka; V. R. Reijnhart, R.; Weisenborn; A.J., 1995, "Method for inhibiting the plugging of conduits by gas hydrates", U.S. Patent No. 5,460,728.

Klomp; U. C, Kruka; V. R. Reijnhart, R.; Weisenborn; A.J., 1997, "Method for inhibiting the plugging of conduits by gas hydrates", U.S. Patent No. 5,648,575.

Kumar, A. and Patwardhan, V.S., 1986,"Prediction of Vapour Pressure of Aqueous Solutions of Single and Mixed Electrolytes", The Canadian Journal of Chemical Engineering, 64, 831-838.

Kurihara, K., Tochigi, K., and Kojima,K., 1987, "Mixing rule containing regular solution and residual excess free energy", *J. Chem. Engng Japan,* **20**, 227-231.

Kvamme, B., Huseby, g., Forrisdahl, O., "Molecular dynamics simulations of PVP kinetic inhibitor in liquid water and hydrate/liquid water systems", pproceedings of 2nd International Conference on Natural Gas Hydrates, pp.347-354,(Monfort, J.P., ed.), Toulouse, 2-6 June (1996).

Lederhos, J.P., Sloan, E.D, 1996, "Transferability of Kinetic Inhibitors Between Laboratory and Pilot Plant", paper presented at the 1996 SPE Annual Conference and Exhibition, Denver, Colorado, USA, SPE 36588.

Lederhos, J.P., Long, J.P., Sum, A., Christiansen, R.L., Sloan E.D.,1996, "Effective kinetic hydrate inhibitors for natural gas hydrates", Chemical Engineering Science, vol. 51, No.8, pp.1221-1229.

Leporcher, E., Peytavy, J. l., Mollier, Y., and Sjôblom, J., 1998, "Multiphase transportation: hydrate plugging prevention through crude oil natural surfactants", paper SPE 49172 presented at the *Annual Technical Conference and Exhibition* held in New Orleans, SPE 49172.

Li, Y.-G. and Pitzer, K. S., 1986, "Thermodynamics of aqueous sodium chloride solutions at high temperatures and pressures (I): thermodynamic properties over 373-573 K and 0.1-100 MPa.'', *J. Chem. Ind. Engng China*, **1**, 40-50.

Li, Y.K., and Nghiem, L.X., 1986, "Phase Equilibria of Oil, Gas and Water/Brine Mixtures From a Cubic Equation of State and Henry's Law", *Canadian Journal of Chemical Engineering*, **64**(3), 486-496.

Long, J.; Lederhos, J.; Sum, A.; Christiansen, R.; Sloan, E.D.., 1994, "Kinetic Inhibitors of Natural Gas Hydrates", Proceedings of the seventy-third GPA Annual Convention, New Orleans, 7-9 March.

Lovell, D., Pakulski, M., 2002, "Hydrate Inhibition in Gas Wells Treated With Two Low Dosage Hydrate Inhibitors", SPE Gas Technology Symposium, 30 April-2 May, Calgary, Alberta, Canada SPE 75668.

Lund, A., Urdahl, O., Kirkhorn, S.S., 1995, "Inhibition of gas hydrate formation by means of chemical additives-2: An evaluation of the screening method", Chemical Engineering Science 51, 3449-3458.

MacDonald, A.W.R., Petrie, M., Wylde, J.J., Chalmers, A.J., Arjmandi, M., 2006, "Field Application of Combined Kinetic Hydrate and Corrosion Inhibitors in the Southern North Sea: Case Studies", SPE Gas Technology Symposium, 15-17 May 2006, Calgary, Alberta, Canada.

Macedo, E.A., Skovborg, P., and Rasmussen, P., 1990, "Calculation of Phase Equilibria for Solutions of Strong Electrolytes in Solvent-Water Mixtures", *Chemical Engineering Science*, **45**(4), 875-882.

Makogon, T. Y., 1997, "Kinetic Inhibition of Natural Gas Hydrates", Ph. D. Thesis, Colorado School of Mines.

Makogon, Y.F., 1981,"Hydrates of natural gas", PennWell Books, Tulsa, Oklahoma.

Makogon T.Y., Sloan E.D., 2002, "Mechanism of Kinetic Hydrate Inhibitors", Proceedings of 4th International Conference on Natural Gas Hydrates, P.498, Yokohama, Japan.

Masoudi, R., Tohidi, B., 2005," Experimental investigation on the effect of commercial oilfield scale inhibitors on the performance of low dosage hydrate inhibitors (ldhi)", Proceedings of the *5th International Conference on Gas Hydrates*, Trondheim, Norway.

Matthews; R. R.; Clark; C. R., 1989, "Inhibition of hydrate formation", US Patent No. 4,856,593.

Mavroyannis, C. and Stephen, M.J., 1962, "Dispersion forces", *Molecular Physics*, **5**, 629-638.

Mckoy, V., and Sinanoglu, O., 1963,"Theory of Dissociation Pressures of Some Gas Hydrates", *Journal of Chemical Physics*, **38**(12), 2946-2956.

Mehta, A.P., and Sloan, E.D., 1993, "Structure H Hydrate Phase Equilibria of Methane + Liquid Hydrocarbon Mixtures", *Journal of Chemical and Engineering Data*, **38**(4), 580-582.

Mehta, A.P., and Sloan, E.D., 1994, "A Thermodynamic Model for Structure-H Hydrates", *AIChE Journal*, **40**(2), 312-320.

Mehta, A.P., Hudson, J., Peters, D., 2001, "Risk of Pipeline Over-Pressurization during Hydrate Remediation by Electrical Heating", Chevron Deepwater pipeline &Riser Conference, Houston.

Mehta, A.P., P.B. Hebert, E. R. Cadena, and J. P. Weatherman, 2002, "Fulfilling the promise of Low-Dosage Hydrate Inhibitors: Journey from Academic Curiosity to Successful Field Implementation", SPE Paper 81927 presented at the Offshore Technology Conference, Houston, USA.

Michelsen, M.L., 1982, "The Isothermal Flash Problem. 1. Stability", *Fluid Phase Equilibria*, **9**(1), 1-19.

Milburn; C. R. ; Sitz; Gary M., 2002, "Amines useful in inhibiting gas hydrate formation", US Patent No. 6,444,852 .

Mitchell, G. F., Talley, L. D., 1999, "Application of Kinetic Hydrate Inhibitor in Black-Oil Flowlines" SPE Annual Technical Conference and Exhibition, 3-6 October, Houston, Texas.

Morris G., 2002, "Deepwater trial tests low-dosage hydrate inhibitor", Oil and Gas Journal, June 17, 2002.

Mullin, J.W., 1997. Crystallization, third ed. Butterworth-Heinemann, Oxford.

Natarajan, V., Bishnoi, P.R., Kalogerakis, N., 1994. Induction phenomena in gas hydrate nucleation. Chemical Engineering Science, 2075–2087.

Notz, P.K., Bumgardner, S.B., Schaneman, B.D., Todd, J.L., 1995,"Application of kinetic inhibitors to gas hydrate problems", *SPE Production & Facilities* **11**, 256-260.

Nygaard, H. F., 1989,"Transportability of hydrates in multiphase systems", *Multi-phase Flow* - Proceedings of the 4th International Conference, pp 1-14.

O'Sullivan, T.D. and Smith, N.O., 1970, "The solubility of partial molar volume of Nitrogen and Methane in water and in Aqueous Sodium Chloride from 50 to 150 °C and 100 to 600 atm.", *The Journal of Physical Chemistry*, **74**(7), 1460-1466.

Pakulski, M., 1998, "Method for Controlling Gas Hydrates in Fluid Mixtures", US Patent No. 5741758.

Pakulski, M., 2000, "Quaternized polyether amines as gas hydrate inhibitors", US Patent No. 6,025,302.

Panchalingham, V., Rudel, M. G., Bodnar, S. H., 2005, "Methods for inhibiting hydrate blockage in oil and gas pipelines using amide compounds", US Patent Office 2005/0081432.

Panchalingham, V., Rudel, M. G., Bodnar, S. H., 2006, "Methods for inhibiting hydrate blockage in oil and gas pipelines using simple quaternary ammonium and phosphonium compounds", UK Patent Office GB2422840.

Parrish, W.R., and Prausnitz, J. M., 1972,"Dissociation Pressures of Gas Hydrates Formed by Gas Mixtures", *Industrial & Engineering Chemistry Process Design and Development*, **11**(1), 26-35.

Patel, N.C., and Teja, A.S., 1982, "A New Cubic Equation of State for Fluids and Fluid Mixtures", *Chemical Engineering Science*, **37**(3), 463-473.

Peiffer; D.G., Costello; C.A., Talley; L. D.; Wright; P.J. 1999, "Method for inhibiting hydrate formation", US Patent 6,194,622.

Phillips, N.J., and Grainger, M., 1998, "Development and Application of Kinetic Hydrate Inhibitors in the North Sea", presented at the SPE Gas Technology Symposium, Calgary, Canada, SPE 40030.

Rasch, A., Mikalsen, A., Austvik, T., Gjertsen, L.H., and Li, X., 2002, "Evaluation of a Kinetic Hydrate Inhibitor with Focus on the Pressure and Fluid Dependency", Proceedings of 4th International Conference on Natural Gas Hydrates, pp.927, Yokohama, Japan.

Rasch, A., Mikalsen, A., Gjertsen, L.H., and Fu, B., 2001, "Evaluation of a low dosage hydrate inhibitor in hydrocarbon systems at high subcooling", Proceedings of the 10th International Conference Multiphase '01, Cannes, France, pp. 239-247.

Ripmeester, J.A., Tse, J.S., Ratcliffe, C.I., and Powell, B.M., 1987,"A New Clathrate Hydrate Structure", *Nature*, **325**(6100), 135-136.

Ripmeester, J.A., Ratcliffe, C.I., and McLaurin, G.E., 1991, "The Role of Heavier Hydrocarbons in Hydrate Formation", *The 1991 AIChE Spring Meeting.*

Sander, B., Fredenslund, A., and Rasmussen, P., 1986, "Calculation of Vapour-Liquid Equilibria in Mixed Solvent/Salt Systems Using an Extended Uniquac Equation", *Chemical Engineering Science*, **41**(5), 1171-1183.

Sinquin, A., Bredzinsky, X., and Beunat, V., 2001, "Kinetic of Hydrates Formation: Influence of Crude Oils", presented at the 2001 SPE Annual Technical Conference and Exhibition held in New Orleans, Louisiana, SPE 71543.

Sinquin, A., Miao, M., Beunat, V., Jussaume, M., 2002, "Kinetic of Hydrates Formation: Influence of Crude Oils-part 2",", *4th International Conference on Gas Hydrates*, Yokohama, Japan, pp.520-525.

Skovborg. P., 1993, "Gas hydrte kinetics", *PhD thesis*, Institute for Kemiteknik, Danmarks Tecniske Hojskole, Lyngby, Denmark.

Skovborg, P., Ng, H.J., Rasmussen, P., Mohn, U., 1993. Measurement of induction times for the formation of methane and ethane gas hydrates. Chemical Engineering Science 48, 445–453.

Sloan, E.D., 1998,"Clathrate Hydrates of Natural Gases", 2nd ed., Marcel Dekker Inc., New York.

Sloan, E.D., Subramanian, S., Matthews, P.N., Lederhos, J.P., Khokhar, A.A., 1998," Quantifying Hydrate Formation and Kinetic Inhibition", *Ind. Eng. Chem. Res.*, 37, 3124.

Sloan, E. D., 2003, "Clathrate hydrate measurements: microscopic, mesoscopic, and macroscopic", Journal of Chemical Thermodynamics, 35 (1): 41-53.

Sohrabi, M., Henderson, G.D., Tehrani, D.H., and Danesh, A., 2000,"Visualisation of Oil Recovery by Water Alternating Gas (WAG) Injection Using High Pressure Micromodels - Water-Wet System. Paper SPE 63000, Proceedings of the SPE Annual Technical Conference and Exhibition, Dallas, Texas.

Spratt, P. A., 2005, "Ion pair amphiphiles as gas hydrate inhibitors" US Patent Office 2005/038572.

Storr, M.T., Monfort, J.P., Taylor, P.C., Rodger, P.M., 2002, "Natural Gas Hydrates: Modifying Stability with Low Dosage Inhibitors", Proceedings of the Fourth international Conference on Gas Hydrates, Yokohama, 504-508.

Storr, M.T., Taylor, P.C., Monfort, J.P, Rodger, P.M., 2004, "Kinetics of hydrate crystallization", Journal of the American Chemical Society, vol.126, pp.1569-1576.

Sugier; A., Bourgmayer, P.; Behar; E., Freund; E.," Method of transporting a hydrate forming fluid", US Patent No. 4,915,176.

Svartaas, T., M., Kelland, M.A., Dybvik, L., 2000, "Experiments Related to the Performance of Gas Hydrate Kinetic Inhibitors", Annals of the New York Academy of Sciences, 912, 744-752.

Swanson, T.A., Petrie, M., Sifferman, T.R., 2005, "The Successful Use of Both Kinetic Hydrate and Paraffin Inhibitors Together in a Deepwater Pipeline with a High Water Cut in the Gulf of Mexico", SPE International Symposium on Oilfield Chemistry, 2-4 February 2005, The Woodlands, Texas.

Takenouchi, S. and Kennedy, G., 1965, "The solubility of Carbon Dioxide in NaCl solutions at high temperatures and pressures", *American Journal of Science*, 263, 445-454.

Tohidi, B., 1995,"Gas Hydrate Equilibria in the Presence of Electrolyte Solutions", *Ph.D. Thesis*, Heriot-Watt University, Edinburgh.

Tohidi, B., Danesh, A., and Todd, A.C., 1995, "Modelling Single and Mixed Electrolyte-Solutions and Its Applications to Gas Hydrates", *Chemical Engineering Research & Design*, 73(A4), 464-472.

Tohidi, B.; Burgass, R.W.; Danesh, A.; Østergaard, K. K.; Todd, A. C., 2000, "Improving the accuracy of gas hydrate dissociation point measurements" *Ann. N.Y. Acad. Sci.*, *912*, 924-931.

Tohidi, B., Anderson, R., Clennell, M.B., Burgess, R.W., and Biderkab, A.-B., 2001, "Visual Observation of Gas-Hydrate Formation and Dissociation in Porous Media by Means of Glass Micromodels", *Geology*, **29**, 867.

Tohidi, B., Anderson, R., Clennell, M.B., Yang, J., Bashir, A., Burgess, R.W., 2002," Application of High Pressure Glass Micromodel to Gas Hydrates Studies", Proceedings of 4th International Conference on Natural Gas Hydrates, pp.761-765, Yokohama, Japan.

Tohidi, B., Anderson, R., Masoudi, R., Arjmandi, M., Burgass, R.W., Yang, J.H., 2003, "A Review of Clathrate Hydrate Research at Heriot-Watt University", *Russian Chemical Journal*, **47**(3), 49-58.

Urdahl, O., Lund, A., Mørk, P., Nilsen, T.N., 1995, "Inhibition of gas hydrate formation by means of chemical additives - I. Development of an experimental set-up for characterization of gas hydrate inhibitor efficiency with respect to flow properties and deposition", *Chemical Engineering Science,* **50**, 863-870.

Urdahl, O., Lund, A., Gjertsen, L.H., and Austvik, T., 1997, "Experimental testing and evaluation of a kinetic gas hydrate inhibitor in different fluid systems", presented at the 213th ACS national meeting, San Francisco, US, Volume 42, No. 2, pp. 498-502.

Valderrama, J.O., and Cisternas, L.A., 1986, "A cubic equation of state for polar and other complex-mixtures", *Fluid Phase Equilibria*, **29**, 431-438.

Valderrama, J.O., 1990, "A generalized Patel-Teja equation of state for polar and nonpolar fluids and their mixtures", *Journal of Chemical Engineering of Japan*, **23**(1), 87-91.

Van der Waals, J.H., and Platteeuw, J.C., 1959, "Clathrate Solutions", *Advances in Chemical Physics*, **2**, 1-57.

Vebenstad, A., Larsen, L., Straume, E., Argo, C. b., Fung, G., 2005, "Assessment of Hydrate Plugging Potentiel of King Gulf of Mexico", Proceedings of the *5th*

International Conference on Gas Hydrates, Vo. 4, pp.1193, Trondheim, Norway.

Vysniauskas, A., Bishnoi, P.R., 1983. A kinetic study of methane hydrate formation. Chemical Engineering Science 38, 1061–1072.

Walas S. M. Phase Equilibria in Chemical Engineering. *Butterworth Publishers,* Boston, 1985.

Washburn (1926-1930), International Critical Tables (ICT) of numerical data, physics, chemistry and technology. National Research council.

Wu, M., Wang, S., Liu, H., 2007, "A Study on Inhibitors for the Prevention of Hydrate Formation in Gas Transmission Pipeline", *Journal of Natural Gas Chemistry, Volume 16, Issue 1, Pages 81-85*

Yousif, M.H., 1998. "The kinetics of hydrate formation". Society of Petroleum Engineers Inc. 69th Annual Technical Conference and Exhibition held in New Orleans, LA, USA, 25–28 September, SPE 28479.

Zuo, Y.X. and Guo, T.M., 1991, "Extension of the Patel-Teja Equation of State to the Prediction of the Solubility of Natural Gas in Formation Water", *Chemical Engineering Science*, **46**(12), 3251-3258.